Exploring gut microbiome – host interactions in the extremes of health and disease

An in-depth analysis of elite athletes and bariatric surgery patients

Nicholas PENNEY

A thesis submitted for the award of the degree of Doctor of Philosophy (PhD)

Supervisors: Professor E Holmes, Professor A Darzi, Mr S Purkayastha

Post-doctoral support: Dr I Garcia-Perez

Department of Surgery and Cancer

Imperial College London

2019

This thesis is dedicated to my wonderful wife Janine for her enduring love and support through the highs and lows of research. Without your endless sacrifices I could never have completed this thesis, or much else for that matter! I hope in the years to come I can come close to repaying you.

Statement of Originality

I certify that this thesis, and the research to which it refers, are the product of my own work, and that any ideas or quotations from the work of other people, published or otherwise, are fully acknowledged in accordance with the standard referencing practices of the discipline. Where my own work resulting from this thesis has been published, this has also been acknowledged.

Copyright Declaration

The copyright of this thesis rests with the author and is made available under a Creative Commons Attribution Non-Commercial No Derivatives licence. Researchers are free to copy, distribute or transmit the thesis on the condition that they attribute it, that they do not use it for commercial purposes and that they do not alter, transform or build upon it. For any reuse or redistribution, researchers must make clear to others the licence terms of this work.

Abstract

Introduction: Multi 'omics analyses, including metabonomic and metagenomic profiling techniques, have enabled new insights into systems biology over the past decade. Using two extremes of a continuum between health and disease – elite athletes and obese patients undergoing bariatric surgery – the work in this thesis aims to apply metabolic phenotyping to further understand the impact of exercise, diet and obesity on human metabolism. Furthermore, through combinatorial analysis of metabonomic and gut microbiome data sets, host – gut microbiome co-metabolism and its influence on health is explored in these two extreme populations.

Methods: Biofluids were collected from three cohorts: i) elite athletes and age and sex matched controls, ii) healthy individuals before and after a high protein diet, exercise regime or both, and iii) obese subjects pre and post bariatric surgery. Multiple analytical platforms were utilised for metabolic profiling including ^{1}H-NMR spectroscopy, UPLC-MS and GC-MS. Gut microbiome analysis was performed using next generation metagenomic sequencing. After pre-processing the metabonomic and metagenomic data; univariate, unsupervised and supervised multivariate analyses were performed as well as gut microbiome-metabolite association studies.

Results: Distinct metabolic and microbial phenotypes existed between both athletes and controls and between obese patients before and after bariatric surgery. Discriminatory metabolites higher in athletes include metabolites associated with muscle turnover, vitamins and recovery supplements, a high protein diet and those derived from gut microbes. Interestingly, increased bacterial diversity seen in athletes correlated with a specific subset of metabolites. Similarly, bariatric surgery resulted in large changes to circulating metabolites. A number of these metabolites were linked to changes in the gut microbiome, including bile acids, short-chain fatty acids and amino acids.

Conclusion: This thesis extends existing knowledge of the gut microbiome's influence on human health through small molecule signalling. Mechanistic studies are now needed to establish causal links between gut microbes, changes to circulating metabolites and disease status.

Objectives

- I hypothesise that elite athletes and healthy controls have distinct metabolic phenotypes and aim to elucidate these differences through metabolic profiling.

- I hypothesise that metabolic changes in athletes are due to a number of influences including exercise levels and diet, resulting in altered microbiome-host co-metabolism. I aim to further elucidate the individual contribution of these lifestyle factors to metabolism.

- I hypothesise that weight-loss and the metabolic benefits seen following bariatric surgery are achieved in part through a functional modification of the gut microbiome, resulting in altered microbiome–host co-metabolism. I aim to further elucidate the metabolic and gut microbiome changes following bariatric surgery.

- In particular, I aim to assess how the gut microbiome influences the metabolic phenotype following bariatric surgery through altered bile acid and short-chain fatty acid signalling

Acknowledgments

I could not have achieved this thesis without the enormous help and generous support that I have received along the way.

Firstly, I would like to thank my supervisors Professor Elaine Holmes, Professor Ara Darzi and Mr Sanjay Purkayastha for the incredible opportunities, guidance and scientific expertise they have provided during the course of this research.

In addition to my primary supervisors, I would like to thank Dr Isabel Garcia-Perez for her invaluable help throughout, in particular with metabonomic analyses. Without her regular help in the laboratory and analysing results I would not have surmounted the steep learning curve in this field. I also thank Dr Lesley Hoyles for her great help and expertise in gut microbiome analysis.

A large number of others have kindly offered significant advice and help. I would like to acknowledge Professor Julian Marchesi, Professor Gary Frost, Dr Joram Posma, Dr James Kinross, Dr Jia Li, Dr Maria Gomez Romero, Dr Verena Horneffer-van der Sluis, Dr Michael Kyriakides, Jerusa Brignardello, Dr Magali Sarafian as well as the staff and patients of the Imperial Weight Centre.

I was also very fortunate to have the opportunity to collaborate with members of the University College Cork and Teagasc Food Research Centre, including Dr Paul Cotter, Dr Orla O'Sullivan and Wiley Barton.

I am indebted to the Diabetes Research and Wellness Foundation for awarding me the Sutherland-Earl Clinical Research Fellowship 2015-2017. This provided vital funding to longitudinally phenotype bariatric surgery patients before and after intervention. Without the DRWFs support this study would not have been feasible and I am very grateful for their belief in this project. In addition, this work was further supported by a National Institute of Health Research (NIHR) – Imperial Biomedical Research Centre (BRC) Surgery and Surgical Technology Grant 2015.

Lastly, I wish to thank my parents for the love, encouragement and wonderful opportunities they have provided me with throughout my life.

Table of Contents

Statement of Originality **4**

Copyright Declaration **4**

Abstract **5**

Objectives **6**

Acknowledgments **7**

List of Figures **15**

List of Tables **18**

Abbreviations **20**

1 Introduction **25**

1.1 The human metabolome 25

1.2 The gut microbiome 26

1.3 Gut microbiome – host metabonome co-metabolism 27

1.3.1 Short Chain Fatty Acids (SCFA) 27

1.3.2 Choline Metabolism 28

1.3.3 Bile Acids 29

1.4 Obesity & Bariatric Surgery 31

1.5 Systematic Review of the role of bile acid co-metabolism in the metabolic effects of bariatric surgery 32

1.5.1 Introduction 32

1.5.2 Methods 32

1.5.3 Results and discussion 33

1.5.4 Bile Acid Metabolism 35

1.5.5 Latest Research 48

1.5.6 Conclusions 49

1.6 Physical activity and Exercise 50
1.7 Chapter Conclusion & Outlook 52
1.8 References 54
2 Analytical Strategies 73
2.1 Metabonomic platforms 73
2.2 NMR principles 74
2.2.1 Nuclear Spin 74
2.2.2 Magnetic resonance 74
2.2.3 Chemical shift & multiplicity 75
2.3 Mass Spectrometry principles 76
2.3.1 Chromatography 76
2.3.2 Mass Spectrometry 77
2.4 Multivariate Data Analysis 79
2.4.1 Unsupervised methods 79
2.4.2 Supervised methods 80
2.5 Metabolite identification 81
2.5.1 1D NMR 82
2.5.2 2D NMR 82
2.5.3 LC-MS 87
2.5.4 Authentic chemical reference spiking 89
2.5.5 Level of assignment 90
2.6 Principles of Next Generation Metagenomic sequencing 90
2.6.1 Statistical handling of NGS data 92
2.7 References 94
3 A cross sectional study to elucidate the metabolic phenotype of elite athletes 98
3.1 Introduction 98

3.2 Methods 99
3.2.1 Patient recruitment 99
3.2.2 Experimental design 99
3.2.3 Preparation of samples for metabolomics analysis 100
3.2.4 LC-MS Metabolic profiling analysis 101
3.2.5 ^{1}H-NMR Metabolic profiling analysis 102
3.2.6 GC-MS SCFAs targeted analysis 102
3.2.7 Gut Microbiota analysis 103
3.2.8 LC-MS data treatment 103
3.2.9 ^{1}H-NMR data treatment 103
3.2.10 Statistical analysis 104
3.2.11 Metabolite identification 104
3.3 Results 105
3.3.1 Demographic and anthropometric differences between athletes and controls 105
3.3.2 Dietary Differences between athletes and controls 106
3.3.3 ^{1}H-NMR spectroscopy of faecal and urine samples in athletes and controls 107
3.3.4 LC-MS of faecal and urine samples in athletes and controls 111
3.3.5 GC-MS of faecal samples in athletes and controls 115
3.3.6 Gut microbiome-host interactions: Correlations between bacterial taxa and faecal SCFA levels. 117
3.4 Discussion 119
3.4.1 Biological interpretation 119
3.4.2 Study limitations and future directions 121
3.5 Conclusion 122
3.6 References 123
4 Unravelling the Diet – Exercise – Microbiome – Metabolome Paradigm 129

4.1 Introduction 129

[Study 1] **A longitudinal trial of diet and exercise's effect on the metabolic phenotype ..131**

4.2 Introduction 131

4.3 Materials and Methods 131

4.3.1 Study population 131

4.3.2 Study Intervention 133

4.3.3 Study Measurements 134

4.3.4 ^{1}H-NMR and LC-MS profiling and SCFA quantitative analysis 134

4.3.5 Metabolite Quantification 134

4.3.6 Statistical Analysis 135

4.4 Results 136

4.4.1 Clinical outcomes 136

4.4.2 ^{1}H-NMR spectroscopy of urine and faecal samples 137

4.4.3 UPLC-MS of urine and faecal samples 139

4.4.4 GC-MS of faecal samples before and after intervention 143

4.4.5 Targeted analysis of selected metabolites of interest 144

4.5 Discussion 145

4.5.1 Biological interpretation 145

4.5.2 Study limitations 147

4.6 Conclusion 147

[Study 2] **Application of an objective dietary healthiness measure to cluster patients according to diet and exercise levels 149**

4.7 Introduction 149

4.8 Materials and Methods 150

4.8.1 Study population 150

4.8.2 Acquisition of clinical exercise and dietary data 150

4.8.3 Gut microbiome analysis and metabolic profiling 150
4.8.4 Objective assessment of dietary intake 150
4.8.5 Statistical Analysis 151
4.8.6 Metabolite identification 152
4.8.7 Metabolite quantification 152
4.9 Results 153
4.9.1 Model generation through clustering of individuals into contrasting groups according to objective dietary healthiness scores and exercise levels. 153
4.9.2 Metabolic characterisation of athletes and sedentary controls stratified by predicted dietary healthiness. 154
4.9.3 Quantitative analysis of short chain fatty acids and organic acids in urine and faeces 160
4.9.4 Bacterial diversity 161
4.9.5 Diet – Gut microbiome – Gut metabolome – Host metabolome interactions .. 162
4.10 Discussion & Biological Interpretation 165
4.10.1 Metabolic phenotype associated with diet and exercise 165
4.10.2 Evidence of altered gut microbial – host co-metabolism 165
4.11 Conclusion 169
4.12 References 178
5 Longitudinal phenotyping of bariatric surgery patients 185
5.1 Introduction 185
5.1.1 Aims and objectives: 187
5.1.2 Preliminary work: 187
5.2 Methods 187
5.2.1 Recruitment 188
5.2.2 Confounding factors 188

5.2.3 Regulatory approvals 188
5.2.4 Clinical, Demographic and Dietary data collection 189
5.2.5 Sample collection 189
5.2.6 Metabolomic analysis 190
5.2.7 Faecal metagenome analysis 195
5.2.8 Statistical analysis 197
5.3 Results 198
5.3.1 Clinical findings after bariatric surgery 198
5.3.2 Dietary behaviour following bariatric surgery 201
5.3.3 Metabolic changes after bariatric surgery 204
5.3.4 Gut microbiome changes after bariatric surgery 230
5.3.5 Gut Microbiome – Host Metabonome Associations 234
5.4 Discussion 238
5.4.1 Clinical findings after bariatric surgery 238
5.4.2 Biological interpretation of metabolic and gut microbiome changes after bariatric surgery 239
5.5 Conclusion 246
5.6 References 247
6 Conclusion and Planned future work 256
6.1 Summary of findings 256
6.2 Impact on host physiology 258
6.3 Future work 259
6.4 References 261

List of Figures

Figure 1.5-1 PRISMA diagram of studies included in the systematic review 34

Figure 1.5-2 BA levels post metabolic procedures..... 36

Figure 1.5-3 The 'SLIMMER' effects. 46

Figure 1.7-1 Overview of experimental design used throughout studies within this thesis... 53

Figure 2.4-1 Example of OPLS-DA correlation coefficient plot. 81

Figure 2.5-1 J-RESolved Spectrum (JRES) 83

Figure 2.5-2 ^{1}H-^{1}H COrrelation SpectroscopY (COSY) 84

Figure 2.5-3 Valerate structure..... 85

Figure 2.5-4 ^{1}H-^{13}C Hetero-nuclear Single Quantum Coherence (HSQC)..... 86

Figure 2.5-5 MS/MS spectrum (positive ionisation mode) of acetylcarnitine (C2)..... 88

Figure 2.5-6 MS/MS spectrum (negative ionisation mode) of CMPF-glucuronide 88

Figure 2.5-7 MS/MS spectrum (negative ionisation mode) of CMPF..... 89

Figure 2.5-8 Chemical reference spiking..... 90

Figure 3.3-1 Dietary intake of Athletes (black) Vs Controls (greeen)..... 107

Figure 3.3-2 PCA scores plots of ^{1}H-NMR spectra..... 108

Figure 3.3-3 Cross validated OPLS-DA scores plots of ^{1}H-NMR spectra..... 109

Figure 3.3-4 PCA scores plots of LC-MS analysis..... 112

Figure 3.3-5 Cross validated OPLS-DA scores plots of LC-MS analysis..... 113

Figure 3.3-6 Median short-chain fatty acid levels in faecal samples of athletes 116

Figure 3.3-7 Heat map of bacterial taxa (family / genus level) that correlate with faecal short-chain fatty acid levels..... 118

Figure 4.3-1 Illustration of semi-quantification using an in-house Matlab script..... 135

Figure 4.4-1 PCA scores plots of ^{1}H-NMR spectra..... 138

Figure 4.4-2 Paired MCCV-PLS-DA scores plots of ^{1}H-NMR analysis 139

Figure 4.4-3 PCA scores plots of LC-MS analysis 140

Figure 4.4-4 Paired MCCV-PLS-DA scores plots of UPLC-MS analysis 142

Figure 4.4-5 Paired MCCV-PLS-DA scores plots of UPLC-MS analysis 143

Figure 4.4-6 Change in faecal SCFA concentrations after intervention with Exercise, Exercise & High Protein Diet or High Protein Diet alone. 144

Figure 4.9-1 Clustering of individuals according to exercise status and predicted adherence to healthy dietary habits, calculated from urinary ^{1}H-NMR spectra of individuals..... 153

Figure 4.9-2 ^{1}H-NMR, SCFA and bacterial diversity results 161

Figure 4.9-3 Linear regression of faecal water ^{1}H-NMR spectra against bacterial diversity (Shannon index), corrected for confounding factors (age, lean mass and fat mass)..... 162

Figure 4.9-4 Faecal – Urinary metabolic interactions 163

Figure 4.9-5 Microbial – Metabolic Superpathway – Metabolite interactions 164

Figure 4.11-1 Diet – Metabolite correlations..... 171

Figure 4.11-2 Gut Species - Metabolite correlations 173

Figure 4.11-3 Metagenome Superpathway – Diversity Indices correlations 175

Figure 4.11-4 Faecal – Faecal Metabolite correlations 176

Figure 4.11-5 Urine – Urine Metabolite correlations..... 177

Figure 5.3-1 Weight loss following VSG and RYGB procedures. 200

Figure 5.3-2 Dietary intake Pre (blue) and Post (green) bariatric surgery. 202

Figure 5.3-3 Dietary intake Pre (blue) and Post (green) RYGB or VSG surgery. 203

Figure 5.3-4 Alternative Healthy Eating Index 2010 (AHEI) scores Pre and Post bariatric surgery 204

Figure 5.3-5 Serum bile acid profile changes following bariatric surgery. 205

Figure 5.3-6 Faecal bile acid profile changes following bariatric surgery. 206

Figure 5.3-7 PCA scores plots of ^{1}H-NMR analysis 217

Figure 5.3-8 PCA scores plots of ^{1}H-NMR analysis 218

Figure 5.3-9 PCA scores plots of ^{1}H-NMR analysis 219

Figure 5.3-10 Serum ^{1}H-NMR paired MCCV-PLS-DA analysis..... 221

Figure 5.3-11 Serum ^{1}H-NMR paired MCCV-PLS-DA subgroup analysis. 222

Figure 5.3-12 Urine ^{1}H-NMR paired MCCV-PLS-DA analysis. 224

Figure 5.3-13 Urine ^{1}H-NMR paired MCCV-PLS-DA subgroup analysis. 225

Figure 5.3-14 Faecal ^{1}H-NMR paired MCCV-PLS-DA analysis. 227

Figure 5.3-15 Faecal ^{1}H-NMR paired MCCV-PLS-DA subgroup analysis. 228

Figure 5.3-16 Phylogenetic tree of differentially abundant taxa post bariatric surgery. 231

Figure 5.3-17 Phylogenetic tree of differentially abundant taxa post RYGB surgery..... 232

Figure 5.3-18 Phylogenetic tree of differentially abundant taxa post VSG surgery. 233

Figure 5.3-19 Gut Species – Bile acid correlations 234

Figure 5.3-20 Gut Species – Faecal SCFA correlations 235

Figure 5.3-21 Gut Species – Serum Amino Acid correlations..... 236

Figure 5.3-22 Gut Species – Serum Acylcarnitine correlations 237

Figure 6.1-1 Summary of findings. 257

List of Tables

Table 2.1-1 Advantages and Disadvantages of Mass Spectrometry versus NMR Spectroscopy 73

Table 2.5-1 HSQC values for ^{1}H and ^{13}C derived from Figure 2.5-4. 87

Table 3.3-1 Summary table of demographic and anthropometric results..... 106

Table 3.3-2 List of significantly associated metabolites whose excretion discriminates between athletes and controls when using ^{1}H-NMR metabolic profiling..... 110

Table 3.3-3 List of significantly associated metabolites whose excretion discriminates between athletes and controls when using LC-MS metabolic profiling models..... 114

Table 3.3-4 Urinary SCFA concentrations (μM) in Athletes Vs Controls. 117

Table 4.3-1 Study inclusion / exclusion criteria 133

Table 4.4-1 Baseline demographic, anthropometric and IPAQ activity measures..... 136

Table 4.9-1 Urinary metabolites discriminating between classes. 157

Table 4.9-2 Faecal metabolites discriminating between classes 160

Table 5.2-1 GC-MS/MS machine settings for targeted SCFA analysis..... 193

Table 5.3-1 Baseline demographics of collected serum samples. 199

Table 5.3-2 Baseline demographics of complete serum, 24hr urine and stool sample sets. 199

Table 5.3-3 Serum SCFA changes after bariatric surgery. 207

Table 5.3-4 Serum SCFA changes after RYGB or VSG surgery. 207

Table 5.3-5 Urine SCFA changes after bariatric surgery..... 208

Table 5.3-6 Urine SCFA changes after RYGB and VSG surgery. 209

Table 5.3-7 Faecal SCFA changes after bariatric surgery. 210

Table 5.3-8 Faecal SCFA changes after RYGB and VSG surgery..... 210

Table 5.3-9 Serum amino acids and sugar levels pre and post bariatric surgery. 212

Table 5.3-10 Serum amino acids and sugar levels pre and post RYGB or VSG surgery..... 213

Table 5.3-11 Serum acylcarnitine levels pre and post bariatric surgery. 214

Table 5.3-12 Serum acylcarnitine levels pre and post RYGB or VSG surgery. 215

Table 5.3-13 Serum metabolites discriminating between classes. 223

Table 5.3-14 Urinary metabolites discriminating between classes. 226

Table 5.3-15 Faecal metabolites discriminating between classes. 229

Abbreviations

- ***^{13}C-NMR: ^{13}Carbon – Nuclear Magnetic Resonance spectroscopy***
- ***^{1}H-NMR: ^{1}Hydrogen – Nuclear Magnetic Resonance spectroscopy***
- ***3IS: 3 Indoxyl Sulfate***
- ***AAA: Aromatic Amino Acid***
- ***ACC2: Acetyl Coenzyme A Carboxylase 2***
- ***ACN: Acetonitrile***
- ***BA: Bile Acid***
- ***BCAA: Branched Chain Amino Acid***
- ***BCKA: Branched Chain KetoAcids***
- ***BH: Benjamini-Hochberg false discovery rate***
- ***BMI: Body Mass Index***
- ***BWA: Burrows-Wheeler Alignment***
- ***CA: Cholic Acid***
- ***cAMP: Cyclic Adenosine MonoPhosphate***
- ***CDCA: ChenoDeoxyCholic Acid***
- ***CKK: Cholecystokinin***
- ***COSY: ^{1}H-^{1}H COrrelation SpectroscopY***
- ***CPT1: Carnitine Palmitoyl Transferase 1***
- ***CV: Cross-Validated***
- ***DCA: DeoxyCholic Acid***
- ***DDBJ: DNA DataBank of Japan***
- ***DIO2: Deiodinase 2***
- ***DMA: DiMethylAmine***
- ***DNA: DeoxyriboNucleic Acid***
- ***DPP-4: DiPeptidyl Peptidase 4***
- ***EMBL: European Molecular Biology Laboratory***

- *ER: Endoplasmic Reticulum*
- *FFQ: Food Frequency Questionnaire*
- *FGF-19: Fibroblast Growth Factor 19*
- *FID: Free Induction Decay*
- *FXR: Farnesoid X Receptor*
- *GC: Gas Chromatography*
- *GCA: GlycoCholic Acid*
- *GCDCS: GlycoChenoDeoxyCholate Sulfate*
- *GDCA: GlycoDeoxyCholic Acid*
- *GenBank: Genetic sequence database of the National Institutes of Health*
- *GIP: Gastric Inhibitory Polypeptide*
- *GLCA: GlycoLithoCholic Acid*
- *GLP-1: Glucagon-Like Peptide-1*
- *GPR: G-Protein coupled Receptor*
- *GUDCA: GlycoUrsoDeoxyCholic Acid*
- *GUDCS: GlycoUrsoDeoxyCholate Sulfate*
- *HDCA: HyoDeoxyCholic Acid*
- *HILIC: Hydrophilic Interaction Liquid Chromatography*
- *HMBC: ^{1}H-^{13}C Hetero-nuclear Multiple-Bond Correlation spectroscopy*
- *HPA: 3-HydroxyPhenylAcetate*
- *HPHPA: 3-(3-HydroxyPhenyl)-3-HydroxyPropionic Acid*
- *HSQC: ^{1}H-^{13}C Hetero-nuclear Single Quantum Coherence spectroscopy*
- *IDO: Indoleamine 2,3-DiOxygenase*
- *IL: InterLeukin*
- *IQR: Inter Quartile Range*
- *IS: Internal Standard*
- *IT: Ileal Transposition*
- *JRES: J-REsolved Spectroscopy*

- *LAGB: Laparoscopic Adjustable Gastric Band*
- *LC: Liquid Chromatography*
- *LCA: LithoCholic Acid*
- *LDL: Low Density Lipoprotein*
- *LoA: Level of Assignment*
- *LSG: Laparoscopic Sleeve Gastrectomy*
- *MAPK: Mitogen-Activated Protein Kinase*
- *MCA: MuroCholic Acid.*
- *MCCV: Monte-Carlo Cross-Validation*
- *MeSH: Medical Subject Headings*
- *MetaPhlAn: Metagenomic Phylogenetic Analysis*
- *MGB: Mini Gastric Bypass*
- *MS: Mass Spectrometry*
- *MVDA: MultiVariate Data Analysis*
- *NASH: Non-Alcoholic SteatoHepatosis*
- *NGS: Next Generation Sequencing*
- *OGTT: Oral Glucose Tolerance Test*
- *OPLS-DA: Orthogonal Partial Least Squares – Discriminant Analysis*
- *OSA: Obstructive Sleep Apnoea*
- *PAG: PhenylAcetylGlutamine*
- *PCA: Principal Component Analysis*
- *PEG: PolyEthylene Glycol*
- *pFDR: p-value corrected for multiple testing using the Benjamini-Hochberg false discovery rate method*
- *ppm: Parts Per Million*
- *PYY: Peptide YY*
- *Q: Quadrupole mass spectrometer*
- *QC: Quality Control*
- *qPCR: Quantitative real-time Polymerase Chain Reaction*

- ***QQQ: Triple Quadrapole mass spectrometer***
- ***RP: Reversed Phase chromatography***
- ***rRNA: Ribosomal RiboNucleic Acid***
- ***RYGB: Roux-en-Y Gastric Bypass***
- ***SCFA: Short Chain Fatty Acid***
- ***SIM: Selected Ion Monitoring***
- ***STOCSY: Statistical TOtal Correlation SpectroscopY***
- ***STORM: SubseT Optimization by Reference Matching***
- ***T2DM: Type 2 Diabetes Mellitus***
- ***TCA: TauroCholic Acid***
- ***TCDCA: TauroChenoDeoxyCholic Acid***
- ***TDCA: TauroDeoxyCholic Acid***
- ***TGR5: G protein-coupled bile acid receptor 1***
- ***TLCA: TauroLithoCholic Acid***
- ***TMA: TriMethylAmine***
- ***TMAO: TriMethylAmine-N-Oxide***
- ***TNF-α: Tumour Necrosis Factor alpha***
- ***TOCSY: ^{1}H-^{1}H TOtal Correlation SpectroscopY***
- ***TOF: Time Of Flight mass spectrometer***
- ***TSH: Thyroid-Stimulating Hormone***
- ***TSP: 3-(TrimethylSilyl)-[2,2,3,3,-$^{2}H_4$]-Propionic acid***
- ***TUDCA: TauroUrsoDeoxyCholic acid***
- ***UDCA: UrsoDeoxyCholic Acid***
- ***UPLC-MS: Ultra Performance Liquid Chromatography – Mass Spectrometry***
- ***UV: Unit Variance***
- ***VSG: Vertical Sleeve Gastrectomy***
- ***WHO: World Health Organization***

1 Introduction

1.1 The human metabolome

Metabonomics is defined as the 'quantitative measurement of the dynamic multiparametric metabolic response of living systems to pathophysiological stimuli or genetic modification'[1]. This focusses on understanding the systemic changes that occur in complex multicellular systems. The related field of metabolomics aims to characterise and quantify all the small molecules within complex biological samples, transformed in the process of metabolism[2].

Many molecules have previously been measured in living systems. However, advances in nuclear magnetic resonance spectroscopy (NMR) and mass spectrometry (MS) now allow large numbers (hundreds and thousands respectively) of metabolites to be measured simultaneously in a high throughput manner. Historically systems biology has employed a 'bottom up' approach to investigate interactions between genetics, proteins and metabolism in isolated cell types or conditions. This new approach allows a 'top down' integrated view of complex biological systems or organisms[2]. Furthermore, it enables measurement of not only the effects of the genome and proteome, but also of further influences on the end metabolic state of living systems such as the gut microbiome, diet, therapeutic drugs and lifestyle factors. Thus, while the study of genetics, transcriptomics and proteomics allows measurement of biological potential in a system, metabonomics allows a more accurate measurement of the global biochemical phenotype of a living system[3, 4].

Metabolome-wide association studies have now been used to identify novel relationships between metabolic profiles and disease states or disease risk. For example, blood pressure has been positively correlated with urinary alanine and an inversely correlated with urinary formate and hippurate[5]. Likewise, plasma levels of five branched-chain and aromatic acids have been shown to be highly significantly correlated with future development of diabetes[6]. Furthermore, metabonomics has enabled investigators to measure the effect of changes in the gut microbiome on host metabolism. For instance, *Faecalibacterium prausnitzii* levels have been associated with modulation of eight urinary metabolites[7]. Moreover, metabonomics has raised the prospect of not only measuring and understanding system wide changes, but also utilising pattern recognition to identify different metabotypes for personalisation of health

care[8]. For example, metabonomic analysis has been utilised to predict toxicity in patients with colorectal cancer treated with capecitabine[9].

1.2 The gut microbiome

The gut microbiome is defined as the collective genomes of the microbes (bacteria, bacteriophage, fungi, protozoa and viruses) that reside within the gastro-intestinal tract[10]. Historically, investigation of gut microbes has relied on the culture of organisms. This has limited studies to analysis of the minority of bacterial species that were able to be cultured, significantly limiting our understanding. The development of anaerobic glove boxes improved the ability to study anaerobic bacteria, the principal group within the gut[11]. In spite of this, it is estimated that 60-80% of gut bacteria have not been cultivated to date[12]. Hence, the introduction of culture-independent metagenomic sequencing technologies over the past decade has provided a paradigm shift in our ability to study the gut microbiome[13]. The gut microbiome has now been linked extensively with both healthy[14, 15] and disease states[16-20], including obesity[20-22], type 2 diabetes mellitus (T2DM)[23], liver disease[24], cardiovascular disease[25, 26], inflammatory bowel disease[27] and autoimmunity[28].

The microbiome therefore represents a potentially significant and novel therapeutic target in the treatment of many pathologies. For example, initial gut microbiome studies in obesity identified a phylum level compositional shift in obese mice, with a relative increase in the abundance of the *Firmicutes* and a proportional decrease in the *Bacteroidetes*[29]. This was confirmed in a human dietary intervention study, demonstrating that weight loss of obese individuals (BMI>30kg/m^2) was accompanied by an increase in the relative abundance of *Bacteroidetes*[22]. Although this finding has not been corroborated in all clinical trials[30], it has now been established that diet is the key modulator of the gut microbiome rather than obesity per se. Indeed, a high fat intake has a direct effect on the microbiota[31-33]. Certainly, a low bacterial richness is associated with increased adiposity, insulin resistance and dyslipidaemia[34] and dieting can modulate this effect[35].

Convincingly, the colonisation of germ free mice with the faecal microbiota of homozygous twin pairs discordant for obesity results in significantly greater increases in body mass and adiposity in mice receiving the faecal microbiota from the obese twin[36]. This may reflect the

fact that the microbiota of obese individuals are able to harvest more energy from the diet[20]. Similarly, it is possible to identify systematic differences in the microbiome of patients with T2DM based on metagenomic phenotyping of their gut microbiota[37]. Furthermore, insulin resistance in obese humans with metabolic syndrome can be improved by transplantation of a lean microbiota, suggesting a causal link between the gut microbiome and host glucose metabolism[38].

Moreover, the effects of bariatric procedures such as Roux-en-Y Gastric Bypass, including weight loss and improved diabetic control, seem to be modulated in part through changes to the gut microbiome. Gut microbial-host metabolic cross-talk has been demonstrated in experiments where the gut microbiota from RYGB treated mice transfected to non-operated germ-free mice lead to significant weight loss and decreased fat mass when compared to the transfer of gut microbiota from mice who had undergone sham surgery[39]. Nonetheless, the overwhelming disruption to the distal gut microbiome caused by bariatric surgery is only just being defined, as is its functional importance.

The effects of the gut microbiome on host factors such as adiposity, metabolism and inflammation are mediated through microbial-host crosstalk. Whereby a chemical superhighway of largely unknown signalling processes that involve many biochemical classes in multiple organs including the gut, liver, brain and the CNS, collectively set the host-microbiome metabolic axes in which the multiple bacterial genomes can sequentially modulate metabolic reactions[40]. A number of specific examples, which appear to be of fundamental importance in health and disease pathogenesis, are outlined below.

1.3 Gut microbiome – host metabonome co-metabolism

1.3.1 Short Chain Fatty Acids (SCFA)

SCFA are produced through the bacterial fermentation of dietary fibre and complex carbohydrates, that would otherwise remain undigested by the host. The most abundant SCFA are acetate (C2), propionate (C3) and butyrate (C4). In addition, valerate and the branched SCFAs isobutyrate, isovalerate and 2-methyl-butyrate are produced by gut bacteria in smaller quantities[41]. Butyrate is particularly important as an energy source for colonic epithelial

cells[42]. Propionate, along with remaining butyrate, is used predominantly by hepatocytes for gluconeogenesis and lipogenesis, while acetate is mainly utilised by myocytes.

In addition to their role as energy sources, SCFAs are now known to have additional important physiological roles. SCFAs regulate gene expression through binding G-protein coupled receptors GPR41 (FFAR3) and GPR43 (FFAR2)[43]. These receptors are expressed by a number of tissues including adipocytes, enteroendocrine cells, pancreatic islet cells and immune cells such as leukocytes, mononuclear cells and splenic tissue[44]. In mouse models of colitis, arthritis and asthma, GPR43 knockout exacerbates inflammation. While germ-free mice, which express little or no SCFAs, also have a similar dysregulation of their inflammatory response, indicating that these effects are microbiome dependent[45]. In addition, GPR43 knockout mice develop obesity, even on a normal diet. Whereas mice overexpressing GPR43 remain lean even on a high fat diet[46]. This is mediated through a GPR43 dependent increase in insulin sensitivity and suppression of insulin-mediated fat accumulation. Again, both $GPR43^{-/-}$ and $GPR43^{+/+}$ genotypes maintain a normal phenotype when raised under germ-free conditions, confirming that these effects are microbiome dependent[46]. Similar findings are also found in GPR41 knockout mice[47].

In further studies SCFAs have been associated with reduced appetite and weight loss through stimulating release of the anorectic gut hormones peptide YY (PYY) and glucagon like peptide-1 (GLP-1) from enteroendocrine L-cells[41, 48]. Furthermore, stimulation of GLP-1 secretion from L cells by SCFAs has been shown to improve insulin sensitivity[49]. In addition, SCFAs, predominantly butyrate, have been shown to modulate colonic gene expression via inhibition of histone deacetylase (HDAC)[50, 51]. This results in suppression of malignant transformation and stimulation of apoptosis in precancerous colonocytes[51]. Furthermore, HDAC suppression leads to both an increase in colonic T regulatory cells[52] and increased AP-1 signalling in intestinal epithelial cells resulting in reduced expression of inflammatory mediators such as TNF-α and IL-2[53]. Thus, reducing intestinal inflammation and its systemic effects.

1.3.2 Choline Metabolism

Choline is an important constituent of cell membranes. Its main source is via dietary phosphatidylcholine (lecithin) and free choline, found in high concentrations in foods such as eggs and red meat. If the dietary intake exceeds the absorption capacity of the small bowel,

choline is delivered to the large bowel. Here it undergoes transformation to trimethylamine (TMA) and dimethylamine (DMA) by the gut flora[54]. Similarly, L-carnitine, found in high concentrations in red meat, dairy products and some supplements, undergoes bacterial conversion to choline and subsequently to TMA and DMA within the large bowel[55, 56]. The majority of TMA is then absorbed into the portal circulation and converted to trimethylamie *N*-oxide (TMAO) by the hepatic enzyme flavin-containing mono-oxygenase-3 (FMO3). Alternatively, gut bacteria may also influence these pathways. Bacterial expression of TMA monooxygenase and TMA dehydrogenase convert TMA to TMAO and DMA respectively. While TMAO reductase, TMAO demethylase convert TMAO to TMA and DMA and respectively[57, 58]. To add further complexity, TMA and TMAO may also be ingested directly via the diet, predominantly through fish intake[59].

Circulating trimethylamine-*N*-Oxide (TMAO) is thought to predict cardiovascular disease and promote atherosclerosis, possibly through modulation of the BA pool, inhibition of macrophage reverse cholesterol transport and increased oxidative stress[26, 56, 60]. In addition, low levels of choline are associated with liver steatosis[24]. Altered gut microbiota can increase conversion of choline to methylamines, reducing the bioavailability of choline and mimicking theses effects, causing non-alcoholic fatty liver disease (NASH)[61, 62]. On the contrary, dietary fibre or intake of plant-based foods appears to inhibit these harmful activities, highlighting the importance of maintaining gut microbiome carbohydrate fermentation[60, 63].

However, the causative effect of cardiovascular disease from high TMAO is disputed and these results may be due to confounders such as reduced kidney function and poor metabolic control[64]. Furthermore, TMAO is present in high concentrations in the tissues of cold water-dwelling fish where it acts as an osmolyte antifreeze agent and is also found in high levels in the urine of Japanese populations whose diet contains a high portion of fish and who do not have high risk for cardiovascular disease[5]. Moreover, TMAO was recently found to protect against impaired glucose tolerance and reduce endoplasmic reticulum stress[65].

1.3.3 Bile Acids

5-10% of bile acids are biotransformed and degraded by intestinal bacteria during enterohepatic circulation. Bacteria normally carry out reductive metabolism, as opposed to humans or mammals which usually perform oxidative metabolism. Indeed, here this duty is

performed by anaerobic bacteria of the genera *Escherichia, Bacteroides*, *Clostridium*, *Lactobacillus* and *Eubacterium*[40, 66]. These microbiota are responsible for the deconjugation of glycine and taurine-conjugated bile acids to the respective unconjugated free bile acids, and then formation of the so-called secondary bile acids such as deoxycholate and lithocholate[67, 68], which in turn undergo reabsorption or secretion. Part of the bile acid pool is utilised as an energy source and completely degraded by various groups of aerobic bacteria, such as *Actinobacteria* and *Betaproteobacteria*.

As well as their role in the emulsification and digestion of fats, bile acids are now known to have a critical role in the modulation of metabolism and the gut-liver axis as well as acting as signalling molecules in other tissues and cells such as cardiomyocytes. This is through their role as signalling molecules via activation of farnesoid X nuclear receptor (FXR) and the transmembrane G protein-coupled receptor TGR5[69, 70]. These receptors are found within a number of organs including the gut, liver and brain and their activation has downstream effects on a number of important metabolic pathways including; lipid and cholesterol metabolism, incretins and glucose homeostasis and energy metabolism[71].

Germ-free and antibiotic treated animals have major changes in bile acid signatures, particularly an increase in the proportion of taurine conjugated bile acids, in multiple body compartments resulting in greatly altered hepatic gene expression patterns with multiple transcript level changes in the cholesterol, steroid and bile acid synthesis pathways[72]. Further, as discussed above, the colonisation of germ free mice with the faecal microbiota of twin pairs discordant for obesity resulted in significantly greater increases in body mass and adiposity in mice receiving the faecal microbiota from the obese twin[36]. Lean mice had higher levels of *Bacteroidetes* and subsequent microbial transformation of their bile acid composition. This altered bile acid composition correlated with altered FXR signalling and was postulated to be a further mechanism contributing to the changes in adiposity in addition to changes in energy harvest[36].

The role of altered bile acid signalling in reducing the metabolic complications of obesity after bariatric surgery is reviewed in detail below[71].

1.4 Obesity & Bariatric Surgery

The World Health Organization (WHO) estimates that 11% of the world's population is obese and the prevalence continues to rise[73]. This global obesity pandemic is having a dramatic impact on the rise of associated chronic disease states such as T2DM, cardiovascular disease and cancer which in turn carry a significant global health and economic burden[73]. Thus, there is an urgent need for effective preventative and therapeutic strategies for treatment of obesity. Disappointingly, the encouragement of lifestyle changes such as improved diet and increased exercise together with pharmacological therapies have predominantly proved ineffectual thus far[74]. Hence surgical procedures have been developed to achieve more sustainable weight loss and are currently the gold standard treatment for morbid obesity. The procedures were originally designed to cause weight loss through gastric restriction and / or malabsorption. Yet, in addition to weight loss they have also been found to be successful in the resolution of T2DM[75-79], heart disease[80], sleep apnoea[81] and in reducing the risk of certain cancers[82]. Interestingly maternal bariatric surgery also appears to confer weight and metabolic improvements to offspring in animal models[83]. Due to these metabolic effects the procedures are termed as 'metabolic' surgery.

The metabolic outcomes are achieved through weight-dependent and weight-independent mechanisms. Indeed, many of the metabolic effects are seen before weight loss has occurred. The most commonly performed metabolic procedure, the Roux-en-Y gastric bypass (RYGB), is thought to achieve its physiological effects through the so-called BRAVE mechanisms (**B**ile flow alteration, **R**eduction of gastric size, **A**natomical gut rearrangement and altered flow of nutrients, **V**agal manipulation and **E**nteric gut hormone modulation)[84].

1.5 Systematic Review of the role of bile acid co-metabolism in the metabolic effects of bariatric surgery

The following review is adapted from the published article[71]: Penney NC, Kinross J, Newton RC, Purkayastha S. The role of bile acids in reducing the metabolic complications of obesity after bariatric surgery: a systematic review. International journal of obesity. 2015;39(11):1565-74.

1.5.1 Introduction

Of the proposed mechanisms discussed above, altered bile acid (BA) metabolism is of critical importance. Certainly, many of the beneficial metabolic effects seen following RYGB are reproduced in rats by simply diverting bile from the common bile duct to the mid to distal jejunum via a catheter[85]. After RYGB surgery, increased volumes of digestate-free BAs are delivered to the distal gut, with increased hepatic flux / enterohepatic circulation, increased plasma BA levels (with altered composition) and subsequent normalisation of the blunted postprandial plasma BA concentration rise seen in obesity[86-88]. However, the impact of 'diversional' surgery on bile metabolism is subtle and highly complex, and BAs exert a systems wide influence on human metabolism in their role as potent small molecular signalling molecules[86, 89-91]. The term 'bile flow alteration' therefore most likely represents a gross over simplification of this critical pathway. In fact, a significant gut-liver axis exists, driven through BA signalling, which is critical in establishing the metabolic complications of obesity and the metabolic response to surgery.

This systematic review therefore assesses the current understanding of the physiological mechanisms by which BAs modulate the metabolic effects seen following metabolic surgery. It explores the available scientific data in both human and animal studies, and provides a systems level overview of BAs role in the resolution of the metabolic phenotype after surgical intervention.

1.5.2 Methods

A systematic literature review was performed to identify all articles investigating the role of BAs in mediating the metabolic effects seen following bariatric surgery in both animal and human models. Embase and Medline databases were searched up to 1st May 2014. Boolean logic was used with search terms including 'bile acids', 'bariatric surgery', 'metabolic surgery', 'obesity surgery', 'gastric bypass', 'sleeve gastrectomy' and 'gastric band'. Controlled

vocabularies (e.g. Medical Subject Heading terms) were used to identify synonyms with the following MeSH terms used in the search: ‘bariatric surgery’, ‘obesity/surgery’, ‘metabolic surgery’, ‘gastrointestinal tract/surgery’, ‘biliopancreatic diversion’ and ‘bile acids and salts’.

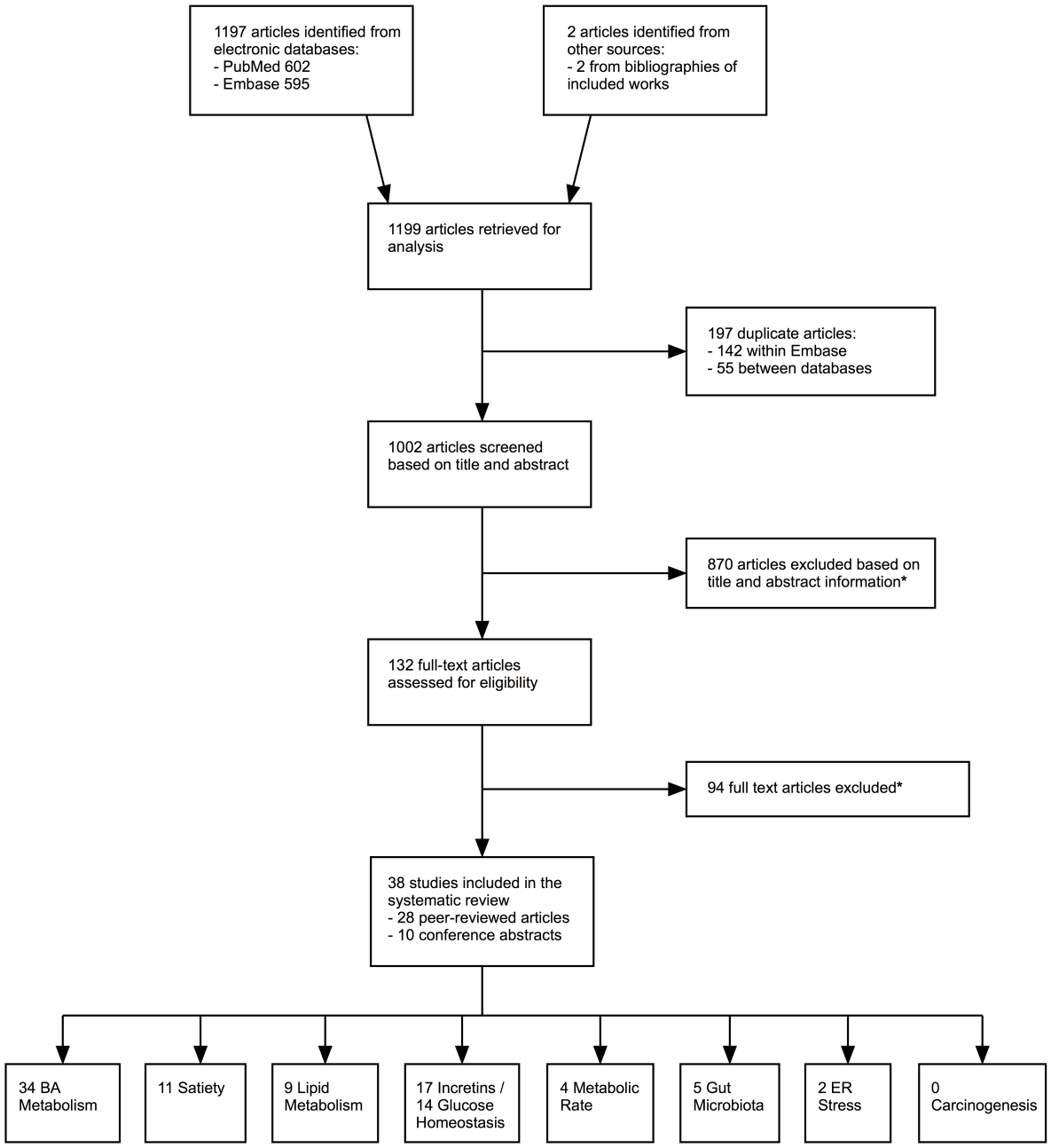
A first iteration search of titles and abstracts was performed to identify candidate articles. A further second iteration review of full text articles was then conducted as required. Additional studies were identified from bibliography searches of retrieved articles. Two researchers independently established study eligibility; any difference in opinion about eligibility was resolved by consensus with a third researcher. All original peer-reviewed articles and published conference abstracts assessing BAs after bariatric surgery, in both humans and animal models, were included in the systematic review. Non-English language articles, articles assessing BAs in vitro or after non-bariatric operations, articles assessing bariatric surgery outcomes without analysis of BAs and articles assessing BA levels in stool only after bariatric surgery were excluded.

1.5.3 Results and discussion

Following database searches (n=1197), inclusion from bibliography searches (n=2) and de-duplication (n=197), 1002 search results were returned. Of these, 132 articles were selected for full-text review of which 38 articles were deemed relevant (see Figure 1.5-1). Evidence was divided into the following domains:

- ***Bile acid metabolism***
- ***Satiety hormones***
- ***Lipid and cholesterol metabolism***
- ***Incretins and glucose homeostasis***
- ***Energy Metabolism***
- ***Gut Microbiota***
- ***ER stress***
- ***Carcinogenesis***

Some articles were relevant to multiple domains.



* Articles assessing BAs in vitro or after non-bariatric operations (n=342), assessing bariatric surgery outcomes but not BAs or assessing BA levels in stool only after bariatric surgery (n=48), not assessing bariatric procedures or BAs (n=302), reviews or editorials (n=248), foreign language articles (n=14) and conference abstracts subsequently included as full articles (n=10), were excluded.

Figure 1.5-1 PRISMA diagram of studies included in the systematic review

Next, secondary searches were conducted in each of the above domains to identify supporting articles that did not directly investigate both BAs and bariatric surgery and hence would not have been identified in the primary search. Further MeSH terms used in addition to the above, again with Boolean logic, included; 'obesity/microbiology', 'gastrointestinal

tract/microbiology', 'microbiota', 'intestines/microbiology', 'metagenome', 'gastrointestinal hormones', 'peptide hormones', 'lipids', 'incretins', 'oxidative stress', 'energy metabolism' and 'thyroid hormones/metabolism'.

Many of the human studies included had low patient numbers (n<10) and lacked proper randomization. Moreover, many of the findings in rats have yet to be proven in humans. Additionally, because of the complexities of studying biliary metabolism in vivo, some studies were unable fully isolate the effects of BAs from that of other physiological confounders such as the increased delivery of fatty acids and other nutrients to the distal ileum after bypass surgery. Therefore, due to the heterogeneity of existing evidence, the results from this review have been structured as a narrative covering each of the above domains with an analysis of the data synthesis provided in each section accordingly.

1.5.4 Bile Acid Metabolism

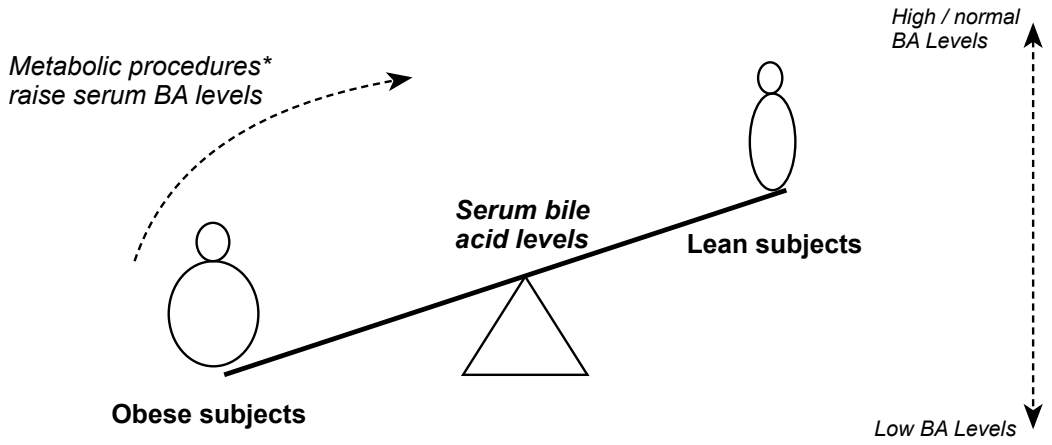
Regulation of BA metabolism involves a number of different pathways. BAs are the main ligands of the Farnesoid X Factor nuclear receptor (FXR, NRIH4)[92-94]. Activation of FXR results in expression of small heterodimer partner 1 (SHP-1), which in turn binds and inhibits liver receptor homolog 1 (LRH-1)[95, 96] and liver X receptor alpha (LXRα)[97]. This results in decreased transcription of cholesterol 7 α-hydroxylase (CYP7A1) within hepatocytes, the rate limiting enzyme in BA biosynthesis from cholesterol. SHP-1 has also been shown to inhibit hepatocyte nuclear factor 4 (HNF4)[98] resulting in decreased CYP8B1 activity, a key enzyme in the control of the CA to CDCA ratio and thus the hydrophobicity of the BA pool[99]. In addition, FXR induces secretion of fibroblast growth factor-19 (FGF-19) from enterocytes, which binds cell-surface FGF receptor 4 (FGFR4) on hepatocytes to induce an alternate pathway suppressing CYP7A1[100-102] in a SHP dependent manner[103].

Many bariatric procedures appear to disrupt the enterohepatic circulation and cause changes to BA homeostasis. In animal[104-107] and human[86-88, 90, 108-115] studies of RYGB, fasting and postprandial levels of plasma BAs were elevated relative to low pre-operative levels and weight-matched controls. Additionally, vertical sleeve gastrectomy (VSG) in animals[70, 116-120] and humans[110] results in elevated plasma BA levels. Although some groups did not find elevated plasma BA levels in humans following VSG[121-123], they did show raised FGF-19 levels[122, 123] and convincingly FXR-null mice had significantly reduced weight loss and glucose

tolerance after VSG compared to wild-type mice implicating the role of altered BA metabolism[70]. Plasma BA levels are also increased after ileal transposition (IT) surgery[89, 124-126] and more recently, the use of duodenal-endoluminal sleeve for the treatment of obesity and diabetes in humans was found to causes an elevation of plasma BA levels[127] (see Figure 1.5-2).

Further, not only does the plasma BA level rise, but the sub fraction composition of the BA pool also changes. Glycine and taurine-conjugated BAs[87, 88, 108], cholic and deoxycholic acid[111] have all been found to increase relative to total BA levels at time points between 5 months and 4 years following RYGB in humans. But, this change is not entirely consistent as a separate study in humans 1 year post RYGB found increases in cholic acid, deoxycholic acid and glycine-conjugated BAs but a decrease in taurine-conjugated BAs[112].

Similarly, IT studies in rats result in raised plasma primary BAs, such as cholic acid[124, 125], with one study showing increased plasma taurine and glycine-conjugated BAs[89] and another showing reduced taurine-conjugated BA levels[124]. Additionally, IT rats have reduced BA levels in the proximal intestinal tract, suggesting an early and efficient reabsorption of BAs[89, 124]. Again the systematic review suggests that there was variability in the sub fraction composition of the BA pool, with one study showing a reduction in primary BAs[89] and another showing elevated primary BAs[124] in the proximal intestine following IT.



* Including; Roux-en-Y gastric bypass (RYGB), Vertical sleeve gastrectomy (VSG), Duodenal endoluminal sleeve (DES), Biliopancreatic diversion (BPD) & Ileal interposition (IT). Raised serum BA levels seen in fasting and post-prandial states.

Figure 1.5-2 BA levels post metabolic procedures

1.5.4.1 Lipid Metabolism

The enterohepatic circulation is highly efficient at retaining BAs; the fractional turnover rates of chenodeoxycholic acid (CDCA) and cholic acid (CA) are calculated to be 0.25 and 0.5 per day respectively[128]. Nonetheless, the resulting faecal loss is balanced by new BA production from cholesterol. This is a major source of cholesterol elimination, accounting for approximately 400mg of excretion per day[129]. Hence BA metabolism is integrally linked to cholesterol homeostasis[92]. For example, disruption of the enterohepatic circulation of BAs using ileal apical sodium co-dependent BA transporter (ASBT) inhibitor therapy causes a significant reduction in plasma cholesterol concentrations and attenuated the progression of atherosclerosis in guinea pigs[130].

As expected, bariatric surgery has a significant impact on lipid metabolism. A recent meta-analysis of the metabolic effects of bariatric surgery found a significant improvement in triglyceride, total cholesterol and LDL levels and a trend towards increased HDL levels when measured at 6 months and up to 10 years post procedure[131]. Recent studies have suggested weight-independent improvements in fasting and post-prandial lipid levels that occurred as soon as 2 weeks after surgery in one study[132-134]. Following RYGB in humans hepatic fat content is decreased within three months[113] and total plasma BA levels were shown to negatively correlate with triglyceride levels[87]. Liver triglyceride levels were also negatively correlated with change in weight and total BA levels following VSG in mice[116, 118]. A similar effect was seen in rats treated with IT, which exhibited lower adiposity, smaller adipocyte size, 25% less ectopic lipid deposition and lower circulating lipids than sham controls despite comparable body weight[126]. Improvement in plasma lipids following VSG in rats was weight independent[120].

BAs are implicated in this process through a variety of molecular signalling pathways. Further to their role regulating CYP7A1, LRH-1 and LXRα induce expression of SREBP1-c[135, 136], a transcription factor that regulates fatty acid and triglyceride synthesis and controls the expression of several genes related to lipogenesis[137]. Hence FXR / SHP mediated inhibition of LRH-1 and LXRα is thought to inhibit lipogenesis[138]. In keeping, SHP levels have been found to be inversely correlated with triglyceride levels in several studies[138]. Additionally, FXR has been shown to induce apolipoprotein C-II (apoC-II)[139, 140] and apoA-V[141] expression, both co-activators of lipoprotein lipase, which acts to lowers serum triglycerides. FXR activation also

reduces expression of apoC-III, an inhibitor of lipoprotein lipase activity[142]. PPARα is another transcription factor, activated by fatty acids, involved in lipid, lipoprotein, and fatty acid metabolism[143]. This pathway is targeted by fibrates to lower lipid levels[144]. PPARα is also involved in modulating bile production and composition[145]. Cross talk between the FXR and PPAR signalling pathways occurs with BAs up-regulating PPARα expression via FXR[146]. Thus FXR is able to control fatty acid, triglyceride and BA metabolism both directly and indirectly[147].

Nevertheless, the changes seen in lipid metabolism following metabolic surgery are likely to be polymodal and isolating the effect of changes in the enterohepatic circulation of BAs on lipid levels has not yet been fully achieved. Furthermore, genomic analysis of FXR has revealed that hepatic transcriptional signalling is altered in obese mice[148] and that genetic variations in FXR contribute to fasting glucose and free fatty acid levels in humans independent of body fat levels[149].

1.5.4.2 Incretins & Glucose Homeostasis

Enteric glucose administration has been shown to have a greater insulinotropic effect than equivalent parenteral administration of glucose. This glucoregulatory role of the gut is known as the 'incretin effect'. The primary mediators are glucagon-like peptide-1 (GLP-1)[150] secreted from L-cells found primarily in the ileum and colon and gastric inhibitory polypeptide (GIP) secreted from K-cells found predominantly in the duodenum and proximal jejunum[151]. GLP-1 and GIP both have a glucose-dependent insulinotropic effect on β cells in the pancreas. GLP-1 has additional anti-diabetic effects including; inhibition of glucagon secretion, reducing gastrointestinal motility and gastric emptying and decreased appetite and food intake[151, 152]. In clinical practice GLP-1 agonists such as liraglutide have been successful in improving glycaemic control, diabetic complications including cardiovascular and renal outcomes and ultimately reducing all-cause mortality in patients with T2DM[153-156]. The secretion of these peptides is stimulated by the arrival of glucose and other macronutrients such as carbohydrates, amino acids and lipids into the intestine. Additionally, BAs have been shown to directly induce incretin secretion[157].

BAs promote GLP-1 and GLP-2 secretion in enteroendocrine cells through the G protein-coupled receptor, TGR5 (GPBAR1). This was shown to be dose dependent via increased intracellular cAMP production in the STC-1[158] and GLUTag cell lines, modelling L-cells[159].

Additionally, BAs were found to have a synergistic effect with glucose on GLP-1 and GLP-2 secretion[159]. Furthermore, in vivo, increased delivery of bile to the distal ileum after duodenal transposition (segment of duodenum containing the hepatopancreatic ampulla transposed 10cm proximal to the caecum), where L-cells occur in greater density and express higher levels of TGR5, resulted in a two fold increase in fasting GLP-2 plasma levels compared with sham-operated controls[159]. Recently Kohli et al[85] diverted BA to the distal jejunum without altering the small bowel anatomy using a catheter inserted into the common bile duct. Rats that underwent biliary diversion again had higher postprandial GLP-1 response in addition to improved glucose tolerance and less fat mass[85]. In obese, type 2 diabetic humans, rectal administration of the BA taurocholate resulted in a dose dependent increase in GLP-1 and insulin and a resulting decrease in plasma glucose levels[160].

RYGB bypasses the foregut and accelerates intestinal transit time. In humans it has been associated with increased GLP-1 levels[108, 109, 114, 161-163], with an associated increase in insulin secretion[164]. Indeed, in a study using GLP-1 antagonist exendin 9–39 after RYGB the expected increase in post-prandial insulin release was prevented[165]. Dipeptidyl peptidase-4 (DPP-4) is an important enzyme in the breakdown of GLP-1 and GIP and has been found to decrease following RYGB[166]. However, the increased peak GLP-1 and GIP levels after RYGB did not correlate with DPP-4 levels and whether this contributes to improved glycaemic control is unclear[166]. Following RYGB increased BA concentrations have been show to positively correlate with peak GLP-1 levels[86, 87, 90] and fasting GIP levels[167]. This association between BA and GLP-1 levels has been demonstrated up to two years following RYGB[168]. A rise in BA levels associated with increased GLP-1 has also been seen following RYGB[104] and IT[89, 125] in rats.

Of clinical importance, a number of animal studies have also correlated the change in BA levels with improved glucose tolerance. In rats, IT delays the onset of diabetes and improves oral glucose tolerance testing (OGTT)[126]. A number of pathways involving BA have been proposed including selective activation of intestinal FXR and LXR[124], and amelioration of ER stress[125]. In addition to incretins, improvement in OGTT has also been correlated with change in BA levels following RYGB in humans[87, 167]. One group found higher FGF-19 and BA levels in patients who underwent diabetic-remission after RYGB compared to those who did not undergo remission following surgery, suggesting a role for the FGF19–CYP7A1–BA pathway in diabetes remission[111]. Indeed, administration of FGF-15 (FGF-19 in humans) to mice has previously

been shown to reverse diet-induced diabetes[169]. Increased FGF-19 and reduced insulin levels are also seen following laparoscopic sleeve gastrectomy (LSG) in humans[122].

Conversely, other studies have questioned the role of proximal gut bypass and hence increased BA delivery to the distal ileum, in enhancing GLP-1 secretion. For example, a variance of GLP-1 levels has been demonstrated at 1 and 2 years following surgery suggesting that additional mechanisms such as adaptation of the gut microbiota and gut mucosa may be involved in increasing GLP-1 secretion[164]. Other studies have reported increased GLP-1 and increased serum BA following bariatric surgery but these followed different patterns and there was no correlation[110]. However, it is possible that levels of individual BA subtypes may be more important than total levels. More convincingly, the blockade of GLP-1 in RYGB patients has demonstrated only a limited deterioration in glucose tolerance suggesting that the resolution of T2DM seen in these patients was due to other mechanisms[170]. A possible explanation for these findings is that the main effects of endogenously secreted GLP-1 are mediated through local activation of sensory afferent nerves[157], hence systemic administration of a GLP-1 antagonist may have limited effect and serum measurements of GLP-1 may not accurately represent local concentrations within the gut.

1.5.4.3 Satiety Hormones

Further to the incretin effect of GLP-1, along with other hormones such as peptide YY (PYY), it is also known to reduce appetite. PYY is secreted from L-cells and is found at higher concentrations in the distal colon[171] and BAs are also known to stimulate its secretion[172, 173]. This is mediated via the BA receptor TGR-5 on L-cells, primarily through systemic exposure to BAs[174]. There is also evidence for intraluminal stimulation. The rectal administration of the BA taurocholic acid induced a dose-dependent secretion of both GLP-1 and PYY and increased fullness in healthy male volunteers[175]. Rectal administration of taurocholate to obese, type 2 diabetic volunteers also increased GLP-1 and PYY and reduced food intake[160].

The attenuation of appetite following RYGB has been associated with corresponding increases in GLP-1 and PYY. The authors of one study found that patients with less weight loss and an increased appetite following RYGB had a reduced GLP-1 and PYY response[176]. The increase in GLP-1 and PYY following RYGB is associated with higher levels of glycine conjugated BAs and a subsequent increase in the post-prandial plasma BA response[90, 108]. BAs have also been

shown to inhibit secretion of the secretagogue and appetite suppressor cholecystokinin (CKK) from the I-cells in the duodenum[177]. Yet, CKK release is under constant suppression by BAs and cannot be further enhanced by the addition of more BAs. In contrast, removal of this inhibition leads to a dramatic increase in plasma CKK levels[178]. This duodenal exclusion after RYGB leads to elevated CKK levels[179].

It was recently shown that patients have markedly reduced brain-hedonistic responses following RYGB compared to restrictive surgery. This was associated with higher levels of BAs, GLP-1 and PYY in the RYGB group[109]. BAs are a potential mediator of this response and two pathways have been suggested[109]. Firstly, bioactive BAs are able to cross the blood-brain barrier[180] and the BA receptor TGR5 is present within the brain[181]. Secondly, as discussed above, FGF-19 increases following RYGB. Intracerebroventricular administration of FGF-19 reduced food intake and improved glycaemic control in rats. Intracerebroventricular administration of an FGF-receptor inhibitor induced the opposite effect[69]. In addition FGF-19 has been shown to act centrally to improve glucose effectiveness (insulin-independent glucose disposal)[182].

1.5.4.4 Energy Metabolism

Energy expenditure was increased after RYGB in obese rats when compared to sham operated controls[183, 184] and in obese humans 1 year after RYGB[185], although this was not seen at 3 weeks following RYGB[186]. Several groups have investigated the potential role of BAs in regulating metabolic rate. It is postulated that BAs binding to TGR5 induce cAMP and mitogen-activated protein kinase (MAPK) pathways, which lead to activation of intracellular type 2 thyroid hormone deiodinase (DIO2)[187]. DIO2 acts to converts T4 to the metabolically active T3[188]. In vivo this was shown to increase the metabolic rate of brown adipose tissue in mice and skeletal muscle in humans[187]. In one prospective study following RYGB in humans total serum BA concentrations were higher compared to obese controls. The total BA levels had a strong inverse correlation with thyroid-stimulating hormone (TSH)[87]. The authors speculated that the reduced TSH in this euthyroid patient group was due to increased conversion of T4 to T3 by D2 resulting in down-regulation of TSH[87]. Confirmatory results were found in another study comparing RYGB to laparoscopic adjustable gastric band (LAGB). Again, TSH levels negatively correlated with the rise in BA levels in the RYGB group[86]. Interestingly, there was also increased skeletal muscle expression of the mitochondrial TGR5 downstream elements,

COX IV and Kir6.2. Nevertheless, this was not associated with a change in resting energy expenditure[86]. Other human studies of RYGB surgery identified by the systematic review identified that fasting total BA levels were doubled, accompanied by a decrease in conjugated BAs[112]. The change in taurine-conjugated BAs negatively correlated with DIO2 mRNA expression in adipose tissue, which correlated negatively with the change in glucose oxidation and positively with the change in lipid oxidation[112]. Yet, there was no correlation between DIO2 mRNA levels and resting energy expenditure or TSH levels[112].

BAs are potent stimulators of the ileum-derived enterokine FGF-19, via FXR[189]. FGF-19, in combination with its obligatory co-receptor β-Klotho[190], binds cell surface FGF receptor 4 (FGFR4) exclusively[191], which is highly expressed in the liver[192]. FGF-19 (FGF-15 in mice) increases basal metabolic rate in mice[169, 193]. There is some evidence that this occurs through the increased delivery of fatty acids into the mitochondria, which subsequently undergo β-oxidation[193]. Carnitine palmitoyl transferase 1 (CPT1), the rate-limiting enzyme involved in the transport of fatty acid into the mitochondria[194], is down regulated by malonyl CoA that is in turn synthesized by acetyl coenzyme A carboxylase 2 (ACC2). Both FGF-19 transgenic mice and mice administered FGF-19 were shown to have reduced levels of ACC2, which in turn (through the mechanisms described above) leads to increased CPT1 and thus increased delivery of fatty acids to mitochondria for β-oxidation[169, 193]. There is good clinical evidence that FGF-19 levels increase following RYGB[90, 111, 113] although one group did not report a significant difference in FGF-19 levels after surgery[87]. Correlation between this and an increased metabolic rate following RYGB has not yet been investigated.

1.5.4.5 Endoplasmic Reticulum (ER) Stress

The BAs tauroursodeoxycholic acid[195] and cholic acid have been shown to reduce ER stress[125]. After IT surgery in a rat model, improvement in glucose tolerance and β-cell mass occurred alongside a reduction in ER stress signalling in hepatic, adipose and pancreatic tissues. BA plasma concentrations are increased following IT with a greater proportional increase in cholic acid. When hepatocytes, white adipocytes and β-cells were incubated with cholic acid in vitro they were protected against the development of ER stress. This suggests that the post-operative increase in circulating cholic acid ameliorates ER stress leading to preservation of β-cell mass and improved insulin sensitivity, in turn improving glucose homeostasis[125]. Reductions in ER stress have also recently been seen following bile diversion to the mid-distal

jejunum in rats[85]. Gavage of taurine-conjugated BA was shown to reduce hepatic steatosis and liver ER stress[85].

1.5.4.6 Gut Microbiota

Germ-free and antibiotic treated animals have greatly altered hepatic gene expression patterns with multiple transcript level changes in the cholesterol, steroid and BA synthesis pathways as well as major increases in conjugated (especially taurine conjugated) BA signatures in multiple body compartments[72]. BA altering micro-organisms have been found not only in the blind loop following RYGB but also the small intestine[196]. *Enterobacteria* cause biotransformation of the BA pool through deamination and 7α-dehydroxylation[197], resulting in increased unconjugated primary BAs and elevated levels of hydrophobic secondary BAs including cholic acid (CA) and taurodeoxycholic acid (TDCA) [198]. *Enterobacteria*-biotransformed BAs (CA & TDCA) cause reduced expression of the ileal apical sodium-dependent BA transporter (SLC10A2) through multiple pathways[198]. Hence a decrease in *Enterobacteria* has been associated with increased BA absorption[198]. The reduced SLC10A2 may be mediated via FXR/SHP[199] and FXR/FGF-19[200] signalling pathways, although further studies are needed to fully elucidate the mechanisms behind this[198]. Nevertheless, studies so far have shown an increase in *Gammaproteobacteria*[105, 201, 202], the class to which *Enterobacteria* belong, following RYGB. Therefore, the increase in BA levels seen after RYGB does not appear to be due to a decrease in *Enterobacteria* causing increased expression of the ileal BA transporter (SLC10A2). Additionally, *Enterobacteria*-mediated deconjugation of taurocholic acid (TCA) enhances ileal FXR signalling. Unconjugated CA has increased potency activating expression of ileal FXR target genes compared to TCA, and this effect is not seen in FXR-null mice[203]. Convincingly, the colonisation of germ free mice with the faecal microbiota of twin pairs discordant for obesity resulted in significantly greater increases in body mass and adiposity in mice receiving the faecal microbiota from the obese twin[36]. Lean mice had higher levels of *Bacteroidetes* and analysis of 37 BA species revealed microbial transformation of BA composition. This correlated with altered FXR signalling and was postulated to be a further mechanism contributing to the changes in adiposity in addition to changes in energy harvest[36].

BAs are also a key determinant of the changes seen in the gut microbiota in response to a high-fat diet[204, 205]. For example, the supplementary intake of CA supports higher levels of 7α-dehydroxylating bacteria, where as a reduction in BAs, as seen in liver cirrhosis, causes a

collapse in the levels of these bacteria[206, 207]. Following RYGB the gut microbiota undergoes significant changes in both rats and humans. The predominant changes include an increased richness of gut microbiota, increased *Proteobacteria*[105, 208] and decreased *Firmicutes*[105, 201, 202]. *Bacteroidetes* increase in human studies[201] but decrease in rat models[105] after RYGB. The factors causing these alterations following RYGB are wide ranging; surgery changes pH levels within the gastric remnant and proximal small bowel, restricts the amount and type of nutrients that can be comfortably consumed, affects gastrointestinal motility and ultimately causes weight loss all of which are likely to alter the gut microbiota[105, 202]. The alteration in bile flow and disruption of the enterohepatic circulation following RYGB is also likely to have fundamental effects on the composition of the gut microbiota and changes in the gut microbiota following RYGB mediate many of the metabolic effects seen via gut microbial-host metabolic cross-talk[105, 106, 168, 209]. The density of microbes increases markedly along the gastrointestinal tract, with 10^3-10^4 microbial cells/g faeces in the duodenum increasing to 10^8 in the ileum, increasing further to 10^{11} in the colon[210, 211]. However, transcriptional analysis found that the gut microbiota modulated the expression of a large number of genes in the small intestine and less genes in the colon suggesting that changes to the small intestine microbiome following bariatric surgery may have more relevance and should be studied further[212]. In keeping with this hypothesis there is also evidence that the choice of surgical approach plays a significant influence on the ecological disruption of the distal gut microbiome and in turn the enterohepatic circulation of BA. Changes to the gut microbiome are also seen following VSG[213]. In addition to reduced body fat and improved glucose tolerance, the relative abundance of *Bacteroides* was reduced after VSG in wild type compared to sham operated mice. However, gut microbiota, body fat and glucose tolerance did not significantly differ in FXR knockout mice after VSG[70]. This suggests that FXR signalling is important in mediating the beneficial effects of VSG, through its modulation by the gut microbiota.

Therefore, the gut microbiota mediate the obese phenotype and its metabolic complications in part through BA co-metabolism in the gut lumen, which in turn influences multiple signalling pathways involved in energy and lipid metabolism, leading to modifications to lipid peroxidation and hepatic fatty acids and triglyceride storage. Other numerous complex host-microbiome axes (such as the endocannabinoid system) are also involved[214]. Nevertheless gut

microbiome – bile acid metabolism represents a significant novel target for the treatment of obesity.

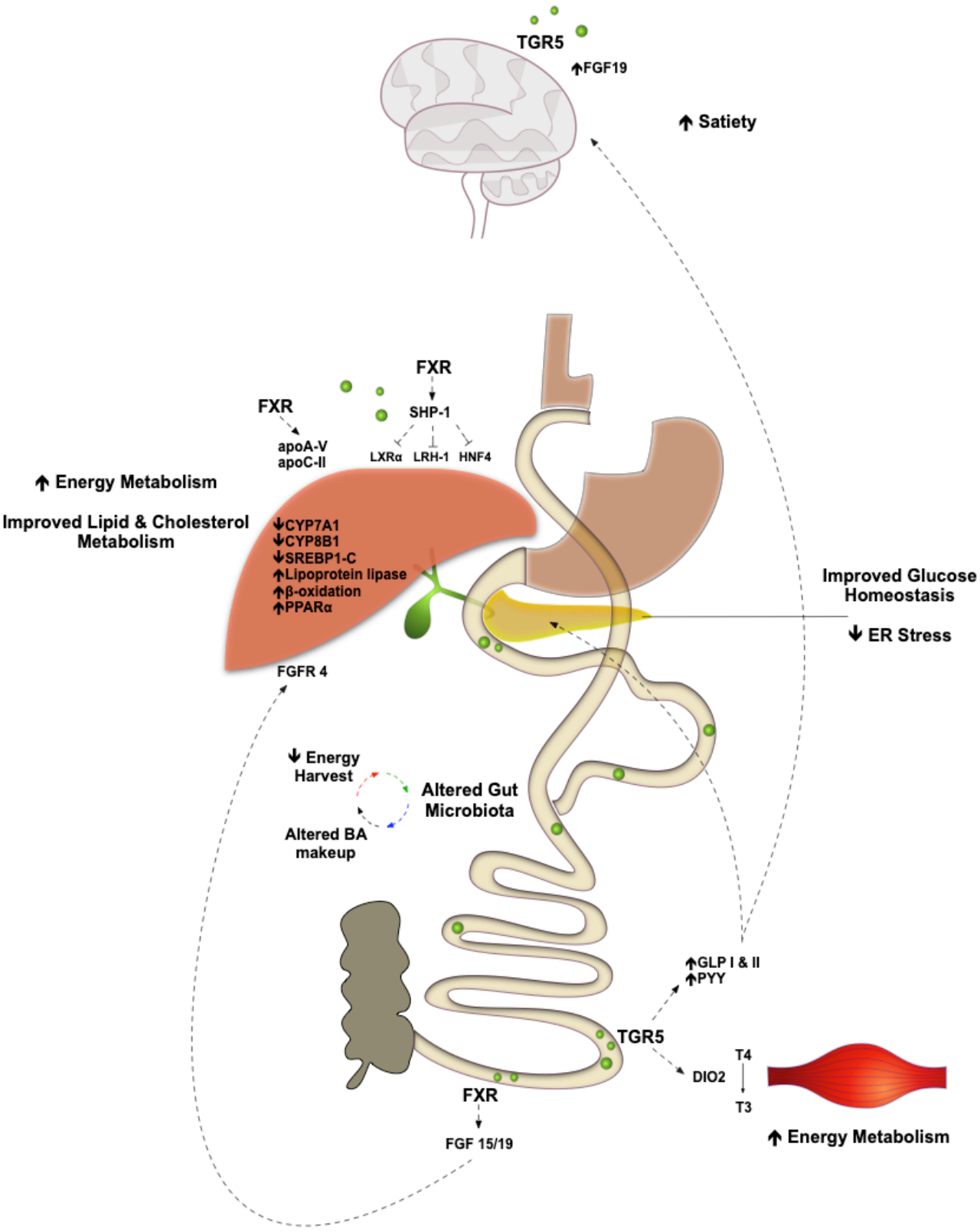


*Figure 1.5-3 The 'SLIMMER' effects. BAs mediate **S**atiety, **L**ipid and cholesterol metabolism, **I**ncretins and glucose homeostasis, energy **M**etabolism, gut **M**icrobiota and **E**ndoplasmic **R**eticulum stress through the downstream effects of their interactions with the FXR and TGR5 receptors.*

1.5.4.7 Carcinogenesis

Metabolic surgery is known to reduce the incidence of cancers overall. The largest effects are seen with female obesity-related tumours[215] and the mechanisms are thought to be both weight-dependent and weight-independent[82]. The mechanisms include reduced inflammation and oxidative stress and modulation of sex steroids, gut hormones and adipokines[82]. Conversely, there is a paradox in the oncological outcomes of patients undergoing bariatric surgical procedures, where epidemiological evidence suggests the risk of colorectal cancer in fact increases[216]. Evidence from mice models has also demonstrated that the faecal water post gastric bypass is highly genotoxic[217] suggesting that the relationship between obesity and colorectal cancer is modulated by the microbiome, and that surgical bariatric interventions may inadvertently alter an individual's colorectal cancer risk by driving the microbiome towards a pro-oncogenic state. Indeed, high levels of BAs are thought to be cytotoxic and promote carcinogenesis through increased production of reactive oxygen and reactive nitrogen species[218, 219] leading to increased DNA damage[220]. Furthermore, it has been suggested that high-fat diets could promote carcinogenesis via faecal BAs[221].

The mechanisms by which BAs promote carcinogen-induced abnormalities in the gut mucosa are complex[222-224]. BAs, particularly secondary BAs at high physiological concentrations, can cause damage to colonic epithelial cells. Resulting inflammation and repair mechanisms lead to hyper-proliferation of undifferentiated cells[225]. Further, BAs induce reactive oxygen and nitrogen species through their stimulating effect on NADPH and phospholipase A2 which causes DNA damage[226]. Furthermore, subsequent chronic exposure to BAs can lead to degradation of the tumour suppressor p53 and upregulate X-linked inhibitor of apoptosis protein (XIAP), reducing apoptosis and leading to the promotion of colorectal cancer[227, 228].

Several groups have used ileal and colonic resection models in rats to alter intraluminal BA levels and found an increased incidence of colonic tumours associated with raised BA levels[229-231]. Although serum levels of BAs increase following bypass surgery, as discussed above, some animal models have suggested that at some points along the intestine levels of intraluminal BAs appear to reduce due to improved absorption[124]. Rats exposed to the carcinogen azoxymethane after partial gastrectomy had lower faecal BA levels and a lower tumour yield relative to sham operated controls[232]. Nevertheless, due to alterations in bile flow, certain areas within the gut are exposed to increased levels of tumour promoting BA. A large

retrospective cohort study of patients following bariatric surgery in Sweden found an increased risk of colorectal cancer following surgery compared to obese controls[216]. Although, a previous large retrospective cohort study assessed the risk of colorectal cancer following BPD, a procedure that significantly increases BA levels in the colon. The authors found a decreased incidence of colorectal cancer compared to obese T2DM controls and a similar level to that of the general population[233]. It was reasoned that the correction of any hyperinsulinaemia following surgery strongly contrasts any possible carcinogenic effect from BAs.

Others have suggested a theoretical increased risk of gastric or oesophageal cancer following a Mini Gastric Bypass / One Anastomosis Gastric Bypass (MGB) due to chronic bile reflux[234]. Though, it is to be noted that so far there have been no reported cases of carcinoma in the gastric pouch or oesophagus following MGB and the theoretical increased risk is disputed[235].

However, this effect is not likely to be FXR mediated as it has recently emerged as a mediator of tumour suppression, with loss of FXR function contributing to tumourgenesis[236]. FXR ligands were able to overcome anti-oestrogen resistance in breast cancer cells via inhibition of HER2/MAPK signalling[237]. In addition, BAs, namely LCA, have been shown to induce apoptosis in colon cancer cells[218]. Similarly, LCA is able to induce apoptosis in neuroblastoma cells[238] and in androgen-dependent and androgen-independent prostate cancer cells[239, 240] via activation of both extrinsic and intrinsic pathways of apoptosis, in a caspase-3 dependent manner. Although, the serum BA levels seen following metabolic surgery are not as high as the levels seen to induce anti-carcinogenic effects in the above studies and hence their contribution to the reduction in cancer rates following surgery remains to be seen.

1.5.5 Latest Research

Recent research has supported a role of increased BA reabsorption following bariatric surgery. Indeed, increased blood BAs occur despite an apparent decrease in BA synthesis after VSG, as measured by the serum marker C4 (7-Hydroxy-4-cholesten-3-one)[241]. Studies in the Gottingen-like minipig found that the portal : systemic conjugated BA ratio decreased after RYGB, indicating that increased systemic BAs after RYGB may be due to a decrease in selective hepatic recapture[242]. A further study of duodenal-jenunal bypass and VSG in rats found higher levels of BAs in both serum and the enterohepatic circulation. In addition, CYP7A1 the rate

limiting enzyme in BA synthesis, was reduced after surgery. Whereas expression of hepatic BA conjugation enzymes and ileal BA transporters was increased. Together indicating that the elevated BA levels was as a results of increased ileal reabsorption and hepatic conjugation, rather than increased synthesis[243]. The importance of the ileum is also highlighted in mouse models of bile flow diversion. Surgical diversion of bile flow to the ileum, but not the jejunum or duodenum, imparted significant weight loss and improved glucose and lipid metabolism similar to RYGB[244].

Recent studies in humans after bariatric surgery have found more specific changes to BA profiles, with secondary BAs appearing to be particularly influenced. One study of RYGB subjects found increases in plasma ursodeoxycholic acid (UDCA) and it's glycine and taurine conjugates 1-month after RYGB as well as increased hepatic insulin sensitivity[245]. In a further study total BA and secondary BA levels were increased at 5-years post RYGB[246]. Blood levels of glycine conjugated UDCA (secondary BA) also increased 6-months after VSG, while glycine and taurine conjugated cholic acid (primary BA) decreased. These changes were associated with increased insulin sensitivity and reduced inflammatory cytokines[247]. Furthermore, increases in secondary bile acids appears to occur independently of both hypocaloric restriction[248] and improved glycaemic control[249]. In diabetic subjects blood bile acids levels increased after RYGB but not intensive medical management[249]. Nonetheless, there appears to be heterogeneity in these findings between studies. Lindqvist et al found a reduction in plasma and faecal BAs, including secondary bile acids, 2-weeks after RYGB in lean pigs[250]. This may have been due to the proximity to the physiological insult of surgery. Although, others found decreased serum C4, UDCA, tauroursodeoxycholic acid (TUDCA), hyodeoxycholic acid (HDCA) and glycoursodeoxycholate sulfate (GUDCS), at 6-months and 1-year post RYGB. Nevertheless, glycochenodeoxycholate sulfate (GCDCS) was increased at both 6-months and 1-year and glycodeoxycholate (GDCA) was increased at 1 year post RYGB[251]. Intriguingly, these changes were more pronounced in the subgroup that underwent diabetic remission and not seen in those that remained diabetic[251].

1.5.6 Conclusions

This systematic review provides convincing evidence for the role of the BAs in the 'SLIMMER' effects of bariatric surgery (see Figure 1.5-3). Moreover, developments in our understanding

of BA signalling suggests that the gut-liver axis is both highly active and closely regulated and furthermore that it is significantly perturbed after bariatric surgery[70, 86, 115, 121]. Most interestingly, the gut microbiome appears to be of critical importance to the mechanism of both weight loss and diabetes resolution after bariatric surgery[39, 208]. This is supported from studies using FXR agonists, FGF-19 analogues and ASBT inhibitors all of which potentially interfere with BA homeostasis and the microbiome, in a bi-directional way. Most critically this review highlights the importance of BAs to the development of the obese phenotype and its metabolic complications. Bariatric surgery provides a unique model through which its disruption may be studied, and this in turn has provided significant new insights into the highly complex and diverse functions of these metabolically active microbial co-metabolites. Thus, it serves as an important target for next generation stratified medical and surgical therapies in obesity.

1.6 Physical activity and Exercise

As discussed above, a sedentary Western lifestyle is implicated in numerous diseases of affluence such as obesity, diabetes and cardiovascular disease[252-254]. The corollary being that exercise therefore represents both a preventative and therapeutic strategy for these diseases[255]. Indeed, exercise is known to have many health benefits including reducing hypertension and cardiovascular disease[256, 257], T2DM[258, 259], colorectal cancer[260], depression[261] and cognitive impairment[262].

Exercise induces a significant challenge to systemic homeostasis causing a number of responses both at the cellular and whole-body multi-organ level, including those that centre around metabolism and immunity[263-265]. Known health-promoting mechanisms include: increasing energy expenditure and carbohydrate metabolism leading to a reduction in obesity related diseases, as well as inducing end-organ and systemic anti-inflammatory effects[266, 267]. Yet, the cellular mechanisms underpinning these health benefits are poorly understood. A recent study revealed that exercise regulates the phosphoproteome via activation of a global network of kinases[268]. Nevertheless, a multitude of signaling pathways are likely to exist due to the widespread perturbation exercise induces to numerous cells, tissues and organs[265].

Exercise is well associated with an improved cholesterol profile with reduced low density lipoprotein (LDL)-cholesterol levels and increased high density lipoprotein (HDL) levels, contributing to a reduction in atherosclerosis and coronary heart disease[269-271]. It has been suggested that, similar to bariatric surgery, bile acid metabolism may be involved in modulating some of these effects[272]. Exercise in mice reduced cholesterol and the atherosclerotic burden. Furthermore, increased cholesterol turnover resulted in increased biliary and faecal BA levels[273, 274]. Other authors have found an increase in the expression of CYP27A1[275] and CYP7A1[276] genes, involved in bile acid synthesis, after exercise training. Moreover, a further study in mice found that altered cholesterol metabolism and increased CYP7A1 was modulated through upregulation of SHP after exercise training[272]. In addition, exercise in rats was shown to reduce the proportion of secondary to primary bile acids within faeces[277]. Nevertheless, these studies have an unknown relevance to humans. In a study of human subjects, exercise induced an immediate decrease in serum BAs which was still present after a 14hr recovery period[278].

Previous studies have focused on a small number of key pathways and metabolites. Preliminary metabonomic studies using ^{1}H-NMR and MS have enabled a global, hypothesis-free analysis of the metabolic changes that occur after exercise. These have demonstrated changes in multiple metabolic pathways including the Krebs cycle, amino acids, SCFAs, branched-chain amino acids[279-281].

Lastly, increasing physical activity offers effective prevention and treatment for many chronic conditions in which the gut microbiome has been implicated[259, 282, 283]. Most elements of lifestyle appear to influence the microbiome. Certainly dietary adaptations to exercise are likely to significantly influence the composition of the microbiota[35, 284]. However, additional mechanisms such as altered gut inflammatory response, splanchnic circulation adaptations and gut-microbiome-brain signaling are also likely to be of importance[255, 266, 285]. A number of different cohorts including elite rugby players and competitive cyclists with increased cardio-respiratory fitness relative to controls have been shown to have higher levels of gut bacterial diversity[281, 286, 287]. Hence the concept that increased physical activity and regular exercise may nurture a preferential gut microbiome has recently emerged[281, 287, 288].

1.7 Chapter Conclusion & Outlook

Due to the many complex and multidirectional interactions that occur between the gut microbiome and host the effects of single components within this relationship are often subtle and difficult to study *in vivo*. Therefore, the key premise underlying this thesis is that the study of extremes in physiology will enable the detection and study of these more subtle interactions.

In this thesis I chose to study two cohorts from opposing extremes of the continuum between health and disease. Namely, elite athletes and obese subjects undergoing bariatric surgery. It is reasoned that studying these extreme physiological states will enable detection of subtler changes in the multidirectional relationship between metabolism and the gut microbiome driven by changes in physical activity, aerobic fitness, diet and adiposity. Furthermore, longitudinally studying bariatric surgery patients before and after surgery will expose subjects to the large physiological changes that occur to the gastrointestinal tract after bariatric surgery while controlling for confounding factors such as subject age and genetics, facilitating further understanding of gut microbiome – host co-metabolism. Third, a prospective interventional study is conducted with the aim of differentiating between the effects of diet and exercise on the gut microbiome and metabolic phenotype. Key metabolites involved in co-metabolism are focused on including, bile acids, SCFAs and choline.

An outline of the experimental strategy employed with each of these studies is shown in Figure 1.7-1 below. The analytical strategies and statistical techniques used are further described in Chapter 2.

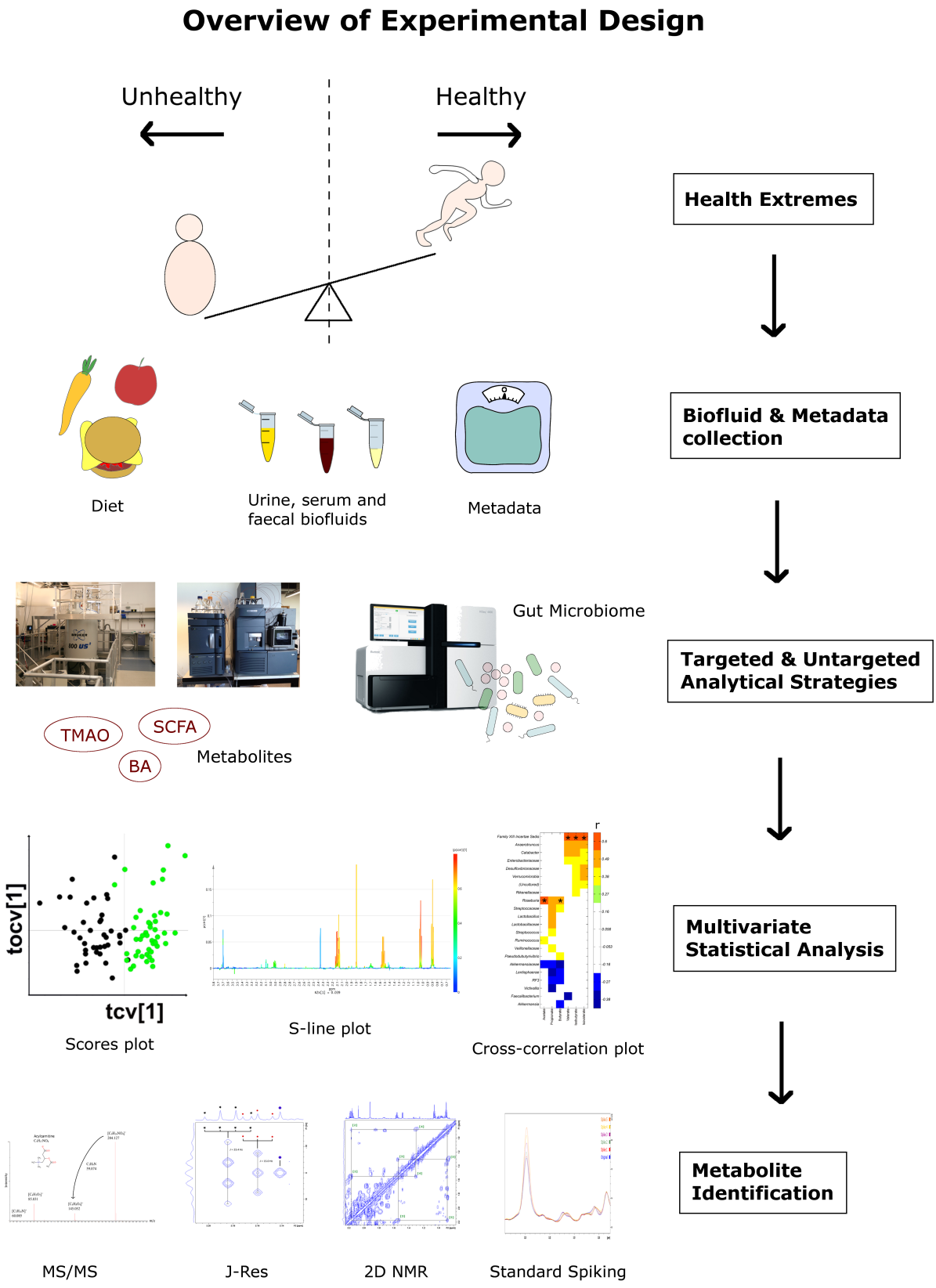


Figure 1.7-1 Overview of experimental design used throughout studies within this thesis. Analytical and statistical strategies used are described further in Chapter 2.

1.8 References

1. Nicholson JK, Lindon JC, Holmes E. 'Metabonomics': understanding the metabolic responses of living systems to pathophysiological stimuli via multivariate statistical analysis of biological NMR spectroscopic data. Xenobiotica. 1999;29(11):1181-9.

2. Nicholson JK, Lindon JC. Systems biology: Metabonomics. Nature. 2008;455(7216):1054-6.

3. Nicholson JK, Wilson ID. Understanding 'global' systems biology: metabonomics and the continuum of metabolism. Nat Rev Drug Discov. 2003;2(8):668-76.

4. Vernocchi P, Del Chierico F, Putignani L. Gut Microbiota Profiling: Metabolomics Based Approach to Unravel Compounds Affecting Human Health. Frontiers in microbiology. 2016;7:1144.

5. Holmes E, Loo RL, Stamler J, Bictash M, Yap IK, Chan Q, et al. Human metabolic phenotype diversity and its association with diet and blood pressure. Nature. 2008;453(7193):396-400.

6. Wang TJ, Larson MG, Vasan RS, Cheng S, Rhee EP, McCabe E, et al. Metabolite profiles and the risk of developing diabetes. Nature medicine. 2011;17(4):448-53.

7. Li M, Wang B, Zhang M, Rantalainen M, Wang S, Zhou H, et al. Symbiotic gut microbes modulate human metabolic phenotypes. Proceedings of the National Academy of Sciences of the United States of America. 2008;105(6):2117-22.

8. Nicholson JK, Holmes E, Kinross JM, Darzi AW, Takats Z, Lindon JC. Metabolic phenotyping in clinical and surgical environments. Nature. 2012;491(7424):384-92.

9. Backshall A, Sharma R, Clarke SJ, Keun HC. Pharmacometabonomic profiling as a predictor of toxicity in patients with inoperable colorectal cancer treated with capecitabine. Clin Cancer Res. 2011;17(9):3019-28.

10. Human Microbiome Project C. A framework for human microbiome research. Nature. 2012;486(7402):215-21.

11. Aranki A, Freter R. Use of anaerobic glove boxes for the cultivation of strictly anaerobic bacteria. The American journal of clinical nutrition. 1972;25(12):1329-34.

12. Suau A, Bonnet R, Sutren M, Godon JJ, Gibson GR, Collins MD, et al. Direct analysis of genes encoding 16S rRNA from complex communities reveals many novel molecular species within the human gut. Appl Environ Microbiol. 1999;65(11):4799-807.

13. Hiergeist A, Glasner J, Reischl U, Gessner A. Analyses of Intestinal Microbiota: Culture versus Sequencing. ILAR J. 2015;56(2):228-40.

14. Human Microbiome Project C. Structure, function and diversity of the healthy human microbiome. Nature. 2012;486(7402):207-14.

15. Claesson MJ, Jeffery IB, Conde S, Power SE, O'Connor EM, Cusack S, et al. Gut microbiota composition correlates with diet and health in the elderly. Nature. 2012;488(7410):178-84.

16. Holmes E, Li JV, Athanasiou T, Ashrafian H, Nicholson JK. Understanding the role of gut microbiome-host metabolic signal disruption in health and disease. Trends in microbiology. 2011;19(7):349-59.

17. Holmes E, Li JV, Marchesi JR, Nicholson JK. Gut microbiota composition and activity in relation to host metabolic phenotype and disease risk. Cell metabolism. 2012;16(5):559-64.

18. Kootte RS, Vrieze A, Holleman F, Dallinga-Thie GM, Zoetendal EG, de Vos WM, et al. The therapeutic potential of manipulating gut microbiota in obesity and type 2 diabetes mellitus. Diabetes, obesity & metabolism. 2012;14(2):112-20.

19. Musso G, Gambino R, Cassader M. Obesity, diabetes, and gut microbiota: the hygiene hypothesis expanded? Diabetes care. 2010;33(10):2277-84.

20. Turnbaugh PJ, Ley RE, Mahowald MA, Magrini V, Mardis ER, Gordon JI. An obesity-associated gut microbiome with increased capacity for energy harvest. Nature. 2006;444(7122):1027-31.

21. Turnbaugh PJ, Hamady M, Yatsunenko T, Cantarel BL, Duncan A, Ley RE, et al. A core gut microbiome in obese and lean twins. Nature. 2009;457(7228):480-4.

22. Ley RE, Turnbaugh PJ, Klein S, Gordon JI. Microbial ecology: human gut microbes associated with obesity. Nature. 2006;444(7122):1022-3.

23. Qin J, Li Y, Cai Z, Li S, Zhu J, Zhang F, et al. A metagenome-wide association study of gut microbiota in type 2 diabetes. Nature. 2012;490(7418):55-60.

24. Henao-Mejia J, Elinav E, Jin C, Hao L, Mehal WZ, Strowig T, et al. Inflammasome-mediated dysbiosis regulates progression of NAFLD and obesity. Nature. 2012;482(7384):179-85.

25. Rak K, Rader DJ. Cardiovascular disease: the diet-microbe morbid union. Nature. 2011;472(7341):40-1.

26. Wang Z, Klipfell E, Bennett BJ, Koeth R, Levison BS, Dugar B, et al. Gut flora metabolism of phosphatidylcholine promotes cardiovascular disease. Nature. 2011;472(7341):57-63.

27. Jostins L, Ripke S, Weersma RK, Duerr RH, McGovern DP, Hui KY, et al. Host-microbe interactions have shaped the genetic architecture of inflammatory bowel disease. Nature. 2012;491(7422):119-24.

28. Berer K, Mues M, Koutrolos M, Rasbi ZA, Boziki M, Johner C, et al. Commensal microbiota and myelin autoantigen cooperate to trigger autoimmune demyelination. Nature. 2011;479(7374):538-41.

29. Ley RE, Backhed F, Turnbaugh P, Lozupone CA, Knight RD, Gordon JI. Obesity alters gut microbial ecology. Proceedings of the National Academy of Sciences of the United States of America. 2005;102(31):11070-5.

30. Schwiertz A, Taras D, Schafer K, Beijer S, Bos NA, Donus C, et al. Microbiota and SCFA in lean and overweight healthy subjects. Obesity. 2010;18(1):190-5.

31. de Wit N, Derrien M, Bosch-Vermeulen H, Oosterink E, Keshtkar S, Duval C, et al. Saturated fat stimulates obesity and hepatic steatosis and affects gut microbiota composition by an enhanced overflow of dietary fat to the distal intestine. American journal of physiology Gastrointestinal and liver physiology. 2012;303(5):G589-99.

32. Ravussin Y, Koren O, Spor A, LeDuc C, Gutman R, Stombaugh J, et al. Responses of gut microbiota to diet composition and weight loss in lean and obese mice. Obesity. 2012;20(4):738-47.

33. Hildebrandt MA, Hoffmann C, Sherrill-Mix SA, Keilbaugh SA, Hamady M, Chen YY, et al. High-fat diet determines the composition of the murine gut microbiome independently of obesity. Gastroenterology. 2009;137(5):1716-24 e1-2.

34. Le Chatelier E, Nielsen T, Qin J, Prifti E, Hildebrand F, Falony G, et al. Richness of human gut microbiome correlates with metabolic markers. Nature. 2013;500(7464):541-6.

35. Cotillard A, Kennedy SP, Kong LC, Prifti E, Pons N, Le Chatelier E, et al. Dietary intervention impact on gut microbial gene richness. Nature. 2013;500(7464):585-8.

36. Ridaura VK, Faith JJ, Rey FE, Cheng J, Duncan AE, Kau AL, et al. Gut microbiota from twins discordant for obesity modulate metabolism in mice. Science. 2013;341(6150):1241214.

37. Karlsson FH, Tremaroli V, Nookaew I, Bergstrom G, Behre CJ, Fagerberg B, et al. Gut metagenome in European women with normal, impaired and diabetic glucose control. Nature. 2013;498(7452):99-103.

38. Vrieze A, Van Nood E, Holleman F, Salojarvi J, Kootte RS, Bartelsman JF, et al. Transfer of intestinal microbiota from lean donors increases insulin sensitivity in individuals with metabolic syndrome. Gastroenterology. 2012;143(4):913-6 e7.

39. Liou AP, Paziuk M, Luevano JM, Jr., Machineni S, Turnbaugh PJ, Kaplan LM. Conserved shifts in the gut microbiota due to gastric bypass reduce host weight and adiposity. Science translational medicine. 2013;5(178):178ra41.

40. Nicholson JK, Holmes E, Kinross J, Burcelin R, Gibson G, Jia W, et al. Host-gut microbiota metabolic interactions. Science. 2012;336(6086):1262-7.

41. Lin HV, Frassetto A, Kowalik EJ, Jr., Nawrocki AR, Lu MM, Kosinski JR, et al. Butyrate and propionate protect against diet-induced obesity and regulate gut hormones via free fatty acid receptor 3-independent mechanisms. PloS one. 2012;7(4):e35240.

42. Donohoe DR, Garge N, Zhang X, Sun W, O'Connell TM, Bunger MK, et al. The microbiome and butyrate regulate energy metabolism and autophagy in the mammalian colon. Cell metabolism. 2011;13(5):517-26.

43. Puertollano E, Kolida S, Yaqoob P. Biological significance of short-chain fatty acid metabolism by the intestinal microbiome. Current opinion in clinical nutrition and metabolic care. 2014;17(2):139-44.

44. Layden BT, Angueira AR, Brodsky M, Durai V, Lowe WL, Jr. Short chain fatty acids and their receptors: new metabolic targets. Translational research : the journal of laboratory and clinical medicine. 2013;161(3):131-40.

45. Maslowski KM, Vieira AT, Ng A, Kranich J, Sierro F, Yu D, et al. Regulation of inflammatory responses by gut microbiota and chemoattractant receptor GPR43. Nature. 2009;461(7268):1282-6.

46. Kimura I, Ozawa K, Inoue D, Imamura T, Kimura K, Maeda T, et al. The gut microbiota suppresses insulin-mediated fat accumulation via the short-chain fatty acid receptor GPR43. Nature communications. 2013;4:1829.

47. Samuel BS, Shaito A, Motoike T, Rey FE, Backhed F, Manchester JK, et al. Effects of the gut microbiota on host adiposity are modulated by the short-chain fatty-acid binding G protein-coupled receptor, Gpr41. Proceedings of the National Academy of Sciences of the United States of America. 2008;105(43):16767-72.

48. Chambers ES, Viardot A, Psichas A, Morrison DJ, Murphy KG, Zac-Varghese SE, et al. Effects of targeted delivery of propionate to the human colon on appetite regulation, body weight maintenance and adiposity in overweight adults. Gut. 2015;64(11):1744-54.

49. Tolhurst G, Heffron H, Lam YS, Parker HE, Habib AM, Diakogiannaki E, et al. Short-chain fatty acids stimulate glucagon-like peptide-1 secretion via the G-protein-coupled receptor FFAR2. Diabetes. 2012;61(2):364-71.

50. Davie JR. Inhibition of histone deacetylase activity by butyrate. The Journal of nutrition. 2003;133(7 Suppl):2485S-93S.

51. Waldecker M, Kautenburger T, Daumann H, Busch C, Schrenk D. Inhibition of histone-deacetylase activity by short-chain fatty acids and some polyphenol metabolites formed in the colon. J Nutr Biochem. 2008;19(9):587-93.

52. Smith PM, Howitt MR, Panikov N, Michaud M, Gallini CA, Bohlooly YM, et al. The microbial metabolites, short-chain fatty acids, regulate colonic Treg cell homeostasis. Science. 2013;341(6145):569-73.

53. Nepelska M, Cultrone A, Beguet-Crespel F, Le Roux K, Dore J, Arulampalam V, et al. Butyrate produced by commensal bacteria potentiates phorbol esters induced AP-1 response in human intestinal epithelial cells. PloS one. 2012;7(12):e52869.

54. Ufnal M, Zadlo A, Ostaszewski R. TMAO: A small molecule of great expectations. Nutrition. 2015;31(11-12):1317-23.

55. Ussher JR, Lopaschuk GD, Arduini A. Gut microbiota metabolism of L-carnitine and cardiovascular risk. Atherosclerosis. 2013;231(2):456-61.

56. Koeth RA, Wang Z, Levison BS, Buffa JA, Org E, Sheehy BT, et al. Intestinal microbiota metabolism of L-carnitine, a nutrient in red meat, promotes atherosclerosis. Nature medicine. 2013;19(5):576-85.

57. Fennema D, Phillips IR, Shephard EA. Trimethylamine and Trimethylamine N-Oxide, a Flavin-Containing Monooxygenase 3 (FMO3)-Mediated Host-Microbiome Metabolic Axis Implicated in Health and Disease. Drug Metab Dispos. 2016;44(11):1839-50.

58. Zhu Y, Jameson E, Parslow RA, Lidbury I, Fu T, Dafforn TR, et al. Identification and characterization of trimethylamine N-oxide (TMAO) demethylase and TMAO permease in Methylocella silvestris BL2. Environ Microbiol. 2014;16(10):3318-30.

59. Cho CE, Taesuwan S, Malysheva OV, Bender E, Tulchinsky NF, Yan J, et al. Trimethylamine-N-oxide (TMAO) response to animal source foods varies among healthy young men and is influenced by their gut microbiota composition: A randomized controlled trial. Mol Nutr Food Res. 2017;61(1).

60. Tang WH, Wang Z, Levison BS, Koeth RA, Britt EB, Fu X, et al. Intestinal microbial metabolism of phosphatidylcholine and cardiovascular risk. The New England journal of medicine. 2013;368(17):1575-84.

61. Dumas ME, Barton RH, Toye A, Cloarec O, Blancher C, Rothwell A, et al. Metabolic profiling reveals a contribution of gut microbiota to fatty liver phenotype in insulin-resistant mice. Proceedings of the National Academy of Sciences of the United States of America. 2006;103(33):12511-6.

62. Tremaroli V, Backhed F. Functional interactions between the gut microbiota and host metabolism. Nature. 2012;489(7415):242-9.

63. Wang D, Zhang Z, Ju J, Wang X, Qiu W. Investigation of piceid metabolites in rat by liquid chromatography tandem mass spectrometry. Journal of chromatography B, Analytical technologies in the biomedical and life sciences. 2011;879(1):69-74.

64. Mueller DM, Allenspach M, Othman A, Saely CH, Muendlein A, Vonbank A, et al. Plasma levels of trimethylamine-N-oxide are confounded by impaired kidney function and poor metabolic control. Atherosclerosis. 2015;243(2):638-44.

65. Dumas ME, Rothwell AR, Hoyles L, Aranias T, Chilloux J, Calderari S, et al. Microbial-Host Co-metabolites Are Prodromal Markers Predicting Phenotypic Heterogeneity in Behavior, Obesity, and Impaired Glucose Tolerance. Cell Rep. 2017;20(1):136-48.

66. Jones BV, Begley M, Hill C, Gahan CG, Marchesi JR. Functional and comparative metagenomic analysis of bile salt hydrolase activity in the human gut microbiome. Proceedings of the National Academy of Sciences of the United States of America. 2008;105(36):13580-5.

67. Groh H, Schade K, Horhold-Schubert C. Steroid metabolism with intestinal microorganisms. Journal of basic microbiology. 1993;33(1):59-72.

68. Fukiya S, Arata M, Kawashima H, Yoshida D, Kaneko M, Minamida K, et al. Conversion of cholic acid and chenodeoxycholic acid into their 7-oxo derivatives by Bacteroides intestinalis AM-1 isolated from human feces. FEMS microbiology letters. 2009;293(2):263-70.

69. Ryan KK, Kohli R, Gutierrez-Aguilar R, Gaitonde SG, Woods SC, Seeley RJ. Fibroblast growth factor-19 action in the brain reduces food intake and body weight and improves glucose tolerance in male rats. Endocrinology. 2013;154(1):9-15.

70. Ryan KK, Tremaroli V, Clemmensen C, Kovatcheva-Datchary P, Myronovych A, Karns R, et al. FXR is a molecular target for the effects of vertical sleeve gastrectomy. Nature. 2014;509(7499):183-8.

71. Penney NC, Kinross J, Newton RC, Purkayastha S. The role of bile acids in reducing the metabolic complications of obesity after bariatric surgery: a systematic review. International journal of obesity. 2015;39(11):1565-74.

72. Swann JR, Want EJ, Geier FM, Spagou K, Wilson ID, Sidaway JE, et al. Systemic gut microbial modulation of bile acid metabolism in host tissue compartments. Proc Natl Acad Sci USA. 2011;108(Suppl. 1):4523-30.

73. World_Health_Organization. Obesity and Overweight: WHO; 2014 [Available from: http://www.who.int/mediacentre/factsheets/fs311/en/.

74. Puterbaugh JS. The emperor's tailors: the failure of the medical weight loss paradigm and its causal role in the obesity of America. Diabetes, obesity & metabolism. 2009;11(6):557-70.

75. Adams TD, Davidson LE, Litwin SE, Kolotkin RL, LaMonte MJ, Pendleton RC, et al. Health benefits of gastric bypass surgery after 6 years. JAMA : the journal of the American Medical Association. 2012;308(11):1122-31.

76. Ikramuddin S, Korner J, Lee WJ, Connett JE, Inabnet WB, Billington CJ, et al. Roux-en-Y gastric bypass vs intensive medical management for the control of type 2 diabetes, hypertension, and hyperlipidemia: the Diabetes Surgery Study randomized clinical trial. JAMA : the journal of the American Medical Association. 2013;309(21):2240-9.

77. Schauer PR, Bhatt DL, Kirwan JP, Wolski K, Brethauer SA, Navaneethan SD, et al. Bariatric surgery versus intensive medical therapy for diabetes--3-year outcomes. The New England journal of medicine. 2014;370(21):2002-13.

78. Eliasson B, Liakopoulos V, Franzen S, Naslund I, Svensson AM, Ottosson J, et al. Cardiovascular disease and mortality in patients with type 2 diabetes after bariatric surgery in Sweden: a nationwide, matched, observational cohort study. The lancet Diabetes & endocrinology. 2015;3(11):847-54.

79. Schauer PR, Bhatt DL, Kirwan JP, Wolski K, Aminian A, Brethauer SA, et al. Bariatric Surgery versus Intensive Medical Therapy for Diabetes - 5-Year Outcomes. The New England journal of medicine. 2017;376(7):641-51.

80. Liang Z, Wu Q, Chen B, Yu P, Zhao H, Ouyang X. Effect of laparoscopic Roux-en-Y gastric bypass surgery on type 2 diabetes mellitus with hypertension: A randomized controlled trial. Diabetes research and clinical practice. 2013;101(1):50-6.

81. Dixon JB, Schachter LM, O'Brien PE, Jones K, Grima M, Lambert G, et al. Surgical vs conventional therapy for weight loss treatment of obstructive sleep apnea: a randomized controlled trial. JAMA : the journal of the American Medical Association. 2012;308(11):1142-9.

82. Ashrafian H, Ahmed K, Rowland SP, Patel VM, Gooderham NJ, Holmes E, et al. Metabolic surgery and cancer: protective effects of bariatric procedures. Cancer. 2011;117(9):1788-99.

83. Cummings BP, Graham JL, Stanhope KL, Chouinard ML, Havel PJ. Maternal ileal interposition surgery confers metabolic improvements to offspring independent of effects on maternal body weight in UCD-T2DM rats. Obesity surgery. 2013;23(12):2042-9.

84. Ashrafian H, Bueter M, Ahmed K, Suliman A, Bloom SR, Darzi A, et al. Metabolic surgery: an evolution through bariatric animal models. Obesity reviews : an official journal of the International Association for the Study of Obesity. 2010;11(12):907-20.

85. Kohli R, Setchell KD, Kirby M, Myronovych A, Ryan KK, Ibrahim SH, et al. A surgical model in male obese rats uncovers protective effects of bile acids post-bariatric surgery. Endocrinology. 2013;154(7):2341-51.

86. Kohli R, Bradley D, Setchell KD, Eagon JC, Abumrad N, Klein S. Weight loss induced by Roux-en-Y gastric bypass but not laparoscopic adjustable gastric banding increases circulating bile acids. The Journal of clinical endocrinology and metabolism. 2013;98(4):E708-12.

87. Patti ME, Houten SM, Bianco AC, Bernier R, Larsen PR, Holst JJ, et al. Serum bile acids are higher in humans with prior gastric bypass: potential contribution to improved glucose and lipid metabolism. Obesity. 2009;17(9):1671-7.

88. Ahmad NN, Pfalzer A, Kaplan LM. Roux-en-Y gastric bypass normalizes the blunted postprandial bile acid excursion associated with obesity. International journal of obesity. 2013;37(12):1553-9.

89. Kohli R, Kirby M, Setchell KD, Jha P, Klustaitis K, Woollett LA, et al. Intestinal adaptation after ileal interposition surgery increases bile acid recycling and protects against obesity-related comorbidities. American journal of physiology Gastrointestinal and liver physiology. 2010;299(3):G652-60.

90. Pournaras DJ, Glicksman C, Vincent RP, Kuganolipava S, Alaghband-Zadeh J, Mahon D, et al. The role of bile after Roux-en-Y gastric bypass in promoting weight loss and improving glycaemic control. Endocrinology. 2012;153(8):3613-9.

91. Pournaras DJ, le Roux CW. Are bile acids the new gut hormones? Lessons from weight loss surgery models. Endocrinology. 2013;154(7):2255-6.

92. Wang H, Chen J, Hollister K, Sowers LC, Forman BM. Endogenous bile acids are ligands for the nuclear receptor FXR/BAR. Molecular cell. 1999;3(5):543-53.

93. Parks DJ, Blanchard SG, Bledsoe RK, Chandra G, Consler TG, Kliewer SA, et al. Bile acids: natural ligands for an orphan nuclear receptor. Science. 1999;284(5418):1365-8.

94. Makishima M, Okamoto AY, Repa JJ, Tu H, Learned RM, Luk A, et al. Identification of a nuclear receptor for bile acids. Science. 1999;284(5418):1362-5.

95. Lu TT, Makishima M, Repa JJ, Schoonjans K, Kerr TA, Auwerx J, et al. Molecular basis for feedback regulation of bile acid synthesis by nuclear receptors. Molecular cell. 2000;6(3):507-15.

96. Goodwin B, Jones SA, Price RR, Watson MA, McKee DD, Moore LB, et al. A regulatory cascade of the nuclear receptors FXR, SHP-1, and LRH-1 represses bile acid biosynthesis. Molecular cell. 2000;6(3):517-26.

97. Brendel C, Schoonjans K, Botrugno OA, Treuter E, Auwerx J. The small heterodimer partner interacts with the liver X receptor alpha and represses its transcriptional activity. Molecular endocrinology. 2002;16(9):2065-76.

98. Lee YK, Dell H, Dowhan DH, Hadzopoulou-Cladaras M, Moore DD. The orphan nuclear receptor SHP inhibits hepatocyte nuclear factor 4 and retinoid X receptor transactivation: two mechanisms for repression. Molecular and cellular biology. 2000;20(1):187-95.

99. Zhang M, Chiang JY. Transcriptional regulation of the human sterol 12alpha-hydroxylase gene (CYP8B1): roles of heaptocyte nuclear factor 4alpha in mediating bile acid repression. The Journal of biological chemistry. 2001;276(45):41690-9.

100. Yu C, Wang F, Kan M, Jin C, Jones RB, Weinstein M, et al. Elevated cholesterol metabolism and bile acid synthesis in mice lacking membrane tyrosine kinase receptor FGFR4. The Journal of biological chemistry. 2000;275(20):15482-9.

101. Holt JA, Luo G, Billin AN, Bisi J, McNeill YY, Kozarsky KF, et al. Definition of a novel growth factor-dependent signal cascade for the suppression of bile acid biosynthesis. Genes & development. 2003;17(13):1581-91.

102. Inagaki T, Choi M, Moschetta A, Peng L, Cummins CL, McDonald JG, et al. Fibroblast growth factor 15 functions as an enterohepatic signal to regulate bile acid homeostasis. Cell metabolism. 2005;2(4):217-25.

103. Kir S, Zhang Y, Gerard RD, Kliewer SA, Mangelsdorf DJ. Nuclear receptors HNF4alpha and LRH-1 cooperate in regulating Cyp7a1 in vivo. The Journal of biological chemistry. 2012;287(49):41334-41.

104. Bhutta HY, White W, Liu Y, Rajpal N, Way J, Rajpal D, et al. Effect of roux-en-y gastric bypass surgery on fecal bile acid excretion in normal and diabetic rats. Diabetes. 2013;62(Suppl. 1):A520 (abstract 2018P).

105. Li JV, Ashrafian H, Bueter M, Kinross J, Sands C, le Roux CW, et al. Metabolic surgery profoundly influences gut microbial-host metabolic cross-talk. Gut. 2011;60(9):1214-23.

106. Ashrafian H, Li JV, Spagou K, Harling L, Masson P, Darzi A, et al. Bariatric surgery modulates circulating and cardiac metabolites. Journal of proteome research. 2014;13(2):570-80.

107. Osto E, Doytcheva P, Corteville C, Spliethoff K, Bueter M, Rohrer L, et al. Increased plasma Glucagon Like Peptide-1 improves endothelial dysfunction immediately after Roux-en-Y gastric bypass prior to body weight loss inhibiting the c-Jun N-terminal Protein Kinase Signaling. European Heart Journal. 2013;34(Suppl. 1):119.

108. Werling M, Vincent RP, Cross GF, Marschall HU, Fandriks L, Lonroth H, et al. Enhanced fasting and post-prandial plasma bile acid responses after Roux-en-Y gastric bypass surgery. Scandinavian journal of gastroenterology. 2013;48(11):1257-64.

109. Scholtz S, Miras AD, Chhina N, Prechtl CG, Sleeth ML, Daud NM, et al. Obese patients after gastric bypass surgery have lower brain-hedonic responses to food than after gastric banding. Gut. 2014;63(6):891-902.

110. Steinert RE, Peterli R, Keller S, Meyer-Gerspach AC, Drewe J, Peters T, et al. Bile acids and gut peptide secretion after bariatric surgery: a 1-year prospective randomized pilot trial. Obesity. 2013;21(12):E660-8.

111. Gerhard GS, Styer AM, Wood GC, Roesch SL, Petrick AT, Gabrielsen J, et al. A role for fibroblast growth factor 19 and bile acids in diabetes remission after Roux-en-Y gastric bypass. Diabetes care. 2013;36(7):1859-64.

112. Simonen M, Dali-Youcef N, Kaminska D, Venesmaa S, Kakela P, Paakkonen M, et al. Conjugated bile acids associate with altered rates of glucose and lipid oxidation after Roux-en-Y gastric bypass. Obesity surgery. 2012;22(9):1473-80.

113. Jansen PL, van Werven J, Aarts E, Berends F, Janssen I, Stoker J, et al. Alterations of hormonally active fibroblast growth factors after Roux-en-Y gastric bypass surgery. Digestive diseases. 2011;29(1):48-51.

114. Dirksen C, Jorgensen NB, Bojsen-Moller KN, Kielgast U, Jacobsen SH, Clausen TR, et al. Gut hormones, early dumping and resting energy expenditure in patients with good and poor weight loss response after Roux-en-Y gastric bypass. International journal of obesity. 2013;37(11):1452-9.

115. Alam M, Agenor KK, Wang G, Reilly D, Vincent R, Alaghband-Zadeh J, et al. Raised plasma bile acids concentrations are related to change of GLP-1 two years after gastric bypass surgery (GBP) in patients with type 2 diabetes. Obesity. 2011;19(Suppl. 1):S156 (abstract 499P).

116. Myronovych A, Kirby M, Seeley RJ, Kohli R. Sleeve gastrectomy in obese mice results in elevated serum bile acids and reduced hepatic steatosis that correlate with weight loss post surgery. Gastroenterology. 2012;142(5 Suppl. 1):S13 (abstract 50).

117. Cummings BP, Bettaieb A, Graham JL, Stanhope KL, Kowala M, Haj FG, et al. Vertical sleeve gastrectomy improves glucose and lipid metabolism and delays diabetes onset in UCD-T2DM rats. Endocrinology. 2012;153(8):3620-32.

118. Myronovych A, Kirby M, Ryan KK, Zhang W, Jha P, Setchell KD, et al. Vertical sleeve gastrectomy reduces hepatic steatosis while increasing serum bile acids in a weight-loss-independent manner. Obesity. 2014;22(2):390-400.

119. Myronovych A, Salazar-Gonzalez RM, Miles L, Ryan KK, Seeley RJ, Kohli R. Short Heterodimer Partner (SHP) is necessary for the improvement in NASH after sleeve gastrectomy in obese mice. Hepatology. 2013;58(4 Suppl. 1):234A (abstract 54).

120. Stefater MA, Sandoval DA, Chambers AP, Wilson-Perez HE, Hofmann SM, Jandacek R, et al. Sleeve gastrectomy in rats improves postprandial lipid clearance by reducing intestinal triglyceride secretion. Gastroenterology. 2011;141(3):939-49 e1-4.

121. Kohli R, Myronovych A, Xanthakos S, Ryan KK, Jenkins T, Salazar-Gonzalez RM, et al. Sleeve gastrectomy in mice and humans results in weight loss independent suppression of hepatic bile acid synthesis. Gastroenterology. 2013;144(5):S319-S20 (abstract Sa1849).

122. Haluzikova D, Lacinova Z, Kavalkova P, Drapalova J, Krizova J, Bartlova M, et al. Laparoscopic sleeve gastrectomy differentially affects serum concentrations of FGF-19 and FGF-21 in morbidly obese subjects. Obesity. 2013;21(7):1335-42.

123. Belgaumkar AP, Vincent RP, Carswell KA, Dew T, Mitry RR, Le Roux CW, et al. Bile acid absorption does not change after laparoscopic sleeve gastrectomy. Obesity surgery. 2011;21(8):1106 (abstract P199).

124. Mencarelli A, Renga B, D'Amore C, Santorelli C, Graziosi L, Bruno A, et al. Dissociation of intestinal and hepatic activities of FXR and LXRalpha supports metabolic effects of terminal ileum interposition in rodents. Diabetes. 2013;62(10):3384-93.

125. Cummings BP, Bettaieb A, Graham JL, Kim J, Ma F, Shibata N, et al. Bile-acid-mediated decrease in endoplasmic reticulum stress: a potential contributor to the metabolic benefits of ileal interposition surgery in UCD-T2DM rats. Disease models & mechanisms. 2013;6(2):443-56.

126. Cummings BP, Strader AD, Stanhope KL, Graham JL, Lee J, Raybould HE, et al. Ileal interposition surgery improves glucose and lipid metabolism and delays diabetes onset in the UCD-T2DM rat. Gastroenterology. 2010;138(7):2437-46, 46 e1.

127. Habegger KM, Al-Massadi O, Heppner KM, Myronovych A, Holland J, Berger J, et al. Duodenal nutrient exclusion improves metabolic syndrome and stimulates villus hyperplasia. Gut. 2014;63(8):1238-46.

128. Stellaard F, Sackmann M, Sauerbruch T, Paumgartner G. Simultaneous determination of cholic acid and chenodeoxycholic acid pool sizes and fractional turnover rates in human serum using 13C-labeled bile acids. Journal of lipid research. 1984;25(12):1313-9.

129. Cohen DE. Balancing cholesterol synthesis and absorption in the gastrointestinal tract. Journal of clinical lipidology. 2008;2(2):S1-3.

130. West KL, Zern TL, Butteiger DN, Keller BT, Fernandez ML. SC-435, an ileal apical sodium co-dependent bile acid transporter (ASBT) inhibitor lowers plasma cholesterol and reduces atherosclerosis in guinea pigs. Atherosclerosis. 2003;171(2):201-10.

131. Li Q, Chen L, Yang Z, Ye Z, Huang Y, He M, et al. Metabolic effects of bariatric surgery in type 2 diabetic patients with body mass index < 35 kg/m2. Diabetes, obesity & metabolism. 2012;14(3):262-70.

132. Benetti A, Del Puppo M, Crosignani A, Veronelli A, Masci E, Frige F, et al. Cholesterol metabolism after bariatric surgery in grade 3 obesity: differences between malabsorptive and restrictive procedures. Diabetes care. 2013;36(6):1443-7.

133. Griffo E, Nosso G, Lupoli R, Cotugno M, Saldalamacchia G, Vitolo G, et al. Early improvement of postprandial lipemia after bariatric surgery in obese type 2 diabetic patients. Obesity surgery. 2014;24(5):765-70.

134. Graessler J, Bornstein TD, Goel D, Bhalla VP, Lohmann T, Wolf T, et al. Lipidomic profiling before and after Roux-en-Y gastric bypass in obese patients with diabetes. The pharmacogenomics journal. 2014;14(3):201-7.

135. Schultz JR, Tu H, Luk A, Repa JJ, Medina JC, Li L, et al. Role of LXRs in control of lipogenesis. Genes & development. 2000;14(22):2831-8.

136. Repa JJ, Liang G, Ou J, Bashmakov Y, Lobaccaro JM, Shimomura I, et al. Regulation of mouse sterol regulatory element-binding protein-1c gene (SREBP-1c) by oxysterol receptors, LXRalpha and LXRbeta. Genes & development. 2000;14(22):2819-30.

137. Horton JD, Goldstein JL, Brown MS. SREBPs: activators of the complete program of cholesterol and fatty acid synthesis in the liver. The Journal of clinical investigation. 2002;109(9):1125-31.

138. Houten SM, Watanabe M, Auwerx J. Endocrine functions of bile acids. The EMBO journal. 2006;25(7):1419-25.

139. Kast HR, Nguyen CM, Sinal CJ, Jones SA, Laffitte BA, Reue K, et al. Farnesoid X-activated receptor induces apolipoprotein C-II transcription: a molecular mechanism linking plasma triglyceride levels to bile acids. Molecular endocrinology. 2001;15(10):1720-8.

140. Kardassis D, Roussou A, Papakosta P, Boulias K, Talianidis I, Zannis VI. Synergism between nuclear receptors bound to specific hormone response elements of the hepatic control region-1 and the proximal apolipoprotein C-II promoter mediate apolipoprotein C-II gene regulation by bile acids and retinoids. The Biochemical journal. 2003;372(Pt 2):291-304.

141. Prieur X, Coste H, Rodriguez JC. The human apolipoprotein AV gene is regulated by peroxisome proliferator-activated receptor-alpha and contains a novel farnesoid X-activated receptor response element. The Journal of biological chemistry. 2003;278(28):25468-80.

142. Claudel T, Inoue Y, Barbier O, Duran-Sandoval D, Kosykh V, Fruchart J, et al. Farnesoid X receptor agonists suppress hepatic apolipoprotein CIII expression. Gastroenterology. 2003;125(2):544-55.

143. Desvergne B, Wahli W. Peroxisome proliferator-activated receptors: nuclear control of metabolism. Endocrine reviews. 1999;20(5):649-88.

144. Staels B, Dallongeville J, Auwerx J, Schoonjans K, Leitersdorf E, Fruchart JC. Mechanism of action of fibrates on lipid and lipoprotein metabolism. Circulation. 1998;98(19):2088-93.

145. Post SM, Duez H, Gervois PP, Staels B, Kuipers F, Princen HM. Fibrates suppress bile acid synthesis via peroxisome proliferator-activated receptor-alpha-mediated downregulation of cholesterol 7alpha-hydroxylase and sterol 27-hydroxylase expression. Arteriosclerosis, thrombosis, and vascular biology. 2001;21(11):1840-5.

146. Pineda Torra I, Claudel T, Duval C, Kosykh V, Fruchart JC, Staels B. Bile acids induce the expression of the human peroxisome proliferator-activated receptor alpha gene via activation of the farnesoid X receptor. Molecular endocrinology. 2003;17(2):259-72.

147. Claudel T, Staels B, Kuipers F. The Farnesoid X receptor: a molecular link between bile acid and lipid and glucose metabolism. Arteriosclerosis, thrombosis, and vascular biology. 2005;25(10):2020-30.

148. Lee J, Seok S, Yu P, Kim K, Smith Z, Rivas-Astroza M, et al. Genomic analysis of hepatic farnesoid X receptor binding sites reveals altered binding in obesity and direct gene repression by farnesoid X receptor in mice. Hepatology. 2012;56(1):108-17.

149. Heni M, Wagner R, Ketterer C, Bohm A, Linder K, Machicao F, et al. Genetic variation in NR1H4 encoding the bile acid receptor FXR determines fasting glucose and free fatty acid levels in humans. The Journal of clinical endocrinology and metabolism. 2013;98(7):E1224-9.

150. Kreymann B, Williams G, Ghatei MA, Bloom SR. Glucagon-like peptide-1 7-36: a physiological incretin in man. Lancet. 1987;2(8571):1300-4.

151. Yabe D, Seino Y. Two incretin hormones GLP-1 and GIP: comparison of their actions in insulin secretion and beta cell preservation. Progress in biophysics and molecular biology. 2011;107(2):248-56.

152. Willard FS, Sloop KW. Physiology and emerging biochemistry of the glucagon-like peptide-1 receptor. Experimental diabetes research. 2012;2012:470851.

153. Garber A, Henry R, Ratner R, Garcia-Hernandez PA, Rodriguez-Pattzi H, Olvera-Alvarez I, et al. Liraglutide versus glimepiride monotherapy for type 2 diabetes (LEAD-3 Mono): a randomised, 52-week, phase III, double-blind, parallel-treatment trial. Lancet. 2009;373(9662):473-81.

154. Zheng SL, Roddick AJ, Aghar-Jaffar R, Shun-Shin MJ, Francis D, Oliver N, et al. Association Between Use of Sodium-Glucose Cotransporter 2 Inhibitors, Glucagon-like Peptide 1 Agonists, and Dipeptidyl Peptidase 4 Inhibitors With All-Cause Mortality in Patients With Type 2 Diabetes: A Systematic Review and Meta-analysis. JAMA : the journal of the American Medical Association. 2018;319(15):1580-91.

155. Marso SP, Daniels GH, Brown-Frandsen K, Kristensen P, Mann JF, Nauck MA, et al. Liraglutide and Cardiovascular Outcomes in Type 2 Diabetes. The New England journal of medicine. 2016;375(4):311-22.

156. Mann JFE, Orsted DD, Brown-Frandsen K, Marso SP, Poulter NR, Rasmussen S, et al. Liraglutide and Renal Outcomes in Type 2 Diabetes. The New England journal of medicine. 2017;377(9):839-48.

157. Knop FK. Bile-induced secretion of glucagon-like peptide-1: pathophysiological implications in type 2 diabetes? American journal of physiology Endocrinology and metabolism. 2010;299(1):E10-3.

158. Katsuma S, Hirasawa A, Tsujimoto G. Bile acids promote glucagon-like peptide-1 secretion through TGR5 in a murine enteroendocrine cell line STC-1. Biochemical and biophysical research communications. 2005;329(1):386-90.

159. Parker HE, Wallis K, le Roux CW, Wong KY, Reimann F, Gribble FM. Molecular mechanisms underlying bile acid-stimulated glucagon-like peptide-1 secretion. British journal of pharmacology. 2012;165(2):414-23.

160. Adrian TE, Gariballa S, Parekh KA, Thomas SA, Saadi H, Al Kaabi J, et al. Rectal taurocholate increases L cell and insulin secretion, and decreases blood glucose and food intake in obese type 2 diabetic volunteers. Diabetologia. 2012;55(9):2343-7.

161. Morinigo R, Moize V, Musri M, Lacy AM, Navarro S, Marin JL, et al. Glucagon-like peptide-1, peptide YY, hunger, and satiety after gastric bypass surgery in morbidly obese subjects. The Journal of clinical endocrinology and metabolism. 2006;91(5):1735-40.

162. Pournaras DJ, Osborne A, Hawkins SC, Vincent RP, Mahon D, Ewings P, et al. Remission of type 2 diabetes after gastric bypass and banding: mechanisms and 2 year outcomes. Annals of surgery. 2010;252(6):966-71.

163. Laferrere B, Heshka S, Wang K, Khan Y, McGinty J, Teixeira J, et al. Incretin levels and effect are markedly enhanced 1 month after Roux-en-Y gastric bypass surgery in obese patients with type 2 diabetes. Diabetes care. 2007;30(7):1709-16.

164. Van der Schueren BJ, Homel P, Alam M, Agenor K, Wang G, Reilly D, et al. Magnitude and variability of the glucagon-like peptide-1 response in patients with type 2 diabetes up to 2 years following gastric bypass surgery. Diabetes care. 2012;35(1):42-6.

165. Salehi M, Prigeon RL, D'Alessio DA. Gastric bypass surgery enhances glucagon-like peptide 1-stimulated postprandial insulin secretion in humans. Diabetes. 2011;60(9):2308-14.

166. Alam ML, Van der Schueren BJ, Ahren B, Wang GC, Swerdlow NJ, Arias S, et al. Gastric bypass surgery, but not caloric restriction, decreases dipeptidyl peptidase-4 activity in obese patients with type 2 diabetes. Diabetes, obesity & metabolism. 2011;13(4):378-81.

167. Nakatani H, Kasama K, Oshiro T, Watanabe M, Hirose H, Itoh H. Serum bile acid along with plasma incretins and serum high-molecular weight adiponectin levels are increased after bariatric surgery. Metabolism: clinical and experimental. 2009;58(10):1400-7.

168. Laferrere B. Gut feelings about diabetes. Endocrinologia y Nutricion. 2012;59(4):254-60.

169. Fu L, John LM, Adams SH, Yu XX, Tomlinson E, Renz M, et al. Fibroblast growth factor 19 increases metabolic rate and reverses dietary and leptin-deficient diabetes. Endocrinology. 2004;145(6):2594-603.

170. Jimenez A, Casamitjana R, Viaplana-Masclans J, Lacy A, Vidal J. GLP-1 action and glucose tolerance in subjects with remission of type 2 diabetes after gastric bypass surgery. Diabetes care. 2013;36(7):2062-9.

171. Adrian TE, Ferri GL, Bacarese-Hamilton AJ, Fuessl HS, Polak JM, Bloom SR. Human distribution and release of a putative new gut hormone, peptide YY. Gastroenterology. 1985;89(5):1070-7.

172. Adrian TE, Ballantyne GH, Longo WE, Bilchik AJ, Graham S, Basson MD, et al. Deoxycholate is an important releaser of peptide YY and enteroglucagon from the human colon. Gut. 1993;34(9):1219-24.

173. Sato M, Shibata C, Kikuchi D, Ikezawa F, Imoto H, Sasaki I. Effects of biliary and pancreatic juice diversion into the ileum on gastrointestinal motility and gut hormone secretion in conscious dogs. Surgery. 2010;148(5):1012-9.

174. Ullmer C, Alvarez Sanchez R, Sprecher U, Raab S, Mattei P, Dehmlow H, et al. Systemic bile acid sensing by G protein-coupled bile acid receptor 1 (GPBAR1) promotes PYY and GLP-1 release. British journal of pharmacology. 2013;169(3):671-84.

175. Wu T, Bound MJ, Standfield SD, Gedulin B, Jones KL, Horowitz M, et al. Effects of rectal administration of taurocholic acid on glucagon-like peptide-1 and peptide YY secretion in healthy humans. Diabetes, obesity & metabolism. 2013;15(5):474-7.

176. le Roux CW, Welbourn R, Werling M, Osborne A, Kokkinos A, Laurenius A, et al. Gut hormones as mediators of appetite and weight loss after Roux-en-Y gastric bypass. Annals of surgery. 2007;246(5):780-5.

177. Mizutani S, Miyata M, Izukura M, Tanaka Y, Matsuda H. Role of bile and trypsin in the release of cholecystokinin in humans. Pancreas. 1995;10(2):194-9.

178. Koop I, Schindler M, Bosshammer A, Scheibner J, Stange E, Koop H. Physiological control of cholecystokinin release and pancreatic enzyme secretion by intraduodenal bile acids. Gut. 1996;39(5):661-7.

179. Lee WJ, Chen CY, Chong K, Lee YC, Chen SC, Lee SD. Changes in postprandial gut hormones after metabolic surgery: a comparison of gastric bypass and sleeve gastrectomy. Surgery for obesity and related diseases : official journal of the American Society for Bariatric Surgery. 2011;7(6):683-90.

180. Ogundare M, Theofilopoulos S, Lockhart A, Hall LJ, Arenas E, Sjovall J, et al. Cerebrospinal fluid steroidomics: are bioactive bile acids present in brain? The Journal of biological chemistry. 2010;285(7):4666-79.

181. Keitel V, Gorg B, Bidmon HJ, Zemtsova I, Spomer L, Zilles K, et al. The bile acid receptor TGR5 (Gpbar-1) acts as a neurosteroid receptor in brain. Glia. 2010;58(15):1794-805.

182. Morton GJ, Matsen ME, Bracy DP, Meek TH, Nguyen HT, Stefanovski D, et al. FGF19 action in the brain induces insulin-independent glucose lowering. The Journal of clinical investigation. 2013;123(11):4799-808.

183. Bueter M, Lowenstein C, Olbers T, Wang M, Cluny NL, Bloom SR, et al. Gastric bypass increases energy expenditure in rats. Gastroenterology. 2010;138(5):1845-53.

184. Nestoridi E, Kvas S, Kucharczyk J, Stylopoulos N. Resting energy expenditure and energetic cost of feeding are augmented after Roux-en-Y gastric bypass in obese mice. Endocrinology. 2012;153(5):2234-44.

185. Faria SL, Faria OP, Cardeal Mde A, Ito MK, Buffington C. Diet-induced thermogenesis and respiratory quotient after Roux-en-Y gastric bypass surgery: a prospective study. Surgery for obesity and related diseases : official journal of the American Society for Bariatric Surgery. 2014;10(1):138-43.

186. Schmidt JBS, Gregersen NTG, Pedersen SP, Nielsen MSN, Nielsen LVN, Holst JJH, et al. The effect of Roux-en-Y gastric bypass surgery on energy expenditure and Appetite: A Randomized Human Study including "Pair fed" control subjects. Obesity Facts. 2013;6(Suppl. 1):28 (abstract T5:OS1.5).

187. Watanabe M, Houten SM, Mataki C, Christoffolete MA, Kim BW, Sato H, et al. Bile acids induce energy expenditure by promoting intracellular thyroid hormone activation. Nature. 2006;439(7075):484-9.

188. Arrojo EDR, Bianco AC. Type 2 deiodinase at the crossroads of thyroid hormone action. The international journal of biochemistry & cell biology. 2011;43(10):1432-41.

189. Zhang JH, Nolan JD, Kennie SL, Johnston IM, Dew T, Dixon PH, et al. Potent stimulation of fibroblast growth factor 19 expression in the human ileum by bile acids. American journal of physiology Gastrointestinal and liver physiology. 2013;304(10):G940-8.

190. Wu X, Lemon B, Li X, Gupte J, Weiszmann J, Stevens J, et al. C-terminal tail of FGF19 determines its specificity toward Klotho co-receptors. The Journal of biological chemistry. 2008;283(48):33304-9.

191. Xie MH, Holcomb I, Deuel B, Dowd P, Huang A, Vagts A, et al. FGF-19, a novel fibroblast growth factor with unique specificity for FGFR4. Cytokine. 1999;11(10):729-35.

192. Hughes SE. Differential expression of the fibroblast growth factor receptor (FGFR) multigene family in normal human adult tissues. The journal of histochemistry and cytochemistry : official journal of the Histochemistry Society. 1997;45(7):1005-19.

193. Tomlinson E, Fu L, John L, Hultgren B, Huang X, Renz M, et al. Transgenic mice expressing human fibroblast growth factor-19 display increased metabolic rate and decreased adiposity. Endocrinology. 2002;143(5):1741-7.

194. Fritz IB, Marquis NR. The role of acylcarnitine esters and carnitine palmityltransferase in the transport of fatty acyl groups across mitochondrial membranes. Proceedings of the National Academy of Sciences of the United States of America. 1965;54(4):1226-33.

195. Ozcan U, Yilmaz E, Ozcan L, Furuhashi M, Vaillancourt E, Smith RO, et al. Chemical chaperones reduce ER stress and restore glucose homeostasis in a mouse model of type 2 diabetes. Science. 2006;313(5790):1137-40.

196. Midtvedt T, Norman A, Nygaard K. Bile acid transforming micro-organisms in rats with an intestinal blind segment. Acta pathologica et microbiologica Scandinavica. 1969;77(1):162-6.

197. Berr F, Kullak-Ublick GA, Paumgartner G, Munzing W, Hylemon PB. 7 alpha-dehydroxylating bacteria enhance deoxycholic acid input and cholesterol saturation of bile in patients with gallstones. Gastroenterology. 1996;111(6):1611-20.

198. Miyata M, Yamakawa H, Hamatsu M, Kuribayashi H, Takamatsu Y, Yamazoe Y. Enterobacteria modulate intestinal bile acid transport and homeostasis through apical sodium-dependent bile acid transporter (SLC10A2) expression. The Journal of pharmacology and experimental therapeutics. 2011;336(1):188-96.

199. Neimark E, Chen F, Li X, Shneider BL. Bile acid-induced negative feedback regulation of the human ileal bile acid transporter. Hepatology. 2004;40(1):149-56.

200. Sinha J, Chen F, Miloh T, Burns RC, Yu Z, Shneider BL. beta-Klotho and FGF-15/19 inhibit the apical sodium-dependent bile acid transporter in enterocytes and cholangiocytes. American journal of physiology Gastrointestinal and liver physiology. 2008;295(5):G996-G1003.

201. Furet JP, Kong LC, Tap J, Poitou C, Basdevant A, Bouillot JL, et al. Differential adaptation of human gut microbiota to bariatric surgery-induced weight loss: links with metabolic and low-grade inflammation markers. Diabetes. 2010;59(12):3049-57.

202. Zhang H, DiBaise JK, Zuccolo A, Kudrna D, Braidotti M, Yu Y, et al. Human gut microbiota in obesity and after gastric bypass. Proceedings of the National Academy of Sciences of the United States of America. 2009;106(7):2365-70.

203. Kuribayashi H, Miyata M, Yamakawa H, Yoshinari K, Yamazoe Y. Enterobacteria-mediated deconjugation of taurocholic acid enhances ileal farnesoid X receptor signaling. European journal of pharmacology. 2012;697(1-3):132-8.

204. Islam KB, Fukiya S, Hagio M, Fujii N, Ishizuka S, Ooka T, et al. Bile acid is a host factor that regulates the composition of the cecal microbiota in rats. Gastroenterology. 2011;141(5):1773-81.

205. Yokota A, Fukiya S, Islam KB, Ooka T, Ogura Y, Hayashi T, et al. Is bile acid a determinant of the gut microbiota on a high-fat diet? Gut microbes. 2012;3(5):455-9.

206. Ridlon JM, Alves JM, Hylemon PB, Bajaj JS. Cirrhosis, bile acids and gut microbiota: unraveling a complex relationship. Gut microbes. 2013;4(5):382-7.

207. Kakiyama G, Pandak WM, Gillevet PM, Hylemon PB, Heuman DM, Daita K, et al. Modulation of the fecal bile acid profile by gut microbiota in cirrhosis. Journal of hepatology. 2013;58(5):949-55.

208. Kong LC, Tap J, Aron-Wisnewsky J, Pelloux V, Basdevant A, Bouillot JL, et al. Gut microbiota after gastric bypass in human obesity: increased richness and associations of bacterial genera with adipose tissue genes. The American journal of clinical nutrition. 2013;98(1):16-24.

209. Sweeney TE, Morton JM. The human gut microbiome: a review of the effect of obesity and surgically induced weight loss. JAMA surgery. 2013;148(6):563-9.

210. Eckburg PB, Bik EM, Bernstein CN, Purdom E, Dethlefsen L, Sargent M, et al. Diversity of the human intestinal microbial flora. Science. 2005;308(5728):1635-8.

211. Scheithauer TP, Dallinga-Thie GM, de Vos WM, Nieuwdorp M, van Raalte DH. Causality of small and large intestinal microbiota in weight regulation and insulin resistance. Mol Metab. 2016;5(9):759-70.

212. Larsson E, Tremaroli V, Lee YS, Koren O, Nookaew I, Fricker A, et al. Analysis of gut microbial regulation of host gene expression along the length of the gut and regulation of gut microbial ecology through MyD88. Gut. 2012;61(8):1124-31.

213. MacHado AD, Forster-Fromme K, Mitra S, Friedrich A, Kramer K, Huson DH, et al. Competence network obesity: An integrated multi -omics approach to study the guest-host metabolic interaction during restrictive obesity intervention. Obesity Facts. 2012;5(Suppl. 2):4-5.

214. Cani PD, Plovier H, Van Hul M, Geurts L, Delzenne NM, Druart C, et al. Endocannabinoids--at the crossroads between the gut microbiota and host metabolism. Nature reviews Endocrinology. 2016;12(3):133-43.

215. Tee MC, Cao Y, Warnock GL, Hu FB, Chavarro JE. Effect of bariatric surgery on oncologic outcomes: a systematic review and meta-analysis. Surgical endoscopy. 2013;27(12):4449-56.

216. Ostlund MP, Lu Y, Lagergren J. Risk of obesity-related cancer after obesity surgery in a population-based cohort study. Annals of surgery. 2010;252(6):972-6.

217. Li JV, Reshat R, Wu Q, Ashrafian H, Bueter M, le Roux CW, et al. Experimental bariatric surgery in rats generates a cytotoxic chemical environment in the gut contents. Frontiers in microbiology. 2011;2:183.

218. Katona BW, Anant S, Covey DF, Stenson WF. Characterization of enantiomeric bile acid-induced apoptosis in colon cancer cell lines. The Journal of biological chemistry. 2009;284(5):3354-64.

219. Bernstein H, Bernstein C, Payne CM, Dvorak K. Bile acids as endogenous etiologic agents in gastrointestinal cancer. World journal of gastroenterology : WJG. 2009;15(27):3329-40.

220. Pearson JR, Gill CI, Rowland IR. Diet, fecal water, and colon cancer--development of a biomarker. Nutrition reviews. 2009;67(9):509-26.

221. Santarelli RL, Pierre F, Corpet DE. Processed meat and colorectal cancer: a review of epidemiologic and experimental evidence. Nutrition and cancer. 2008;60(2):131-44.

222. Cohen BI, Raicht RF. Effects of bile acids on colon carcinogenesis in rats treated with carcinogens. Cancer research. 1981;41(9 Pt 2):3759-60.

223. Koga S, Kaibara N, Takeda R. Effect of bile acids on 1,2-dimethylhydrazine-induced colon cancer in rats. Cancer. 1982;50(3):543-7.

224. Reiss B, Weiss CJ, Tanaka T, Reddy B, Williams GM. Effects of bile acids on carcinogen-exposed rat colon in organ culture and as subsequent long-term transplants. Journal of the National Cancer Institute. 1987;78(1):107-13.

225. Payne CM, Bernstein C, Dvorak K, Bernstein H. Hydrophobic bile acids, genomic instability, Darwinian selection, and colon carcinogenesis. Clin Exp Gastroenterol. 2008;1:19-47.

226. Ignacio Barrasa J, Olmo N, Perez-Ramos P, Santiago-Gomez A, Lecona E, Turnay J, et al. Deoxycholic and chenodeoxycholic bile acids induce apoptosis via oxidative stress in human colon adenocarcinoma cells. Apoptosis. 2011;16(10):1054-67.

227. Nguyen TT, Ung TT, Kim NH, Jung YD. Role of bile acids in colon carcinogenesis. World J Clin Cases. 2018;6(13):577-88.

228. Qiao D, Gaitonde SV, Qi W, Martinez JD. Deoxycholic acid suppresses p53 by stimulating proteasome-mediated p53 protein degradation. Carcinogenesis. 2001;22(6):957-64.

229. Morvay K, Szentleleki K, Torok G, Pinter A, Borzsonyi M, Nawroth R. Effect of change of fecal bile acid excretion achieved by operative procedures on 1,2-dimethylhydrazine-induced colon cancer in rats. Diseases of the colon and rectum. 1989;32(10):860-3.

230. Savage AP, Sian MS, Matthews JL, Bloom SR, Cooke T. Experimental colonic carcinogenesis: changes in faecal bile acids after promotion of intestinal tumours by small bowel resection in the rat. Gut. 1988;29(4):495-502.

231. Kanamoto R, Azuma N, Suda H, Saeki T, Tsuchihashi Y, Iwami K. Elimination of Na+-dependent bile acid transporter from small intestine by ileum resection increases [correction of increase] colonic tumorigenesis in the rat fed deoxycholic acid. Cancer letters. 1999;145(1-2):115-20.

232. Houghton PW, Owen RJ, Henly PJ, Mortensen NJ, Hill MJ, Williamson RC. Experimental colonic carcinogenesis after gastric surgery. The British journal of surgery. 1990;77(7):774-8.

233. Adami GF, Papadia FS, Marinari GM, Camerini GB, Scopinaro N. Does biliopancreatic diversion carry increased risk for colorectal cancer? A cohort study. Obesity surgery. 2008;18(2):212-5.

234. Mahawar KK, Carr WR, Balupuri S, Small PK. Controversy surrounding 'mini' gastric bypass. Obesity surgery. 2014;24(2):324-33.

235. Musella M, Milone M. Still "controversies" about the mini gastric bypass? Obesity surgery. 2014;24(4):643-4.

236. Modica S, Murzilli S, Salvatore L, Schmidt DR, Moschetta A. Nuclear bile acid receptor FXR protects against intestinal tumorigenesis. Cancer research. 2008;68(23):9589-94.

237. Giordano C, Catalano S, Panza S, Vizza D, Barone I, Bonofiglio D, et al. Farnesoid X receptor inhibits tamoxifen-resistant MCF-7 breast cancer cell growth through downregulation of HER2 expression. Oncogene. 2011;30(39):4129-40.

238. Goldberg AA, Beach A, Davies GF, Harkness TA, Leblanc A, Titorenko VI. Lithocholic bile acid selectively kills neuroblastoma cells, while sparing normal neuronal cells. Oncotarget. 2011;2(10):761-82.

239. Kim ND, Im E, Yoo YH, Choi YH. Modulation of the cell cycle and induction of apoptosis in human cancer cells by synthetic bile acids. Current cancer drug targets. 2006;6(8):681-9.

240. Goldberg AA, Titorenko VI, Beach A, Sanderson JT. Bile acids induce apoptosis selectively in androgen-dependent and -independent prostate cancer cells. PeerJ. 2013;1:e122.

241. Escalona A, Munoz R, Irribarra V, Solari S, Allende F, Francisco Miquel J. Bile acids synthesis decreases after laparoscopic sleeve gastrectomy. Surgery for obesity and related diseases : official journal of the American Society for Bariatric Surgery. 2016;12(4):763-9.

242. Chavez-Talavera O, Baud G, Spinelli V, Daoudi M, Kouach M, Goossens JF, et al. Roux-en-Y gastric bypass increases systemic but not portal bile acid concentrations by decreasing hepatic bile acid uptake in minipigs. International journal of obesity. 2017;41(4):664-8.

243. Wei M, Shao Y, Liu QR, Wu QZ, Zhang X, Zhong MW, et al. Bile acid profiles within the enterohepatic circulation in a diabetic rat model after bariatric surgeries. American journal of physiology Gastrointestinal and liver physiology. 2018;314(5):G537-G46.

244. Flynn CR, Albaugh VL, Cai S, Cheung-Flynn J, Williams PE, Brucker RM, et al. Bile diversion to the distal small intestine has comparable metabolic benefits to bariatric surgery. Nature communications. 2015;6:7715.

245. Albaugh VL, Flynn CR, Cai S, Xiao Y, Tamboli RA, Abumrad NN. Early Increases in Bile Acids Post Roux-en-Y Gastric Bypass Are Driven by Insulin-Sensitizing, Secondary Bile Acids. The Journal of clinical endocrinology and metabolism. 2015;100(9):E1225-33.

246. Risstad H, Kristinsson JA, Fagerland MW, le Roux CW, Birkeland KI, Gulseth HL, et al. Bile acid profiles over 5 years after gastric bypass and duodenal switch: results from a randomized clinical trial. Surgery for obesity and related diseases : official journal of the American Society for Bariatric Surgery. 2017;13(9):1544-53.

247. Belgaumkar AP, Vincent RP, Carswell KA, Hughes RD, Alaghband-Zadeh J, Mitry RR, et al. Changes in Bile Acid Profile After Laparoscopic Sleeve Gastrectomy are Associated with Improvements in Metabolic Profile and Fatty Liver Disease. Obesity surgery. 2016;26(6):1195-202.

248. Jahansouz C, Xu H, Hertzel AV, Serrot FJ, Kvalheim N, Cole A, et al. Bile Acids Increase Independently From Hypocaloric Restriction After Bariatric Surgery. Annals of surgery. 2016;264(6):1022-8.

249. Sachdev S, Wang Q, Billington C, Connett J, Ahmed L, Inabnet W, et al. FGF 19 and Bile Acids Increase Following Roux-en-Y Gastric Bypass but Not After Medical Management in Patients with Type 2 Diabetes. Obesity surgery. 2016;26(5):957-65.

250. Lindqvist A, Ekelund M, Garcia-Vaz E, Stahlman M, Pierzynowski S, Gomez MF, et al. The impact of Roux-en-Y gastric bypass surgery on normal metabolism in a porcine model. PloS one. 2017;12(3):e0173137.

251. Luo P, Yu H, Zhao X, Bao Y, Hong CS, Zhang P, et al. Metabolomics Study of Roux-en-Y Gastric Bypass Surgery (RYGB) to Treat Type 2 Diabetes Patients Based on Ultraperformance Liquid Chromatography-Mass Spectrometry. Journal of proteome research. 2016;15(4):1288-99.

252. Biswas A, Oh PI, Faulkner GE, Bajaj RR, Silver MA, Mitchell MS, et al. Sedentary time and its association with risk for disease incidence, mortality, and hospitalization in adults: a systematic review and meta-analysis. Annals of internal medicine. 2015;162(2):123-32.

253. Same RV, Feldman DI, Shah N, Martin SS, Al Rifai M, Blaha MJ, et al. Relationship Between Sedentary Behavior and Cardiovascular Risk. Curr Cardiol Rep. 2016;18(1):6.

254. Wilmot EG, Edwardson CL, Achana FA, Davies MJ, Gorely T, Gray LJ, et al. Sedentary time in adults and the association with diabetes, cardiovascular disease and death: systematic review and meta-analysis. Diabetologia. 2012;55(11):2895-905.

255. O'Sullivan O, Cronin O, Clarke SF, Murphy EF, Molloy MG, Shanahan F, et al. Exercise and the microbiota. Gut microbes. 2015;6(2):131-6.

256. Rebholz CM, Gu D, Chen J, Huang JF, Cao J, Chen JC, et al. Physical activity reduces salt sensitivity of blood pressure: the Genetic Epidemiology Network of Salt Sensitivity Study. Am J Epidemiol. 2012;176 Suppl 7:S106-13.

257. Carnethon MR, Evans NS, Church TS, Lewis CE, Schreiner PJ, Jacobs DR, Jr., et al. Joint associations of physical activity and aerobic fitness on the development of incident hypertension: coronary artery risk development in young adults. Hypertension. 2010;56(1):49-55.

258. Tuomilehto J, Lindstrom J, Eriksson JG, Valle TT, Hamalainen H, Ilanne-Parikka P, et al. Prevention of type 2 diabetes mellitus by changes in lifestyle among subjects with impaired glucose tolerance. The New England journal of medicine. 2001;344(18):1343-50.

259. Schwingshackl L, Missbach B, Dias S, Konig J, Hoffmann G. Impact of different training modalities on glycaemic control and blood lipids in patients with type 2 diabetes: a systematic review and network meta-analysis. Diabetologia. 2014;57(9):1789-97.

260. Kyu HH, Bachman VF, Alexander LT, Mumford JE, Afshin A, Estep K, et al. Physical activity and risk of breast cancer, colon cancer, diabetes, ischemic heart disease, and ischemic stroke events: systematic review and dose-response meta-analysis for the Global Burden of Disease Study 2013. Bmj. 2016;354:i3857.

261. Harkin A. Muscling in on depression. The New England journal of medicine. 2014;371(24):2333-4.

262. Bherer L, Erickson KI, Liu-Ambrose T. A review of the effects of physical activity and exercise on cognitive and brain functions in older adults. J Aging Res. 2013;2013:657508.

263. Benatti FB, Pedersen BK. Exercise as an anti-inflammatory therapy for rheumatic diseases-myokine regulation. Nat Rev Rheumatol. 2015;11(2):86-97.

264. Hawley JA, Krook A. Metabolism: One step forward for exercise. Nature reviews Endocrinology. 2016;12(1):7-8.

265. Hawley JA, Hargreaves M, Joyner MJ, Zierath JR. Integrative biology of exercise. Cell. 2014;159(4):738-49.

266. Hoffman-Goetz L, Pervaiz N, Packer N, Guan J. Freewheel training decreases pro- and increases anti-inflammatory cytokine expression in mouse intestinal lymphocytes. Brain Behav Immun. 2010;24(7):1105-15.

267. Mul JD, Stanford KI, Hirshman MF, Goodyear LJ. Exercise and Regulation of Carbohydrate Metabolism. Prog Mol Biol Transl Sci. 2015;135:17-37.

268. Hoffman NJ, Parker BL, Chaudhuri R, Fisher-Wellman KH, Kleinert M, Humphrey SJ, et al. Global Phosphoproteomic Analysis of Human Skeletal Muscle Reveals a Network of Exercise-Regulated Kinases and AMPK Substrates. Cell metabolism. 2015;22(5):922-35.

269. Halverstadt A, Phares DA, Wilund KR, Goldberg AP, Hagberg JM. Endurance exercise training raises high-density lipoprotein cholesterol and lowers small low-density lipoprotein and very low-density lipoprotein independent of body fat phenotypes in older men and women. Metabolism: clinical and experimental. 2007;56(4):444-50.

270. Durstine JL, Grandjean PW, Cox CA, Thompson PD. Lipids, lipoproteins, and exercise. J Cardiopulm Rehabil. 2002;22(6):385-98.

271. Paffenbarger RS, Jr., Hyde RT, Wing AL, Lee IM, Jung DL, Kampert JB. The association of changes in physical-activity level and other lifestyle characteristics with mortality among men. The New England journal of medicine. 1993;328(8):538-45.

272. Farahnak Z, Magri Tomaz L, Bergeron R, Chapados N, Lavoie JM. The effect of exercise training on upregulation of molecular markers of bile acid metabolism in the liver of ovariectomized rats fed a cholesterol-rich diet. ARYA Atheroscler. 2017;13(4):184-92.

273. Meissner M, Lombardo E, Havinga R, Tietge UJ, Kuipers F, Groen AK. Voluntary wheel running increases bile acid as well as cholesterol excretion and decreases atherosclerosis in hypercholesterolemic mice. Atherosclerosis. 2011;218(2):323-9.

274. Meissner M, Nijstad N, Kuipers F, Tietge UJ. Voluntary exercise increases cholesterol efflux but not macrophage reverse cholesterol transport in vivo in mice. Nutr Metab (Lond). 2010;7:54.

275. Wilund KR, Feeney LA, Tomayko EJ, Chung HR, Kim K. Endurance exercise training reduces gallstone development in mice. J Appl Physiol (1985). 2008;104(3):761-5.

276. Pinto PR, Rocco DD, Okuda LS, Machado-Lima A, Castilho G, da Silva KS, et al. Aerobic exercise training enhances the in vivo cholesterol trafficking from macrophages to the liver independently of changes in the expression of genes involved in lipid flux in macrophages and aorta. Lipids Health Dis. 2015;14:109.

277. Hagio M, Matsumoto M, Yajima T, Hara H, Ishizuka S. Voluntary wheel running exercise and dietary lactose concomitantly reduce proportion of secondary bile acids in rat feces. J Appl Physiol (1985). 2010;109(3):663-8.

278. Nieman DC, Shanely RA, Gillitt ND, Pappan KL, Lila MA. Serum metabolic signatures induced by a three-day intensified exercise period persist after 14 h of recovery in runners. Journal of proteome research. 2013;12(10):4577-84.

279. Pechlivanis A, Kostidis S, Saraslanidis P, Petridou A, Tsalis G, Mougios V, et al. (1)H NMR-based metabonomic investigation of the effect of two different exercise sessions on the metabolic fingerprint of human urine. Journal of proteome research. 2010;9(12):6405-16.

280. Pechlivanis A, Chatziioannou AC, Veskoukis AS, Kouretas D, Mougios V, Theodoridis GA. GC-MS analysis of blood for the metabonomic investigation of the effects of physical exercise and allopurinol administration on rats. Journal of chromatography B, Analytical technologies in the biomedical and life sciences. 2014;966:127-31.

281. Estaki M, Pither J, Baumeister P, Little JP, Gill SK, Ghosh S, et al. Cardiorespiratory fitness as a predictor of intestinal microbial diversity and distinct metagenomic functions. Microbiome. 2016;4(1):42.

282. Johannesson E, Simren M, Strid H, Bajor A, Sadik R. Physical activity improves symptoms in irritable bowel syndrome: a randomized controlled trial. The American journal of gastroenterology. 2011;106(5):915-22.

283. Robsahm TE, Aagnes B, Hjartaker A, Langseth H, Bray FI, Larsen IK. Body mass index, physical activity, and colorectal cancer by anatomical subsites: a systematic review and meta-analysis of cohort studies. Eur J Cancer Prev. 2013;22(6):492-505.

284. Ou J, Carbonero F, Zoetendal EG, DeLany JP, Wang M, Newton K, et al. Diet, microbiota, and microbial metabolites in colon cancer risk in rural Africans and African Americans. The American journal of clinical nutrition. 2013;98(1):111-20.

285. Grenham S, Clarke G, Cryan JF, Dinan TG. Brain-gut-microbe communication in health and disease. Front Physiol. 2011;2:94.

286. Clarke SF, Murphy EF, O'Sullivan O, Lucey AJ, Humphreys M, Hogan A, et al. Exercise and associated dietary extremes impact on gut microbial diversity. Gut. 2014;63(12):1913-20.

287. Petersen LM, Bautista EJ, Nguyen H, Hanson BM, Chen L, Lek SH, et al. Community characteristics of the gut microbiomes of competitive cyclists. Microbiome. 2017;5(1):98.

288. Cronin O, Molloy MG, Shanahan F. Exercise, fitness, and the gut. Curr Opin Gastroenterol. 2016;32(2):67-73.

2 Analytical Strategies

The analytical pipeline for metabonomics involves analysis of biofluid samples using a variety of analytical platforms, followed by computational modelling in order to detect multicomponent metabolic patterns that enable biomarker identification or elucidation of biological mechanisms of physiology / pathology.

2.1 Metabonomic platforms

Metabolites within a biofluid are commonly measured using either nuclear magnetic resonance (NMR) spectroscopy or mass spectrometry (MS). Each technique carries inherent strengths and weaknesses as detailed below:

	Mass Spectrometry	**NMR Spectroscopy**
Advantages	• ***Highly sensitive to metabolites in low concentrations (several orders of magnitude more sensitive than NMR)*** • ***Can deliver quantitative information on specific pathways or metabolite classes when run in targeted mode*** • ***Can obtain structural information of metabolites***	• ***Simple and non-destructive sample preparation*** • ***Quantification of metabolites is precise*** • ***Readily reproducible*** • ***Can obtain structural information of metabolites***
Disadvantages	• ***Difficulties in accurately quantifying metabolites*** • ***Analysis requires sample destruction*** • ***Less reproducible (LC-MS)*** • ***Difficult metabolite identification (LC-MS)***	• ***Less sensitive to metabolites in low concentrations***

Table 2.1-1 Advantages and Disadvantages of Mass Spectrometry versus NMR Spectroscopy

2.2 NMR principles

2.2.1 Nuclear Spin

Nuclear magnetic resonance (NMR) spectroscopy relies on the quantum mechanical property of atomic nuclei termed 'spin'. This was first demonstrated by Gerlach and the Nobel laureate Stern in 1922, who split a beam of silver atoms into two beams using an externally applied magnetic field, representing the two, α and β spin states of the silver nucleus[289]. When the neutrons and protons of a nucleus are an even number, the particle rotations are paired against each other, such that there is no overall spin. Whereas an odd number of protons or neutrons or both results in unbalanced spins, creating an overall net spin. If the overall number of neutrons plus protons is odd then the nucleus has a half integer spin, while if the number of neutrons and protons are both odd the nucleus has an integer spin[290].

A nucleus with spin (S) has 2S + 1 possible orientation states. Hence, in organic chemistry the elemental isotopes ^{1}H, ^{13}C, ^{19}F and ^{31}P are of particular interest as they each possess a spin (S) of ½. Thus, resulting in 2 possible spin states, which greatly simplifies subsequent spectral interpretation[290].

2.2.2 Magnetic resonance

When placed under a magnetic field, nuclei with two spin states adopt a spin state parallel or anti-parallel to the applied magnetic field axis. The energy states of these two spin configurations is non-equivalent and the initial populations of each state are governed by thermodynamics, as described by the Boltzmann distribution[291]. Accordingly, more nuclei exist in the low energy state than high energy. Low energy nuclei can be excited to the high energy state when subjected to electromagnetic radiation at the Larmor frequency, which is determined by the frequency with which the nucleus precesses around the magnetic field axis[291, 292]. When the radiofrequency electromagnetic pulse is withdrawn the nuclei revert back to their prior low energy state. In the process, they emit an oscillating radiofrequency signal, called a Free Induction Decay (FID). The FID detected in the NMR receiver coils undergoes a Fourier transformation to convert the signal from the time domain to the frequency domain and subsequently generates the NMR spectrum[293].

2.2.3 Chemical shift & multiplicity

The mainstay of NMR analysis in organic chemistry relies on ^{1}H-NMR due to the high abundance of ^{1}H in organic compounds. NMR is based on quantum mechanics and is therefore inherently quantitative. The peak area of a derived signal for a specific molecule is proportional to the number of nuclei present and hence the molecules concentration in the sample. Compounds can be differentiated from each other using their characteristic chemical shift and multiplicity which are influenced by the immediate electron density surrounding a proton and the number of neighbouring protons in the molecule:

When a magnetic field is applied, the magnetic field at the nucleus is not equal to this applied field due to shielding of the nucleus from surrounding electrons. The nuclear shielding of the same type of nucleus (e.g. ^{1}H) varies according to local factors such as binding partners, bond lengths and angles. This causes changes in the resonance frequency of the nuclei of different compounds, known as chemical shift. Chemical shift, measured in part per million (ppm), is defined as nuclear shielding / applied magnetic field. It is measured relative to a reference sample with a low distortion of the electron distribution[292, 293]. In the NMR experiments within this thesis 3-(trimethylsilyl)-[2,2,3,3,-$^{2}H_4$]-propionic acid (TSP) is used and has a designated chemical shift of 0.0 ppm.

A nucleus in isolation will result in a single peak. However, neighbouring nuclei can create spin-spin *J*-coupling resulting in splitting of the resonance frequency into multiple peaks. The multiplicity of a signal reflects the number of adjacent protons (n), equivalent to themselves but non-equivalent to the coupled proton. The number of possible magnetically different combinations of these adjacent protons is given by n+1. In a first order spectrum, this results in a multiplicity of the coupled proton of n+1. The distance between the peaks is termed the coupling constant (*J*) and is measured in Hertz. Since *J*-coupling results from the magnetic field of other nuclei it is constant and not affected by the applied magnetic field[292, 293].

A second frequency domain can be added to 1D NMR experiments (2D NMR) to provide further ^{1}H or ^{13}C spectral information and is useful to help determine molecular structures.

2.3 Mass Spectrometry principles

2.3.1 Chromatography

Mass spectrometry is commonly performed in combination with a chromatography technique to allow separation of compounds in the time domain (Retention Time). Different techniques have been used successfully with mass spectrometry including: liquid chromatography (LC), gas chromatography (GC) and capillary electrophoresis. In this thesis liquid and gas chromatography are used.

Liquid chromatography is well suited to water soluble compounds such as those found in urine and blood. Liquid chromatography employs the use of a mobile phase run against a stationary phase to separate analytes. Technological advances, including packing stationary columns with smaller particles and delivering mobile phases at higher pressures, has enabled superior separation of compounds while also reducing analysis time compared to standard chromatography columns: so called ultra-performance liquid chromatography (UPLC). UPLC can be performed in a number of different ways in order to optimise separation of metabolites of interest and minimise co-elution. Reversed-phase (RP) chromatography employs a hydrophobic stationary phase and a polar mobile phase. This is well suited to separation of non-polar and medium polar analytes. To ensure retention of polar compounds the mobile phase is initially mainly aqueous and acidified, hence is of low elutropic strength. A gradient of increasing levels of organic solvent is then used to elute the analytes. This technique has been adapted for use with both urine and blood samples[294]. Within blood, lipids are of particular interest and their separation is enhanced through the use of a stationary phase with a low positively charged surface[295]. However, using RP techniques highly polar compounds are not retained and elute with the initial void volume. For highly polar analytes hydrophilic interaction chromatography (HILIC) is well suited. This employs a polar mobile phase but hydrophilic stationary phase[294].

Gas chromatography is well suited to volatile compounds. It is more stable and readily reproducible than LC-MS based techniques and highly sensitive. As a result, at present there are more compounds defined in GC-MS databases than for LC-MS. However, GC typically requires derivatisation and is reliant on the compounds of interest being volatile or able to be made volatile after derivatisation. GC utilises an inert carrier gas as the mobile phase, while

the stationary phase is a coated column. The stationary phase can vary in polarity, as well as column length and diameter. Analytes start in the liquid phase and are subjected to a gradient of increasing temperature within the column[296].

2.3.2 Mass Spectrometry

Mass spectrometry (MS) is founded on the measurement of mass-to-charge (m/z) ratios of charged molecules, where z is the charge value divided by the elementary charge constant (e, 1.6022 x 10^{-9}). MS relies on a number of different modules within the mass spectrometer including: injection, ion source, analyser and detection modules.

The injection can either be direct or in combination with chromatography techniques such as LC or GC as described previously, to allow separation of compounds in the time domain before injection into the mass spectrometer.

Positively or negatively charged ions are then generated within the ion source module. A number of different ionisation methods have been described. The experiments conducted using UPLC-MS within this thesis utilise electrospray ionisation (ESI), developed by Fenn, for which he was awarded a Nobel Prize in Chemistry[297]. ESI is known as a 'soft' ionisation technique as it allows the generation of intact ions of organic molecules of interest, that are fragile and otherwise susceptible to fragmentation using other ionisation methods. ESI generates an aerosol of charged particles through the application of high voltage to the injection liquid as it is sprayed from a narrow capillary. Compounds that increase solution conductivity, such as acetic acid, can be added to provide a source of protons and facilitate the ionisation process and in doing so reduce the initial droplet size. Evaporation of solvent from each droplet occurs through a combination of heat and inert gas flow. Desolvation occurs until the electrostatic repulsion of like charges outweighs droplet surface tension (Rayleigh's limit) and a 'Coulomb explosion' occurs, whereby the droplet 'explodes' into multiple smaller daughter droplets. This continues until the electrostatic charge density is strong enough to desorb ions from the droplet into the ambient gas. Ultimately the solvent and neutral molecules are removed and a stream of charged ions enters into the MS vacuum[298, 299]. This stage can be susceptible to ion suppression, a form of matrix effect. This causes some analytes to ionise more or less than expected due to the effects of co-eluting compounds. Thus, ion

suppression has a deleterious effect on downstream quantification accuracy and limits the ability to compare the measured intensities of different analytes against each other.

In GC-MS electron impact ionisation (EI) is commonly used. Here the sample enters the ion source in a gaseous state. A heated filament, usually of tungsten or rhenium, produces electrons which collide with the gas molecules, removing an electron from it and producing the corresponding positively charged ion[300]. This technique uses high energy electrons and hence creates a large number of fragmented ions, thus is considered a 'hard' ionisation technique. Other methods include matrix-assisted laser desorption ionisation (MALDI), another 'soft' ionisation technique. Here laser energy is used to ionise molecules mixed with a matrix material and applied to a metal plate.

Charged ions are then transported to the analyser where the mass-to-charge ratio of arriving ions and their abundance is detected. This is commonly performed using a time of flight (TOF) or quadrupole (Q) analyser or a combination of these, for example a Q-TOF or triple quadrupole (QQQ). TOF analysers accelerate particles using an electric field across a known distance. Particles with a lower m/z ratio will reach a higher velocity and cross the distance in less time than those with a higher m/z ratio. Accordingly, for a given electric potential difference, distance and measured time to detection a m/z ratio can be calculated[301]. TOF analysers have high acquisition rates and spectral deconvolution and are able to measure the m/z ratio with a high degree of accuracy over a broad mass range[302]. This comes at the cost of lowered sensitivity. Alternatively, quadrupole analysers can be used. These were developed by Paul for which he was awarded a Nobel Prize in Physics[303]. Quadrupoles utilise oscillating (AC) radio frequency voltage applied to four parallel metal rods with a static (DC) voltage offset applied between one pair and the other. Under these conditions only ions with a specific m/z ratio will pass down the quadrapole between the rods, other ions will develop unstable paths and collide with the rods before they reach the detector. This can either be used to select ions at a given m/z ratio or to measure a range of m/z values through a continuous alteration of the applied voltage[303]. To acquire a mass spectrum the DC and AC potential must be scanned across a range. The broader the mass range the longer the scan time, resulting in reduced spectral deconvolution[304]. To increase selectivity a tandem triple quadrupole (QQQ) can be used. The first acts as an initial mass filter, the selected ion enters the second quadrupole which acts as a collision chamber to fragment the ion into smaller daughter ions. The third

quadrupole then measures targeted fragment ions. This analysis is both highly sensitive and specific. However, it will only measure targeted ions[305].

2.4 Multivariate Data Analysis

Metabonomic analysis through NMR or MS produces a huge quantity of raw data. There are routinely many more variable measurements than samples or subjects. This necessitates the use of appropriate statistical tools to extract meaningful information from this raw data. This is performed through multivariate data analysis (MVDA). MVDA is particularly suitable when there are more variables than samples, many highly correlated variables and multiple Y variables[306]. Analytical tests can be unsupervised or supervised.

2.4.1 Unsupervised methods

In unsupervised tests, such as Principal Component Analysis (PCA), the algorithm does not know the true outcome, for example class, of the samples analysed. Therefore, PCA is useful at the beginning of an analysis to provide an unbiased exploratory data overview. PCA reduces the dimensionality of a dataset by transforming the data matrix into a coordinate system of principal components[307]. The greatest variance within the data matrix is described through the first principal component. Whereas the second principal component describes the maximal variance after the first principal component has been removed and is orthogonal to it. This can be continued to explain successively more variance in the matrix. An R^2 value is calculated which describes the variation explained by the model, in other words the 'goodness of fit'. However, with each further addition of a principal component to the model there is a risk of overfitting. To prevent this a Q^2 value is calculated through k-fold cross-validation. This describes the variation predictable by the model, or 'goodness of prediction' and hence is a measure of its reliability. Accordingly, to avoid overfitting, when the Q^2 value of a model begins to decrease no further principal components should be added[308].

The model can be visualised graphically in two ways: a scores plot and a loadings plot. The scores plot projects the individual observations onto principal components and plots each successive principal component to a coordinate axis (x, y, z). Thus, the observations can be graphically represented in two or three dimensions. In doing so a scores plot is able to produce a visually interpretable data summary identifying natural groupings of observations or

outliers, typically accommodating the main variance in the dataset within the first few principal components. Meanwhile the loadings plot projects the variables onto the principal components and summarises the relationship among the variables in the model[306, 308].

2.4.2 Supervised methods

In supervised statistical tests the algorithm knows the assigned class membership of the analysed samples and attempts to find which rule predicts the defined class output for a given data matrix. Partial Least Squares (PLS) analysis identifies latent variables that account for the largest amount of variation predictive of the outcome (Y)[306]. Again, the process can be repeated with successive principal components. PLS can be performed as a regression with a continuous Y, for example blood pressure values, or as a discriminant analysis between categorical classes. PLS can be enhanced through the addition of an orthogonal signal correction filter to remove systematic variation that is not related to the class of interest: Orthogonal – Partial Least Squares (O-PLS)[309]. This separates the systematic variation into predictive and orthogonal components. The orthogonal component is the variation within X, due to biological or experimental factors, that is orthogonal to Y. This facilitates easier interpretation of the class-separating variables through interrogation of the predictive component[309]. Derived parameters to describe the quality of the model are: R^2X which explains how much of the variance in the dataset is explained by the model; R^2Y which describes the percentage of the outcome (Y) explained by the predictive component; Q^2Y which describes the reliability of the R^2Y value through cross-validation.

For NMR matrices O-PLS-DA models are commonly visualised using a coefficient loadings plot. The intensity and direction of the displayed line represents the covariance of the scaled variables, appearing as a pseudo NMR spectrum. The line is then colour coded according to the strength of the correlation coefficient (scale of red to blue representing the strongest to weakest correlations respectively) between each measured data point and class discrimination[310]. An example is shown in Figure 2.4-1. Here the ^{1}H-NMR spectral peaks from the metabolites acetate, butyrate and propionate correlate with Class A. Propionate, coloured red, correlates with Class A more strongly than acetate and butyrate, coloured yellow. An unknown metabolite (Unknown 1) correlates with Class B, although this is a weaker correlation (coloured green).

Longitudinally paired data is susceptible to overfitting due to the symmetrical nature of the data. Therefore in this thesis longitudinally paired global metabolic data, pre and post-intervention, was analysed using Partial Least Squares – Discriminant Analysis (PLS-DA) with Monte-Carlo cross-validation (MCCV)[311]. Data was centred and scaled to account for the repeated-measures design. 1000 MCCV models were generated and used to calculate the mean cross-validated predictive component score (T_{pred}) and variance for each sample[311]. The fit and predictability of the models obtained was determined by the R^2 and Q^2 values respectively. Gaussian kernel density estimates of the T_{pred} in each group were generated for visual interpretation[311].

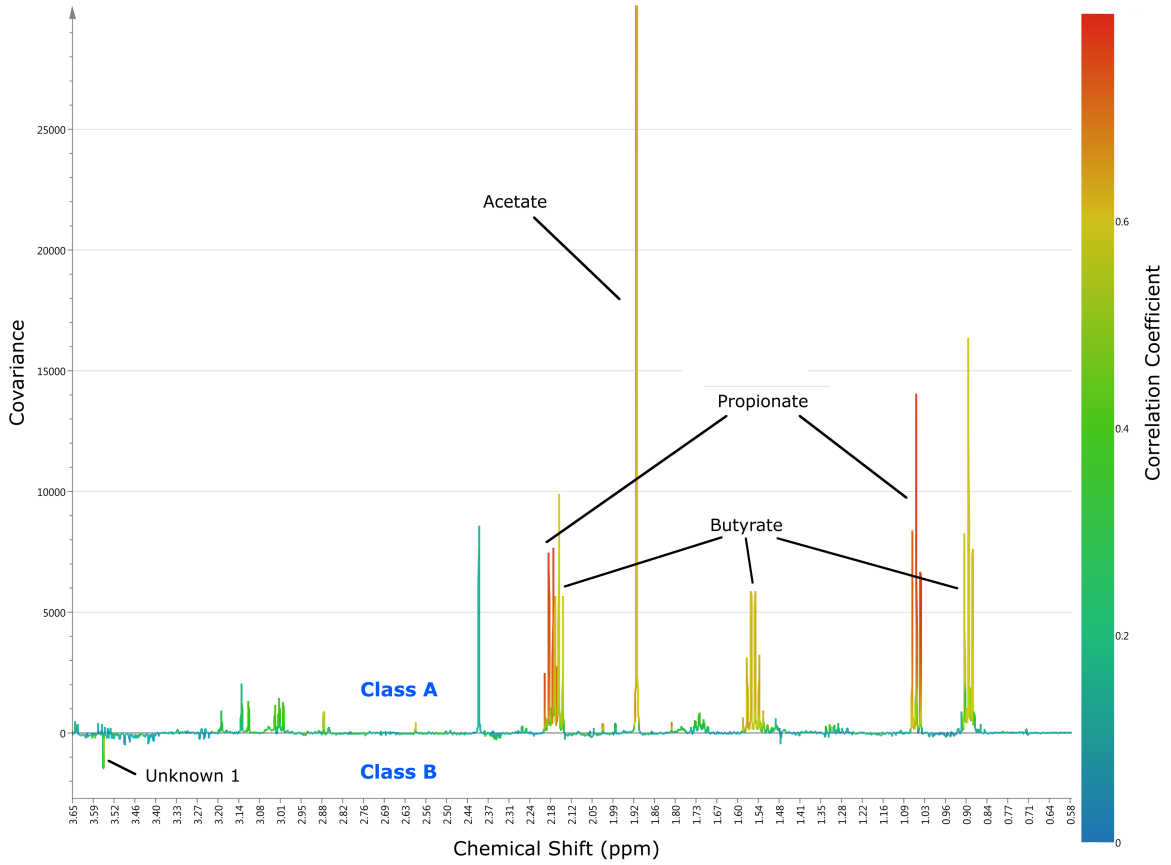


Figure 2.4-1 Example of OPLS-DA correlation coefficient plot.

2.5 Metabolite identification

Significant spectral peaks (NMR) or m/z (MS) values were assigned to their respective metabolites using a catalogue of spectroscopy strategies, analytical techniques and statistical tools, as described below.

2.5.1 1D NMR

2.5.1.1 Chemical shift & multiplicity

Chemical shift (δ) and multiplicity of significant spectra obtained using 1D ^{1}H-NMR were noted. These were compared to known compounds in open source databases such as the Human Metabolome Database[312] and in-house reference libraries. If possible, compounds were putatively assigned.

2.5.1.2 Statistical spectral correlation

In addition, statistical tools such as Statistical TOtal Correlation SpectroscopY (STOCSY)[313] and SubseT Optimization by Reference Matching (STORM)[314] were applied to link spectra from the same metabolite in different areas of the spectrum. The methods rely on using statistical correlation within a data set to identify data points across a spectrum that are consistently correlated and therefore, likely to belong to the same molecule. Care was taken not to link spectral associations due to shared biological pathways, rather than spectra from the same metabolite, such as metabolites in the Krebs cycle.

2.5.2 2D NMR

2D NMR, the addition of a second frequency domain, was used to glean further structural information on unidentified metabolites or to help confirm their identity. This included ^{1}H-^{1}H and ^{1}H-^{13}C experiments.

2.5.2.1 J-Resolved spectroscopy

Multiplicity was confirmed using 2D J-Resolved (JRes) spectroscopy, in which the second dimension (F2) is used to capture the multiplicity of the peak. The JRES example shown illustrates how this technique can be used to derive the multiplicity of overlapping spectra (see Figure 2.5-1).

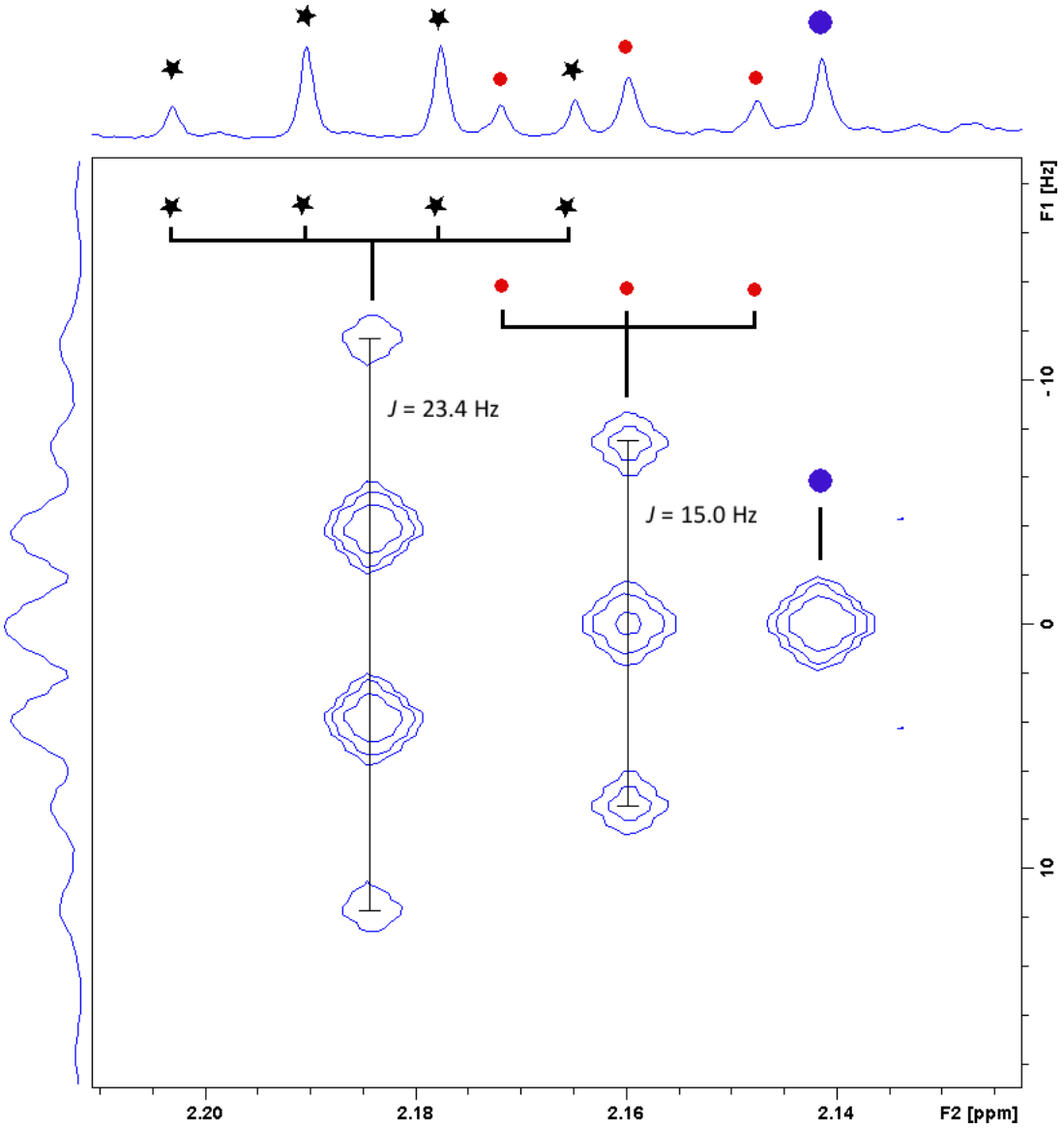


Figure 2.5-1 J-RESolved Spectrum (JRES) of faecal water sample. Black stars denote the quartet of propionate at δ 2.19. Red circles denote the triplet of butyrate at δ 2.16. The magnitude of the J-couplings are 23.4 Hz and 15.0 Hz respectively. The blue circle denotes the singlet of acetyl carnitine at δ 2.14.

2.5.2.2 Homonuclear (^{1}H-^{1}H) correlation

^{1}H-^{1}H COrrelation SpectroscopY (COSY)[315] and ^{1}H-^{1}H TOtal Correlation SpectroscopY (TOCSY)[316] were utilised to identify proton spectra from the same metabolites. COSY experiments demonstrate protons linked directly through scalar (*J*) coupling whereas TOCSY is able to demonstrate spins that are not directly coupled but exist within the same spin system. As such, TOCSY acts as a 'long range' COSY. These techniques were used to confirm coupled protons, either *de novo* or as inferred from statistical correlations using STORM and STOCSY.

In the example below four separate proton signals [δ 0.89 (t), δ 1.30 (m), δ 1.54 (m), δ 2.17 (t)], derived from 1D NMR spectroscopy of athlete faecal water, are linked using COSY (See Figure 2.5-2). These coupled signals represent protons positioned at C2-C5 of valerate (see Figure 2.5-3).

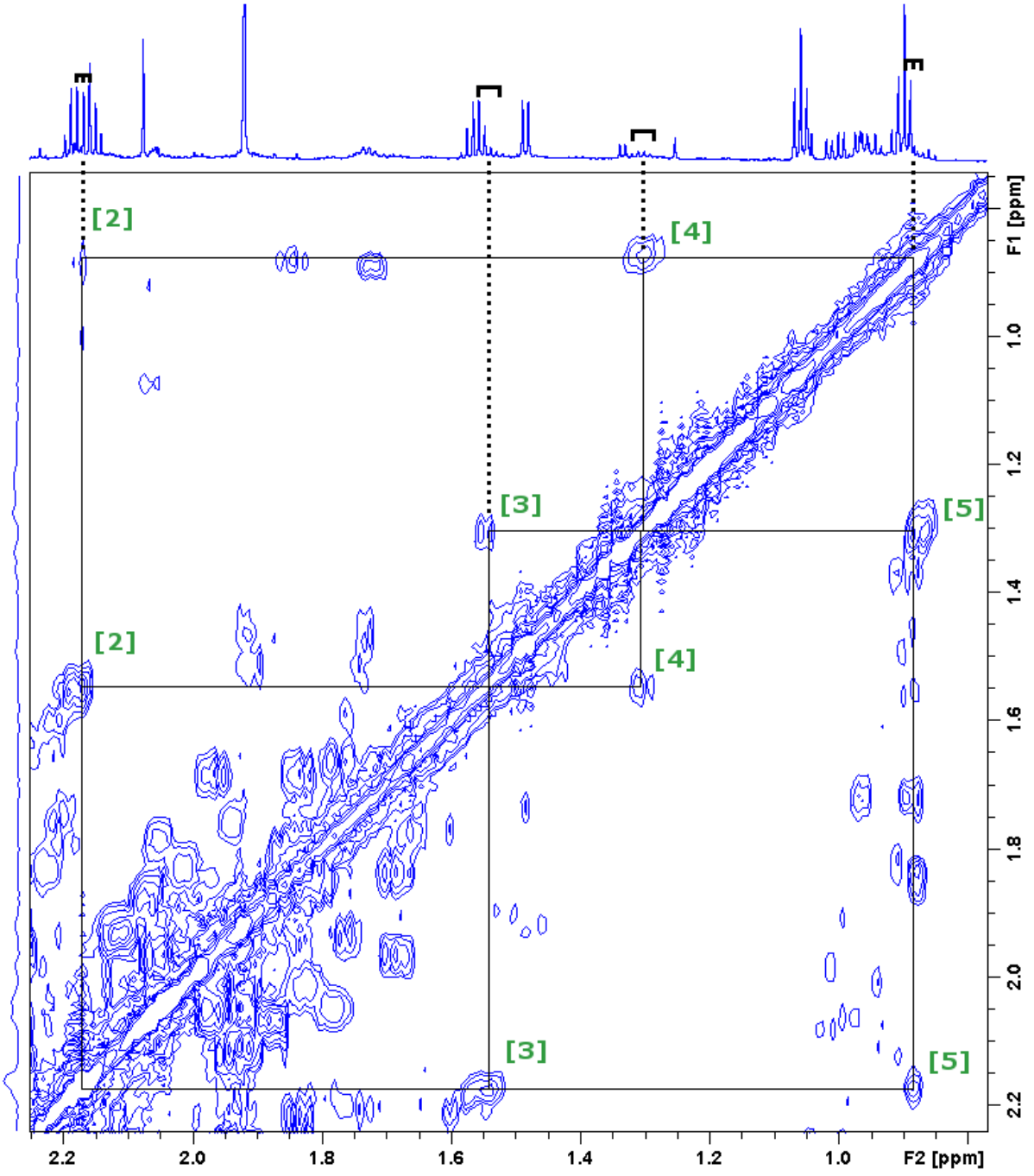


Figure 2.5-2 ^{1}H-^{1}H COrrelation SpectroscopY (COSY) of athlete faecal water sample. Labelling shows the ^{1}H-^{1}H J coupling between protons within valerate at the carbon positions C2-C5 (See Figure 2.5-3). Corresponding 1D ^{1}H spectral peaks for valerate are labelled (δ 0.89 t, 1.30 m, 1.54 m, 2.18 t).

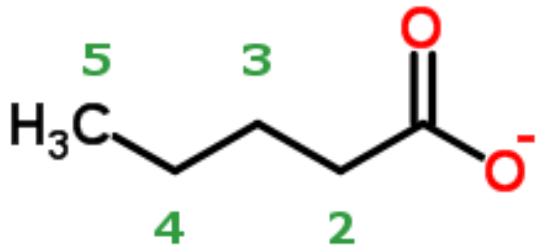


Figure 2.5-3 Valerate structure ($C_5H_{10}O_2$). Carbons C2 to C5 are labelled.

2.5.2.3 Heteronuclear (^{1}H-^{13}C) correlation

^{1}H-^{13}C Hetero-nuclear Single Quantum Coherence (HSQC)[317] and ^{1}H-^{13}C Hetero-nuclear Multiple-Bond Correlation (HMBC)[318] spectroscopy were used to detect correlations between proton and carbon atoms from the same metabolites. HSQC experiments demonstrate correlations between nuclei separated by one bond whereas HMBC experiments are able to detect correlations over approximately two to four bonds. In the example below, the ^{13}C δ value derived from the F1 frequency axis was used in combination with the ^{1}H δ value to confirm the identity of metabolites against known values for the metabolites in reference databases.

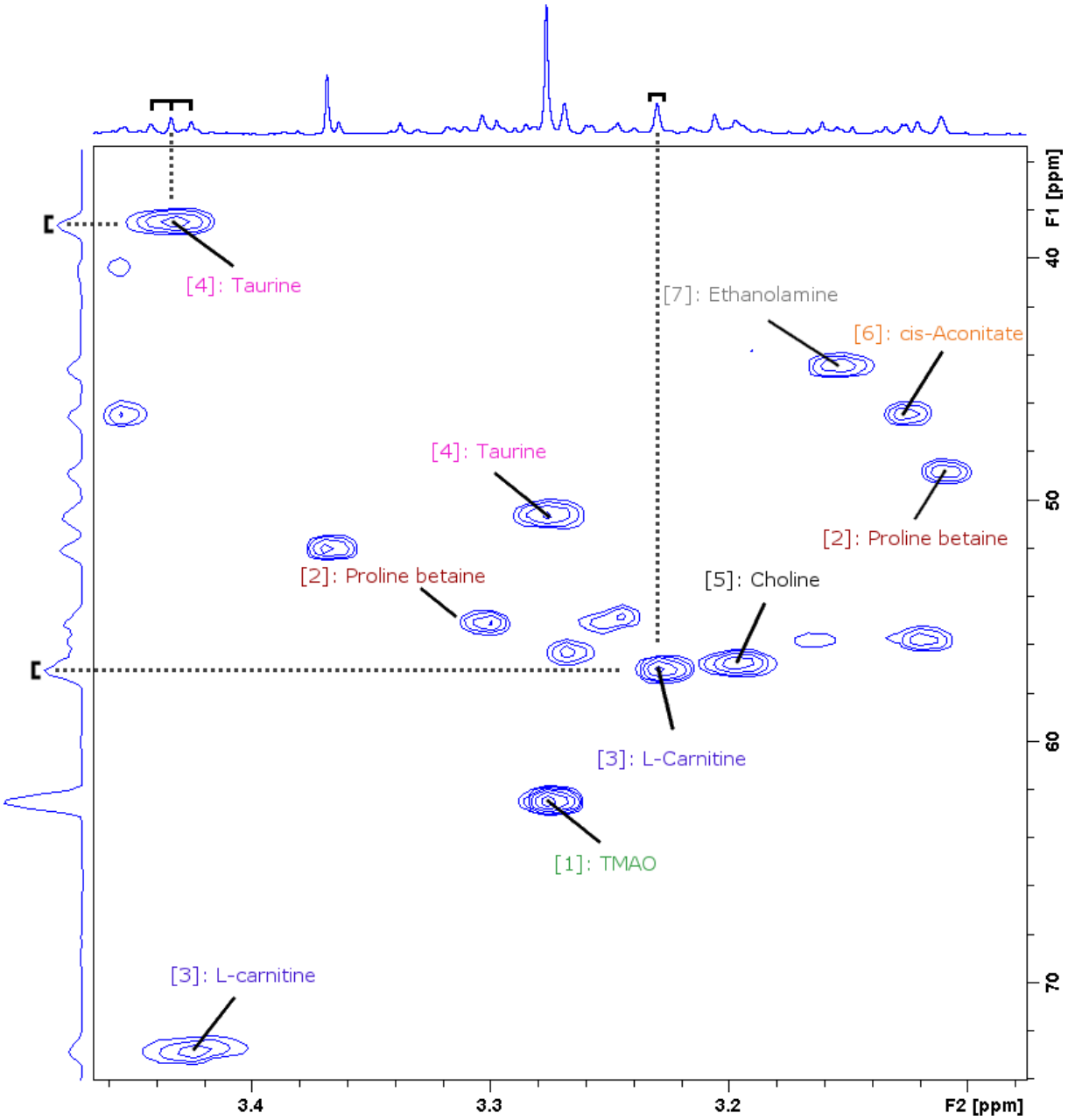


Figure 2.5-4 ^{1}H-^{13}C Hetero-nuclear Single Quantum Coherence (HSQC) spectrum of athlete urine sample to help confirm metabolite identification. Corresponding ^{1}H and ^{13}C spectral peaks respectively are labelled for Taurine (δ 3.44 triplet, δ 38.4 singlet) and L-Carnitine (δ 3.23 singlet, δ 56.9 singlet).

Metabolite	^{1}H value	^{13}C value
[1]: TMAO	3.27	62.4
[2]: Proline Betaine	3.11 3.30	48.8 55.0
[3]: L-Carnitine	3.23 3.43 2.43* 4.56*	56.9 72.8 45.7* 66.8*
[4]: Taurine	3.27 3.44	50.5 38.4
[5]: Choline	3.20 3.52* 4.05*	56.7 70.5* 58.5*
[6]: cis-Aconitate	3.13 5.73*	46.4 127.3*
[7]: Ethanolamine	3.15 3.84*	44.4 60.7*

* = Not shown

Table 2.5-1 HSQC values for ^{1}H and ^{13}C derived from Figure 2.5-4.

2.5.3 LC-MS

2.5.3.1 Mass charge (m/z) ratio & retention time

Mass charge ratios and retention times were compared against known values derived from published reference databases such as the Human Metabolome Database[312] and METLIN[319].

2.5.3.2 MS/MS

Confirmation of metabolite identities was obtained using Tandem MS (MS/MS) on selected target ions at their respective retention time. Target ions were fragmented with an energy ramp of 5-20eV to yield product ions. These metabolite finger prints were used to distinguish metabolites with similar m/z ratios from each other and identify the metabolite at a higher level. Some classes of metabolites, such as acylcarnitines and glucuronides, gave characteristic fragmentation patterns (see Figure 2.5-5 and Figure 2.5-6).

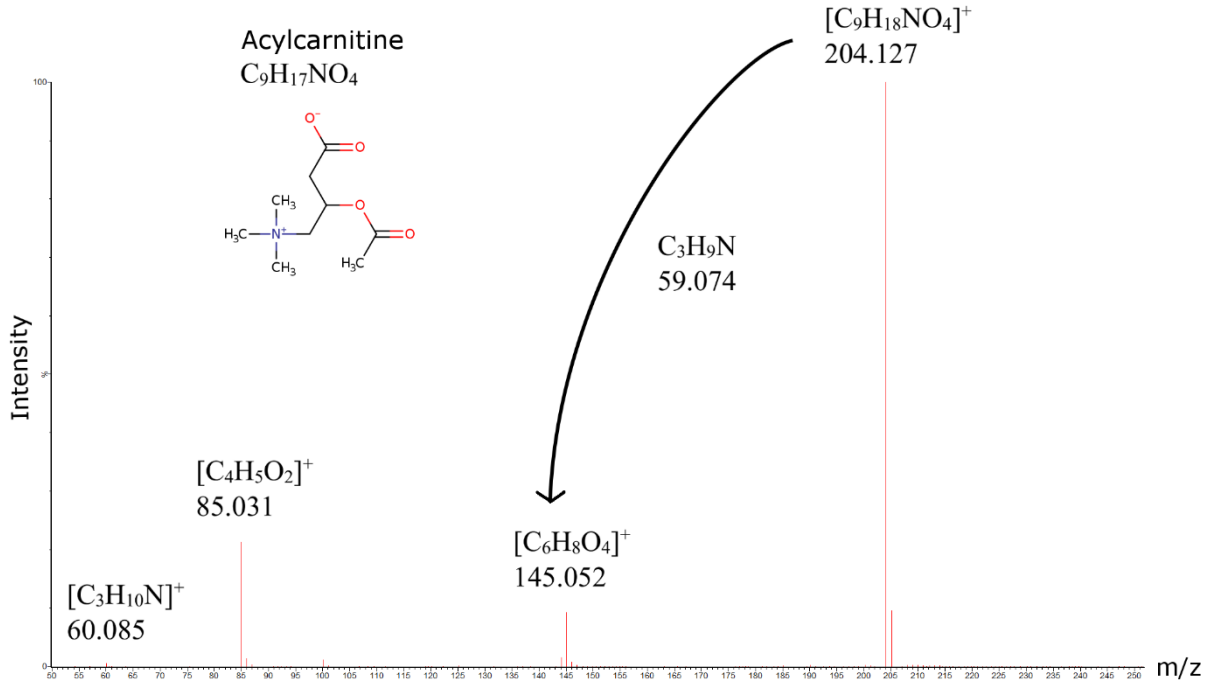


Figure 2.5-5 MS/MS spectrum (positive ionisation mode) of acetylcarnitine (C2). Shows neutral loss of 59 m/z and 85 m/z product ion characteristic of acylcarnitines.

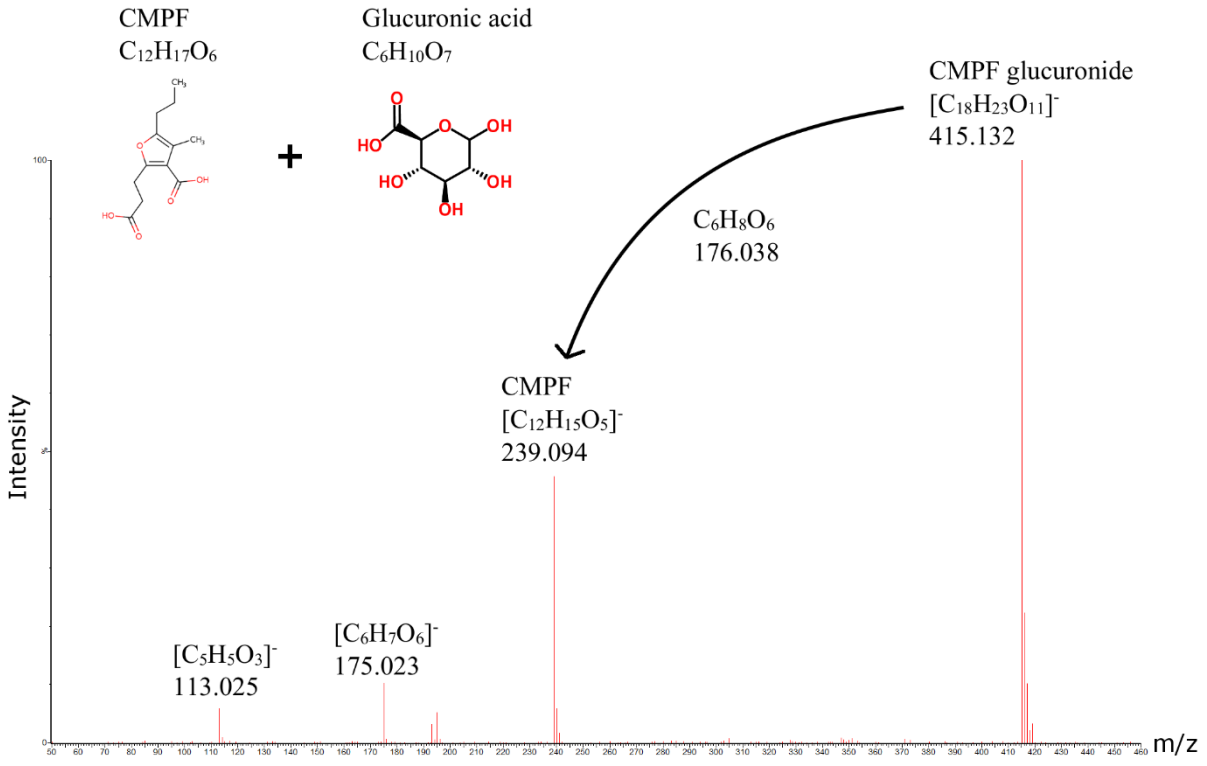


Figure 2.5-6 MS/MS spectrum (negative ionisation mode) of CMPF-glucuronide. Shows neutral loss of 176 m/z (loss of monodehydrated glucuronic acid) and 175 m/z + 113 m/z product ions characteristic of glucuronides.

In the selected case above, the aglycone at 239.09 m/z underwent a further separate MSMS experiment to confirm its identity (see Figure 2.5-7). The aglycone parent ion (239 m/z) yielded product ions at 195.102 (44.0 neutral loss = decarboxylation) and 151.112 (44.0 neutral loss from 195 = further decarboxylation) as well as an additional product ion at 221.086 (18.0 neutral loss = dehydration). These findings are consistent with the human metabolome database entries for the MS/MS of CMPF (3-Carboxy-4-methyl-5-propyl-2-furanpropionic acid).

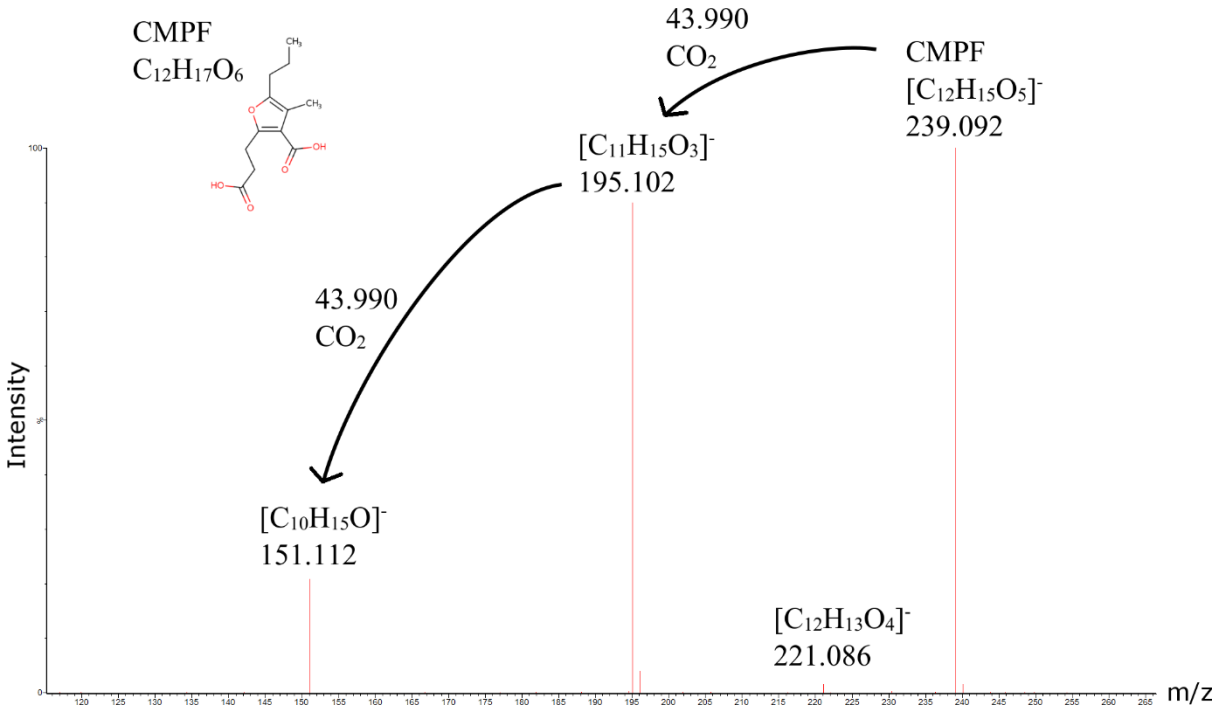


Figure 2.5-7 MS/MS spectrum (negative ionisation mode) of CMPF. Shows the expected 221, 195 & 151 m/z product ions of CMPF, produced through the neutral loss of H_20 and CO_2 and further CO_2 loss from the 195 product ion respectively.

2.5.4 Authentic chemical reference spiking

Metabolites putatively identified through the NMR and MS pipelines described above underwent spiking with an authentic chemical reference standard to confirm the identity. In the example below, serial additions of small volumes of dimethylglycine were added to an aliquot of urine, prepared in an identical manner to the original ^{1}H-NMR analysis (see Figure 2.5-8). Thus, confirming that the spectral peak at δ 3.23 is that of dimethylglycine.

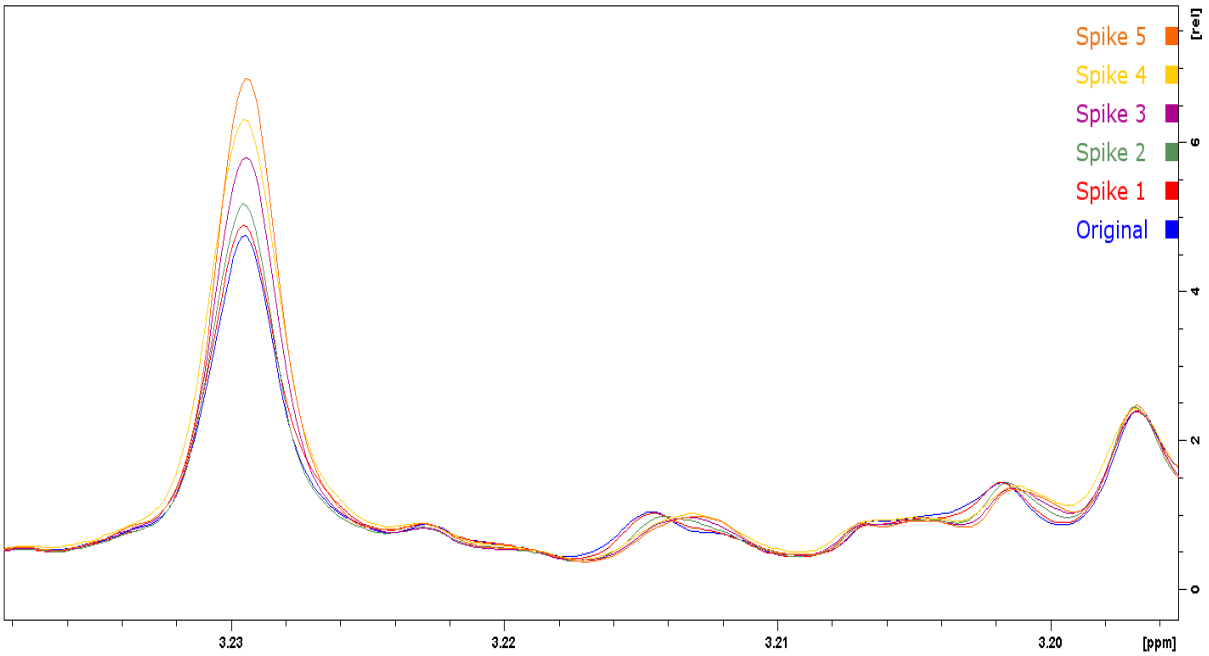


Figure 2.5-8 Chemical reference spiking to confirm identification of dimethylglycine at δ 3.23 (s) in urine.

2.5.5 Level of assignment

Metabolite identification was characterized by a level of assignment (LoA) score that describes how the identification was made. These were consistent with the identification levels described by the Chemical Analysis Working Group (CAWG) as part of the Metabolomics Standards Initiative (MSI)[320]. The levels used were as follows: LoA 1: Identified compound, confirmed by comparison to an authentic chemical reference. LoA 2: MS/MS target and product ions or 1D+2D NMR chemical shifts and multiplicity match to a reference database or literature to putatively annotate compound. LoA 3: Chemical shift (δ) and multiplicity matches a reference database to tentatively assign the compound.

2.6 Principles of Next Generation Metagenomic sequencing

The development of the Sanger chain termination sequencing technique in 1977 enabled reliable and reproducible sequencing of DNA[321]. Later the introduction of automated capillary electrophoresis based sequencing increased throughput and enabled the Human Genome Project[322-324]. These so called 'first-generation' sequences were developed further through the introduction of short read, massively parallel sequencing. The introduction of "next generation sequencing" (NGS) delivered a paradigm shift in both the speed and cost of data

output[325]. By way of example the first human genome took 15 years to sequence using laboratories around the world and cost nearly three billion dollars[322, 323]. Whereas the latest NGS machines can sequence approximately 50 whole genomes in a day for around 1000 dollars each[326].

NGS accomplishes this through sequencing by synthesis. First, DNA fragments are hybridised to the flow cell surface. Each bound fragment then undergoes bridge amplification using DNA polymerase to create identical copies, or 'cluster', of the original molecule on the flow cell surface. Subsequently, all four nucleotides are simultaneously added to the flow cell with DNA polymerase and incorporated into the primed DNA fragments. Each nucleotide is labelled with a base-specific fluorescent label and acts as a terminator of polymerisation. After incorporation into the nucleic acid chain, laser excitation causes emission of fluorescence, with a different wavelength emitted for each of the four nucleotides. The nucleotide at each cluster is then recorded, the base enzymatically cleaved and the next nucleotide in the chain added. This is performed on multiple clusters on each flow cell in a massively parallel fashion, for a predefined number of cycles (read length). In addition, DNA fragments can be sequenced using paired-end sequencing, where adapters are added to both ends of the DNA strands and strands are sequenced from both ends. Reads are then aligned to a reference sequence or assembled *de novo* using bioinformatics software[325, 327].

NGS can be applied to sequence bacterial DNA from faecal or gut samples. Previous studies of gut bacteria have relied on the culture of organisms. This limited studies to analysis of the minority of species that were able to be cultured, significantly restricting our understanding. The advent of DNA sequencing has enabled novel insight into gut microbial communities through culture-independent analysis[13]. Previously culture-independent studies analysing the gut microbiome have relied on amplicon sequencing of the highly conserved 16S ribosomal RNA gene. Relative to 16S rRNA sequencing, next generation metagenomic sequencing enables enhanced analysis of 'who is there', with increased sensitivity and accuracy of species detection within the microbial community. Further it allows insight into 'what they are doing' with increased prediction of genes and the functional capability of the microbiome. In addition, NGS removes bias inherent in 16S rRNA sequencing, resulting from differences in the copy number of 16S rRNA genes between different species and chimeric amplification[328].

2.6.1 Statistical handling of NGS data

Previously, Sanger sequencing produced long reads (~900bp) with low coverage (<10x) and extreme cost. NGS has enabled a significant reduction in cost and high coverage levels but has the disadvantage of shorter reads (25-150bp). As a result, there are a number of statistical challenges in reconstructing the genome. These include; small read lengths, gigabytes of data, genomic repeats and sequencing errors such as mismatches or indels. Analysis of metagenome data is further complicated by having multiple different genomes, including different strains, mixed into one data set, difference coverage for different bacteria and conserved genomic regions between different bacteria.

There are two main branches of statistical methods used to approach these challenges. First, sequences can be mapped to existing reference genomes. A number of different alignment algorithms have been described. Many were developed when sequence reads were short and as a consequence reasonably required every base read to be aligned to the reference. However, these algorithms do not allow for gapped alignment where indels may be present or mismatches potentially due to misassembly of the reference genome of structural variations[329]. Longer reads, now possible with later generations of NGS, are more likely to contain mismatches and indels making these algorithms unsuitable. In addition, they require large amounts of computational processing power and data memory resulting in slow alignments when scaled up to hundreds of samples[329]. A number of long-read alignment algorithms have now been developed including BWA[329], Bowtie2[330] and GEM[331]. Each have weakness in terms of accuracy, speed or ability to tolerate mismatches and indels. Within this thesis the Burrows-Wheeler Alignment Maximal Exact Matches (BWA-MEM)[332] algorithm is used. This utilises string matching theory via back searching with Burrow-Wheeler transform to provide a fast and accurate algorithm for alignment of a wide range of sequence lengths against a large reference genome, allowing mismatches and gaps[329]. When extending seeds (exact matches) a best extension score is calculated. If this is below a threshold the extension will be rejected. The algorithm utilises this score to automatically choses between local and end-to-end alignment and consequently avoids introducing excessive mismatches and gaps, making the algorithm robust to sequencing errors and chimeric reads[332].

This is first used to map reads against human, plant and other non-bacterial genomes, so that they can be filtered from the metagenome analysis. In addition, reads are mapped to clade-specific marker genes identified from reference genomes to achieve taxonomic assignments using the Metagenomic Phylogenetic Analysis (MetaPhlAn) tool[333, 334].

Second, genomes can be assembled *de-novo*. A number of challenges exist when assembling metgenome data. These include; different abundance levels of species resulting in non-uniform read coverage across different genomes, species within a microbial community sharing highly conserved genomic regions and multiple related bacterial strains with varying abundances that share most of their genetic sequence but contain regions of significant variation (microdiversity)[335]. Again, a number of assemblers have been described. Here metagenome assembly is performed in two rounds using the metaSPAdes[335] algorithm. This adapts the SPAdes algorithm[336] for metagenomic data. By working across a wide range of coverage depths metaSPAdes attempts to maintain both contiguity and accuracy. Additionally, to tackle microdiversity a 'consensus backbone' is constructed, thus ignoring some rare strain-specific features[335]. An initial independent assembly is carried out for each sample, then unassembled reads are pooled and subjected to a second round of assembly to improve the representation of low-abundance sequences. The assembled metagenome is subsequently used to make gene predictions and a non-redundant gene catalogue. Filtered sequences are then mapped against this generated gene catalogue using the BWA-MEM algorithm to determine gene abundance. Furthermore, functional annotation of this gene catalogue is achieved by comparing the catalogue to gene databases such as KEGG (Kyoto Encyclopedia of Genes and Genomes)[337] and InterPro[338].

2.7 References

13. Hiergeist A, Glasner J, Reischl U, Gessner A. Analyses of Intestinal Microbiota: Culture versus Sequencing. ILAR J. 2015;56(2):228-40.

289. Gerlach W, Stern O. Der experimentelle Nachweis der Richtungsquantelung im Magnetfeld. Zeitschrift für Physik. 1922;9(1):349-52.

290. Lindon JC, Nicholson JK, Holmes E. The handbook of metabonomics and metabolomics. Amsterdam; London: Elsevier; 2007.

291. Hore PJ, Jones JA, Wimperis S. NMR: the toolkit. Oxford: Oxford University Press; 2000.

292. Rule GS, Hitchens TK. Fundamentals of protein NMR spectroscopy. 1st ed. Dordrecht: Springer; 2010.

293. Friebolin H. Basic one- and two-dimensional NMR spectroscopy. 5th ed. Weinheim: Wiley-VCH; 2011.

294. Want EJ, Wilson ID, Gika H, Theodoridis G, Plumb RS, Shockcor J, et al. Global metabolic profiling procedures for urine using UPLC-MS. Nat Protoc. 2010;5(6):1005-18.

295. Damen CW, Isaac G, Langridge J, Hankemeier T, Vreeken RJ. Enhanced lipid isomer separation in human plasma using reversed-phase UPLC with ion-mobility/high-resolution MS detection. Journal of lipid research. 2014;55(8):1772-83.

296. Garcia A, Barbas C. Gas chromatography-mass spectrometry (GC-MS)-based metabolomics. Methods Mol Biol. 2011;708:191-204.

297. Fenn JB. Electrospray Wings for Molecular Elephants (Nobel Lecture). Angewandte Chemie International Edition. 2003;42(33):3871-94.

298. Whitehouse CM, Dreyer RN, Yamashita M, Fenn JB. Electrospray interface for liquid chromatographs and mass spectrometers. Analytical chemistry. 1985;57(3):675-9.

299. Fenn JB, Mann M, Meng CK, Wong SF, Whitehouse CM. Electrospray ionization for mass spectrometry of large biomolecules. Science. 1989;246(4926):64-71.

300. Bleakney W. A New Method of Positive Ray Analysis and Its Application to the Measurement of Ionization Potentials in Mercury Vapor. Physical Review. 1929;34(1):157-60.

301. Cameron AE, Jr. DFE. An Ion ``Velocitron''. Review of Scientific Instruments. 1948;19(9):605-7.

302. Mirsaleh-Kohan N, Robertson WD, Compton RN. Electron ionization time-of-flight mass spectrometry: historical review and current applications. Mass Spectrom Rev. 2008;27(3):237-85.

303. Paul W. Electromagnetic traps for charged and neutral particles (Nobel Lecture). Reviews of Modern Physics. 1990;62(3):531-40.

304. von Muhlen C, Zini CA, Caramao EB, Marriott PJ. Comparative study of Eucalyptus dunnii volatile oil composition using retention indices and comprehensive two-dimensional gas chromatography coupled to time-of-flight and quadrupole mass spectrometry. J Chromatogr A. 2008;1200(1):34-42.

305. Yost RA, Enke CG. Selected Ion Fragmentation with a Tandem Quadrupole Mass-Spectrometer. J Am Chem Soc. 1978;100(7):2274-5.

306. Eriksson L, Byrne T, Johansson E, Trygg J, Vikstrom C. Multi- and megavariate data analysis: basic principles and applications. Third ed: Umetrics; 2013.

307. Wold S, Esbensen K, Geladi P. Principal component analysis. Chemometrics and Intelligent Laboratory Systems. 1987;2(1):37-52.

308. Jackson JE. A user's guide to principal components. Hoboken, N.J.: Wiley-Interscience; 2003.

309. Trygg J, Wold S. Orthogonal projections to latent structures (O-PLS). Journal of Chemometrics. 2002;16(3):119-28.

310. Holmes E, Cloarec O, Nicholson JK. Probing latent biomarker signatures and in vivo pathway activity in experimental disease states via statistical total correlation spectroscopy (STOCSY) of biofluids: application to HgCl2 toxicity. Journal of proteome research. 2006;5(6):1313-20.

311. Garcia-Perez I, Posma JM, Gibson R, Chambers ES, Hansen TH, Vestergaard H, et al. Objective assessment of dietary patterns by use of metabolic phenotyping: a randomised, controlled, crossover trial. The lancet Diabetes & endocrinology. 2017;5(3):184-95.

312. Wishart DS, Feunang YD, Marcu A, Guo AC, Liang K, Vazquez-Fresno R, et al. HMDB 4.0: the human metabolome database for 2018. Nucleic Acids Res. 2017.

313. Cloarec O, Dumas ME, Craig A, Barton RH, Trygg J, Hudson J, et al. Statistical total correlation spectroscopy: an exploratory approach for latent biomarker identification from metabolic 1H NMR data sets. Analytical chemistry. 2005;77(5):1282-9.

314. Posma JM, Garcia-Perez I, De Iorio M, Lindon JC, Elliott P, Holmes E, et al. Subset optimization by reference matching (STORM): an optimized statistical approach for recovery of metabolic biomarker structural information from 1H NMR spectra of biofluids. Analytical chemistry. 2012;84(24):10694-701.

315. Aue WP, Bartholdi E, Ernst RR. 2-Dimensional Spectroscopy - Application to Nuclear Magnetic-Resonance. J Chem Phys. 1976;64(5):2229-46.

316. Braunschweiler L, Ernst RR. Coherence Transfer by Isotropic Mixing - Application to Proton Correlation Spectroscopy. J Magn Reson. 1983;53(3):521-8.

317. Bodenhausen G, Ruben DJ. Natural Abundance N-15 Nmr by Enhanced Heteronuclear Spectroscopy. Chem Phys Lett. 1980;69(1):185-9.

318. Bax A, Summers MF. H-1 and C-13 Assignments from Sensitivity-Enhanced Detection of Heteronuclear Multiple-Bond Connectivity by 2d Multiple Quantum Nmr. J Am Chem Soc. 1986;108(8):2093-4.

319. Smith CA, O'Maille G, Want EJ, Qin C, Trauger SA, Brandon TR, et al. METLIN: a metabolite mass spectral database. Ther Drug Monit. 2005;27(6):747-51.

320. Sumner LW, Amberg A, Barrett D, Beale MH, Beger R, Daykin CA, et al. Proposed minimum reporting standards for chemical analysis Chemical Analysis Working Group (CAWG) Metabolomics Standards Initiative (MSI). Metabolomics. 2007;3(3):211-21.

321. Sanger F, Nicklen S, Coulson AR. DNA sequencing with chain-terminating inhibitors. Proceedings of the National Academy of Sciences of the United States of America. 1977;74(12):5463-7.

322. Consortium IHGS. Initial sequencing and analysis of the human genome. Nature. 2001;409(6822):860-921.

323. Venter JC, Adams MD, Myers EW, Li PW, Mural RJ, Sutton GG, et al. The sequence of the human genome. Science. 2001;291(5507):1304-51.

324. Collins FS, Morgan M, Patrinos A. The Human Genome Project: lessons from large-scale biology. Science. 2003;300(5617):286-90.

325. Mardis ER. Next-generation DNA sequencing methods. Annu Rev Genomics Hum Genet. 2008;9:387-402.

326. Hayden EC. Technology: The $1,000 genome. Nature. 2014;507(7492):294-5.

327. Mardis ER. Next-generation sequencing platforms. Annu Rev Anal Chem (Palo Alto Calif). 2013;6:287-303.

328. Angly FE, Dennis PG, Skarshewski A, Vanwonterghem I, Hugenholtz P, Tyson GW. CopyRighter: a rapid tool for improving the accuracy of microbial community profiles through lineage-specific gene copy number correction. Microbiome. 2014;2:11.

329. Li H, Durbin R. Fast and accurate short read alignment with Burrows-Wheeler transform. Bioinformatics. 2009;25(14):1754-60.

330. Langmead B, Salzberg SL. Fast gapped-read alignment with Bowtie 2. Nat Methods. 2012;9(4):357-9.

331. Marco-Sola S, Sammeth M, Guigo R, Ribeca P. The GEM mapper: fast, accurate and versatile alignment by filtration. Nat Methods. 2012;9(12):1185-8.

332. Li H. Aligning sequence reads, clone sequences and assembly contigs with BWA-MEM. arXiv. 2013.

333. Truong DT, Franzosa EA, Tickle TL, Scholz M, Weingart G, Pasolli E, et al. MetaPhlAn2 for enhanced metagenomic taxonomic profiling. Nat Methods. 2015;12(10):902-3.

334. Segata N, Waldron L, Ballarini A, Narasimhan V, Jousson O, Huttenhower C. Metagenomic microbial community profiling using unique clade-specific marker genes. Nat Methods. 2012;9(8):811-4.

335. Nurk S, Meleshko D, Korobeynikov A, Pevzner PA. metaSPAdes: a new versatile metagenomic assembler. Genome Res. 2017;27(5):824-34.

336. Bankevich A, Nurk S, Antipov D, Gurevich AA, Dvorkin M, Kulikov AS, et al. SPAdes: a new genome assembly algorithm and its applications to single-cell sequencing. J Comput Biol. 2012;19(5):455-77.

337. Kanehisa M, Goto S. KEGG: kyoto encyclopedia of genes and genomes. Nucleic Acids Res. 2000;28(1):27-30.

338. Finn RD, Attwood TK, Babbitt PC, Bateman A, Bork P, Bridge AJ, et al. InterPro in 2017-beyond protein family and domain annotations. Nucleic Acids Res. 2017;45(D1):D190-D9.

3 A cross sectional study to elucidate the metabolic phenotype of elite athletes

Results from the following chapter have been published as part of the following article[339]: Barton W, Penney NC, Cronin O, Garcia-Perez I, Molloy MG, Holmes E, et al. The microbiome of professional athletes differs from that of more sedentary subjects in composition and particularly at the functional metabolic level. Gut. 2018;67(4):625-33.

3.1 Introduction

Regular exercise challenges systemic homeostasis causing a number of physiological multi-organ responses, including those that centre around metabolism, immunity and the gut-microbiome-brain axis[261, 263, 264, 266]. Exercise induces end-organ and systemic anti-inflammatory effects, as well as increasing carbohydrate metabolism efficiency[266, 267]. A sedentary lifestyle is implicated in an increased risk of numerous diseases, such as obesity, diabetes, cardiovascular disease and asthma[252-254, 340]. Recent evidence supports an influential role for the gut microbiome in these diseases, partially mediated by its impact on inflammatory processes[22, 26, 56, 60, 341-348]. Conversely, increasing physical activity offers effective prevention and treatment for many chronic conditions in which the gut microbiome has been implicated[259, 282, 283]. Hence the concept that increased physical activity and regular exercise may nurture a preferential gut microbiome has recently emerged[281, 287, 288]. For the purposes of this thesis we assume that increased exercise equates with increased healthiness and that this holds true for the extreme levels of physical activity seen in elite athletes.

Previously, taxonomic differences in gut microbiota between an elite athlete cohort of professional rugby players and a group of high and low BMI, age and sex matched controls were demonstrated using 16S rRNA amplicon sequencing[286]. The study found a significantly higher intestinal microbial diversity amongst the athletes compared to both high and low control groups. This taxonomic diversity was significantly correlated with higher levels of exercise and protein consumption, as seen in the athlete group. Here, further analysis of the same cohort using metabolic phenotyping is undertaken. The aims of the study were to assess the impact of high levels of exercise, associated dietary changes and the subsequent change in microbial diversity on the metabolic phenotypes of participants through the metabolic profiling of urine and faecal samples. The results confirm enhanced microbial diversity in

athletes compared with controls. Furthermore, additional insights into the influence of intense physical exercise and the associated dietary changes on the resultant metabolic changes that occur are achieved. Through combination of dietary, metagenomic and metabonomic information this study extends the paradigm to include links between physical fitness and the functional potential of the gut microbiota and its metabolites.

3.2 Methods

3.2.1 Patient recruitment

Patients were recruited to the study as previously described[286]. Elite male professional rugby players from the National Irish Rugby Union team and healthy male controls from Ireland were recruited. In an effort to represent the varied sizes and body morphologies of a professional rugby team, two groups of age-matched controls were recruited based on their physical size (BMI). Group 1 had a BMI ≤25 and group 2 had a BMI >28kg/m^2. Exclusion criteria included having a BMI between 25-28, antibiotic treatment within the previous 2 months or suffering from any cardiovascular, gastrointestinal or immunological condition. The study was approved by the Cork Clinical Research Ethics Committee.

3.2.2 Experimental design

Faecal and urine samples were collected from participants, then aliquoted and stored at -80°C until further analysis.

Dietary data were collected using a food frequency questionnaire (FFQ), administered by a research nutritionist. The FFQ used was an adapted version from the UK arm of the European Prospective Investigation into Cancer (EPIC) study[349], which was based on the original Willet FFQ[350]. Subjects were asked to recall their dietary intake over the preceding four weeks. Foods and beverages were quantified using a photographic food atlas.

Body composition analysis data were obtained using dual-energy X-ray absorptiometry scans and waist:hip measurements.

3.2.3 Preparation of samples for metabolomics analysis

Frozen urine samples (-80°C) were thawed, vortexed and then centrifuged at 1600 × g for 10 min to remove particulates and precipitated proteins. Urine samples were prepared for metabolic profiling analysis by reversed phase (RP) and hydrophilic interaction chromatography (HILIC) ultra-performance liquid chromatography – mass spectrometry (UPLC-MS) as follows: 200 µl of supernatant was diluted (1:1) with high purity (HPLC grade) water, vortexed, centrifuged at 2700 × g for 20 min and aliquoted for HILIC and RP methods. Quality control (QC) samples were prepared by pooling 50 µl volumes of each sample. During the analysis, the samples were maintained at 4°C in the autosampler. For ^{1}H-NMR spectroscopy, 540 µL of urine samples were mixed with 60 µL of 1.5M KH_2PO_4 buffer (pH 7.4, 80% D2O) containing 1 mM of the internal reference standard, 3-(trimethylsilyl)-[2,2,3,3,-$^{2}H_4$]-propionic acid (TSP) and 2mM sodium azide (NaN_3), as described previously[351].

Frozen faecal samples (-80°C) underwent x2 freeze thaw cycles to lyse the cells. After thawing for a second time, 100mg of homogenised sample was placed in a microtube containing 250 µl of 25% acetonitrile (1 ACN : 3 H_2O), 2mM sodium azide and ~0.05g 1mm Zirconia beads. The microtubes underwent 10 seconds in a Biospec bead beater. Samples were then centrifuged at 16000 x g for 20 mins. Following this the faecal water supernatant were centrifuged through centrifuge tube filters (cellulose acetate membrane, pore size 0.22 µm) to remove any remaining particular matter. The centrifuge tube filters were washed prior to use three times with 25% acetonitrile. The resulting faecal water was prepared for metabolic profiling analysis by HILIC and bile acid profiling UPLC-MS as follows: 150µl of faecal water was diluted 3:1 with acetonitrile. Samples were vortexed and incubated at -20°C for 1 hour. Following this samples were centrifuged at 4°C at 16000 x g for 1 hour. Quality control (QC) samples were prepared by pooling 20µl volumes of each faecal water sample and then preparing as above. For ^{1}H NMR spectroscopy, 50µl of the filtered faecal water was added to a Pyrex glass tube and placed under Nitrogen gas flow for 30 mins or until all the liquid had evaporated. The dried sample was reconstituted with 540µl of D_2O and 60µl of phosphate buffer solution as described above. The solution was mixed and sonicated for 5 minutes before undergoing further centrifugation at 16000 x g for 10 mins prior to transferring 600µl of supernatant to a NMR tube for ^{1}H-NMR spectral acquisition.

Faecal samples were prepared for targeted analysis of short-chain fatty acids (SCFAs) using gas chromatography – mass spectrometry (GC-MS) as previously described[352]. In brief, 100mg of thawed faecal sample was suspended in 1ml of water with 0.5% phosphoric acid. After acidification, samples were vortexed for 2 min and centrifuged for 10 min at 16000 x g. 1ml of the resulting faecal water supernatant was added to 1 ml of ethyl acetate for 2 min and then centrifuged for 10 min at 16000 x g. Prior to analysis, a 600µl volume of the organic phase was transferred into a silanised vial with 4-methyl valeric acid added as the internal standard (IS) at a final concentration of 500uM. Samples were analysed in a random order with QCs interspersed every ten samples. Calibration curves of the measured SCFAs were derived through analysis of duplicate dilution series of the purchased chemical standards at the beginning and end of the run.

Urine samples were prepared for targeted analysis of SCFAs using GC-MS as follows. 100µl of urine was acidified with 2µl of hydrochloric acid and added to 500µl of MTBE + internal standard (methyl stearate 100 ppm). Samples were vortexed and shaken for 20 minutes then centrifuged at 16000 x g for 5 minutes at 4 °C. 300µl of the resulting polar phase was placed into silanized vials and 20µl of derivatiser MTBSTF + 1% TBDMSCI added (*N*-tert-Butyldimethylsilyl-*N*-methyltrifluoroacetamide with 1 % tert-Butyldimethylchloro-silane). After vortexing samples were incubated at 60°C for 45 minutes and then aliquoted for analysis.

3.2.4 LC-MS Metabolic profiling analysis

Reversed-phased (RP), HILIC and bile acid UPLC-MS metabolic profiling experiments were performed using a Waters Acquity Ultra Performance LC system (Waters, Milford, MA, USA) coupled to Xevo G2 quadrupole – time of flight (Q-TOF) mass spectrometer (Waters, Milford, MA, USA) with an electrospray source. Samples were analysed in a random order, with QCs interspersed every ten samples.

Urine samples were first analysed using UPLC-MS, with a RP chromatographic method with both positive and negative MS ionisation detection. Secondly, to separate and detect more polar molecules, a HILIC chromatographic stage was used with positive MS ionisation detection. Faecal water samples underwent analysis using HILIC and bile acid profiling chromatographic methods in positive and negative ionisation detection modes respectively.

HILIC, Reversed-Phase and bile acid profiling liquid chromatographic separation was performed as previously described[294, 353]. Mass spectrometry was performed with the following settings: capillary and cone voltages were set at 1.5 kV and 30 V, respectively. The desolvation gas was set to 1000 L/hr at a temperature of 600°C; the cone gas was set to 50 L/hr and the source temperature was set to 120°C. For mass accuracy a lock-spray interface was used with leucine enkephalin [556.27741 Da ($[M+H]^+$), 554.2615 Da ($[M-H]^-$)] solution used as the lock mass at a concentration of 2000 ng/ml and at a flow rate of 15 µl/min.

3.2.5 ^{1}H-NMR Metabolic profiling analysis

^{1}H-NMR spectroscopy was performed on the aqueous phase extracts at 300 K on a Bruker 600 MHz spectrometer (Bruker Biospin, Germany) using the following standard one-dimensional pulse sequence: RD – g_{z1} – 90° – t_1 – 90° – t_m – g_{z2} – 90° – ACQ[351]. The relaxation delay (RD) was set at 4s, 90° represents the applied 90° radio frequency pulse, interpulse delay (t_1) was set to an interval of 4 µs, mixing time (tm) was 10 ms, magnetic field gradients (g_{z1} and g_{z2}) were applied for 1 ms and the acquisition period (AQA) was 2.7 s. Water suppression was achieved through irradiation of the water signal during RD and t_m. For the urine samples, each spectrum was acquired using 4 dummy scans followed by 32 scans while faecal spectra were acquired using 256 scans and 4 dummy scans and collected into 64K data points. A spectral width of 12 000Hz was used for all the samples. Prior to Fourier transformation, the free induction decays (FIDs) were multiplied by an exponential function corresponding to a line broadening of 0.3 Hz.

3.2.6 GC-MS SCFAs targeted analysis

The GC-MS targeted SCFAs analysis was conducted on an Agilent 7890B GC system, coupled to an Agilent 5977A quadrupole mass selective detector (Agilent Technologies, USA). The analysis was performed to detect levels of the SCFAs acetate, propionate, butyrate, valerate, isobutyrate, isovalerate, according to a previously described method[352].

In brief, the GC was fitted with a high polarity, polyethylene glycol (PEG) capillary column (Agilent J&W DB-WAXetr, 30m, 0.25mm internal diameter, 0.25µm film thickness) and helium was used as the carrier gas at 1 mL/min. Injections were made in splitless mode with an injection volume of 1 µL and an injector temperature of 250°C. A glass liner with a glass wool plug at the lower end of the liner was used to avoid contamination of the GC column with non-

volatile material. The column temperature was initially 90°C, then increased to 150°C at 15°C/min, to 170°C at 5°C/min, and finally to 250°C at 20°C/min and kept at this temperature for 2 min (total time 14 min). The solvent delay used was set to 3.5 min. The detector was operated in selected ion monitoring (SIM) mode (electron energy 70 eV), scanning the selected characteristic target ion for each measured SCFA, at the corresponding retention times. Retention times were confirmed prior to analysis through analysis of authentic SCFAs in full scan mode. The temperature of the ion source, quadrupole, and interface were 230, 150, and 280°C, respectively.

3.2.7 Gut Microbiota analysis

DNA extraction from faecal samples, 16S rRNA amplicon sequencing and bioinformatic processing of data generated was performed by collaborators from the University College Cork and Teagasc Food Research Centre as previously described[286].

3.2.8 LC-MS data treatment

The raw mass spectrometric data acquired were pre-processed using xcms in R and the centwave peak picking methods were used to detect chromatographic peaks[354]. The xcms-centwave parameters were dataset specific. Feature grouping across samples was performed using the 'nearest' method within xcms. Peak filling, Minimum Fraction (0.5) and QC coefficient of variation (0.3) filters were applied to the features. Data were normalised using median fold change normalisation using the median data set as the reference[355].

3.2.9 ^{1}H-NMR data treatment

^{1}H-NMR spectra were automatically corrected for phase and baseline distortions and referenced to the TSP singlet at δ 0.0 using TopSpin 3.1 software. Spectra were then digitized into 20k data points at a resolution of 0.0005ppm using an in-house MATLAB R2014a (Mathworks) script. Subsequently, spectral regions corresponding to the internal standard (δ -0.5 to 0.5) and water (δ 4.6 to 5) peaks were removed. In addition, urea (δ 5.4 to 6.3) was removed from the urinary spectra. All spectra were normalised using median fold change normalisation using the median spectrum as the reference[355].

3.2.10Statistical analysis

The resulting ^{1}H-NMR and LC-MS data sets were imported into SIMCA 14.1 (Umetrics) to conduct multivariate statistical analysis. Principal Component Analysis (PCA), followed by an Orthogonal Partial Least Squares Discriminant Analysis (OPLS-DA) was performed to examine the data sets and to observe clustering in the results according to the predefined classes. The OPLS-DA models in the current study were established based on one PLS component and one orthogonal component. Unit variance scaling was applied to ^{1}H-NMR data, Pareto scaling was applied to MS data. The fit of the models obtained was determined by the R^2X and R^2Y values. While the predictability of the models was determined by the Q^2Y values, derived from 7-fold cross validation.

Significant metabolites were obtained from UPLC-MS OPLS-DA models through division of regression coefficients by the jack-knife interval standard error to give an estimate of the t-statistic. Variables with a t-statistic ≥1.96 (z-score, corresponding to the 97.5 percentile) were considered significant. Differentiating metabolites were obtained from ^{1}H-NMR OPLS-DA models after identifying spectral peaks with correlation coefficients values higher than a selected cut off value of 0.4.

Univariate statistical analysis was used to examine the SCFA data set. The data were not normally distributed, hence the Mann-Whitney U test was performed to examine differences between classes. p-values were adjusted for multiple testing using the Benjamini-Hochberg False Discovery Rate (pFDR) method.

Linear regression of NMR spectra was performed against bacterial diversity indices adjusting for confounding factors (age, lean mass and fat mass). For each NMR variable, a regression coefficient was obtained from the linear regression model, and was converted to a t-score and subsequently to a p-value. These p-values were adjusted for multiple testing using the Benjamini-Hochberg False Discovery Rate (pFDR) method. All variables with a pFDR ≤ 0.01 were considered to be significantly associated with bacterial diversity.

3.2.11Metabolite identification

Initially, metabolites were tentatively assigned by matching spectra chemical shift (δ) and multiplicity or m/z ratios, for NMR and MS data respectively, to in-house and external

metabolite databases, such as the Human Metabolome Database (HMDB)[312]. Confirmation of metabolite identities in the NMR data was obtained using a combination of statistical tools such as SubseT Optimization by Reference Matching (STORM)[314] and Statistical TOtal Correlation SpectroscopY (STOCSY)[313] applied to 1D ^{1}H NMR sequence data and 2D NMR experiments such as J-Resolved spectroscopy (JRes), ^{1}H-^{1}H COrrelation SpectroscopY (COSY)[315], ^{1}H-^{1}H TOtal Correlation SpectroscopY (TOCSY)[316], ^{1}H-^{13}C Hetero-nuclear Single Quantum Coherence (HSQC)[317] and ^{1}H-^{13}C Hetero-nuclear Multiple-Bond Correlation (HMBC)[318] spectroscopy.

Confirmation of metabolites identities in the LC-MS data was obtained using Tandem MS (MS/MS) on selected target ions with an energy ramp 5-20eV and measurement of resulting product ions.

Metabolite identification was characterized by a level of assignment (LoA) score that describes how the identification was made[320]. The levels used were as follows: LoA 1: Identified compound, confirmed by comparison to an authentic chemical reference. LoA 2: MS/MS precursor and product ions or 1D+2D NMR chemical shifts and multiplicity match to a reference database or literature to putatively annotate compound. LoA 3: Chemical shift (δ) and multiplicity matches a reference database to tentatively assign the compound.

3.3 Results

3.3.1 Demographic and anthropometric differences between athletes and controls

Forty male elite professional rugby players were recruited to the study. The mean age of the athletes was 29 years and they had a mean BMI of 29.1kg/m^2. Forty-six healthy male controls were recruited. They had a mean age of 29 years and all bar one subject were of Irish ethnicity. The control arm consisted of both low BMI (≤25kg/m^2, n=23) and high BMI (>28kg/m^2, n=23) subjects.

	Elite athletes (n=40)	Low BMI controls (n=23)	High BMI controls (n=23)
Age (years)	28.8 (3.8)	28.1 (5.1)	30.8 (5.6)
BMI (kg/m^2)	29.1 (3.0)$^{+}$	22.7 (1.8)**	31.2 (3.0)$^{¥}$
Body mass (kg)	101.3 (13.8)	74.3 (6.3)	103.1 (13.8)
Body fat (%)	16.9 (6.1)$^{++}$	15 (4.6)*	33.9 (8.8)$^{¥}$
Lean body mass (kg)	80 (8.9)$^{++}$	55.4 (5.6)**	65 (8)$^{¥}$
Waist/hip ratio	0.8 (0.04)$^{++}$	0.8 (0.05)	0.9 (0.07)$^{¥}$

*Table 3.3-1 Summary table of demographic and anthropometric results. Data shown as mean (SD), *p<0.01 or **p<0.0005 athletes versus low BMI controls $^{+}$p<0.01 or $^{++}$p<0.0005 athletes versus high BMI controls $^{¥}$p<0.0005 high BMI versus low BMI controls.*

3.3.2 Dietary Differences between athletes and controls

Athletes had significantly higher dietary intake of all food groups, including carbohydrate (pFDR<0.001), protein (pFDR<0.001), fat (pFDR<0.001), sugar (pFDR<0.001), fibre (pFDR<0.001), cholesterol (pFDR<0.001) and starch (pFDR=0.017). The largest increase was in protein intake with a median intake of 248g/day in athletes Vs 110g/day in controls (see Figure 3.3-1).

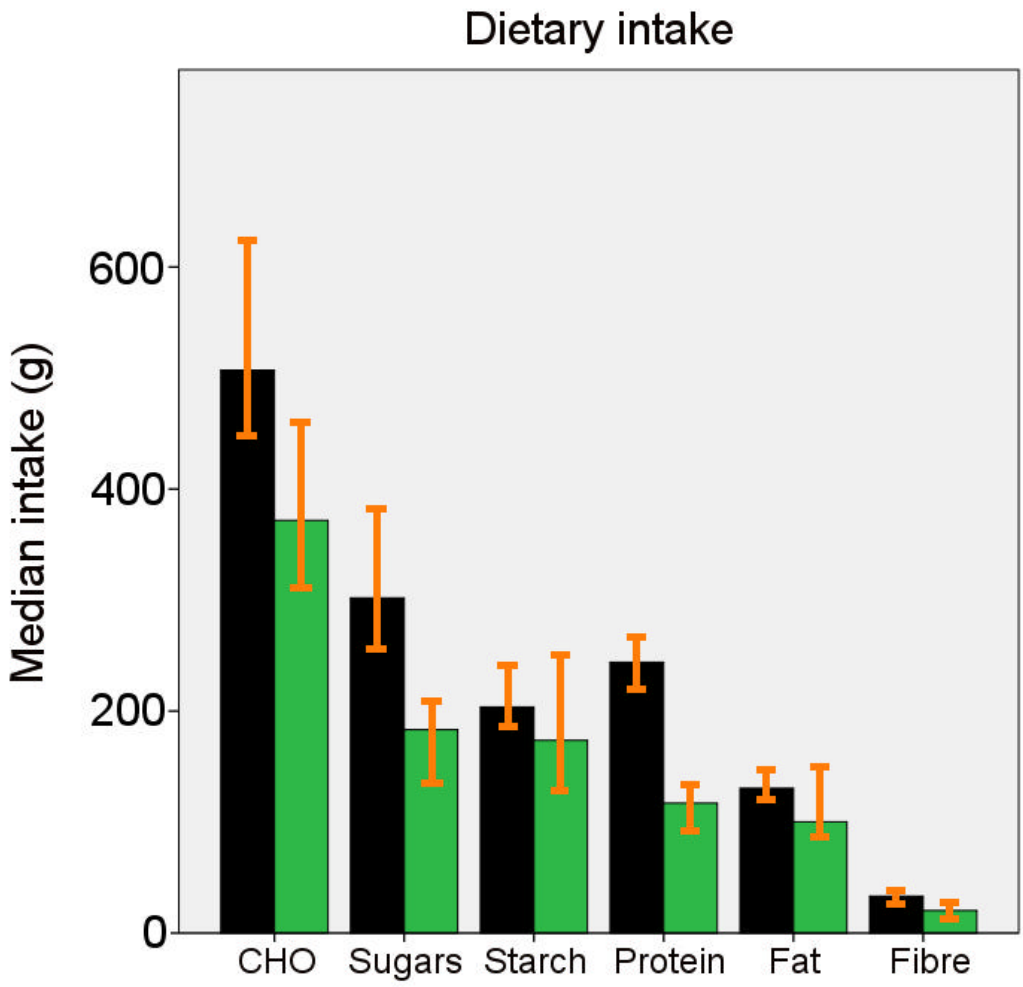


Figure 3.3-1 Dietary intake of Athletes (black) Vs Controls (greeen). Error bars = 95% confidence intervals. All food groups were significantly different between classes (pFDR<0.05).

3.3.3 ^{1}H-NMR spectroscopy of faecal and urine samples in athletes and controls

A combination of multiplatform metabolic phenotyping and multivariate analysis based on Principal Component Analysis (PCA) and Orthogonal Partial Least Squares Discriminant Analysis (OPLS-DA) was used to compare urinary and faecal samples from athletes and controls.

3.3.3.1 PCA models comparing ^{1}H-NMR spectra of athlete and control samples

Unsupervised analysis using PCA models of ^{1}H-NMR spectra from urine and faecal samples demonstrated clustering of participants according to their class (see Figure 3.3-2). The low R^2X and Q^2X scores indicate that the dataset contains multiple sources of variation that are not fully captured in the first three components.

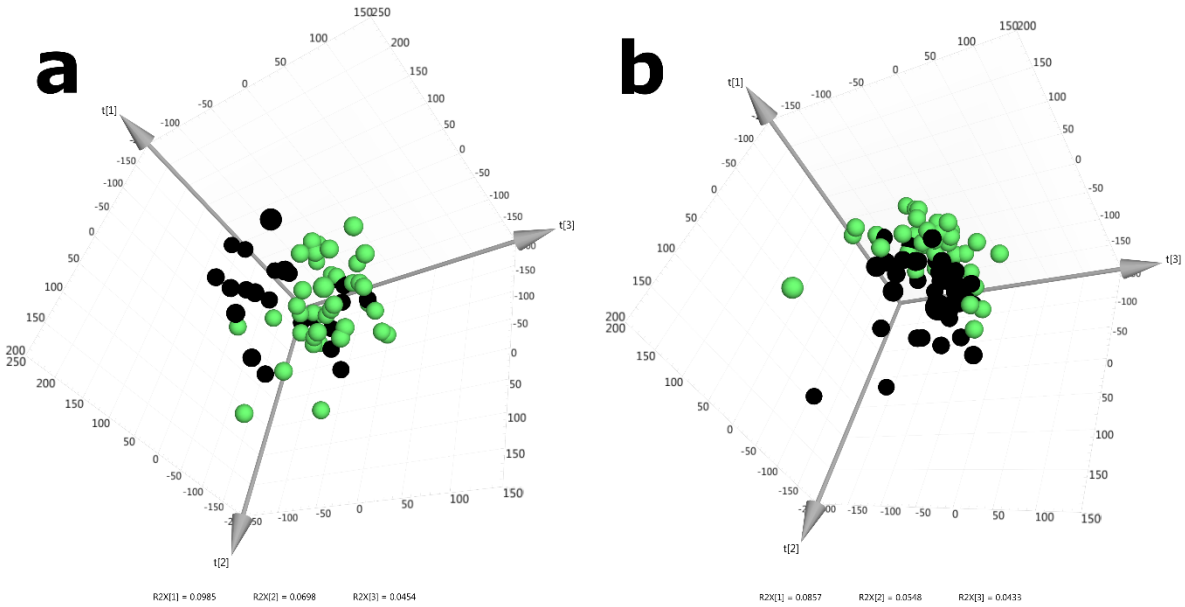


Figure 3.3-2 PCA scores plots of ^{1}H-NMR spectra comparing athletes (green) to controls (black). Models are comprised of 3 principal components. a) ^{1}H-NMR faecal sample analysis (R^2X=0.21, Q^2X=0.11), b) ^{1}H-NMR urine sample analysis (R^2=0.18, Q^2=0.05).

3.3.3.2 OPLS-DA models comparing ^{1}H-NMR spectra of athlete and control samples

Further differentiation between classes was achieved using supervised models. The cross-validated (CV) OPLS-DA models found strong differences between athletes and controls in urine and faecal samples analysed by ^{1}H-NMR analysis. Urine gave the strongest model, although both were significant. CV-OPLS-DA of ^{1}H-NMR spectra of urine samples gave a model score of R^2Y=0.86, Q^2Y=0.60 (see Figure 3.3-3a). The CV-OPLS-DA model comparing ^{1}H-NMR spectra of faecal samples gave a model score of R^2Y=0.86, Q^2Y=0.52 (see Figure 3.3-3b).

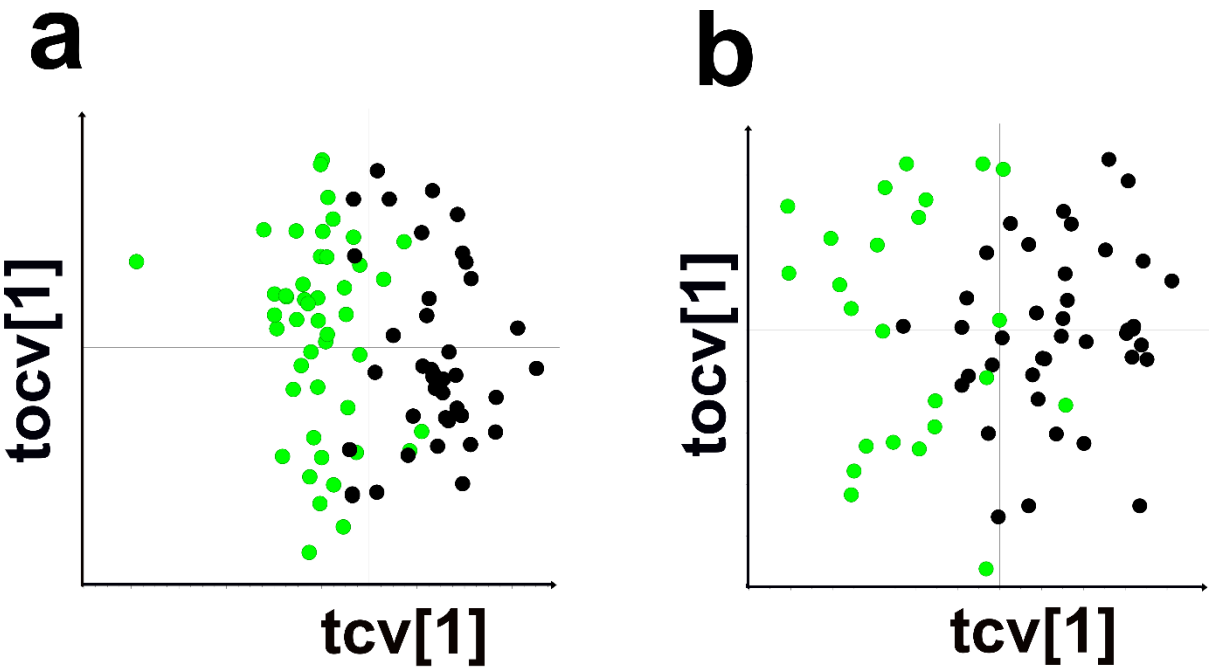


Figure 3.3-3 Cross validated OPLS-DA scores plots of ^{1}H-NMR spectra comparing athletes (green) to controls (black). Models are comprised of 1 predictive (tcv[1]) and 1 orthogonal (tocv[1]) principal component. a) ^{1}H-NMR urine sample analysis (R^2Y=0.86, Q^2Y=0.60), b) ^{1}H-NMR faecal sample analysis (R^2Y=0.86, Q^2Y=0.52).

3.3.3.3 Loadings of OPLS-DA ^{1}H-NMR spectroscopy models differentiating between athletes and controls

The loadings of the pairwise OPLS-DA models were used to identify metabolites discriminating between the two classes. Athletes' ^{1}H-NMR metabolic phenotypes were characterised by higher levels of TMAO, L-carnitine, dimethylglycine, O-acetyl carnitine, proline betaine, creatinine, acetoacetate, 3-hydroxy-isovaleric acid, acetone, *N*-methylnicotinate, *N*-methylnicotinamide, phenylacetylglutamine (PAG) and 3-methylhistidine in urine samples and higher levels of propionate, acetate, butyrate, trimethylamine, lysine, methylamine in faecal samples, relative to controls. Beta alanine betaine was higher in both faecal and urine samples of athletes. Athletes were further characterised by lower levels of glycerate, allantoin and succinate and lower levels of glycine and tyrosine relative to controls in urine and faecal samples respectively (see Table 3.3-2).

Table 3.3-2 List of significantly associated metabolites whose excretion discriminates between athletes and controls when using ^{1}H-NMR metabolic profiling models of urine (Figure 3.3-3a) and faecal water (Figure 3.3-3b).

Lists the metabolite name, significant chemical shift values and multiplicity, LoA and direction of association (↑ indicates higher excretion in the athletes group, ↓ indicates lower excretion in the athletes group) for urine and faecal biofluids.

Metabolite	**^{1}H chemical shift δ (multiplicity) [a]** **[Linked with STOCSY / TOCSY]**	**^{13}C chemical shift δ [HSQC]**	**LoA[b]**	**Association**	**Biofluid**
TMAO	3.27 (s)	62.39	1	↑	Urine
L-Carnitine	3.23 (s), 2.45 (dd), 3.43 (m)	56.96, 40.4/45.8, 38.4	1	↑	Urine
Dimethylglycine	2.93 (s), 3.72 (s)	46.53	1	↑	Urine
O-Acetyl Carnitine	3.19 (s), 2.15 (s)	56.76	2	↑	Urine
Proline Betaine	3.30 (s), 3.11 (s)	55.8	2	↑	Urine
Creatinine	3.05 (s), 4.06 (s)	33.1, 59.3	2	↑	Urine
Acetoacetate	2.29 (s), 3.45 (s)	32.68	2	↑	Urine
3-hydroxy-isovaleric acid	1.27 (s), 2.37 (s)	30.93, 52.33	2	↑	Urine
Acetone	2.24 (s)	33.3	2	↑	Urine
N-methylnicotinate	4.44 (s), 8.84 (d), 9.12 (s), 8.10 (t)	-	3	↑	Urine
N-methylnicotinamide	4.486 (s), 8.19 (t), 8.90 (d), 8.96 (d), 9.29 (s)	-	3	↑	Urine
Phenylacetylglutamine (PAG)	2.11 (m), 2.27 (m), 3.67 (m), 4.19 (m), 7.36 (t), 7.43 (t)	-	3	↑	Urine
3-Methylhistidine	3.32 (dd), 3.34 (dd), 3.76 (s), 3.98 (dd), 7.16 (s), 8.27 (s)	-	3	↑	Urine
Unknown A	3.12 (s)	55.73	-	↑	Urine
Unknown B	6.67 (d)	-	-	↑	Urine
Unknown C	2.90 (t), 4.42 (s), 4.43 (d)	-	-	↑	Urine
Unknown D	2.13 (d)	-	-	↑	Urine
Glycerate	3.70(m), 3.87 (dd)	66.15	1	↓	Urine
Allantoin	5.39 (s)	66.24	1	↓	Urine
Succinate	2.41 (s)	36.98	1	↓	Urine
Propionate	1.06 (t), 2.19 (q)	11.55, 25.7	2	↑	Faeces
Acetate	1.92 (s)	26.19	2	↑	Faeces

Butyrate	0.90 (t), 1.56 (m), 2.16 (t)	17.7, 28.7, 42.3*	2	↑	Faeces
Trimethylamine	2.88 (s)	41.3	1	↑	Faeces
Lysine	1.46 (m), 1.73 (q), 3.02 (t)	24.4, 29.4, 40.6	1	↑	Faeces
Methylamine	2.60 (s)	33.98	1	↑	Faeces
Unknown A	3.12 (s) (STOCSY 2.26 (s), 3.32-3.35)	55.73	-	↑	Faeces
Unknown E[§]	4.43 (d), 5.49 (d)	-	-	↑	Faeces
Glycine	3.56 (s)	44.54	2	↓	Faeces
Tyrosine	6.91 (d), 7.20 (d), 3.94 (dd), 3.06 (dd), 3.20 (dd)	-	3	↓	Faeces

[§]overlapping region – multiple candidate saccharides

[a]Multiplicity key is as follows: s=singlet, d=doublet, t=triplet, q=quartet, dd=doublet of doublets, m=multiplet.

[b]The Level of Assignment (LoA) used for the molecules identified by NMR are LoA 1: Identified compound, confirmed by adding the authentic chemical compound to the urine samples (spike-in experiments). LoA 2: ^{1}H and ^{13}C NMR chemical shifts and their multiplicity matched to database or literature to putatively annotate compound. LoA 3: ^{1}H NMR chemical shifts and their multiplicity matched to database or literature to putatively annotate compound.

^{13}C shifts marked by an asterisk (*) were not confirmed experimentally due to the absence of unambiguous resonance values and are taken from the Human Metabolome Database (HMDB).

3.3.4 LC-MS of faecal and urine samples in athletes and controls

3.3.4.1 PCA models comparing LC-MS spectra of athlete and control samples

Similar to ^{1}H-NMR, the unsupervised analysis using PCA models of urine and faecal LC-MS data demonstrated clustering of participants according to their class (see Figure 3.3-4). The low R^2X and Q^2X values in the urinary datasets suggest a high degree of metabolite variance between participant urine samples not fully captured in the first three components.

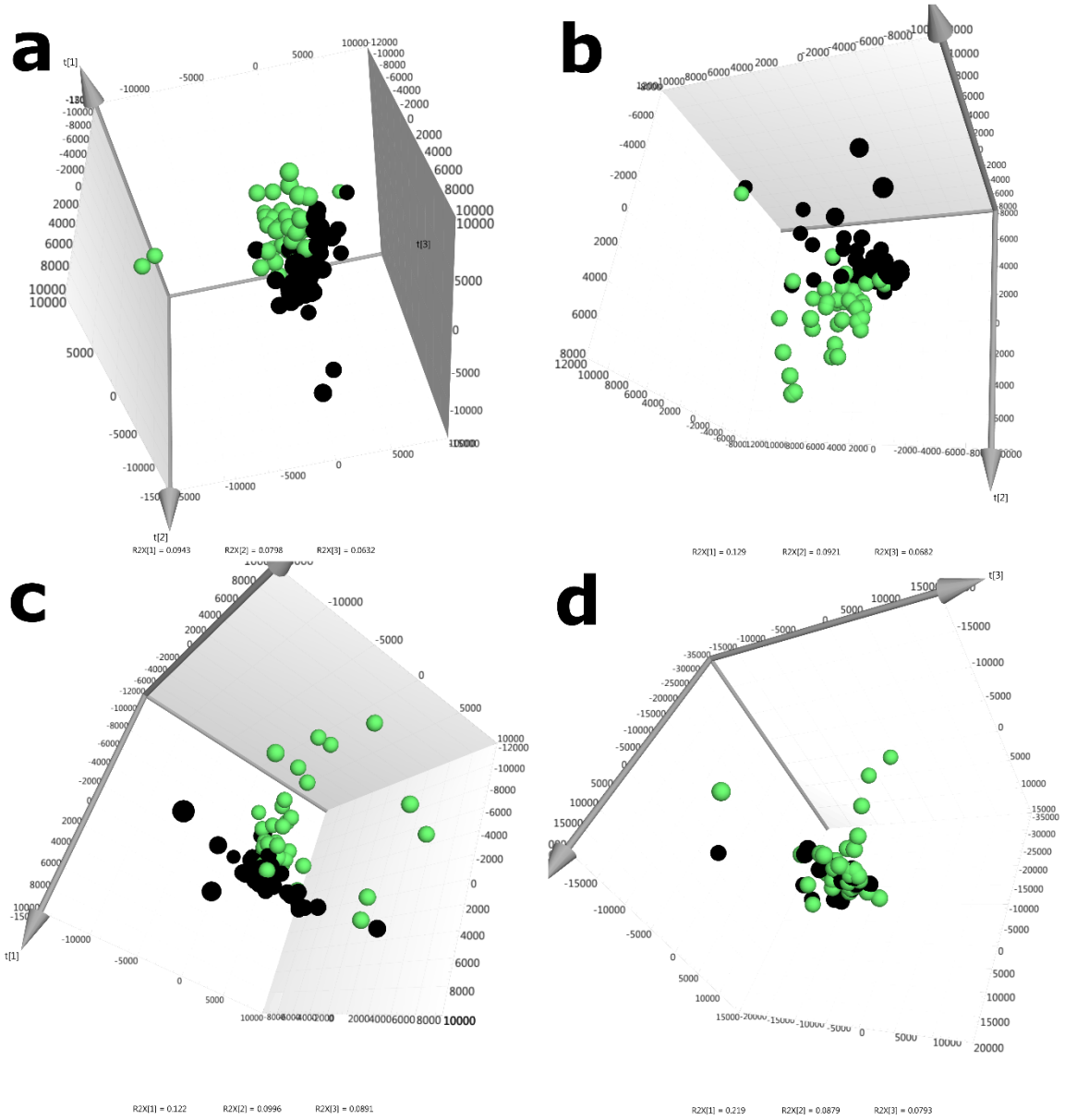


Figure 3.3-4 PCA scores plots of LC-MS analysis comparing athletes (green) to control (black) participants. Models are comprised of 3 principal components. a) UPLC-MS (RP, negative mode) urine sample analysis (R^2X=0.24, Q^2X=0.07), b) UPLC-MS (RP, positive mode) urine sample analysis (R^2X=0.29, Q^2X=0.15), c) UPLC-MS (HILIC, positive mode) urine sample analysis (R^2X=0.31, Q^2X=0.03), d) UPLC-MS (HILIC, positive mode) faecal sample analysis (R^2X=0.39, Q^2X=0.21).

3.3.4.2 OPLS-DA models comparing LC-MS spectra of athlete and control samples

Again, further differentiation between classes was achieved using supervised models. The cross-validated (CV) OPLS-DA models show strong differences between athletes (green circles) and controls (black circles) in urine samples analysed by HILIC UPLC-MS positive mode (R^2Y=0.85, Q^2Y=0.74, see Figure 3.3-5a), RP UPLC-MS positive mode (R^2Y=0.83, Q^2Y=0.73, see Figure 3.3-5b) and RP UPLC-MS negative mode (R^2Y=0.83, Q^2Y=0.67, see Figure 3.3-5c). Likewise, the CV-OPLS-DA models comparing faecal samples reveal differences between

athletes and controls analysed by HILIC UPLC-MS positive mode (R^2Y=0.65, Q^2Y=0.34, see Figure 3.3-5d). In addition, the semi-targeted analysis of bile acids shows separation between athletes and controls faecal samples in the CV-OPLS-DA model (R^2Y=0.70, Q^2Y=0.41).

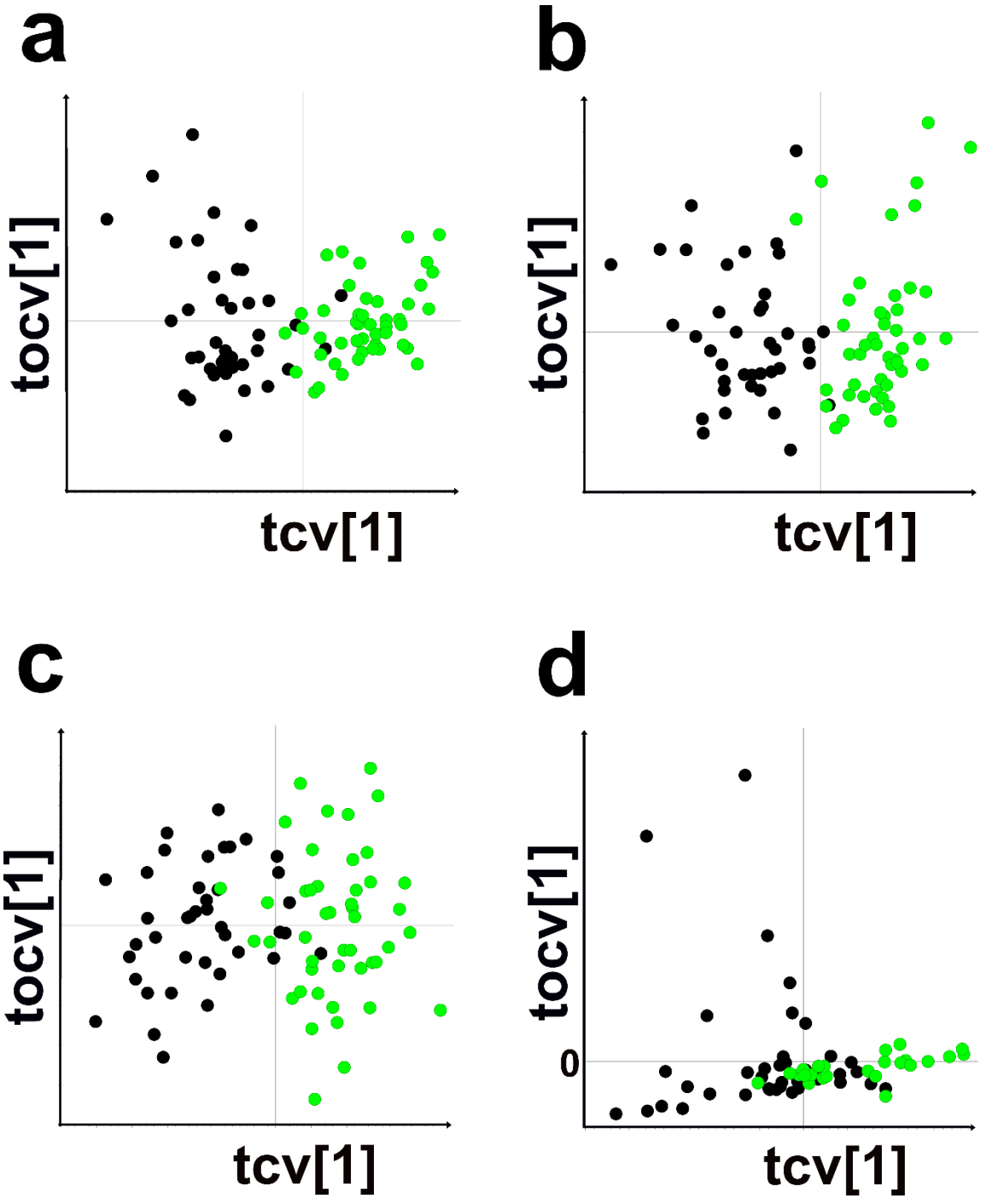


Figure 3.3-5 Cross validated OPLS-DA scores plots of LC-MS analysis comparing athletes (green) to controls (black). Models are comprised of 1 predictive (tcv[1]) and 1 orthogonal (tocv[1]) principal component. a) UPLC-MS (HILIC, positive mode) urine sample analysis (R^2Y=0.85, Q^2Y=0.74), b) UPLC-MS (reversed phase, positive mode) urine sample analysis (R^2Y=0.83, Q^2Y=0.73), c) UPLC-MS (reversed phase, negative mode) urine sample analysis (R^2Y=0.83, Q^2Y=0.67), d) UPLC-MS (HILIC, positive mode) faecal sample analysis (R^2Y=0.65, Q^2Y=0.34).

3.3.4.3 Loadings of OPLS-DA UPLC-MS models differentiating between athletes and controls

UPLC-MS analyses revealed higher urinary excretion of *N*-formylanthranilic acid, hydantoin-5-propionic acid, 3-Carboxy-4-methyl-5-propyl-2-furanpropionic acid (CMPF), CMPF glucuronide, trimetaphosphoric acid, acetylcarnitine - C2, propionylcarnitine - C3, isobutyrylcarnitine – C4, 2-Methylbutyroylcarnitine - C5, Hexanoylcarnitine - C6, C9:1-carnitine, L-valine, nicotinuric acid, 4-pyridoxic acid and creatinine in athletes relative to controls. While levels of glutamine, 7-methylxanthine, imidazoleacetic acid, isoquinoline / quinolone were lower in athletes' urinary samples relative to controls. Additionally, 16 unknown glucuronides were lower in the athlete samples (see Table 3.3-3).

Table 3.3-3 List of significantly associated metabolites whose excretion discriminates between athletes and controls when using LC-MS metabolic profiling models of urine (Figure 3.3-5a-d).

Lists the metabolite name, liquid chromatography (LC)-platform, mass charge ratio (m/z), MSMS fragments, retention time (RT), level of assignment (LoA) and direction of association (↑ indicates higher excretion in the athletes group, ↓ indicates lower excretion in the athletes group) in urine.

Metabolite	LC-platform	m/z	MSMS product ions (5-20eV)	RT	LoA	Association
N-formylanthranilic acid	RP -	164.034	120.04, 136.04, 92.05	4.52	2	↑
Hydantoin-5-propionic acid	RP -	171.040	100.04, 127.06, 128.04	1.43	2	↑
3-Carboxy-4-methyl-5-propyl-2-furanpropionic acid (CMPF)	RP -	239.091	195.10, 151.11	6.16	2	↑
CMPF glucuronide x1	RP -	-	Aglycone: CMPF *(239.09 – see above)*	-	*	↑
Trimetaphosphoric acid	RP -	238.891	96.96, 220.90, 78.96	0.42	2	↑
Glucuronide x1	RP -	-	Aglycone: 239.09	-	*	↑
Acetylcarnitine - C2	RP +	204.125	145.05, 85.03	0.85	2	↑
Propionylcarnitine - C3	RP +	218.139	159.07, 85.03	1.99	2	↑
(Iso)Butyrylcarnitine - C4	RP +	232.155	173.08. 85.03	2.83	2	↑
2-Methylbutyroylcarnitine - C5	RP +	246.171	187.10, 85.03	3.60	2	↑
C9:1-carnitine	RP +	300.217	241.14, 139.11, 85.03	5.32	2	↑
L-Valine	RP +	118.086	72.08	2.43	2	↑
Nicotinuric acid	RP +	181.061	135.06	3.33	2	↑

Hexanoylcarnitine - C6	HILIC +	260.185	201.11, 85.03	5.72	2	↑
4-Pyridoxic acid	HILIC +	184.062	166.05, 148.04, 138.06	1.14	2	↑
Creatinine	HILIC +	114.067	87.06	6.49	2	↑
Glutamine	RP -	145.061	127.05, 102.95, 101.94, 128.04, 84.05, 109.04	2.89	2	↓
Unknown glucuronides x9	RP -	-	Aglycones: 195.06, 271.07, 285.12, 237.14, 209.12, 143.07, 269.18, 257.17, 217.06	-	*	↓
7-Methylxanthine	RP +	167.059	124.05, 150.03, 142.06	1.98	2	↓
Imidazoleacetic acid	RP +	127.051	81.05	0.67	2	↓
Isoquinoline / quinoline	RP +	130.065	103.06	4.79	2	↓
Unknown glucuronides x7	RP +	-	Aglycones: 303.15, 219.06, 297.14, 383.14, 281.17, 239.16, 265.18	-	*	↓

The Level of Assignment (LoA) used for the molecules identified by MS are LoA 1: Identified compound, confirmed by comparison to an authentic chemical reference. LoA 2: MS/MS spectrum matched to database or literature to putatively annotate compound.

**Glucuronides characterised by a neutral loss of 176.03 Da (loss of monodehydrated glucuronic acid) in positive and negative modes. Further characterised by 175 m/z (anhydrous glucuronic acid) + 113 m/z (fragment of glucuronic acid) product ions in negative mode. If unable to unambiguously identify resulting aglycone, aglycone m/z stated.*

Although semi-targeted bile acid analysis of faecal water through UPLC-MS provided a good CV-OPLS-DA model (R^2Y=0.70, Q^2Y=0.41), interrogation of the metabolite loadings did not reveal any significant difference in 58 measured bile acids as defined by our previous criteria where t-statistic ≥ 1.96. Significant metabolites tentatively identified as higher in this profiling method included butyrate / iosbutyrate, valerate / isovalerate, caproate / isocaproate and D-urobilinogen (LoA 3).

3.3.5 GC-MS of faecal samples in athletes and controls

Univariate analysis, using the Mann Whitney U test, of SCFA levels in faeces measured by targeted GC-MS showed significantly higher levels of acetate (pFDR = 0.0001), propionate (pFDR < 0.0001), butyrate (pFDR = 0.0001) and valerate (pFDR=0.0112) in athletes relative to controls. Isobutyrate and Isovalerate did not differ significantly between the groups (see Figure 3.3-6).

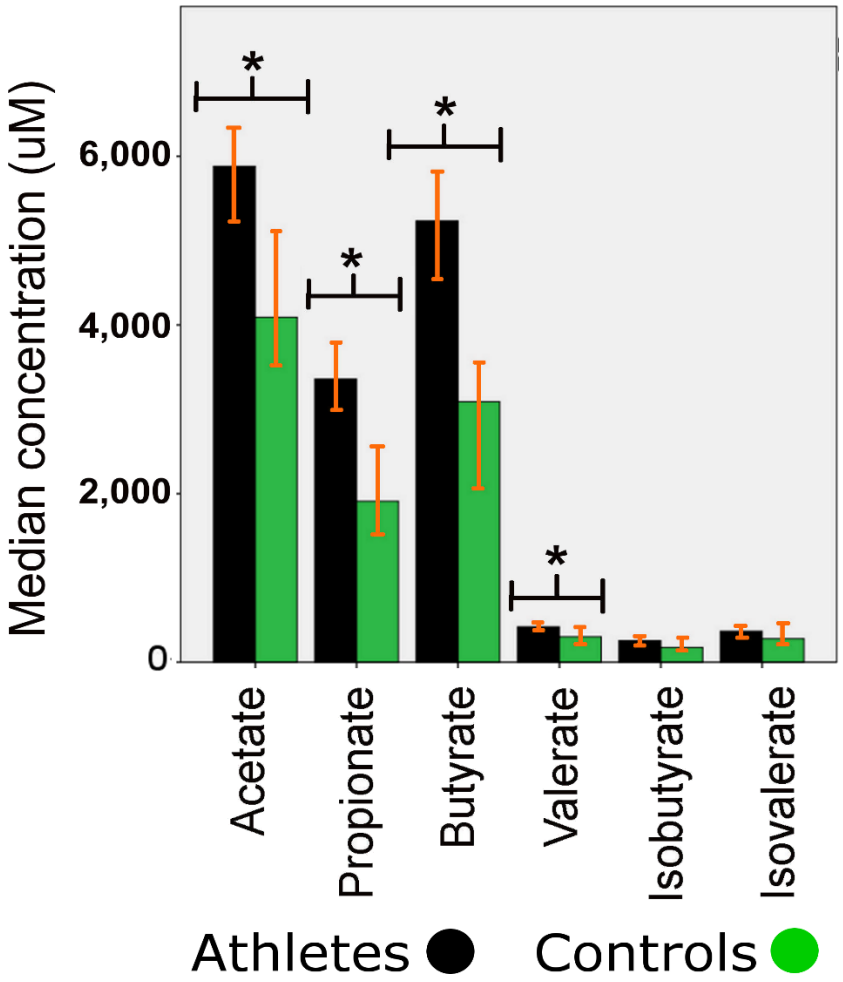


*Figure 3.3-6 Median short-chain fatty acid levels in faecal samples of athletes (black) and controls (green). Error bars represent 95% confidence intervals. * = p<0.05 after false discovery rate corrections using the Benjamini-Hochberg method.*

Univariate analysis of SCFA levels in urine found significantly lower levels of acetate (pFDR = 0.0074), propionate (pFDR = 0.0074), isobutyrate (pFDR = 0.0347), isovalerate (pFDR = 0.0011), 2-Methylbutyrate (pFDR = 0.0001) and lactate (pFDR = 0.0034) in athletes relative to controls. Butyrate, valerate, caproate and 2-hydroxybutyrate did not differ significantly between the groups.

		Median (μM)	IQR	Mann Whintey U (pFDR)
Acetate	Athlete	41.1	32.2	0.0074
	Control	61.4	39.3	
Propionate	Athlete	0.30	0.15	0.0074
	Control	0.39	0.15	

Isobutyrate	Athlete	0.51	0.37	0.0347
	Control	0.69	0.46	
Butyrate	Athlete	0.36	0.32	NS
	Control	0.33	0.23	
2 Methylbutyrate	Athlete	0.16	0.07	0.0001
	Control	0.28	0.18	
Isovalerate	Athlete	0.09	0.06	0.0011
	Control	0.13	0.09	
Valerate	Athlete	0.13	0.08	NS
	Control	0.11	0.07	
Caproate	Athlete	0.83	0.46	NS
	Control	0.73	0.49	
Lactate	Athlete	51.6	37.9	0.0034
	Control	91.6	61.8	
2 Hydroxybutyrate	Athlete	12.6	4.8	NS
	Control	12.3	4.5	

Table 3.3-4 Urinary SCFA concentrations (μM) in Athletes Vs Controls. IQR = Interquartile range, NS = Not significant.

3.3.6 Gut microbiome-host interactions: Correlations between bacterial taxa and faecal SCFA levels.

Taxonomic differences between the gut microbiota of athletes and controls in this cohort were previously published[286]. Here Spearman correlation was carried out between targeted measurements of faecal SCFAs and taxonomic data from 16S rRNA sequencing to assess if differences in taxonomic abundance influenced faecal SCFA levels. After FDR correction, Roseburia was positively correlated with acetate (r=0.53, pFDR=0.004) and butyrate (r=0.48, pFDR=0.018) while Family XII Incertae Sedis was positively correlated with isobutyrate (r=0.60, pFDR=0.000), isovlaerate (r=0.58, pFDR=0.000) and valerate (r=0.51, pFDR=0.008) (see Figure 3.3-7).

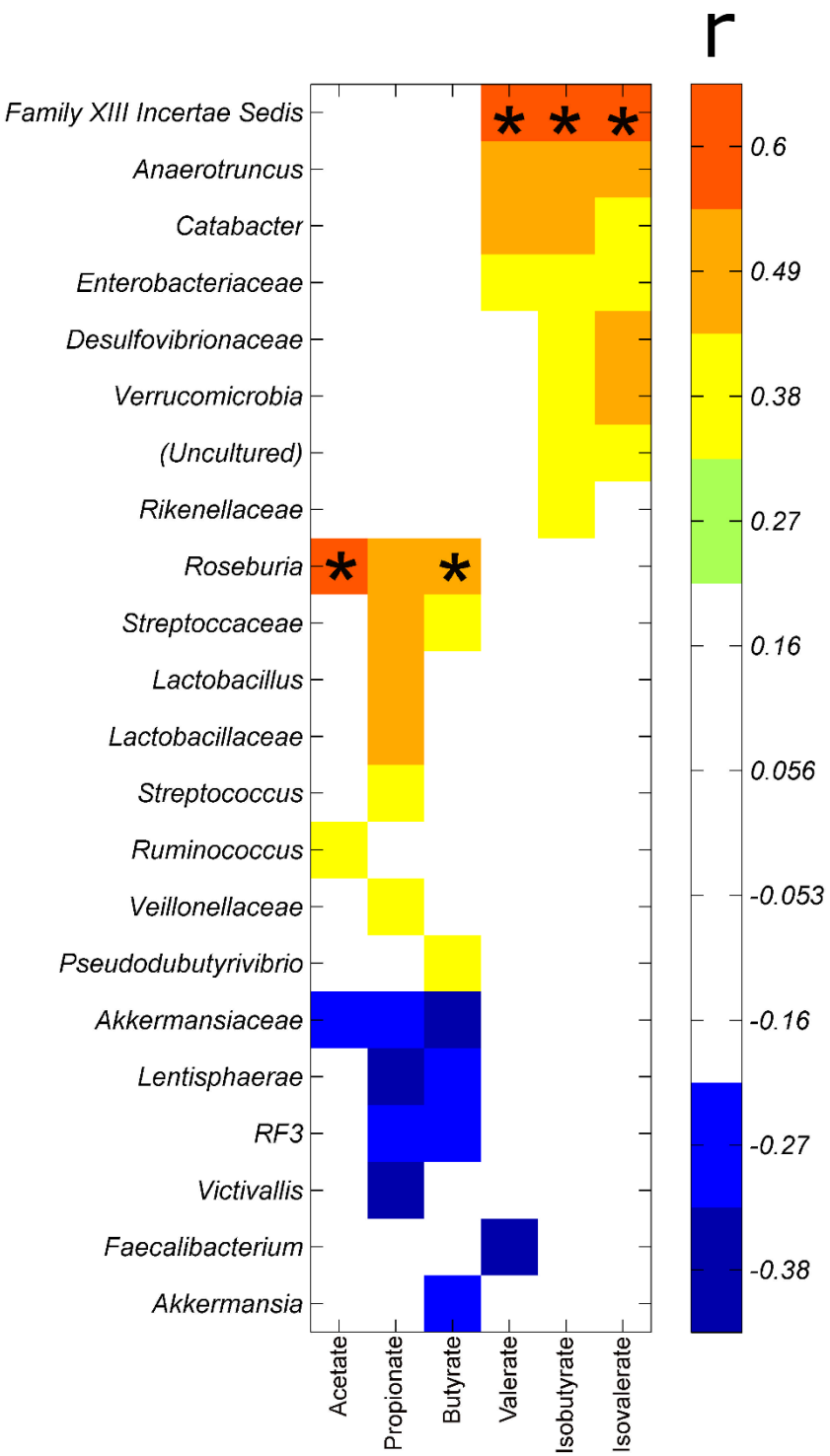


*Figure 3.3-7 Heat map of bacterial taxa (family / genus level) that correlate with faecal short-chain fatty acid levels using Spearman's correlation. Bright colours represent positive correlations, cool colours represent negative correlations (r). All correlations shown had a p-value <0.01. Those marked * represent correlations with a pFDR <0.01 after Benjamini-Hochberg multiple testing corrections.*

3.4 Discussion

3.4.1 Biological interpretation

These results shown that distinct metabolic phenotypes exist between athletes and controls. Phenotypic differences were dominated by metabolites associated with muscle turnover, those derived from vitamins and recovery supplements, metabolites derived from a high protein diet and metabolites derived from gut microbes.

Athletes have an enriched faecal SCFA profile, previously associated with a lean phenotype and numerous health benefits[36, 356, 357]. Within the faecal SCFAs, two distinct correlation clusters were observed; acetic acid, propionic acid and butyric acid correlated predominantly with dietary contributors (fibre with butyric acid and protein with propionic acid), while isobutyric acid, isovaleric acid and valeric acid correlated with microbial diversity. The same clusters are observed when correlating SCFAs with individual bacterial taxa. In keeping with these results, high levels of *Roseburia*, a known butyrate producer has previously been associated with high cardiovascular fitness[281]. Furthermore, low levels of *Roseburia* have been associated with Crohn's disease and chronic kidney disease progression[358, 359]. The association of *Family XIII Incertae Sedis* with levels of valerate, isobutyrate and isovalerate within the gut has not been previously reported and may be of importance to colonic health. Interestingly, SCFA were excreted in lower levels in athletes' urine relative to controls. The mechanism behind this is not fully understood. I postulate that this may be due to reduced systemic absorption due to decreased permeability of the gut as a result of increased delivery of SCFAs such as butyrate to the colonocytes leading to healthier intercellular tight junctions in the athletes. Alternatively, there could be increased utilisation of systemically absorbed SCFAs as an energy source in athletes.

Athletes' diets consisted of a higher proportion of protein and a higher intake overall of other nutrient classes such as carbohydrates, fat and fibre. The impact of higher protein intake in the athletes' relative to both control groups was seen in the metabolic phenotyping results. Numerous by-products of dietary protein metabolism, mostly by microbes, were elevated in the athlete cohort. These include TMAO, carnitines, trimethylamine, 3-Carboxy-4-methyl-5-propyl-2-furanpropionic acid, and 3-hydroxy-isovaleric acid. L-carnitine is obtained predominantly from meat or supplementation. L-carnitine transports long-chain acyl groups

from fatty acids into the mitochondrial matrix, there they are broken down through β-oxidation to acetyl CoA to obtain usable energy via the Krebs cycle. It has been suggested that L-carnitine supplementation can enhance exercise endurance capacity[360, 361].

Bacterial degradation of carnitine and choline by certain *Proteobacteria* and *Firmicutes* within the gut results in the by-product trimethylamine (TMA), which is subsequently oxidised in the liver via the flavin mono-oxygenase enzyme family to trimethylamine-*N*-oxide (TMAO)[54, 362, 363]. In turn, TMAO can be reduced to TMA, also elevated in the athlete group, by bacterial reductases in the human gut in certain *Actinobacteria*, *Firmicutes* and *Proteobacteria*[364, 365]. Highlighting a potential downside to these dietary changes, elevated TMAO seen here with increased protein intake, has been observed in patients with atherosclerosis and cardiovascular disease[26, 56, 60, 341, 366]. However, TMAO is present in cold water dwelling fish in high concentrations acting as an osmolyte and an antifreeze agent. This is consistent with TMAO being found in high levels in the urine of Japanese populations, who are not high risk for cardiovascular disease[5]. Similarly of interest is 3-hydroxy-isovaleric acid which has been shown to inhibit muscle wasting when used in conjunction with physical exercise. The compound can originate from the diet, potentially from egg consumption[367], however it is also commonly used as a supplement by athletes to increase exercise-induced gains in muscle size and muscle strength, reduce exercise-induced muscle damage, and speed up recovery from high intensity exercise[368, 369]. Proline betaine is likely a direct reflection of increased fruit consumption, specifically citrus fruit, in athletes[370].

Numerous metabolites associated with muscle turnover including creatinine, L-valine and 3-methylhistidine were elevated in the athlete groups. Similarly, metabolites derived from vitamins and recovery supplements common in professional sports, including glutamine, lysine and niacin breakdown products were found in higher concentrations in athletes.

Interestingly, PAG – a microbial conversion product of phenylalanine – is found in higher concentrations in the athletes. This has previously been associated with a lean phenotype[16]. In addition, PAG is the strongest biomarker of patients post bariatric surgery, where it is associated with an increase in the relative proportions of *Proteobacteria*[105]. This is also found here in the athlete group. However, contrary to our findings here, increased *Proteobacteria* has previously been labelled as a microbial signature of gut dysregulation[371, 372]. Studies have observed higher abundance of gut *Proteobacteria* in disease states such as obesity, T2DM and

non-alcoholic steatohepatitis (NASH) relative to controls[372]. Although, high Proteobacteria levels are also observed in non-disease states such as the neonatal period[371]. Therefore, the causative role of gut *Proteobacteria* abundance in disease remains to be established.

3.4.2 Study limitations and future directions

Shortcomings were introduced through the use of BMI to select controls. This was utilised in an effort to represent the varied sizes and body morphologies of a professional rugby team. Traditionally the 'backs' of a rugby team are leaner that the 'forwards'. However, in the athlete arm the majority of BMI increase was due to increased lean mass whereas in sedentary controls with a high BMI (>28kg/m^2) this was due to increased adiposity. In addition, Athletes' diets consisted of a higher proportion of protein and a higher intake overall of other nutrient classes such as carbohydrates, fat and fibre. Where possible the impact of higher protein intake on the metabolic differences between classes was identified and explained. However, this limited the ability to fully discriminate the effects of exercise and those originating from dietary differences between the two cohorts. The ideal control group would have a matched diet composition.

A technical limitation was the lack of normalisation of quantified metabolites. Unlike blood samples which have tightly regulated solute levels, urine and stool samples vary considerably in their volume according to water consumption and other physiological factors such as exercise levels. Hence the concentration of metabolites in these samples can be significantly altered. Untargeted metabolites measured through ^{1}H-NMR or LC-MS were normalised using median fold change normalisation[355, 373], a widely accepted technique to correct for these factors. However, this is an unsuitable method for a small panel of quantified metabolites. In stool, a possible solution would be to normalise using total stool volume or weight over a period of 24-hours or more. This would be highly unpractical to undertake. Similarly, urine could be normalised through volume over a 24-hour collection, or alternatively using urinary osmolality or creatinine levels. Indeed, ideally a combination of two of these techniques is recommended[374]. However, unfortunately these metrics were not available.

Lastly, sample collection was not fully standardised between participants. Samples were collected from subjects at variable times in the day and at variable times relative to their last meal and last period of exercise. Circadian rhythm, fasting status and time after exercise have

all been shown to introduce or influence metabolic changes[375-377]. However, the intra-individual changes introduced by these sampling variations are likely to be small relative to the inter-individual differences between these extreme cohorts[377].

3.5 Conclusion

These results have shown distinct metabolic phenotypes between athletes and sedentary controls, with changes likely resulting from both dietary differences and levels of aerobic and anaerobic exercise and fitness. However, the study does not allow the separation of these components and indeed conflates changes due to exercise and those due to diet. Nevertheless, this study has enabled novel insights into the exercise and diet microbiome-metabonome paradigm and the large differences between these extreme cohorts have overcome some of the limitations in study design. Elaboration and further exploration of the separate components of this paradigm, through better controlled studies, is now required and may inform the composition of exercise and fitness programs.

3.6 References

5. Holmes E, Loo RL, Stamler J, Bictash M, Yap IK, Chan Q, et al. Human metabolic phenotype diversity and its association with diet and blood pressure. Nature. 2008;453(7193):396-400.

16. Holmes E, Li JV, Athanasiou T, Ashrafian H, Nicholson JK. Understanding the role of gut microbiome-host metabolic signal disruption in health and disease. Trends in microbiology. 2011;19(7):349-59.

22. Ley RE, Turnbaugh PJ, Klein S, Gordon JI. Microbial ecology: human gut microbes associated with obesity. Nature. 2006;444(7122):1022-3.

26. Wang Z, Klipfell E, Bennett BJ, Koeth R, Levison BS, Dugar B, et al. Gut flora metabolism of phosphatidylcholine promotes cardiovascular disease. Nature. 2011;472(7341):57-63.

36. Ridaura VK, Faith JJ, Rey FE, Cheng J, Duncan AE, Kau AL, et al. Gut microbiota from twins discordant for obesity modulate metabolism in mice. Science. 2013;341(6150):1241214.

54. Ufnal M, Zadlo A, Ostaszewski R. TMAO: A small molecule of great expectations. Nutrition. 2015;31(11-12):1317-23.

56. Koeth RA, Wang Z, Levison BS, Buffa JA, Org E, Sheehy BT, et al. Intestinal microbiota metabolism of L-carnitine, a nutrient in red meat, promotes atherosclerosis. Nature medicine. 2013;19(5):576-85.

60. Tang WH, Wang Z, Levison BS, Koeth RA, Britt EB, Fu X, et al. Intestinal microbial metabolism of phosphatidylcholine and cardiovascular risk. The New England journal of medicine. 2013;368(17):1575-84.

105. Li JV, Ashrafian H, Bueter M, Kinross J, Sands C, le Roux CW, et al. Metabolic surgery profoundly influences gut microbial-host metabolic cross-talk. Gut. 2011;60(9):1214-23.

252. Biswas A, Oh PI, Faulkner GE, Bajaj RR, Silver MA, Mitchell MS, et al. Sedentary time and its association with risk for disease incidence, mortality, and hospitalization in adults: a systematic review and meta-analysis. Annals of internal medicine. 2015;162(2):123-32.

253. Same RV, Feldman DI, Shah N, Martin SS, Al Rifai M, Blaha MJ, et al. Relationship Between Sedentary Behavior and Cardiovascular Risk. Curr Cardiol Rep. 2016;18(1):6.

254. Wilmot EG, Edwardson CL, Achana FA, Davies MJ, Gorely T, Gray LJ, et al. Sedentary time in adults and the association with diabetes, cardiovascular disease and death: systematic review and meta-analysis. Diabetologia. 2012;55(11):2895-905.

259. Schwingshackl L, Missbach B, Dias S, Konig J, Hoffmann G. Impact of different training modalities on glycaemic control and blood lipids in patients with type 2 diabetes: a systematic review and network meta-analysis. Diabetologia. 2014;57(9):1789-97.

261. Harkin A. Muscling in on depression. The New England journal of medicine. 2014;371(24):2333-4.

263. Benatti FB, Pedersen BK. Exercise as an anti-inflammatory therapy for rheumatic diseases-myokine regulation. Nat Rev Rheumatol. 2015;11(2):86-97.

264. Hawley JA, Krook A. Metabolism: One step forward for exercise. Nature reviews Endocrinology. 2016;12(1):7-8.

266. Hoffman-Goetz L, Pervaiz N, Packer N, Guan J. Freewheel training decreases pro- and increases anti-inflammatory cytokine expression in mouse intestinal lymphocytes. Brain Behav Immun. 2010;24(7):1105-15.

267. Mul JD, Stanford KI, Hirshman MF, Goodyear LJ. Exercise and Regulation of Carbohydrate Metabolism. Prog Mol Biol Transl Sci. 2015;135:17-37.

281. Estaki M, Pither J, Baumeister P, Little JP, Gill SK, Ghosh S, et al. Cardiorespiratory fitness as a predictor of intestinal microbial diversity and distinct metagenomic functions. Microbiome. 2016;4(1):42.

282. Johannesson E, Simren M, Strid H, Bajor A, Sadik R. Physical activity improves symptoms in irritable bowel syndrome: a randomized controlled trial. The American journal of gastroenterology. 2011;106(5):915-22.

283. Robsahm TE, Aagnes B, Hjartaker A, Langseth H, Bray FI, Larsen IK. Body mass index, physical activity, and colorectal cancer by anatomical subsites: a systematic review and meta-analysis of cohort studies. Eur J Cancer Prev. 2013;22(6):492-505.

286. Clarke SF, Murphy EF, O'Sullivan O, Lucey AJ, Humphreys M, Hogan A, et al. Exercise and associated dietary extremes impact on gut microbial diversity. Gut. 2014;63(12):1913-20.

287. Petersen LM, Bautista EJ, Nguyen H, Hanson BM, Chen L, Lek SH, et al. Community characteristics of the gut microbiomes of competitive cyclists. Microbiome. 2017;5(1):98.

288. Cronin O, Molloy MG, Shanahan F. Exercise, fitness, and the gut. Curr Opin Gastroenterol. 2016;32(2):67-73.

294. Want EJ, Wilson ID, Gika H, Theodoridis G, Plumb RS, Shockcor J, et al. Global metabolic profiling procedures for urine using UPLC-MS. Nat Protoc. 2010;5(6):1005-18.

312. Wishart DS, Feunang YD, Marcu A, Guo AC, Liang K, Vazquez-Fresno R, et al. HMDB 4.0: the human metabolome database for 2018. Nucleic Acids Res. 2017.

313. Cloarec O, Dumas ME, Craig A, Barton RH, Trygg J, Hudson J, et al. Statistical total correlation spectroscopy: an exploratory approach for latent biomarker identification from metabolic 1H NMR data sets. Analytical chemistry. 2005;77(5):1282-9.

314. Posma JM, Garcia-Perez I, De Iorio M, Lindon JC, Elliott P, Holmes E, et al. Subset optimization by reference matching (STORM): an optimized statistical approach for recovery of metabolic biomarker structural information from 1H NMR spectra of biofluids. Analytical chemistry. 2012;84(24):10694-701.

315. Aue WP, Bartholdi E, Ernst RR. 2-Dimensional Spectroscopy - Application to Nuclear Magnetic-Resonance. J Chem Phys. 1976;64(5):2229-46.

316. Braunschweiler L, Ernst RR. Coherence Transfer by Isotropic Mixing - Application to Proton Correlation Spectroscopy. J Magn Reson. 1983;53(3):521-8.

317. Bodenhausen G, Ruben DJ. Natural Abundance N-15 Nmr by Enhanced Heteronuclear Spectroscopy. Chem Phys Lett. 1980;69(1):185-9.

318. Bax A, Summers MF. H-1 and C-13 Assignments from Sensitivity-Enhanced Detection of Heteronuclear Multiple-Bond Connectivity by 2d Multiple Quantum Nmr. J Am Chem Soc. 1986;108(8):2093-4.

320. Sumner LW, Amberg A, Barrett D, Beale MH, Beger R, Daykin CA, et al. Proposed minimum reporting standards for chemical analysis Chemical Analysis Working Group (CAWG) Metabolomics Standards Initiative (MSI). Metabolomics. 2007;3(3):211-21.

339. Barton W, Penney NC, Cronin O, Garcia-Perez I, Molloy MG, Holmes E, et al. The microbiome of professional athletes differs from that of more sedentary subjects in composition and particularly at the functional metabolic level. Gut. 2018;67(4):625-33.

340. Chen YC, Tu YK, Huang KC, Chen PC, Chu DC, Lee YL. Pathway from central obesity to childhood asthma. Physical fitness and sedentary time are leading factors. Am J Respir Crit Care Med. 2014;189(10):1194-203.

341. Tang WH, Hazen SL. Microbiome, trimethylamine N-oxide, and cardiometabolic disease. Translational research : the journal of laboratory and clinical medicine. 2016.

342. Conlon MA, Bird AR. The impact of diet and lifestyle on gut microbiota and human health. Nutrients. 2014;7(1):17-44.

343. Woting A, Pfeiffer N, Loh G, Klaus S, Blaut M. Clostridium ramosum promotes high-fat diet-induced obesity in gnotobiotic mouse models. MBio. 2014;5(5):e01530-14.

344. Utzschneider KM, Kratz M, Damman CJ, Hullarg M. Mechanisms Linking the Gut Microbiome and Glucose Metabolism. The Journal of clinical endocrinology and metabolism. 2016;101(4):1445-54.

345. Hartstra AV, Bouter KE, Backhed F, Nieuwdorp M. Insights into the role of the microbiome in obesity and type 2 diabetes. Diabetes care. 2015;38(1):159-65.

346. Williams NC, Johnson MA, Shaw DE, Spendlove I, Vulevic J, Sharpe GR, et al. A prebiotic galactooligosaccharide mixture reduces severity of hyperpnoea-induced bronchoconstriction and markers of airway inflammation. The British journal of nutrition. 2016;116(5):798-804.

347. Falony G, Joossens M, Vieira-Silva S, Wang J, Darzi Y, Faust K, et al. Population-level analysis of gut microbiome variation. Science. 2016;352(6285):560-4.

348. Zhernakova A, Kurilshikov A, Bonder MJ, Tigchelaar EF, Schirmer M, Vatanen T, et al. Population-based metagenomics analysis reveals markers for gut microbiome composition and diversity. Science. 2016;352(6285):565-9.

349. Ekelund U, Ward HA, Norat T, Luan J, May AM, Weiderpass E, et al. Physical activity and all-cause mortality across levels of overall and abdominal adiposity in European men and women: the European Prospective Investigation into Cancer and Nutrition Study (EPIC). The American journal of clinical nutrition. 2015;101(3):613-21.

350. Willett WC, Sampson L, Stampfer MJ, Rosner B, Bain C, Witschi J, et al. Reproducibility and validity of a semiquantitative food frequency questionnaire. American journal of epidemiology. 1985;122(1):51-65.

351. Dona AC, Jimenez B, Schafer H, Humpfer E, Spraul M, Lewis MR, et al. Precision high-throughput proton NMR spectroscopy of human urine, serum, and plasma for large-scale metabolic phenotyping. Analytical chemistry. 2014;86(19):9887-94.

352. Garcia-Villalba R, Gimenez-Bastida JA, Garcia-Conesa MT, Tomas-Barberan FA, Carlos Espin J, Larrosa M. Alternative method for gas chromatography-mass spectrometry analysis of short-chain fatty acids in faecal samples. J Sep Sci. 2012;35(15):1906-13.

353. Sarafian MH, Lewis MR, Pechlivanis A, Ralphs S, McPhail MJ, Patel VC, et al. Bile acid profiling and quantification in biofluids using ultra-performance liquid chromatography tandem mass spectrometry. Analytical chemistry. 2015;87(19):9662-70.

354. Tautenhahn R, Bottcher C, Neumann S. Highly sensitive feature detection for high resolution LC/MS. BMC bioinformatics. 2008;9:504.

355. Veselkov KA, Vingara LK, Masson P, Robinette SL, Want E, Li JV, et al. Optimized preprocessing of ultra-performance liquid chromatography/mass spectrometry urinary metabolic profiles for improved information recovery. Analytical chemistry. 2011;83(15):5864-72.

356. Koh A, De Vadder F, Kovatcheva-Datchary P, Backhed F. From Dietary Fiber to Host Physiology: Short-Chain Fatty Acids as Key Bacterial Metabolites. Cell. 2016;165(6):1332-45.

357. Hamer HM, Jonkers DM, Bast A, Vanhoutvin SA, Fischer MA, Kodde A, et al. Butyrate modulates oxidative stress in the colonic mucosa of healthy humans. Clinical nutrition (Edinburgh, Scotland). 2009;28(1):88-93.

358. Jiang S, Xie S, Lv D, Zhang Y, Deng J, Zeng L, et al. A reduction in the butyrate producing species Roseburia spp. and Faecalibacterium prausnitzii is associated with chronic kidney disease progression. Antonie Van Leeuwenhoek. 2016;109(10):1389-96.

359. Takahashi K, Nishida A, Fujimoto T, Fujii M, Shioya M, Imaeda H, et al. Reduced Abundance of Butyrate-Producing Bacteria Species in the Fecal Microbial Community in Crohn's Disease. Digestion. 2016;93(1):59-65.

360. Kim JH, Pan JH, Lee ES, Kim YJ. L-Carnitine enhances exercise endurance capacity by promoting muscle oxidative metabolism in mice. Biochemical and biophysical research communications. 2015;464(2):568-73.

361. Huang A, Owen K. Role of supplementary L-carnitine in exercise and exercise recovery. Med Sport Sci. 2012;59:135-42.

362. Meadows JA, Wargo MJ. Carnitine in bacterial physiology and metabolism. Microbiology. 2015;161(6):1161-74.

363. Fennema D, Philips IR, Shephard EA. Trimethylamine and trimethylamine N-oxide, a flavin-containing monooxygenase 3 (FMO3)-mediated host-microbiome metabolic axis implicated in health and disease. Drug Metab Dispos. 2016.

364. Arata H, Shimizu M, Takamiya K. Purification and properties of trimethylamine N-oxide reductase from aerobic photosynthetic bacterium Roseobacter denitrificans. J Biochem. 1992;112(4):470-5.

365. Kwan HS, Barrett EL. Purification and properties of trimethylamine oxide reductase from Salmonella typhimurium. J Bacteriol. 1983;155(3):1455-8.

366. Bennett BJ, de Aguiar Vallim TQ, Wang Z, Shih DM, Meng Y, Gregory J, et al. Trimethylamine-N-oxide, a metabolite associated with atherosclerosis, exhibits complex genetic and dietary regulation. Cell metabolism. 2013;17(1):49-60.

367. Stratton SL, Bogusiewicz A, Mock MM, Mock NI, Wells AM, Mock DM. Lymphocyte propionyl-CoA carboxylase and its activation by biotin are sensitive indicators of marginal biotin deficiency in humans. The American journal of clinical nutrition. 2006;84(2):384-8.

368. Wilson GJ, Wilson JM, Manninen AH. Effects of beta-hydroxy-beta-methylbutyrate (HMB) on exercise performance and body composition across varying levels of age, sex, and training experience: A review. Nutr Metab (Lond). 2008;5:1.

369. Wilson JM, Fitschen PJ, Campbell B, Wilson GJ, Zanchi N, Taylor L, et al. International Society of Sports Nutrition Position Stand: beta-hydroxy-beta-methylbutyrate (HMB). J Int Soc Sports Nutr. 2013;10(1):6.

370. Heinzmann SS, Brown IJ, Chan Q, Bictash M, Dumas ME, Kochhar S, et al. Metabolic profiling strategy for discovery of nutritional biomarkers: proline betaine as a marker of citrus consumption. The American journal of clinical nutrition. 2010;92(2):436-43.

371. Shin NR, Whon TW, Bae JW. Proteobacteria: microbial signature of dysbiosis in gut microbiota. Trends Biotechnol. 2015;33(9):496-503.

372. Rizzatti G, Lopetuso LR, Gibiino G, Binda C, Gasbarrini A. Proteobacteria: A Common Factor in Human Diseases. Biomed Res Int. 2017;2017:9351507.

373. Dieterle F, Ross A, Schlotterbeck G, Senn H. Probabilistic quotient normalization as robust method to account for dilution of complex biological mixtures. Application in 1H NMR metabonomics. Analytical chemistry. 2006;78(13):4281-90.

374. Warrack BM, Hnatyshyn S, Ott KH, Reily MD, Sanders M, Zhang H, et al. Normalization strategies for metabonomic analysis of urine samples. Journal of chromatography B, Analytical technologies in the biomedical and life sciences. 2009;877(5-6):547-52.

375. Dallmann R, Viola AU, Tarokh L, Cajochen C, Brown SA. The human circadian metabolome. Proceedings of the National Academy of Sciences of the United States of America. 2012;109(7):2625-9.

376. Berton R, Conceicao MS, Libardi CA, Canevarolo RR, Gaspari AF, Chacon-Mikahil MP, et al. Metabolic time-course response after resistance exercise: A metabolomics approach. J Sports Sci. 2017;35(12):1211-8.

377. Kim K, Mall C, Taylor SL, Hitchcock S, Zhang C, Wettersten HI, et al. Mealtime, temporal, and daily variability of the human urinary and plasma metabolomes in a tightly controlled environment. PloS one. 2014;9(1):e86223.

4 Unravelling the Diet – Exercise – Microbiome – Metabolome Paradigm

4.1 Introduction

The human gut microbiome has been implicated in a number of different pathologies, including obesity[20, 21], diabetes[23], cardiovascular disease[26] and cancer[378, 379]. Metabolic diseases in particular have been strongly associated with reduced bacterial diversity[34, 348, 380, 381]. A high fat, low fibre "Western diet" and sedentary lifestyle are well known risk factors for these morbidities. Importantly diet modulates many of its effects through the gut microbiome[382]. Recent studies have shown that increased physical activity and aerobic fitness may also mediate some of its known health benefits through modulation of gut bacteria[383-386]. Human studies, including results from the study described in Chapter 3, have shown changes to the gut microbiome, including increased diversity, in both habitual exercisers[281, 387] and professional athletes[65, 286, 287].

However, in humans the relationship between increased physical activity and microbial changes is confounded by the dietary adaptations that typically accompany physical activity. In this Chapter, two independent studies are performed in an effort to unravel this complex inter-dependent relationship:

1. ***A longitudinal study of the effects of high protein diet, exercise and combined regimes on the metabolic phenotype***
2. ***Multi-level modelling of individuals according to dietary habits and exercise levels based on objective diet healthiness scores derived from ^{1}H-NMR profiling***

The first study is a longitudinal study to measure the effects of three separate interventions. Namely a high protein diet, an exercise regime and the combination of a high protein diet with the exercise regime. Whereas the second study builds upon the analysis of professional athletes and sedentary controls in Chapter 3. Here I apply a novel objective dietary healthiness score, based on urine ^{1}H-NMR spectra, to cluster subjects based on both diet and exercise parameters in an attempt to separate these confounding factors.

[Study 1] A longitudinal trial of diet and exercise's effect on the metabolic phenotype

Results from the following chapter have been published as part of the following article[388]: Cronin O, Barton W, Skuse P, Penney NC, Garcia-Perez I, Murphy EF, et al. A Prospective Metagenomic and Metabolomic Analysis of the Impact of Exercise and/or Whey Protein Supplementation on the Gut Microbiome of Sedentary Adults. mSystems. 2018;3(3).

4.2 Introduction

In an endeavour to differentiate between the effects of diet and exercise on the human gut microbiome and metabolic phenotype a prospective interventional study was conducted. Participants were randomised into three arms consisting of; a high (whey) protein diet, an exercise regime, and a combined high protein diet and exercise regime. Samples of urine and stool were collected before and after intervention for metabolomic and gut microbiome analysis.

4.3 Materials and Methods

4.3.1 Study population

Ethical approval for the study was granted by the Cork Clinical Research Ethics Committee (CREC). Healthy male and female participants, aged between 18-40 and with low levels of physical activity were recruited to the study. To enable measurement of the effect of de novo exercise training, subjects were required not to have engaged in regular activities beyond light physical activities of daily life for a minimum of three months prior to enrolment into the study. Baseline levels of physical activity were assessed using the International Physical Activity Questionnaire short form[389].

Volunteers were assessed for medical conditions including; diabetes mellitus, cardiovascular disease, autoimmune disorders or regular medication use. In addition, volunteers who had experienced factors likely to disrupt the gut microbiome were excluded. These included individuals that had suffered gastroenteritis, received oral antibiotics or received bowel preparation one month prior to enrolment. Full inclusion and exclusion criteria are outlined in Table 4.3-1.

Inclusion Criteria
• Low physical activity level as per the International Physical Activity Questionnaire (Short form) • Not currently or recently (last 3 months) involved in regular or organised amateur sport or exercise • Non-smoker • Not on regular medications • Aged 18 to 40 • Body Mass Index between 22 to 35 (inclusive)
Exclusion Criteria
• Coronary artery disease, congenital heart disease or any cardiovascular disease • Family history of known coronary artery disease before 45 years of age • Uncontrolled hypertension (>140/90 mmHg) • Renal or hepatic impairment • Type 1 or type 2 diabetes mellitus • Pulmonary disease – not including well-controlled, mild asthma • Primary or secondary immunodeficiency or autoimmune disorder • Current smoker or ex-smoker of less than 3 months duration • Psychiatric disorders including previous history of depression • A history of substance abuse • Current or recent involvement in another clinical research study • Known or suspected hypersensitivity to the dietary supplementation

• Gastro-intestinal disease e.g. coeliac disease, inflammatory bowel disease, Irritable Bowel Syndrome • Previous significant gastro-intestinal surgery e.g. colectomy • Suspected or confirmed pregnancy

Table 4.3-1 Study inclusion / exclusion criteria

4.3.2 Study Intervention

Eligible volunteers were randomised into one of three intervention groups: High Protein Diet, Exercise, Combined High Protein Diet and Exercise. All interventions lasted eight weeks.

In the Protein Diet group, participants received daily 30g protein supplementation and were instructed to maintain their usual levels of physical inactivity. This contained 24g of whey protein and consisted of a blend of whey protein isolate, concentrate, and hydrolysed whey protein concentrate. Compliance was encouraged through the use of daily text message reminders. In addition, participants were required to return empty sachets each fortnight before collecting further supplements. Participants with a compliance below 90% were withdrawn from the study.

The exercise program consisted of standardised, mixed resistance and aerobic training, with participants required to train three times per week. Aerobic exercise was progressive and similar to a 'couch to 5km' running program, whereby individuals with minimal aerobic fitness were able to complete sessions at the start of the program and subsequent exercise sessions progressively increased in difficulty over the eight-week program to match improved fitness. The aerobic exercise was moderate intensity and graded 5-7 / 10 on the modified Borg rating of perceived exertion scale[390]. In addition, volunteers undertook resistance training using seven machine-based resistance exercises. Subjects performed a minimum of three sets of eight repetitions with starting weights calculated at induction as 70% of the participant's one repetition maximum value. The resistance training was progressive and aimed to increase the resistance weight by 15-20% over the course of the program. A FitLinxx® activity monitoring system was used to remotely monitor compliance to the exercise program. Individuals not complying for more than seven days were withdrawn from the study.

The combined group followed the same exercise and protein supplementation regimens as the individual groups. All participants were instructed to maintain their usual dietary intake and not to take additional dietary, vitamin or herbal supplementation during the study period. In addition, participants requiring antibiotics during the study period were withdrawn.

4.3.3 Study Measurements

Initial baseline measurements were performed within four days preceding the intervention and again at the end of the eight-week intervention period. Subjects were instructed to refrain from alcohol and exercise for 24 hours prior to the measurement. In addition, to reduce the effects of diurnal variation, measurements were taken between 0700-1030. Clinical variables including heart rate, blood pressure and weight as well as body composition, assessed using Dual-Energy X-ray Absorptiometry (DEXA) scan, were measured. Participants were then asked to provide fresh faecal and urine samples. These were aliquoted and stored at -80°c until further analysis.

Volunteers then underwent a cardio-respiratory fitness assessment. To prevent injury from unaccustomed vigorous exercise, a validated submaximal assessment of peak aerobic capacity (VO_{2max}), the Rockport one-mile walk test, was utilised[391]. The test was performed in a standardised temperature environment at an indoor running track.

Dietary intake was assessed using a food frequency questionnaire (FFQ). Subjects were asked to record their dietary intake based on the preceding eight weeks. The FFQ used was an 146-item questionnaire, adapted from the UK arm of the European Prospective Investigation into Cancer (EPIC) study[349], which was based on the original Willet FFQ[350].

4.3.4 ^{1}H-NMR and LC-MS profiling and SCFA quantitative analysis

^{1}H-NMR profiling, LC-MS profiling and GC-MS SCFA quantitative analysis of urinary and faecal samples was performed as previously described in Chapter 3.

4.3.5 Metabolite Quantification

Semi-quantification of identified metabolites was performed using an in-house Matlab script to annotate maximal intensity of MFC normalised spectral peaks. The highest intensity spectral peak was identified for each measured metabolite and precisely quantified for each individual. Manual annotation enabled precise marking of peaks, allowing for variations in

chemical shift in individual samples. Where spectral peaks overlapped with other metabolites the highest intensity unambiguous spectral region was used. The example below (Figure 4.3-1) shows the variation in peak intensity of TMAO between participants.

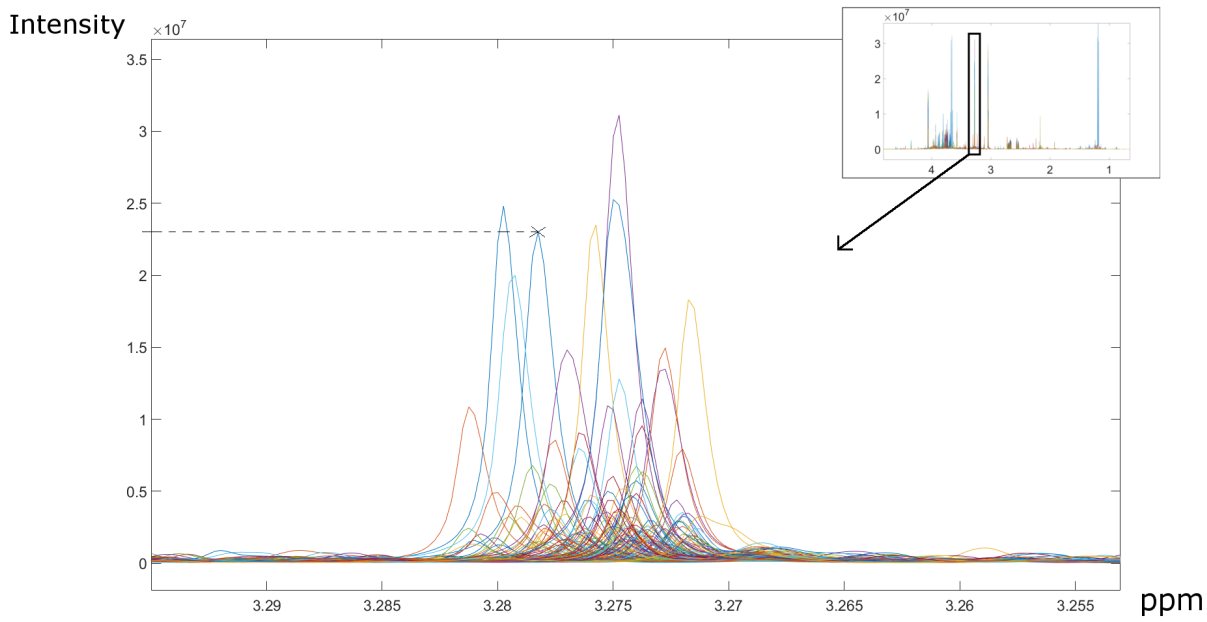


Figure 4.3-1 Illustration of semi-quantification using an in-house Matlab script. The figure shows the labelling of each participant's singlet at 3.275ppm (TMAO), to identify the peak intensity.

4.3.6 Statistical Analysis

4.3.6.1 Paired analysis

Data were centred and scaled to account for the repeated-measures design and then modelled using Partial Least Squares – Discriminant Analysis (PLS-DA) with Monte-Carlo cross-validation (MCCV)[311]. The fit and predictability of the models obtained was determined by the R^2Y and Q^2Y values respectively.

4.3.6.2 Univariate analysis

Differences in quantitative and semi-quantitative analyses of targeted metabolites between longitudinally paired samples were assessed for significance using the Wilcoxon Rank test. P values were corrected using Benjamini-Hochberg multiple testing corrections.

4.4 Results

4.4.1 Clinical outcomes

Healthy Irish male and female Caucasian volunteers (n=90) aged 18 to 40 years and with a body mass index (BMI) of between 22-35kg/m^2, were recruited in 2014.

Seventy-four of the 90 participants enrolled in the study completed the 8-week study period. At baseline, there was not significant difference in participants' clinical and anthropometric characteristics (see Table 4.4-1). Subjects were predominantly classed as overweight, with the median BMI over 27kg/m^2 in all groups. There were no significant differences in the participants' baseline level of physical activity, assessed using the International Physical Activity Questionnaire (IPAQ)[392].

Table 4.4-1 Baseline demographic, anthropometric and IPAQ activity measures. Values are expressed as medians (IQR). PA = Physical activity.

	Exercise (n=25)	**Exercise + Protein (n=22)**	**Protein only (n=27)**	**p-value (Kruskal-Wallis test)**
Age (years)	35 (28-38)	32 (28-35)	34 (28-36)	0.53
Sex (female)	n=14 (56%)	n=12 (55%)	n=11 (41%)	0.48
Height (cm)	172 (165-181)	169 (166-183)	172 (163-178)	0.67
Weight (kg)	78.8 (70.1-94.5)	82.3 (69-98.9)	76.4 (69.8-87)	0.67
BMI (kg/m^2)	27.9 (25.1-29.2)	27.5 (25.7-30)	27.0 (24.9-28.7)	0.76
Resting heart rate (BPM)	72 (65-81)	68 (61-79)	74 (66-78)	0.36
Systolic BP (mmHg)	128 (117-134)	125 (121-136)	125 (118-130)	0.71
Diastolic BP (mmHg)	78 (74-89)	76 (72-84)	79 (75-84)	0.54
Waist:Hip ratio	0.85 (0.83-0.89)	0.84 (0.8-0.93)	0.83 (0.78-0.88)	0.37
Body fat (%)	32.8 (29-38.7)	34.7 (29-37.2)	34.5 (29.3-39.4)	0.66
Fat mass (kg)	26.3 (22.6-30.6)	26.0 (23-33.1)	26.8 (20.7-32.9)	0.96
Lean tissue mass (kg)	52.4 (40.7-61.4)	51.3 (41.5-61.5)	47.2 (42.9-53.3)	0.44
Weekly PA (METS)	462 (298-1139)	564 (413-844)	657 (424-1145)	0.60
Weekly PA (kCals)	761 (381-1618)	748 (525-1127)	762 (512-1773)	0.77
Sitting time (hours per week)	56 (40-61)	62 (47-76)	51 (33-62)	0.11

Motorized transport (hours per week)	5 (3.25-8.3)	3.5 (2-6)	4.1 (0.8-7)	0.27

Following intervention participants in the Exercise and Combined groups both demonstrated significantly improved maximal aerobic capacities (VO_2max) and reduced resting heart rates ($p<0.05$). In addition, the Exercise and Combined groups, in contrast to the Protein only group, had a significant reduction in total fat mass, percentage fat mass and trunk fat mass as well as an increase in total lean tissue mass at the end of the intervention ($p<0.05$). Other than Whey protein supplementation, dietary frequency patterns did not deviate from participants' baseline intake over the course of the intervention.

4.4.2 ^{1}H-NMR spectroscopy of urine and faecal samples

4.4.2.1 PCA models comparing ^{1}H-NMR spectra of samples before and after intervention

Principal component analysis of participant samples of urine and faeces pre and post intervention did not reveal any clustering according to class, or other factor (see Figure 4.4-1). Models are comprised of 2 principal components. Model scores were as follows; ^{1}H-NMR urine sample analysis ($R^2X=0.16$, $Q^2X=0.12$), ^{1}H-NMR faecal sample analysis ($R^2X=0.36$, $Q^2X=0.30$).

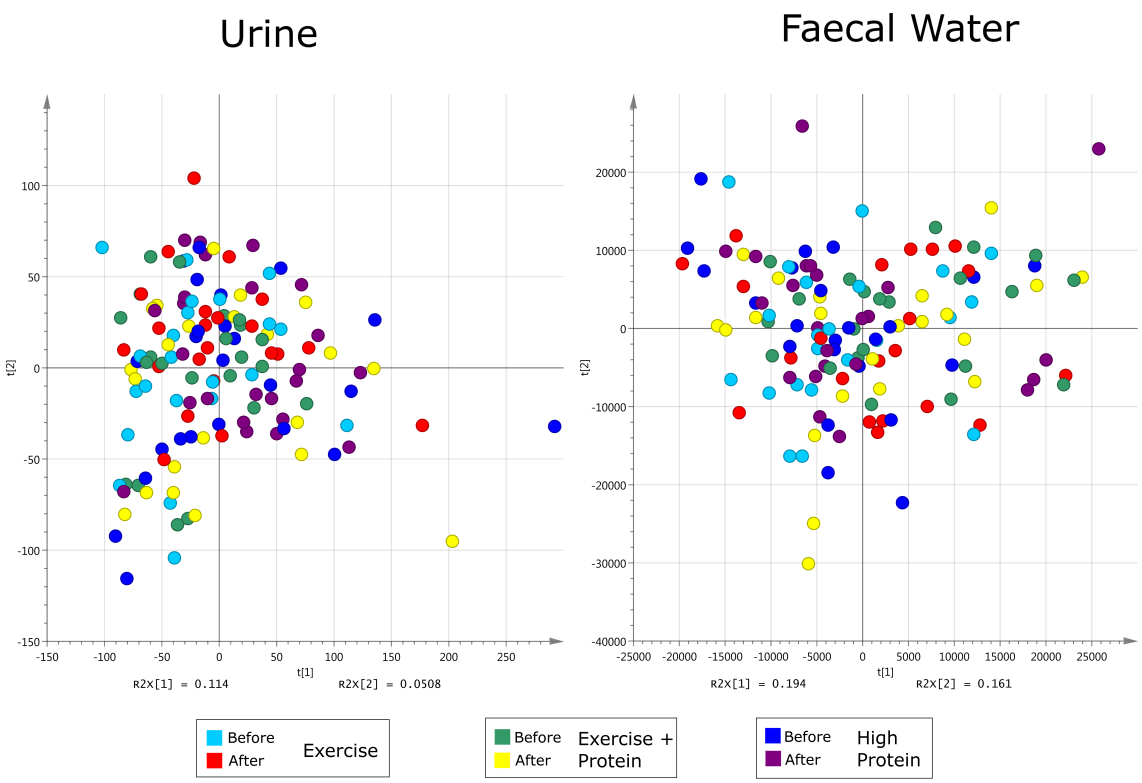


Figure 4.4-1 PCA scores plots of ^{1}H-NMR spectra comparing participants samples pre and post intervention with either Exercise, Exercise & High Protein Diet or High Protein Diet alone. Models are comprised of 2 principal components. a) ^{1}H-NMR urine sample analysis (R^2X=0.16, Q^2X=0.12), b) ^{1}H-NMR faecal sample analysis (R^2X=0.36, Q^2X=0.30).

4.4.2.2 Paired OPLS-DA models comparing ^{1}H-NMR spectra of samples before and after intervention

Paired MCCV-PLS-DA analysis or urine and faecal ^{1}H-NMR spectral profiles did not reveal any significant metabolic differences after intervention in any group (see Figure 4.4-2). Scores from analysis of urine samples were as follows: Exercise R^2Y: 0.95, Q^2Y: -0.33; Exercise + Protein R^2Y: 0.97, Q^2Y: -0.10; Protein: R^2Y: 0.97, Q^2Y: -0.27. Scores from analysis of faecal samples were as follows: Exercise R^2Y: 0.96, Q^2Y: -0.05; Exercise + Protein R^2Y: 0.97, Q^2Y: -0.12; Protein: R^2Y: 0.95, Q^2Y: -0.08.

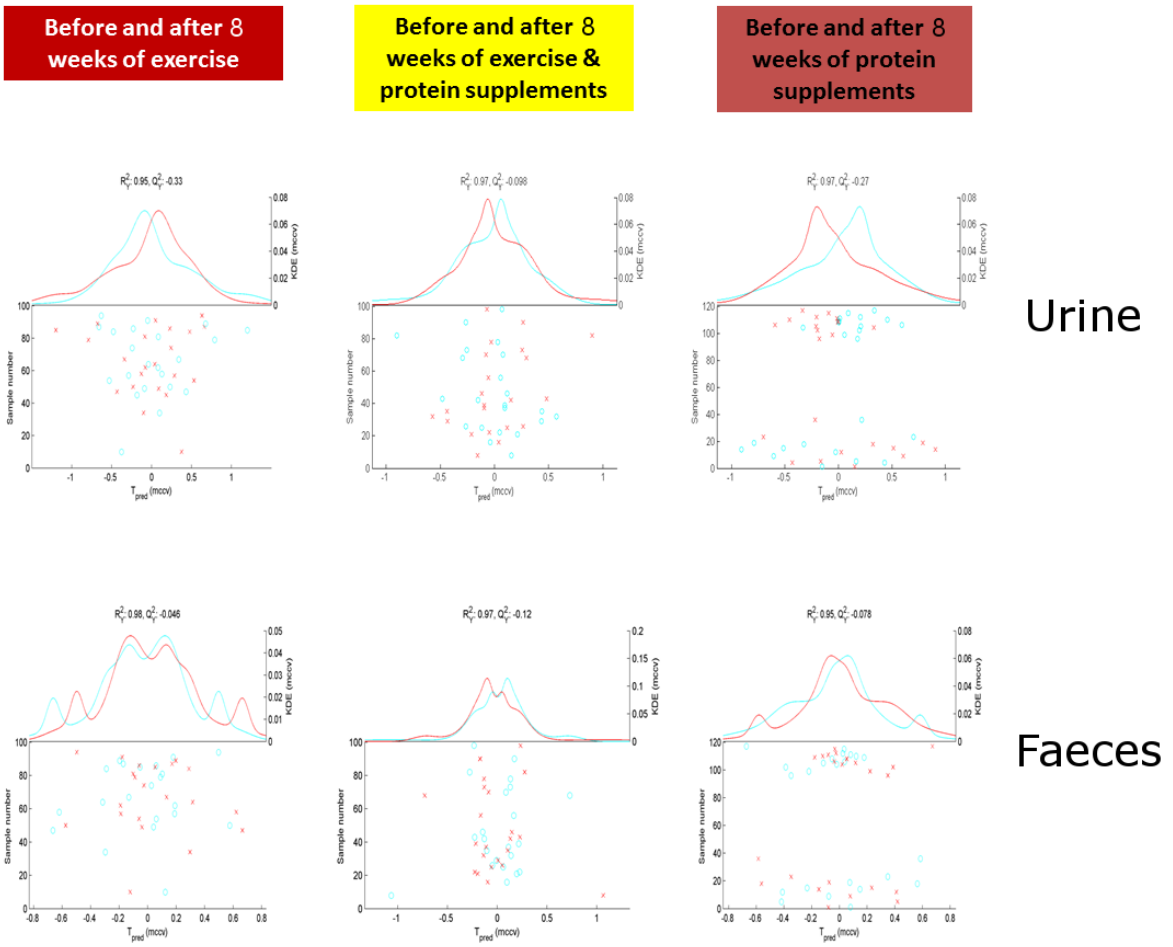


Figure 4.4-2 Paired MCCV-PLS-DA scores plots of ^{1}H-NMR analysis comparing participants samples pre and post intervention with either Exercise, Exercise & High Protein Diet or High Protein Diet alone. Models are comprised of 1 predictive and 1 orthogonal component. i) ^{1}H-NMR urine sample analysis (Exercise R^2Y: 0.95, Q^2Y: -0.33; Exercise + Protein R^2Y: 0.97, Q^2Y: -0.10; Protein: R^2Y: 0.97, Q^2Y: -0.27), ii) ^{1}H-NMR faecal sample analysis (Exercise R^2Y: 0.96, Q^2Y: -0.05; Exercise + Protein R^2Y: 0.97, Q^2Y: -0.12; Protein: R^2Y: 0.95, Q^2Y: -0.08).

4.4.3 UPLC-MS of urine and faecal samples

4.4.3.1 PCA models comparing LC-MS spectra of samples before and after intervention

Similar to unsupervised PCA of ^{1}H-NMR spectra of urine and faecal samples pre and post intervention, analysis by LC-MS did not cluster according to class, or other factors (see Figure 4.4-3). Model scores, comprising 2 principal components, were as follows; Urine Reversed Phase LC-MS Negative Mode (R^2X=0.18, Q^2X=0.12), Urine Reversed Phase LC-MS Positive Mode (R^2X=0.19, Q^2X=0.13), Urine HILIC LC-MS Positive Mode (R^2X=0.21, Q^2X=0.01), Faeces HILIC LC-MS Positive Mode (R^2X=0.21, Q^2X=0.01). The scores indicate an extremely high degree of variation within the dataset.

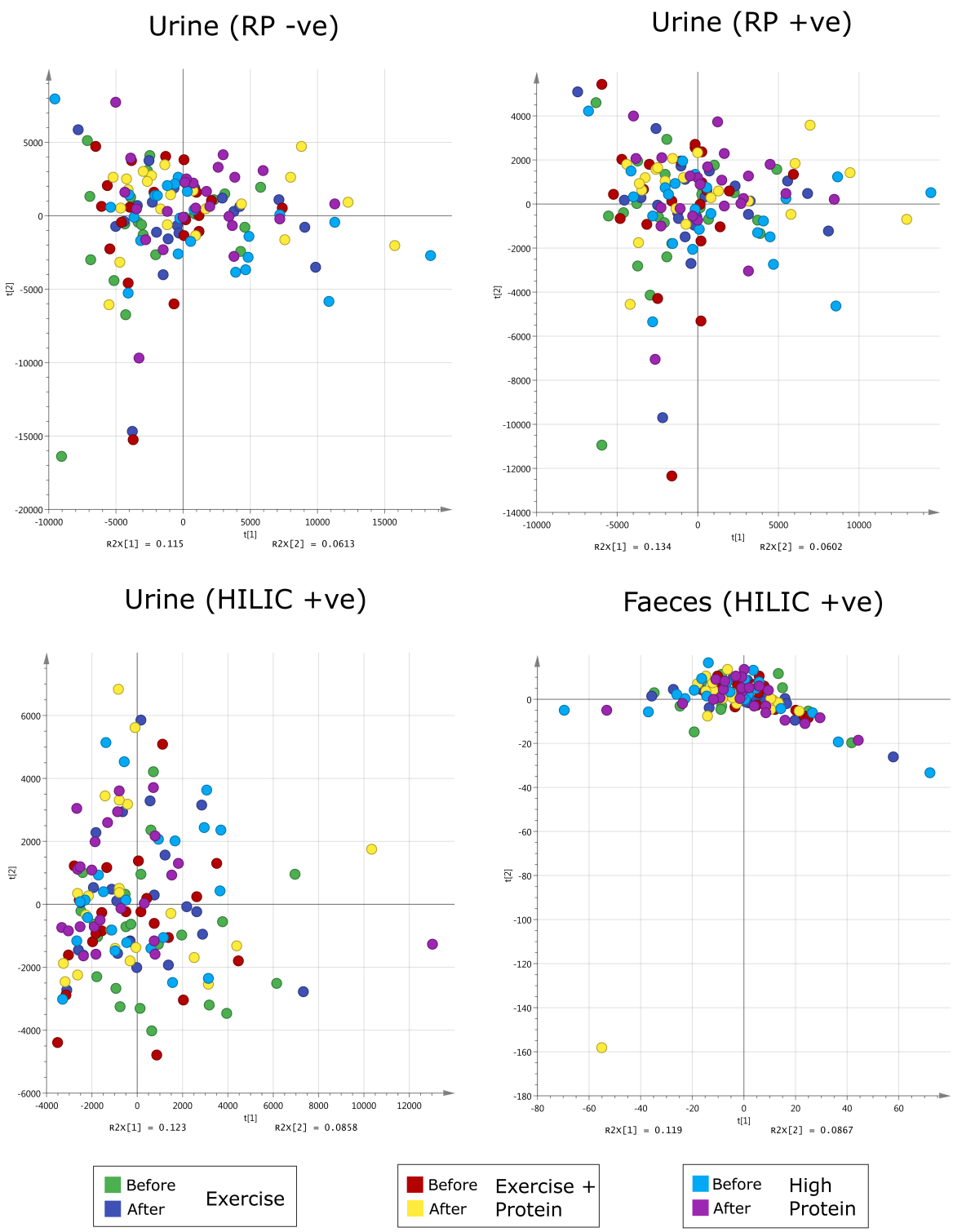


Figure 4.4-3 PCA scores plots of LC-MS analysis comparing participants samples pre and post intervention with either Exercise, Exercise & High Protein Diet or High Protein Diet alone. Models are comprised of 2 principal components. a) Urine Reversed Phase UPLC-MS Negative Mode (R^2X=0.18, Q^2X=0.12), b) Urine Reversed Phase UPLC-MS Positive Mode (R^2X=0.19, c) Q^2X=0.13), Urine HILIC UPLC-MS Positive Mode (R^2X=0.21, Q^2X=0.01), d) Faeces HILIC UPLC-MS Positive Mode (R^2X=0.21, Q^2X=0.01).

4.4.3.2 Paired OPLS-DA models comparing LC-MS spectra of samples before and after intervention

Paired MCCV-PLS-DA analysis or urine and faecal UPLC-MS profiles pre and post intervention did not reveal any significant metabolic differences in any intervention group (see Figure 4.4-4 and Figure 4.4-5). Scores from analysis of urine samples were as follows: UPLC-MS (reversed phase chromatography, positive polarity) Exercise R^2Y: 0.96, Q^2Y: -3.90; Exercise + Protein R^2Y: 0.94, Q^2Y: 0.30; Protein: R^2Y: 0.92, Q^2Y: -0.12. UPLC-MS (reversed phase chromatography, negative polarity) Exercise R^2Y: 0.97, Q^2Y: -7.10; Exercise + Protein R^2Y: 0.95, Q^2Y:0.24; Protein: R^2Y: 0.94, Q^2Y: 0.05. UPLC-MS (HILC chromatography, positive polarity) Exercise R^2Y: 0.98, Q^2Y: -7.50; Exercise + Protein R^2Y: 0.97, Q^2Y: -0.06; Protein: R^2Y: 0.94, Q^2Y: 0.05. Scores from analysis of faecal samples were as follows: UPLC-MS (HILIC chromatography, positive polarity) Exercise R^2Y: 0.95, Q^2Y: -4.80; Exercise + Protein R^2Y: 0.95, Q^2Y: -6.80; Protein: R^2Y: 0.93, Q^2Y: -0.00.

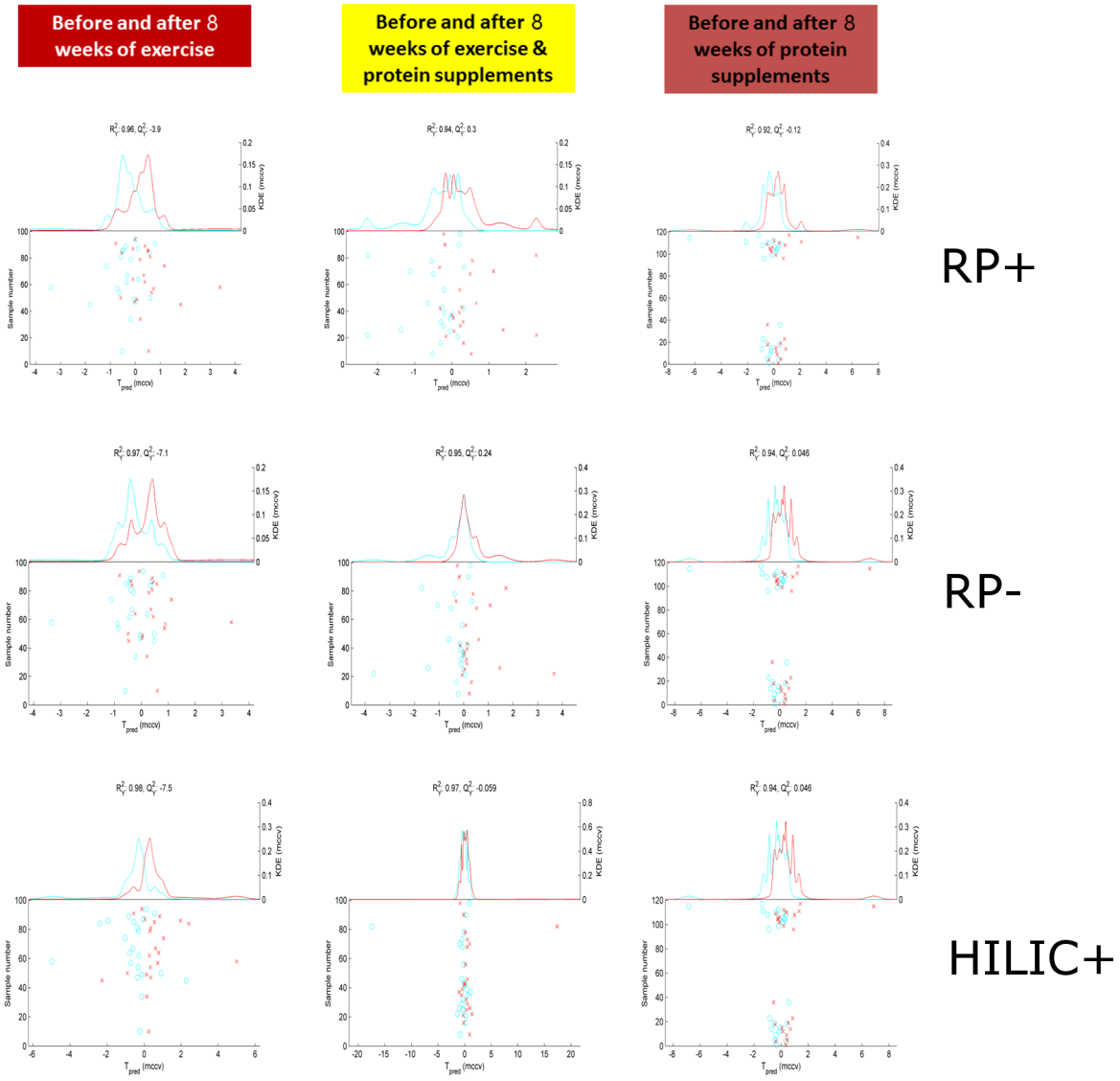


Figure 4.4-4 Paired MCCV-PLS-DA scores plots of UPLC-MS analysis comparing participants samples pre and post intervention with either Exercise, Exercise & High Protein Diet or High Protein Diet alone. Models are comprised of 1 predictive and 1 orthogonal component. i) RP+ urine sample analysis (Exercise R^2Y: 0.96, Q^2Y: -3.90; Exercise + Protein R^2Y: 0.94, Q^2Y: 0.30; Protein: R^2Y: 0.92, Q^2Y: -0.12), ii) RP- urine sample analysis (Exercise R^2Y: 0.97, Q^2Y: -7.10; Exercise + Protein R^2Y: 0.95, Q^2Y:0.24; Protein: R^2Y: 0.94, Q^2Y: 0.05), iii) HILIC+ urine sample analysis (Exercise R^2Y: 0.98, Q^2Y: -7.50; Exercise + Protein R^2Y: 0.97, Q^2Y: -0.06; Protein: R^2Y: 0.94, Q^2Y: 0.05).

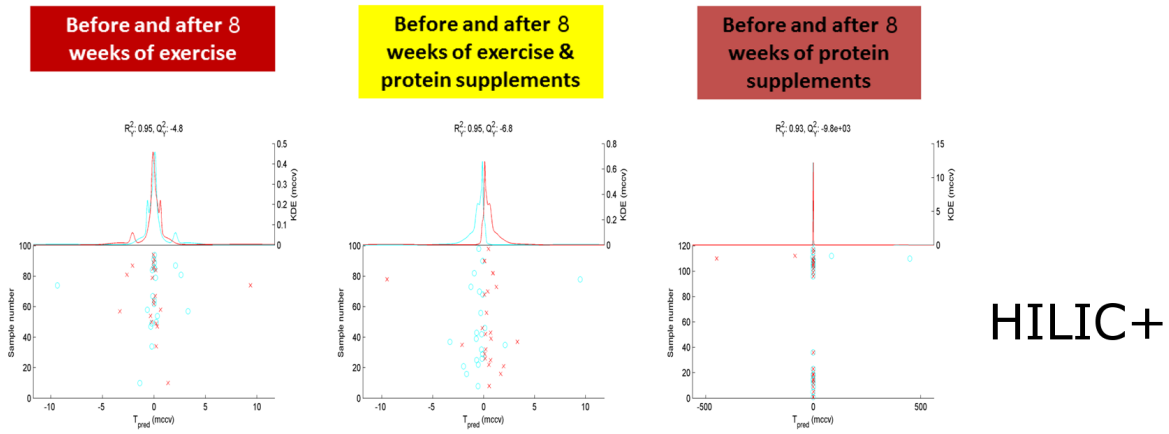


Figure 4.4-5 Paired MCCV-PLS-DA scores plots of UPLC-MS analysis comparing participants samples pre and post intervention with either Exercise, Exercise & High Protein Diet or High Protein Diet alone. Models are comprised of 1 predictive and 1 orthogonal component. i) HILIC+ faecal sample analysis (Exercise R^2Y: 0.95, Q^2Y: -4.80; Exercise + Protein R^2Y: 0.95, Q^2Y: -6.80; Protein: R^2Y: 0.93, Q^2Y: -0.00).

4.4.4 GC-MS of faecal samples before and after intervention

There were no significant differences in measured concentrations of faecal acetate, propionate, butyrate, valerate, isobutyrate or isovalerate after intervention in any group. In addition, there were no differences in the intervention effect between groups. Mean changes are shown in Figure 4.4-6.

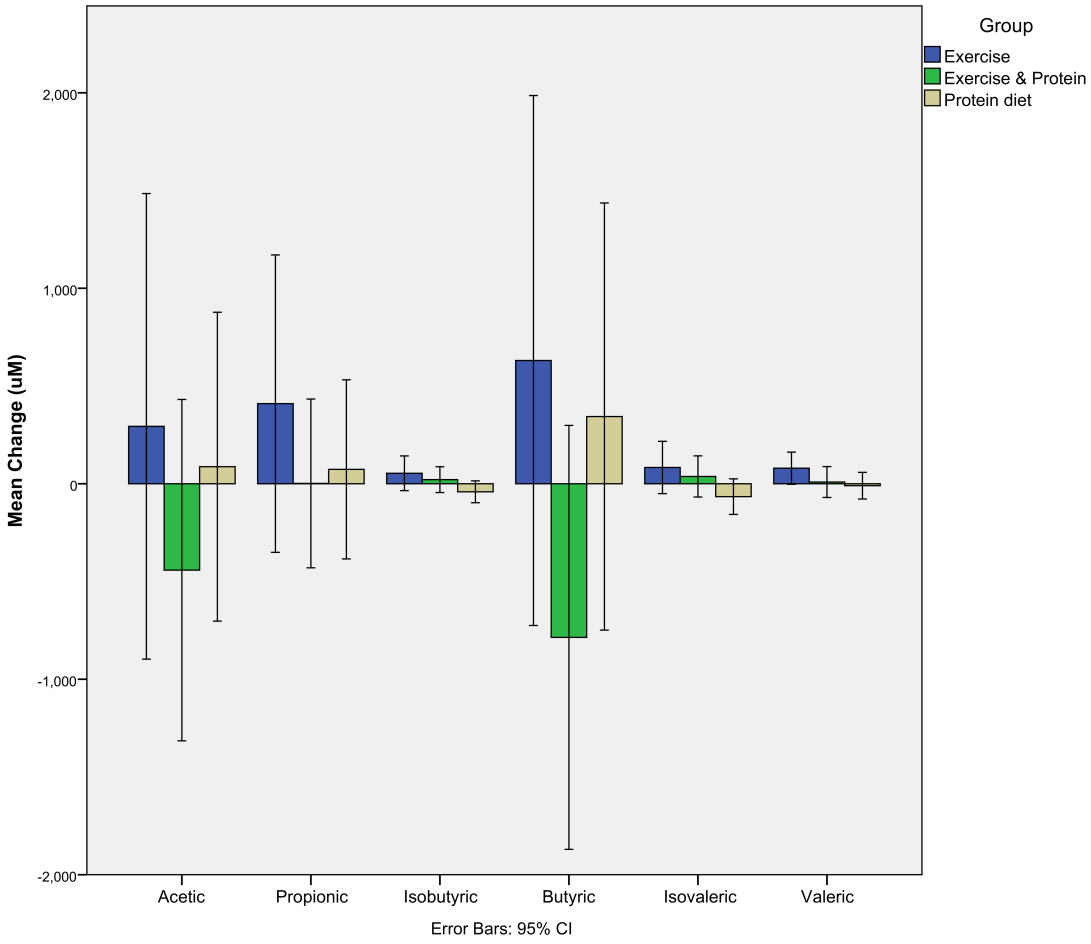


Figure 4.4-6 Change in faecal SCFA concentrations after intervention with Exercise, Exercise & High Protein Diet or High Protein Diet alone. 95% confidence interval bars are shown.

4.4.5 Targeted analysis of selected metabolites of interest

The following metabolites were semi-quantified in urine; allantoin, carnitine, citrate, glycine, hippurate, leucine, phenylacetylglutamine (PAG), proline betaine, succinate, trans aconitate, TMAO, valine. In the exercise group, there was a significant increase in glycine (Wilcoxon Rank p=0.019) and leucine (p=0.030) and a significant decrease in TMAO (p=0.042) after intervention. In the high protein diet group, there was a significant increase in PAG (p=0.023) and a decrease in trans-aconitate (p=0.004) after intervention. There were no significant changes in the combined exercise and high protein diet group. The high protein diet group had a larger increase in TMAO relative to both the exercise group (Mann Whitney U p=0.006, pFDR=0.036) and combined exercise and high protein diet group (p=0.046). In addition, the high protein diet participants had a larger increase in PAG relative to those in the exercise group (p=0.001, pFDR=0.014).

Within the faeces, dimethylamine, glutamate, methylamine, phenylacetate, serine, trimethylamine and tyrosine were semi-quantified. After eight weeks protein supplementation participants had lower faecal glutamate (Wilcoxon Rank p=0.023). The reduction in glutamate was greater than that seen in the combined exercise and high protein diet group (Mann Whitney U p=0.005, pFDR=0.035).

4.5 Discussion

4.5.1 Biological interpretation

Overall these interventions of: i) high protein diet; ii) exercise regime and iii) combined high protein and exercise over and eight-week period appear to result in a minimal metabolic impact on the trial participants. An intriguing exception is the controversial metabolite TMAO.

As discussed, bacterial degradation of carnitine and choline by certain *Proteobacteria* and *Firmicutes* within the gut results in the by-product trimethylamine (TMA), which is subsequently oxidised in the liver via the flavin mono-oxygenase enzyme family to trimethylamine-*N*-oxide (TMAO)[54, 362, 363]. Alternatively, TMAO can be consumed directly from sources such as fish[393]. As previously discussed, TMAO has been framed as a disease factor. Elevated TMAO has been associated with atherosclerosis and cardiovascular disease in a number of studies[26, 56, 60, 341, 366], possibly through altered cholesterol metabolism and oxidative stress[26, 60]. TMAO has now also been associated with diabetes risk[394, 395]. However, the causative effect in humans is uncertain. The association of high TMAO with cardiometabolic risk may be due to confounders such as kidney function and poor metabolic control[64]. Although others suggest that a strong independent risk remains after adjusting for these confounders[396, 397]. Furthermore, some studies investigating the cardiovascular risks of TMAO have found contrasting results. A study investigating patients with ischaemic stroke found they had lower levels of TMAO. Although again, this may be due to confounders in stroke patients such as a reduced food intake following a stroke, aspirin use which has been demonstrated to lower TMAO as well as possibly the stroke event itself[398-400]. While exposure of atherosclerosis-prone apolipoprotein E deficient ($ApoE^{-/-}$) mice transfected with human cholesteryl ester transfer protein to high levels of TMAO through a L-carnitine rich diet led unexpectedly to a reduced area of aortic atherosclerosis[401]. Further TMAO did not affect foam

cell formation *in vitro*[401]. Moreover, TMAO was recently found to protect against impaired glucose tolerance and reduce endoplasmic reticulum stress[65]. In addition, TMAO has a number of important biological functions, such as maintaining cell volume under conditions of osmotic and hydrostatic stress[54]. It is present in cold water dwelling fish in high concentrations acting as an osmolyte and an antifreeze agent. This is consistent with TMAO being found in high levels in the urine of Japanese populations, who are not high risk for cardiovascular disease[5]. Again though, the causation is not clear and this may be due to the beneficial effects of omega-3 fatty acids found in fish rather than TMAO[400].

Indeed, elevated levels of urinary TMAO were seen in the previous Chapter in elite athletes, who in addition to high levels of exercise consumed significantly higher levels of protein relative to controls[339]. Here we see a decrease in urinary TMAO in the exercise group and an increase in TMAO in the high protein group relative to the other trial arms. Suggesting that while it may or may not have deleterious health implications, exercise and high protein diet confer potential opposing modulatory effects on urinary TMAO levels. While a promising paradigm, further work is necessary to determine specific mechanisms, and to rule out unintended dietary influences or influences on host biology from exercise.

Similarly, urinary PAG increased significantly in the high protein group after intervention and increased relative to the changes in other study arms, implying that a high protein diet causes changes within the gut microbiome leading to increased production of this microbially derived metabolite. The physiological relevance of PAG is not fully understood. PAG results from glutamine conjugation of phenylacetic acid, which is almost solely derived from microbial conversion of the amino acid phenylalanine[402]. PAG is a major nitrogenous metabolite that accumulates in uraemia[403]. In patients with chronic kidney disease high PAG levels were an independent risk factor for mortality and cardiovascular disease[402]. However, although this may be a result of altered microbial metabolism it may be explained by tubular dysfunction in chronic kidney disease[402, 404]. Nevertheless, PAG has also been associated with higher risk of carotid atherosclerosis despite no significant difference in renal function between groups. To the contrary, a number of other studies have associated PAG with healthy outcomes including a lean phenotype[16, 105], longevity in centurions[405], reduced arterial stiffness[406]. Furthermore, PAG holds anti-inflammatory effects through inhibition of T cell activation and

Toll-like receptor 4 signalling[407]. Thus, more work is needed to establish the clinical significance of higher PAG levels resulting from a high protein diet.

Lower levels of faecal glutamate following protein supplementation is not readily explained as this would be expected to increase due to the increased amino acid load resulting from the whey protein supplementation. It may be that this change is relative to greater increases in other metabolites, such as other amino acids, within the sample and is an artefact of median fold change normalisation.

4.5.2 Study limitations

Participants were asked to refrain from exercise for 24 hours prior to sample collection. This was in order to limit any temporary metabolic changes resulting from exercise manifesting in the results. Indeed, many of the short-term effects are likely to have returned to baseline after a 24hour period of abstinence. Thus, in effect this study aimed to look for permanent or longer lasting changes. However, it is likely that these may not have manifested themselves over the relatively short intervention period of eight weeks. An additional time point immediately after cessation of exercise would have been useful to identify any immediate metabolic changes that subsequently returned to baseline after 24hrs of no exercise.

In addition, some of these results may have resulted from subtle alterations in diet. This study attempted to control for the potential impact of dietary variation by instructing participants to maintain a usual ad libitum diet. Food frequency dietary analysis indicated stability in the volunteers' dietary patterns, however like all self-reported methods of dietary intake assessment, FFQ assessment is subject to limitations[408].

4.6 Conclusion

In conclusion, this prospective study demonstrates that short-to-medium term combined exercise and/or whey protein supplementation in healthy, physically inactive adults does not induce significant metabolic alterations.

Similarly, results from the gut microbiome analysis in this study (not presented here) indicate that these interventions do not significantly influence bacterial, viral or archaeal diversity. Furthermore, functional activity of the gut microbiota does not appear to be majorly

manipulated, although some changes are evident including alteration of urinary TMAO and PAG excretion. The alterations in microbial diversity, composition, and metabolomic profiles that we and others have observed in habitual exercisers and professional athletes may be a late response to exercise or fitness that occurs over months or years[65, 279, 281, 286].

[Study 2] Application of an objective dietary healthiness measure to cluster patients according to diet and exercise levels

4.7 Introduction

As discussed, the human gut microbiome has been implicated in a number of different pathologies, including obesity[20, 21], diabetes[23], cardiovascular disease[26] and cancer[378, 379]. Metabolic diseases in particular have been strongly associated with reduced bacterial diversity[34, 347, 380, 381]. It is proposed that changes within the gut microbiome, implicated in metabolic diseases, are driven by a high fat, low fibre "Western diet" and sedentary lifestyle. Whereas, both a healthy diet and exercise have been shown to increase diversity of the gut bacteria[382, 383]. Studies have also suggested that increased physical activity and aerobic fitness may mediate some of its known health benefits through modulation of gut bacteria, including increased diversity compared to sedentary individuals[65, 281, 286, 287, 383-387].

True understanding of the relationship between the gut microbiome, diet and exercise remains elusive since, in humans, the relationship between increased physical activity and microbial changes is confounded by the dietary adaptations that often accompany physical activity. This is further compounded by the lack of accuracy in assessing dietary habits, with an estimated 30-80% misreporting of food intake using traditional self-reported assessment tools. In our previous analysis, elite athletes' increased taxonomic and functional diversity positively correlated with dietary protein intake, in addition to increased physical activity[65, 286]. Here, in order to unravel the contribution of diet and exercise to modulation of the gut microbiota, we apply metabolic profiling combined with a novel mathematical modelling strategy to provide objective evidence of adherence to healthy dietary habits [311], thereby facilitating the removal of the confounding effects of individuals' dietary misreporting. This enables individuals to be characterised more accurately according to both their physical activity and dietary status. Thus, the current study provides novel functional insights into the distinct influences of each of these factors on host metabolism, the gut microbiome and subsequent gut microbiome–host co-metabolism. Lastly, we further explore the functional

and metabolic implications of increased bacterial diversity on the host through multivariate regression analyses.

4.8 Materials and Methods

4.8.1 Study population

As described in Chapter 3, elite professional male athletes (n=40) and healthy controls (n=46) matched for age and gender were enrolled in this study in 2011[286]. Approval was granted by the Cork Clinical Research Ethics Committee. Urine and faecal samples were collected from both groups and stored at -80°C until analysis.

4.8.2 Acquisition of clinical exercise and dietary data

Urine and faecal samples were collected from professional athletes while attending an intensive training camp. While samples were collected from healthy controls who had predominantly sedentary lifestyles. Activity levels were validated using the EPIC-Norfolk questionnaire[409] and creatine kinase levels. Dietary intake was calculated from food frequency questionnaires (FFQ) administered by a research nutritionist[286].

4.8.3 Gut microbiome analysis and metabolic profiling

DNA extraction from faecal samples, library preparation, next generation sequencing and bioinformatical processing of data generated was performed by collaborators from the University College Cork and Teagasc Food Research Centre as previously described[339]. ^{1}H-NMR urine and faecal metabolic profiling analysis and GC-MS targeted SCFA analysis was conducted using established methods[351, 352] as described in Chapter 3.

4.8.4 Objective assessment of dietary intake

Here, we have applied a novel mathematical tool capable of objectively assessing free-living individuals' dietary patterns based on their urine composition, without the need to collect dietary data. The tool is based on a Monte Carlo cross-validated PLS-DA model built from urinary metabolic profiles derived from a highly controlled environment (in-patient randomised controlled clinical trial) to assure healthy participants were fully adherent to four dietary interventions that reflected four different levels of adherence to World Health

Organization (WHO) healthy eating recommendations[311]. The application of this model has been successfully validated in free living populations.

^{1}H-NMR urinary metabolic profiles from athletes and controls were projected into the MCCV-PLS-DA model to calculate a predicted score for each participant that reflected their adherence to healthy eating. This score was used to cluster participants in the three groups: i) sedentary controls with a ≤35% adherence to healthy eating; ii) sedentary controls with a ≥100% adherence to healthy eating; iii) athletes with a ≥100% adherence to healthy eating. A cut off value of ≤35% adherence to healthy eating was chosen arbitrarily and designed to select the two extreme dietary healthiness clusters (see Figure 4.9-1). These groups were compared using OPLS-DA.

4.8.5 Statistical Analysis

^{1}H-NMR spectra were phased and digitised over the range δ0·5–9·5 and imported into MATLAB to undergo median fold change normalisation[355]. Multivariate statistical analysis was performed using SIMCA 14.1 (Umetrics)[355]. The three groups previously defined by extreme dietary habits and physical activity levels were compared using Orthogonal Partial Least Squares – Discriminant Analysis (OPLS-DA): sedentary controls with a ≤35% adherence to healthy eating versus controls with a ≥100% adherence to healthy eating [Model 1]; sedentary controls with a ≥100% adherence to healthy eating versus athletes with a ≥100% adherence to healthy eating [Model 2]; controls with a ≤35% adherence to healthy eating versus athletes with a ≥100% adherence to healthy eating [Model 3]. The OPLS-DA models in this study were established based on one predictive component and one orthogonal component. Unit variance scaling was applied to ^{1}H-NMR spectral data. The fit and predictability of the models obtained were determined by the R^2Y and Q^2Y values, respectively. Metabolites differentiating between exercise and/or diet groups were obtained from ^{1}H-NMR OPLS-DA models after investigating spectra with correlation coefficients values higher than 0.4.

Univariate statistical analysis (Mann-Whitney U test) was used to identify discriminatory metabolites in SCFA quantitative datasets. p values were adjusted for multiple testing using the Benjamini-Hochberg (BH) False Discovery Rate method (pFDR).

Linear Regression analysis of ^{1}H-NMR global spectra was performed against Shannon, Simpson and Whole Tree bacterial diversity indices, corrected for confounding factors (age, lean mass and fat mass), using an in-house MATLAB (release 2104a) script. Metabolites with adjusted p-values <0.01, after correcting for multiple testing using the Benjamini-Hochberg False Discovery Rate method, were considered significant and were subsequently visualised in a Manhattan plot.

Finally, HeatMaps showing significant Spearman's correlations between datasets were generated using the ComplexHeatmap script in R[410]. Spearman's correlations were first calculated in MATLAB, with p-values corrected for multiple testing using the Benjamini-Hochberg False Discovery Rate (pFDR) method. Correlations between metabolite-metabolite data sets with a pFDR <0.05 were included. Due to the large number of variables, a false discovery rate of 1% was set for correlations including microbiome taxa and pathway datasets. Hierarchical clustering of correlations was performed using Euclidean distances.

4.8.6 Metabolite identification

A combination of data-driven strategies such as such as SubseT Optimization by Reference Matching (STORM)[314] and Statistical TOtal Correlation SpectroscopY (STOCSY)[313] and analytical identification strategies were used to aid structural identification of significant discriminatory metabolites. Specifically, a catalogue of 1D ^{1}H-NMR sequence with water pre-saturation and 2D NMR experiments such as J-Resolved spectroscopy, ^{1}H–^{1}H TOtal Correlation SpectroscopY (TOCSY), ^{1}H–^{1}H COrrelation SpectroscopY (COSY), ^{1}H–^{13}C Hetero-nuclear Single Quantum Coherence (HSQC) and ^{1}H–^{13}C Hetero-nuclear Multiple-Bond Correlation (HMBC) spectroscopy were performed. Finally, metabolites were confirmed by in situ spiking experiments using authentic chemical standards.

4.8.7 Metabolite quantification

Semi-quantification of identified metabolites was performed using an in-house MATLAB script to annotate the maximal intensity of median fold change normalised spectral peaks. The dominant (highest intensity) spectral peak was identified for each of the measured metabolites and precisely quantified for each individual. Manual annotation allowed for variations in chemical shift in individual samples, enabled precise annotation of peak

intensities. Where spectral peaks overlapped with other metabolites the highest intensity unambiguous spectral region was used.

4.9 Results

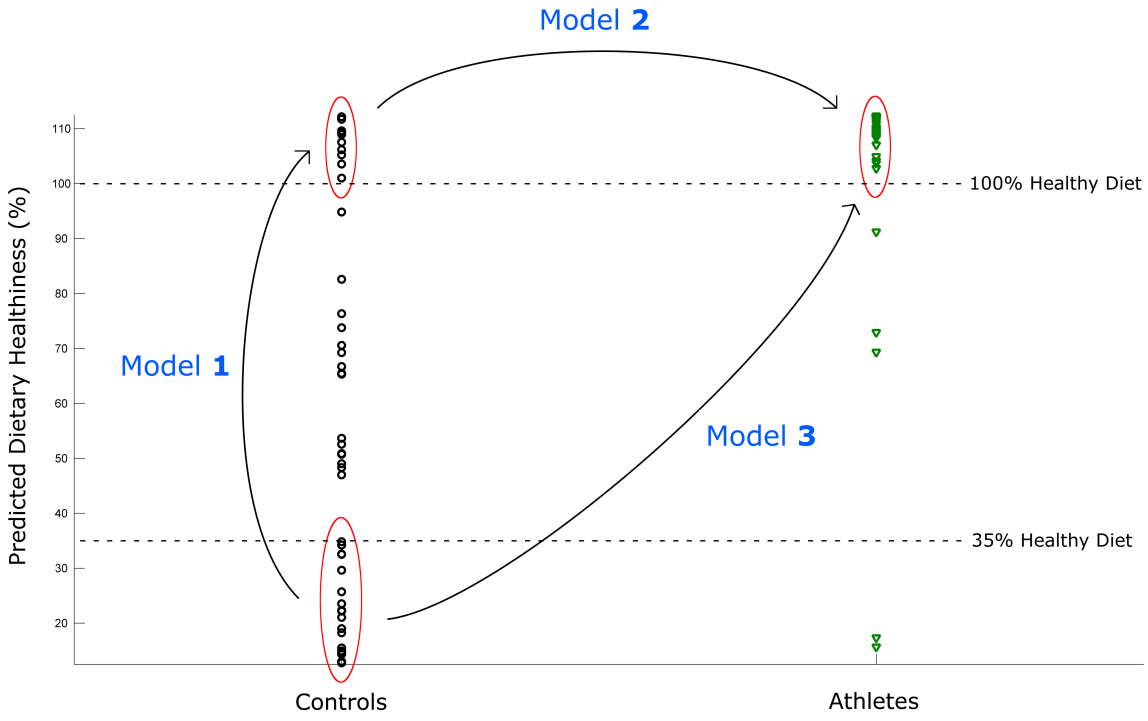


Figure 4.9-1 Clustering of individuals according to exercise status and predicted adherence to healthy dietary habits, calculated from urinary ^{1}H-NMR spectra of individuals, to form comparative models. Model 1 (Dietary Healthiness): sedentary controls with a ≤35% adherence to healthy diet Vs controls with a ≥100% adherence to healthy diet. Model 2 (Exercise): sedentary controls with a ≥100% adherence to healthy diet versus athletes with a ≥100% adherence to a healthy diet. Model 3 (Combined Healthy Diet and Exercise): sedentary controls with a ≤35% adherence to a healthy diet versus athletes with a ≥100% adherence to a healthy diet.

4.9.1 Model generation through clustering of individuals into contrasting groups according to objective dietary healthiness scores and exercise levels.

Scores corresponding to participants' adherence to healthy eating habits were generated from ^{1}H-NMR urinary profiles using a validated metabolic profiling dietary assessment tool[311] (see Figure 4.9-1). As expected, sedentary controls had diverse dietary healthiness scores, whilst professional athletes were predominantly assigned to scores with ≥100% adherence to healthy eating, reflecting the known association between habitual exercise and healthy

eating[411]. Individuals were then clustered according to their score for dietary healthiness to construct comparative groups, with subsequent comparisons made between the contrasting groups as described (see Figure 4.9-1). The models were generated to assess both the combined [Model 3] and discrete effects of a healthy diet [Model 1] and exercise [Model 2] on host metabolism, the gut microbiome and subsequent gut microbiome – host co-metabolism.

4.9.2 Metabolic characterisation of athletes and sedentary controls stratified by predicted dietary healthiness.

Based on the urine spectral data, three robust Orthogonal Partial Least Squares Discriminant Analysis (OPLS-DA) models were obtained for assessment of the metabolic impact of diet, exercise and the combination of diet and exercise. The model to investigate the combined effect of diet healthiness and exercise (Model 3a) was the strongest (R^2Y=0.94, Q^2Y=0.74), with robust models also defining the impact of diet healthiness (R^2Y=0.97, Q^2Y=0.55; Model 1a) or exercise alone (R^2Y=0.92, Q^2Y=0.45; Model 2a). With regard to the faecal profiles, the strongest model was that defining the effect of exercise (R^2Y=0.92, Q^2Y=0.45, Model 2b) whilst the combination of diet and exercise healthiness produced a relatively robust model (R^2Y=0.91, Q^2Y=0.39; Model 3b) with diet showing the least impact (R^2Y=0.95, Q^2Y=0.21; Model 1b).

The loadings of the pairwise OPLS-DA models were used to identify metabolites discriminating between the two classes in each model. Metabolites discriminating between classes are listed in Table 4.9-1 (urine) and Table 4.9-2 (faeces). As expected, in Model 1 (Healthy Diet effect) urinary metabolites with well-known dietary associations such as proline-betaine (associated with citrus intake) and hippurate (associated with the consumption of fruits and vegetables) were significantly higher in the group with healthier eating scores, whereas markers of oxidative stress (2-hydroxybutyrate) and anaerobic metabolism (lactate) were found in lower concentrations within the healthier eating group. Faecal metabolites associated with healthier diet scores included lower concentrations of 2-aminobutyrate and 2-hydroxybutyrate and higher levels of markers of cruciferous vegetable intake (SMCSO derivatives). In the Exercise effect model (Model 2) the athlete group was characterised by a number of urinary metabolites derived from the gut microbiome, such as

phenylacetylglutamine (PAG) and 3-Indoxyl sulphate, as well as the ketone body acetoacetate and markers of red meat intake and fatty-acid metabolism (carnitine, o-acetyl carnitine). While markers of oxidative stress (allantoin) and Krebs cycle intermediates (succinate) were higher in the sedentary group. Analysis of faecal metabolites found higher concentrations of the SCFAs acetate, propionate, butyrate and valerate and lower levels of the amino acids glycine, phenylalanine and tyrosine in the athlete group compared to sedentary controls consuming a comparatively healthy diet. Model 3 (Combined effect) consisted predominantly of metabolites derived from models 1 and 2. Healthy eating, exercise and the combined effect of both (Models 1-3), were all characterised by higher markers of choline metabolism; with higher urinary TMAO. In the exercise effect model (Model 2) this corresponded with higher faecal methylamine, and trimethylamine and lower dimethylamine in athletes relative to sedentary controls.

Urinary Metabolites

<35% controls Vs >100% control [Model 1 – Diet healthiness]			
Metabolite	**^{1}H chemical shift δ (multiplicity)[a]**	**Association[#]**	**Source / Role**
Acetone	2.24 (s)	↑	Ketone
Citrate	2.55~ (d), 2.69~ (d)	↑	Fruit / Krebs cycle
Creatinine	3.05 (s), 4.06 (s)	↑	Muscle mass
TMAO	3.27 (s)	↑	Choline metabolism, fish, meat
Proline Betaine	3.30 (s), 3.11 (s)	↑	Citrus fruits
3-Hydroxyphenylacetate	3.48(s), 6.79 (m), 6.81 (m), 6.86 (m), 7.26 (t)	↑	Gut microbial - Tyrosine metabolism
Hippurate	7.55 (t), 7.64 (t), 7.84 (d), 3.98 (d)	↑	Fruits & vegetables
Formate	8.46 (s)	↑	Fruits & vegetables
Lactate	Targeted GC-MS	↓	Anaerobic metabolism
2-hydroxybutyrate	Targeted GC-MS	↓	Glutathione synthesis
N-methylnicotinamide (NMND)	4.486 (s), 8.19 (t), 8.90 (d), 8.97 (d), 9.28 (s)	↓	Vit B3 / Endogenous Tryptophan metabolism
Pyroglutamate	2.04 (m), 2.41 (m), 2.51 (m), 4.18 (q)	↓	Glutamate metabolism
Sucrose	4.23 (d), 3.46 (t), 3.55 (dd), 3.67 (s), 3.75 (t), 3.82 (m), 3.87 (dd), 3.89 (dd), 4.04 (t), 5.40 (d)	↓	Sugars
>100% controls Vs >100% athletes [Model 2 - Exercise]			
Acetoacetate	2.29 (s), 3.45 (s)	↑	Ketone
Phenylacetylglutamine (PAG)	2.11 (m), 2.27 (m), 3.67 (m), 4.19 (m), 7.36 (t), 7.43 (t)	↑	Gut microbial – Phenylalanine metabolism
Carnitine	3.23 (s), 2.45 (dd), 3.43 (m)	↑	Red meat
N-methylnicotinamide	4.486 (s), 8.19 (t), 8.90 (d), 8.97 (d), 9.28 (s)	↑	Niacin (B3)
3-Indoxyl sulfate *[UV]*	7.51(d), 7.71 (d), 7.21 (m), 7.28 (m)	↑	Gut microbial – Tryptophan metabolism
TMAO	3.27 (s)	↑	Choline metabolism, fish, meat
N-methyl-2-pyridone-5-carboxamide (2PY)	3.65 (d), 6.67 (d), 7.83 (dd), 8.34 (d)	↑	NAD degradation, Tryptophan metabolism
O-Acetyl Carnitine	3.19 (s), 2.15 (s)	↑	Red meat
2-methylbutyrate	Targeted GC-MS	↓	Branched SCFA
Succinate	2.41 (s)	↓	Krebs cycle
Citrate *[UV]*	2.55~ (d), 2.69~ (d)	↓	Fruit / Krebs cycle
3-Hydroxyphenylacetate	3.48(s), 6.79 (m), 6.81 (m), 6.86 (m), 7.26 (t)	↓	Gut microbial / Tyrosine metabolism
Allantoin	5.39 (s)	↓	Gut microbial – oxidative stress
3-(3-hydroxyphenyl)-3-hydroxypropionic acid (HPHPA)	2.62 (dd), 2.71 (dd)*, 5.02 (dd), 6.85 (ddd), 6.91 (t), 6.98 (m), 7.30 (t)	↓	Gut microbial - dysbiosis

<35% controls Vs >100% athletes [Model 3 – Diet healthiness & Exercise]			
Acetoacetate	2.29 (s), 3.45 (s)	↑	Ketone
Phenylacetylglutamine (PAG)	2.11 (m), 2.27 (m), 3.67 (m), 4.19 (m), 7.36 (t), 7.43 (t)	↑	Gut microbial – Phenylalanine metabolism
Carnitine	3.23 (s), 2.45 (dd), 3.43 (m)	↑	Red meat
TMAO	3.27 (s)	↑	Choline metabolism, fish, meat
Proline Betaine	3.30 (s), 3.11 (s)	↑	Citrus fruits
3-Indoxyl sulfate	7.51(d), 7.71 (d), 7.21 (m), 7.28 (m)	↑	Gut microbial
Hippurate	7.55 (t), 7.64 (t), 7.84 (d), 3.98 (d)	↑	Fruits & vegetables
N-methyl-2-pyridone-5-carboxamide (2PY)	3.65 (d), 6.67 (d), 7.83 (dd), 8.34 (d)	↑	NAD degradation, Tryptophan metabolism
O-Acetyl Carnitine	3.19 (s), 2.15 (s)	↑	Red meat
Acetate	Targeted GC-MS	↓	SCFA
Propionate	Targeted GC-MS	↓	SCFA
2-methylbutyrate	Targeted GC-MS	↓	Branched SCFA
Isovalerate	Targeted GC-MS	↓	Branched SCFA
Lactate	Targeted GC-MS	↓	Anaerobic metabolism
Alanine	1.49 (d), 3.79 (q)	↓	Amino acid
Pyroglutamate	2.04 (m), 2.41 (m), 2.51 (m), 4.18 (q)	↓	Glutamate metabolism
Sucrose	4.23 (d), 3.46 (t), 3.55 (dd), 3.67 (s), 3.75 (t), 3.82 (m), 3.87 (dd), 3.89 (dd), 4.04 (t), 5.40 (d)	↓	Sugars
Allantoin	5.39 (s)	↓	Gut microbial – oxidative stress

Table 4.9-1 Urinary metabolites discriminating between classes. [#]Association: Tables show urinary metabolites increasing (↑) or decreasing (↓) with increased diet healthiness, exercise and combined diet healthiness and exercise in models 1, 2 and 3 respectively. [¤]Multiplicity key is as follows: s=singlet, d=doublet, t=triplet, q=quartet, dd=doublet of doublets, m=multiplet. [1]H shifts marked by an asterisk (*) were not confirmed experimentally due to the absence of unambiguous resonance values and are taken from the Human Metabolome Database (HMDB).

Faecal Metabolites

<35% controls Vs >100% control [Model 1 – Diet healthiness]			
Metabolite	**^{1}H chemical shift δ (multiplicity)[a]**	**Association[#]**	**Source / Role**
SMCSO metabolite 1	2.78 (s)	↑	Cruciferous vegetables
SMCSO metabolite 2	2.81 (s)	↑	Cruciferous vegetables
S-methyl-L-cysteine-sulfoxide (SMCSO)	2.83 (s)	↑	Cruciferous vegetables
3-hydroxyphenylpropionate	2.47 (t), 2.84 (t), 6.75 (m), 6.81 (t), 6.87 (m), 7.25 (t)	↑	Gut microbial / Caffeine
Bile Salts 1	0.73 (s)	↓	Bile acids
2-aminobutyrate	0.98 (t)	↓	Glutathione synthesis
Methylsuccinate (citramalate)	1.09 (d), 2.13 (dd)*, 2.53 (dd), 2.63 (m)*	↓	Microbial, malate analogue
2-hydroxybutyrate	1.20 (d)	↓	Glutathione synthesis
Acetate	1.92 (s)	↓	SCFA
N-acetylglucosamine	2.06 (s), 3.47-3.85 (m), 5.21 (d)	↓	Amino sugar, bacterial cell wall constituent
Beta-alanine	2.56 (t), 3.18 (t)	↓	Beta amino acid Uracil metabolism
Ribose	3.52 (dd), 4.11 (t), 4.93 (d), 5.25 (d) +…	↓	Monosaccharide, RNA constituent
Hypoxanthine	8.21 (d)	↓	Purine derivative
>100% controls Vs >100% athletes [Model 2 - Exercise]			
Bile salts 3	0.79 (s)	↑	Bile acids
Valerate	0.89 (t), 1.30 (m), 1.54 (m), 2.18 (t)	↑	SCFA
Butyrate	0.90 (t), 1.56 (m), 2.16 (t) + Targeted GC-MS	↑	SCFA
Propionate	1.06 (t), 2.19 (q) + Targeted GC-MS	↑	SCFA
Threonine	1.33 (d), 3.59 (d), 4.26 (dqt)	↑	Amino acid
Acetate	1.92 (s) + Targeted GC-MS	↑	SCFA
Methylamine	2.60 (s)	↑	Choline metabolism
Trimethylamine	2.88 (s)	↑	Choline metabolism
Uracil	5.81 (d), 7.55 (d)	↑	RNA nucleobase
Anserine	7.17 (s), 8.35 (s), 3.65 (s)	↑	Dipeptide
3-hydroxyphenylpropionate	2.47 (t), 2.84 (t), 6.75 (m), 6.81 (t), 6.87 (m), 7.25 (t)	↓	Gut microbial / Caffeine
Dimethylamine	2.73 (s)	↓	Choline metabolism
Glycine	3.56 (s)	↓	Amino acid

Phenylalanine	3.20 (dd), 3.29 (dd), 3.99 (dd), 7.34 (d), 7.38 (m), 7.43 (m)	↓	Amino acid
Tyrosine	6.91 (d), 7.21 (d)	↓	Amino acid
<35% controls Vs >100% athletes [Model 3 – Diet healthiness & Exercise]			
Acetate	1.92 (s)	↑	SCFA
Anserine	7.17 (s), 8.35 (s), 3.65 (s)	↑	Dipeptide
Bile salts 3	0.79 (s)	↑	Bile acids
Butyrate	0.90 (t), 1.56 (m), 2.16 (t) + Targeted GC-MS	↑	SCFA
Methylamine	2.60 (s)	↑	Choline metabolism
Propionate	1.06 (t), 2.19 (q) + Targeted GC-MS	↑	SCFA
Trimethylamine	2.88 (s)	↑	Choline metabolism
Valerate	0.89 (t), 1.30 (m), 1.54 (m), 2.18 (t) + Targeted GC-MS	↑	SCFA
2-hydroxybutyrate	1.20 (d)	↓	Glutathione synthesis
Proline	2.01 (m), 2.35 (m), 4.14 (dd)	↓	Amino acid
N-acetylglucosamine	2.06 (s), 3.47-3.85 (m), 5.21 (d)	↓	Amino sugar, bacterial cell wall constituent
Glycine	3.56 (s)	↓	Amino acid
Bacterial Diversity (Shannon / Simpson / Whole Tree) [Model 4 - Diversity]			
Bile Salts 2	0.76 (s)	↑	Bile acids
2-methylbutyrate	0.86 (t), 1.05 (d), 1.39 (m), 1.5 (m), 2.21 (m)	↑	Branched SCFA
Caproate	0.86 (t), 1.27 (m), 1.53 (m), 2.17 (t)	↑	MCFA
Valerate	0.89 (t), 1.30 (m), 1.54 (m), 2.18 (t)	↑	SCFA
Isovalerate	0.91 (d), 1.96 (m), 2.06 (d)	↑	Branched SCFA
α-ketoisocaproate (2-oxoisocaproate)	0.94 (d), 2.10 (m), 2.62 (d)	↑	BCAA degradation
Isobutyrate	1.07 (d), 2.35 (m)	↑	Branched SCFA
α-ketoisovalerate (2-oxoisovalerate)	1.13 (d), 3.02 (m)	↑	BCAA degradation
Glutamate	2.05 (m), 2.12 (m), 2.35 (m), 3.75 (dd)	↑	Amino acid
Malate	2.36 (dd), 2.67 (dd), 4.32 (dd)	↑	Krebs cycle
Ureidopropionate	2.39 (t), 3.29 (q)*	↑	Uracil metabolism
3-phenylpropionate (Hydrocinnamate)	2.49 (t), 2.90 (t), 7.30 (m)	↑	Phenylalanine metabolism
Dimethylamine	2.73 (s)	↑	Choline metabolism
2-methylproline	2.75 (s), [3.60-61 (s)]	↑	Arginine & Proline metabolism
Phenylacetate	3.54 (s), 7.31 (m), 7.39 (m)	↑	Phenylalanine metabolism
Isoleucine	0.94 (t), 1.02 (d), 1.28 (m), 1.48(m), 1.98 (m), 3.68 (d)	↓	BCAA

Asparagine	2.95 (dd), 2.87 (dd), 4.01 (dd)	↓	Amino acid
Glucose	3.25 (dd), 3.42 (m), 3.49 (m), 3.54 (dd), 3.74 (m), 3.84 (m), 3.91 (dd), 4.65 (d), 5.24 (d)	↓	Sugars
Uridine	3.80 (dd)*, 3.91 (dd)*, 4.12 (m)*, 4.22 (dd)*, 4.34 (dd)*, 5.91 (d), 5.92 (d), 7.88 (d)	↓	Nucleoside
Histidine	7.11 (s), 7.93 (s)	↓	Amino acid
Nicotinate	7.53 (dd)*, 8.26 (m), 8.62 (dd), 8.94 (d)	↓	Vit B3

Table 4.9-2 Faecal metabolites discriminating between classes. [#]Association: Tables show faecal metabolites increasing (↑) or decreasing (↓) with increased diet healthiness, exercise, combined diet healthiness and exercise, and gut bacterial diversity in models 1, 2, 3 and 4 respectively. [α]Multiplicity key is as follows: s=singlet, d=doublet, t=triplet, q=quartet, dd=doublet of doublets, m=multiplet. [1]H shifts marked by an asterisk (*) were not confirmed experimentally due to the absence of unambiguous resonance values and are taken from the Human Metabolome Database (HMDB).

4.9.3 Quantitative analysis of short chain fatty acids and organic acids in urine and faeces

Targeted GC-MS of SCFA level in faeces revealed significantly higher levels of acetate (pFDR<0.001), propionate (pFDR<0.001) and butyrate (pFDR=0.006) in healthy eating athletes relative to healthy eating controls (Model 2 – Exercise Effect). In addition to propionate (pFDR=0.004) and butyrate (pFDR=0.019), valerate (pFDR=0.043) was higher in healthy eating athletes relative to sedentary controls with unhealthy eating, while acetate was significantly higher before but not after Benjamini-Hochberg (BH) multiple testing corrections (pFDR=0.056) (Model 3 – Combined effect). There were no significant differences in the diet healthiness model (Model 1) and no differences in isobutyrate or isovalerate concentrations in any model.

Targeted analysis of ten organic acids in urine by GC-MS demonstrated lower levels of lactate (pFDR=0.002) and 2-hydroxybutyrate (pFDR=0.014) in controls ≥100% adherence to healthy eating versus controls with a ≤35% adherence to healthy eating (Model 1 – Healthy Diet effect). 2-Methylbutyrate levels (pFDR=0.043) were lower in healthy eating athletes versus healthy eating controls (Model 2 – Exercise effect). In contrast to the faecal SCFA model, acetate (pFDR=0.006), propionate (pFDR=0.003), 2-methylbutyrate (pFDR=0.001), isovalerate (pFDR=0.001) and lactate (pFDR<0.001) were all lower in athletes with ≥100% adherence to healthy eating versus controls with ≤35% adherence to healthy eating (Model 3 – Combined Effect).

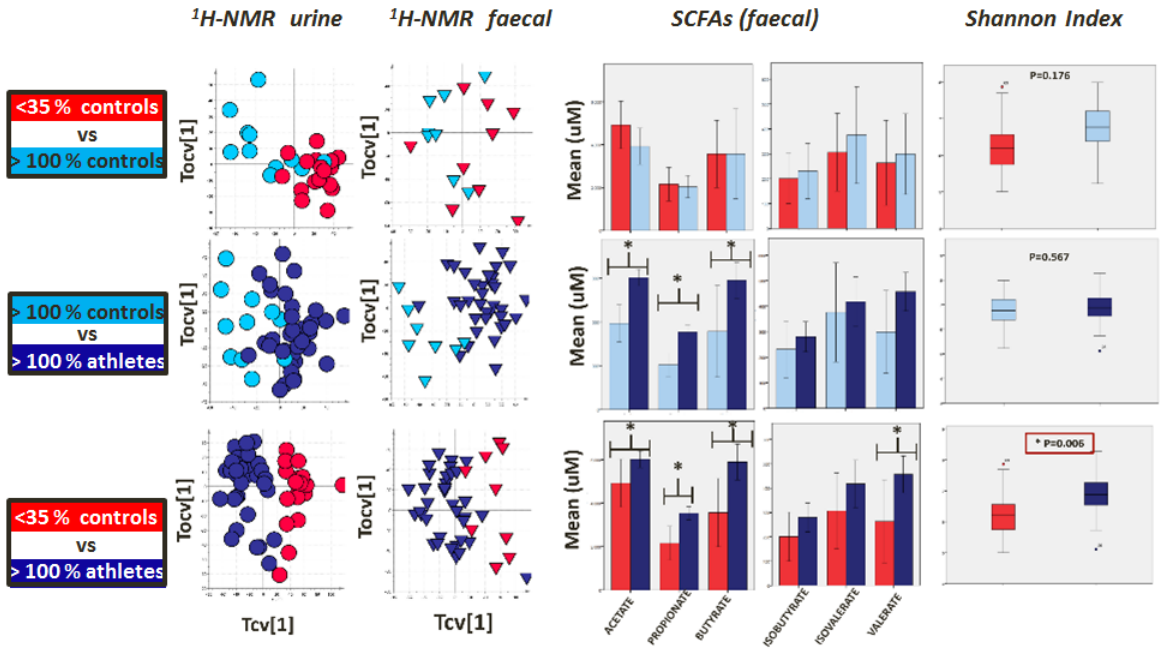


*Figure 4.9-2 ¹H-NMR, SCFA and bacterial diversity results. Cross-validated OPLS-DA scores plots of a) 1H-NMR urinary profiles, b) 1H-NMR faecal profiles. Bar charts of c) mean SCFA levels measured through quantitative GC-MS and d) mean Shannon diversity index levels, with 95% CI shown. Significant results (pFDR<0.05) marked with *. Rows 1,2&3 represent Model 1 (Diet Healthiness), Model 2 (Exercise) and Model 3 (Combined Diet Healthiness and Exercise) respectively.*

4.9.4 Bacterial diversity

No difference in gut bacterial diversity was found between classes in Models 1 or 2. However, there was increased bacterial diversity in healthy eating athletes versus unhealthy eating controls (Model 3 – Combined Diet & Exercise effect) using Shannon (pFDR=0.012), Simpson (pFDR=0.020), Whole Tree (pFDR=0.001), Chao1 (pFDR=0.025) and observed species (pFDR=0.012) indices.

Linear regression analysis of ¹H-NMR faecal water global spectra against Shannon, Simpson and Whole Tree bacterial diversity indices, corrected for confounding factors (age, lean mass and fat mass), revealed multiple metabolites associated with bacterial diversity (see Figure 4.9-3 and Table 4.9-2). Whereas no urinary ¹H-NMR global spectra were found to significantly correlate with measures of gut bacterial diversity. Levels of faecal metabolites associated with an increased bacterial diversity include increased short/medium chain FAs valerate and caproate, branched SCFAs isobutyrate, isovalerate and 2-methylbutyrate, branched chain amino acid (BCAA) degradation products 2-oxoisocaproate and 2-oxoisovalerate as well as products of phenylalanine (phenylacetate and 3-phenylpropionate), choline (dimethylamine), proline (2-methylproline) and uracil (ureidopropionate) metabolism. Increased diversity was

also associated with lower glucose levels in addition to reduced isoleucine, asparagine and histidine.

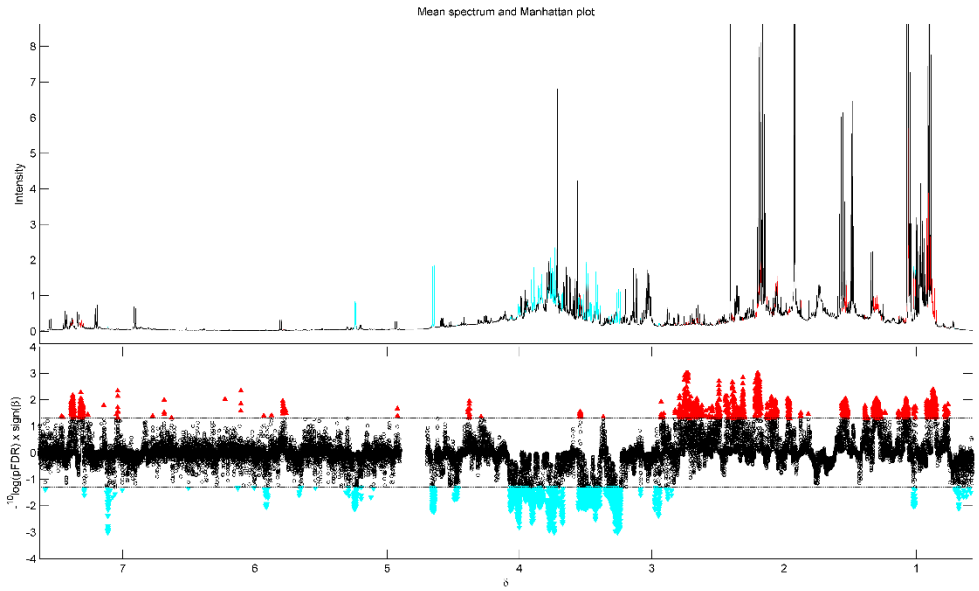


Figure 4.9-3 Linear regression of faecal water ^{1}H-NMR spectra against bacterial diversity (Shannon index), corrected for confounding factors (age, lean mass and fat mass). Metabolites with a pFDR of <0.01 were considered significant and are highlighted in the Manhattan plot and mean spectrum. Spectra highlighted red increase with bacterial diversity, spectra highlighted blue decrease with increased bacterial diversity.

4.9.5 Diet – Gut microbiome – Gut metabolome – Host metabolome interactions

A total of 47 faecal and 27 urinary metabolites of interest, based on discriminatory capacity from Models 1-3 and/or metabolites associated with bacterial diversity, were quantified. Gut metabolome – host metabolome interactions (faecal vs urinary metabolites respectively) were derived from Spearman's correlations between the two data sets (see Figure 4.9-4). Diet – Gut bacterial metabolome and Diet – host metabolome relationships were derived from Spearman's correlations between dietary food groups calculated from food frequency questionnaires and faecal and urinary metabolite levels (see Figure 4.11-1). Furthermore, Spearman's correlations of metabolite levels against bacterial species (Figure 4.11-2) and microbial metabolic superpathway (Figure 4.9-5) relative abundances revealed numerous significant correlations with one or more urinary or faecal metabolite (Species pFDR<0.01 = 257, Metabolic Superpathways pFDR<0.01 = 58). Similarly, relative abundance of 206 microbial metabolic superpathways was significantly correlated to measures of bacterial diversity (pFDR<0.01, Figure 4.11-3). Lastly, correlations within faecal-faecal and urinary-

urinary metabolite datasets were used to highlight known or unknown metabolic pathways (see Figure 4.11-4 and Figure 4.11-5).

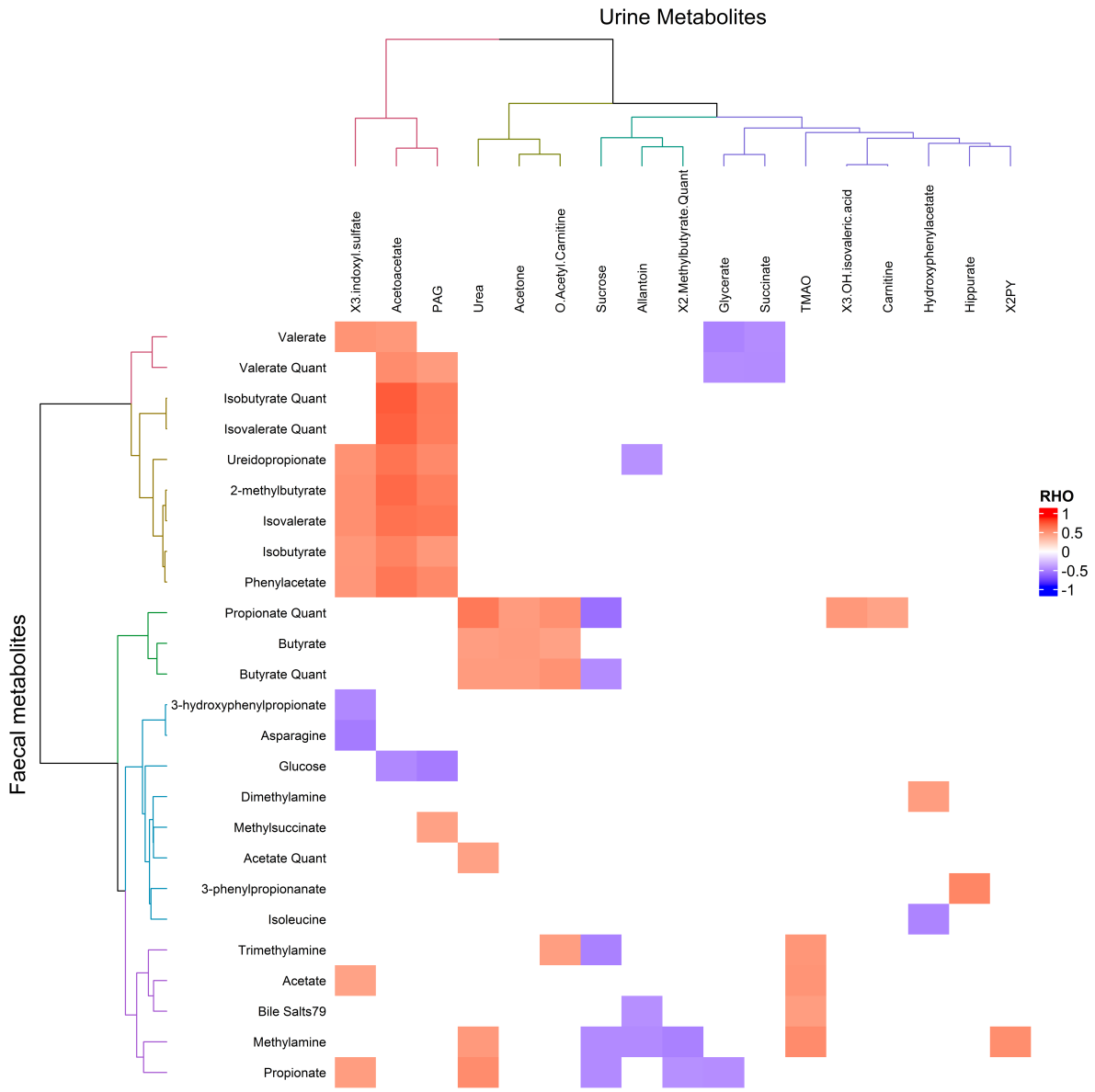


Figure 4.9-4 Faecal – Urinary metabolic interactions. Significant Spearman's correlations (pFDR <0.05) between faecal and urinary metabolic datasets are shown, shaded according to strength of correlation coefficient (Rho). Correlations are clustered according to Euclidean distances.

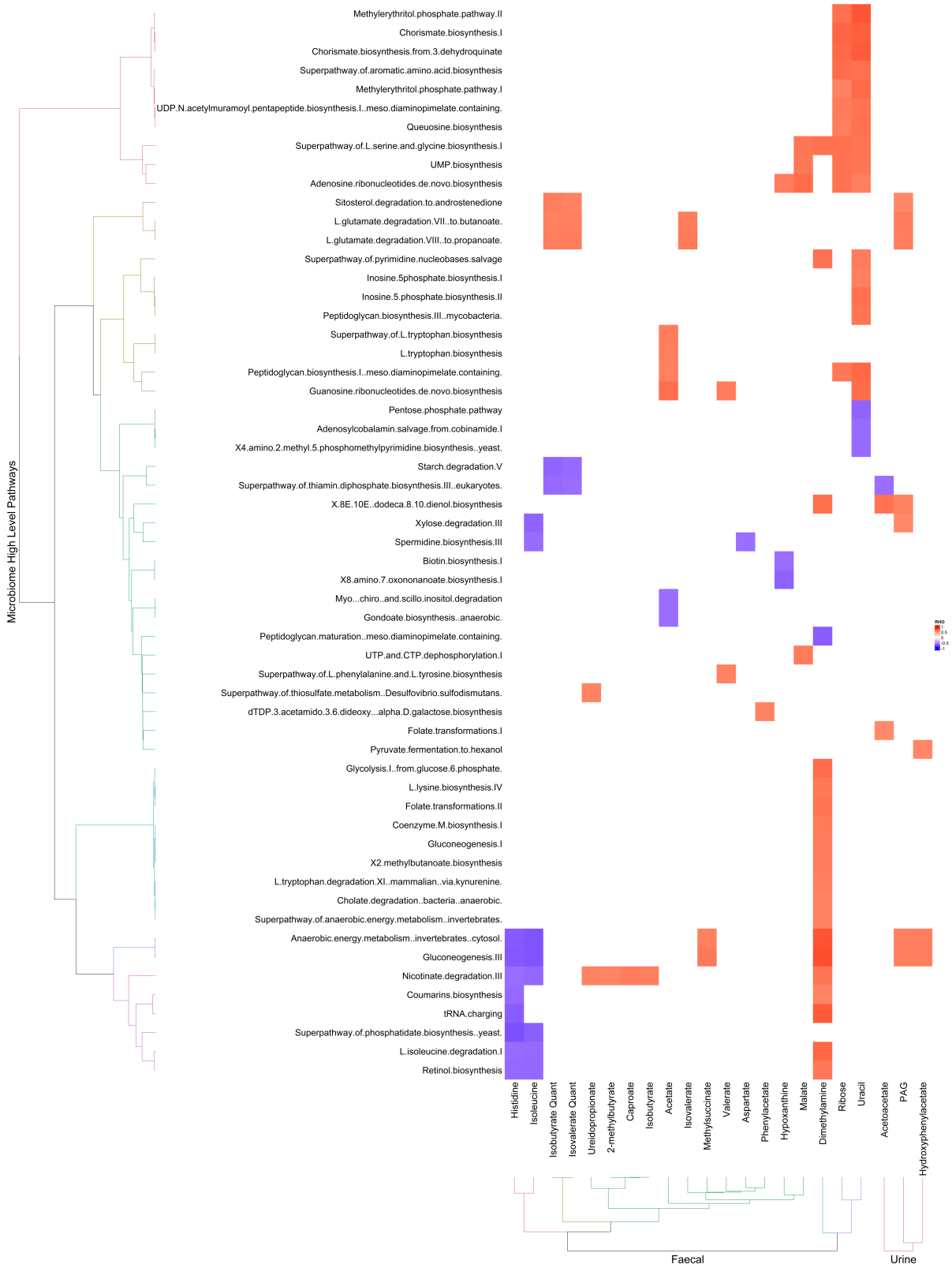


Figure 4.9-5 Microbial – Metabolic Superpathway – Metabolite interactions. Significant Spearman's correlations (pFDR <0.01) between microbial metabolic superpathways Vs faecal and urinary metabolic datasets are shown, shaded according to strength of correlation coefficient (Rho). Correlations are clustered according to Euclidean distances.

4.10 Discussion & Biological Interpretation

Each of the models pertaining to diet healthiness, exercise or a combination of both displayed a unique metabolic and functional microbial signature, with a significant proportion of identified metabolites discriminating between the various pairwise comparisons resulting from gut-host co-metabolism. Bacterial diversity was associated with a combination of increased diet healthiness and exercise and was correlated with a distinct array of microbially derived metabolites.

4.10.1 Metabolic phenotype associated with diet and exercise

As expected, the effect of adherence to healthy dietary habits was associated with higher concentrations of markers of fruit and vegetable intake in the form of proline-betaine, formate and hippurate in addition to lower sugar levels[279, 311].

While investigating changes related with a high level of physical activity, we found higher levels of O-acetyl carnitine, associated with the intake of animal protein. Indeed, protein consumption was higher in the athlete group and included whey protein supplementation. Although higher O-acetyl carnitine may also be due to increased fatty acid mobilisation and oxidation in this group[412]. Additionally, there were lower concentrations of urinary succinate in athletes, likely due to increased systemic utilisation through the Krebs cycle. While sedentary controls assigned healthy diet scores were characterised by lower urinary levels of lactate and 2-hydroxybutyrate, markers of anaerobic respiration and oxidative stress respectively. Oxidative stress raises the rate of hepatic glutathione synthesis, causing homocysteine to be metabolised through the transulfuration pathway to replace depleted cysteine, with 2-hydroxybutyrate produced as a byproduct[279].

4.10.2 Evidence of altered gut microbial – host co-metabolism

4.10.2.1Tryptophan Metabolism

In participants assigned healthy eating scores (Model 1) we find lower levels of methylnicotinamide (NMND). In humans, the amino acid tryptophan is predominantly metabolised through the kynurenine pathway. The resulting nicotinamide is methylated by nicotinamide *N*-methyltransferase (NNMT), to form *N*-methylnicotinamide (NMND), which is then further metabolised to N-methyl-2-pyridone-5-carboxamide (2PY)[413]. Nicotinamide

serves an important role in energy regulation. NNMT knockout in mice – resulting in higher nicotinamide and reduced NMND and 2PY – is protective of diet induced obesity[414]. Thus, the lower levels of NMND seen here suggest increased energy expenditure in healthy eaters.

Conversely, in the exercise effect model we find higher levels of 2PY associated with physical activity (Model 2). In addition, there is increased gut microbial metabolism of tryptophan through the indole pathway leading to increased 3 indoxyl-sulfate (3IS). This is a similar metabolic signature to that seen in malnourished children[413]. In this case, however, increased 2PY is more readily explained through indoleamine 2,3-dioxygenase (IDO) mediated activation of the kynurenine pathway due to increased inflammation[286]. While increased 3IS is likely due to a shift towards proteolytic fermentation of increased colonic protein by gut bacteria due to higher protein intake in healthy eating athletes relative to healthy eating sedentary controls (median intake 240g/day Vs 104 g/day, $p<0.001$).

4.10.2.2 Phenylalanine Metabolism

Higher physical activity (Model 2) and the combined effect of healthy diet and exercise (Model 3) result in higher levels of urinary PAG, produced through gut microbial conversion of phenylalanine to phenylacetate and subsequent conversion to PAG in the liver. In keeping, we also see a resulting reduction in faecal phenylalanine and tyrosine. Consistent with these findings, PAG has previously been associated with a lean phenotype[415]. In our study PAG levels predominantly correlate with bacterial species from the *Actinobacteria* and *Proteobacteria* phyla as well as a number of bacterial pathways including increased gluconeogenesis, anaerobic energy metabolism and glutamate degradation to SCFAs. The ketone body acetoacetate, likewise raised with higher physical activity and the combined effect of healthy diet and exercise, can also be produced through ketogenic metabolism of phenylalanine.

Whilst PAG is positively associated with the group of healthy eating athletes (Model 2), the more minor microbial phenylalanine metabolites 3-hydroxyphenylacetate (HPA) and 3-(3-hydroxyphenyl)-3-hydroxypropionic acid (HPHPA) are inversely correlated, whereas HPA levels are higher in the urine of healthy eating controls (Model 1). The biological role of HPA and HPHPA is disputed. Some studies have associated HPA and HPHPA with neurological disorders[416]. Others, however, have shown the contrary[417] and furthermore HPA is thought to be a dietary marker of the rutin intake, a flavonoid and antioxidant.

4.10.2.3 Benzoate Metabolism

Alternatively, phenylalanine and other dietary aromatic compounds such as catechin can be metabolised to benzoate, which is further metabolised to hippurate[418]. Here we find higher hippurate in individuals with a healthy diet scores (Model 1). Higher hippurate levels have been correlated with a lean phenotype and lower blood pressure as well as fruit intake[5, 419]. In this study urinary hippurate levels correlate strongly with faecal 3-phenylpropionate, suggesting that the main source of hippurate production observed here is through degradation of catechin from the diet.

4.10.2.4 Choline Metabolism

We find higher levels of TMAO in both the healthy diet and exercise effect models in addition to the combined model. Circulating trimethylamine-*N*-Oxide (TMAO) is thought to predict cardiovascular disease (CVD), possibly through altered cholesterol metabolism and oxidative stress[26, 60]. However, the causative effect in humans is disputed and may be due to confounders such as kidney function and poor metabolic control[64]. Furthermore, as discussed in chapter 3, TMAO is present in high concentrations in the tissues of cold water-dwelling fish where it acts as an antifreeze agent and is also found in high levels in the urine of Japanese populations whose diet contains a high portion of fish and who do not have high risk for CVD[5]. Moreover, TMAO was recently found to protect against impaired glucose tolerance and reduce endoplasmic reticulum stress[65].

As expected, we find urinary TMAO levels correlate with faecal trimethylamine and methylamine, although not dimethylamine. Further, TMAO correlates with urinary carnitine, acetyl-carnitine and urea levels, all markers of protein intake, which is consistent with the higher reported intake of protein in the healthy eating athletes represented in the exercise and combined models. The bacterial abundance data also show a dichotomy with respect to association between TMAO and DMA. For example, we identify a large number of bacterial species and pathways whose abundance correlates with faecal dimethylamine excretion but which do not appear to influence TMAO levels. Whereas the heterofermentative lactic acid bacterium *Leuconostoc citreum* correlates with higher TMAO levels. Intriguingly we also identify a number of lactococcal phages that correlate with TMAO. This raises the possibility that changes to the gut environment, such as altered pH from changes to lactic acid bacteria,

can alter levels of TMA / TMAO producing and metabolising bacteria leading to subsequent changes in host TMAO levels. Indeed, lactococcal phage levels also correlate with increased TMAO:DMA and TMA:DMA ratios, suggesting they may influence bacterial TMA dehydrogenase or TMAO aldolase activity.

4.10.2.5SCFA and Branched chain amino acid metabolism

Faecal SCFAs are found in higher concentrations in subjects with increased physical activity (Model 2) and combined healthy eating and increased exercise (Model 3) relative to controls. SCFAs are produced through the bacterial fermentation of dietary fibre and complex carbohydrates. The most abundant SCFAs are acetate (C2), propionate (C3) and butyrate (C4). In addition, valerate and the branched SCFAs isobutyrate, isovalerate and 2-methyl-butyrate are produced by gut bacteria in smaller quantities[41]. Butyrate is the preferred source of energy for colonic epithelial cells[42]. Whereas propionate, along with remaining butyrate, is used predominantly by hepatocytes for gluconeogenesis, while acetate is mainly utilised by muscle cells to generate energy. Importantly SCFAs have been associated with reduced appetite and weight loss through stimulating release of the anorectic gut hormones peptide YY (PYY) and glucagon like peptide-1 (GLP-1)[41, 48]. Interestingly, it has been reported that undigested proteins and amino acids in the colon may serve as an additional substrate for SCFA production. Indeed, in this cohort we find that while faecal butyrate correlates strongly with fibre intake, propionate correlates most strongly with protein intake – increased in healthy eating athletes.

Alternatively, medium chain fatty acids, branched SCFAs and branched chain keto acids (BCKAs) are correlated with higher bacterial diversity, seen after modelling the combined effects of healthy diet and exercise. The branched SCFAs isobutyrate, isovalerate and 2-methylbutyrate are produced through the fermentation of BCAAs and have also been shown to modulate energy metabolism[420]. Here, isobutyrate and isovalerate are both correlated with bacterial amino acid (glutamate) degradation pathways to propionate and butyrate and show an inverse correlation to pathways encoding starch degradation. It is likely that bacteria here are using similar pathways to ferment BCAAs in place of glutamate. Further, in faecal samples with higher bacterial diversity we detect higher BCKAs 2-oxoisocaproate and 2-oxoisovalerate, produced through the catabolism of the BCAA leucine and valine respectively.

This initial transamination reaction, catalysed by branched chain aminotransferase, produces glutamate (also higher) and the respective BCKA[421, 422]. Subsequent leucine metabolism via 2-oxoisocaproate is ketogenic, while valine metabolism via 2-oxoisovalerate is glucogenic[423]. This constellation of raised BCKAs, glutamate and branched-SCFAs suggests that the increased diversity observed here is associated with an adaptation towards increased degradation of protein and amino acids in the colon. Additionally, we see reduced glucose and amino acid levels (histidine, asparagine, isoleucine) with increased bacterial diversity. It is not clear whether these changes are a result of bacterial adaptation to a high protein / low sugar environment in the distal colon or whether they are driven by an increase in bacterial utilisation of amino acids. Intriguingly the reduction in faecal amino acid levels, seen here with increased diversity, appears to indicate that enhanced protein degradation increases beyond increased intake. Corresponding changes are also seen in bacterial pathways related with increased diversity. Increased diversity correlates with higher; amino acid, BCAA and nicotinate degradation, co-factor and amino acid biosynthesis and gluconeogenesis pathways, along with reduced; starch degradation, methionine and fatty acid biosynthesis pathways.

In addition, SCFA can also be utilised by bacteria for *de novo* amino acid biosynthesis[424]. Here increased valerate, seen with increased exercise (Model 2 & 3) and bacterial diversity, is associated with bacterial phenylalanine and tyrosine biosynthesis pathways. While increased acetate, seen with increased exercise (Model 2 & 3), is associated with tryptophan biosynthesis pathways. Lastly, acetate is associated with guanosine ribonucleotide biosynthesis, suggesting that acetate has an important role in enabling the biosynthesis of aromatic compounds.

4.11 Conclusion

The analysis of individuals' gut microbiome and metabolic profiles according to groupings based on an objective measure of their dietary habits, exercise levels and further analysis according to bacterial diversity has elicited novel insights into this complex, multi-factorial paradigm. Each exercise/diet group appears to exhibit a distinct metabolic and functional microbial phenotype.

Model synthesis using an objective measure of dietary healthiness has enabled us to better control for a number of closely related confounders, and more accurately ascertain the individual biological sequelae of diet healthiness and exercise respectively. However, although reduced, a number of confounders in this paradigm still exist. Some changes exhibited in the exercise effect model may be due to increased meat and protein intake in this group. Where possible this has been explained. Additionally, a subgroup of athletes consumed the probiotics *lactobacillus casei* or *lactobacillus acidophilus* regularly. However, their relative abundance in the faecal metagenomic data did not significantly correlate with any faecal or urinary metabolites.

Importantly, increased microbial diversity has previously been associated with a healthy state[34, 347, 380, 381]. Certainly, many microbial derived metabolites such as SCFA are known to be beneficial and furthermore an increase in diversity is associated with a low glycaemic state. However, in this cohort we also see higher diversity relating to an increase towards proteolytic fermentation by gut bacteria. Protein metabolism within the gut has been associated with the production of toxic compounds such as ammonia, amines and sulphides[425, 426]. Thus, indicating that in this cohort the effects of higher diversity may include deleterious as well as beneficial effects on the host. This illustrates the importance of more in-depth analysis at a pathway and taxonomic level in future microbiome studies.

4.11.1.1.1 Supplementary Figures

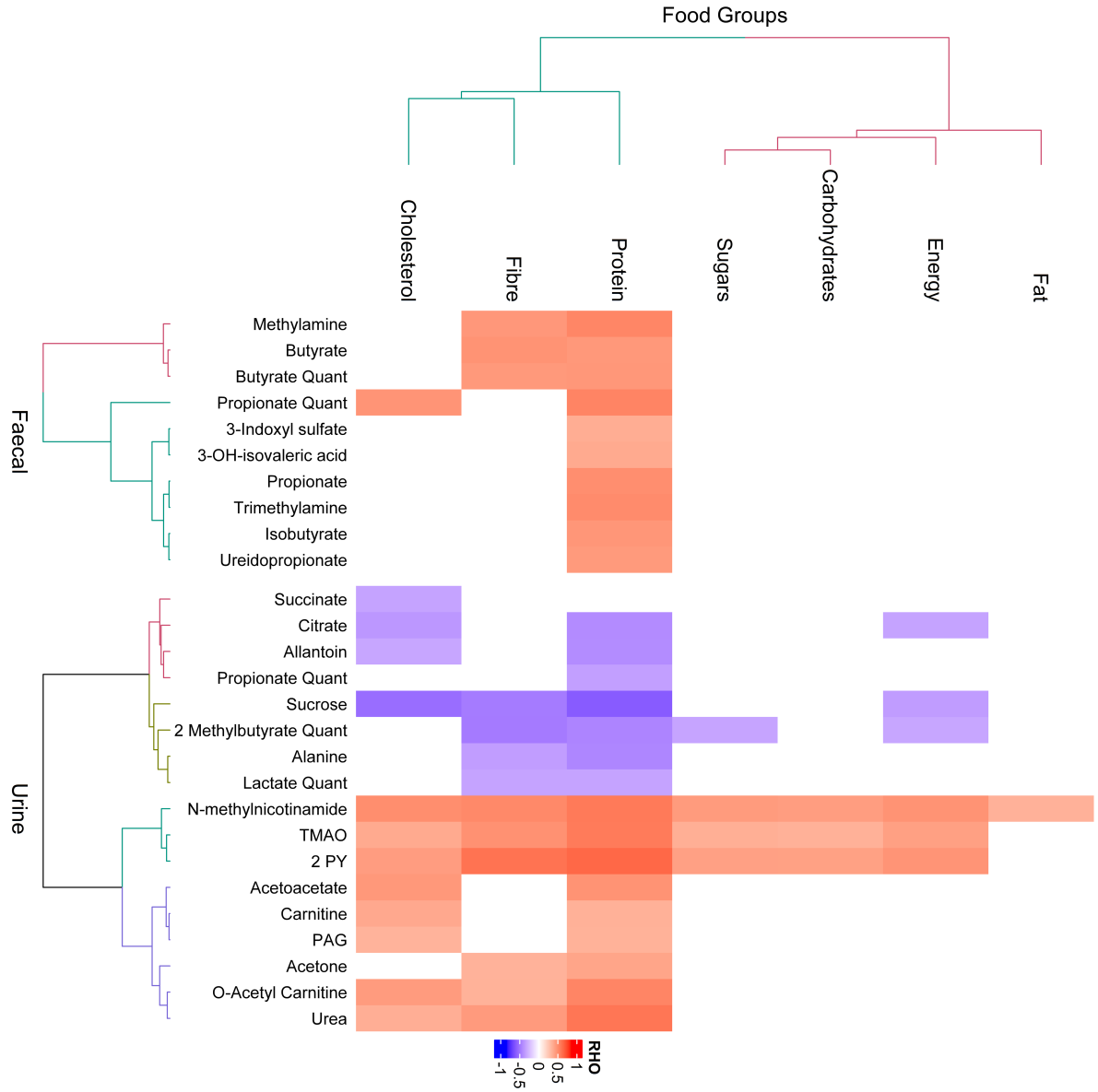
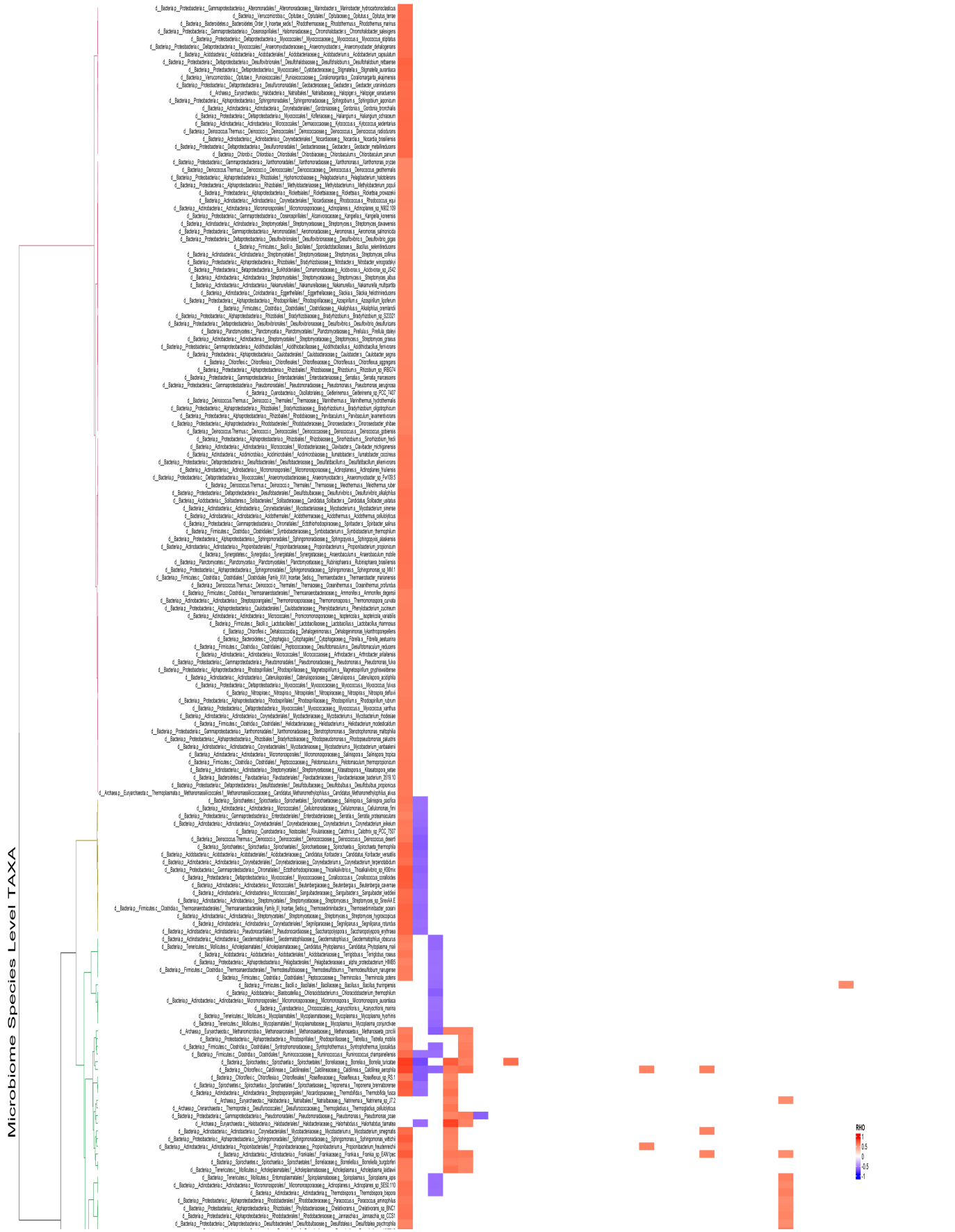


Figure 4.11-1 Diet – Metabolite correlations. Significant Spearman's correlations (pFDR <0.05) between diet Vs faecal and urinary metabolic datasets are shown, shaded according to strength of correlation coefficient (Rho). Correlations are clustered according to Euclidean distances.


Microbiome Species Level TAXA
RHO
1
0.5
0
-0.5
-1

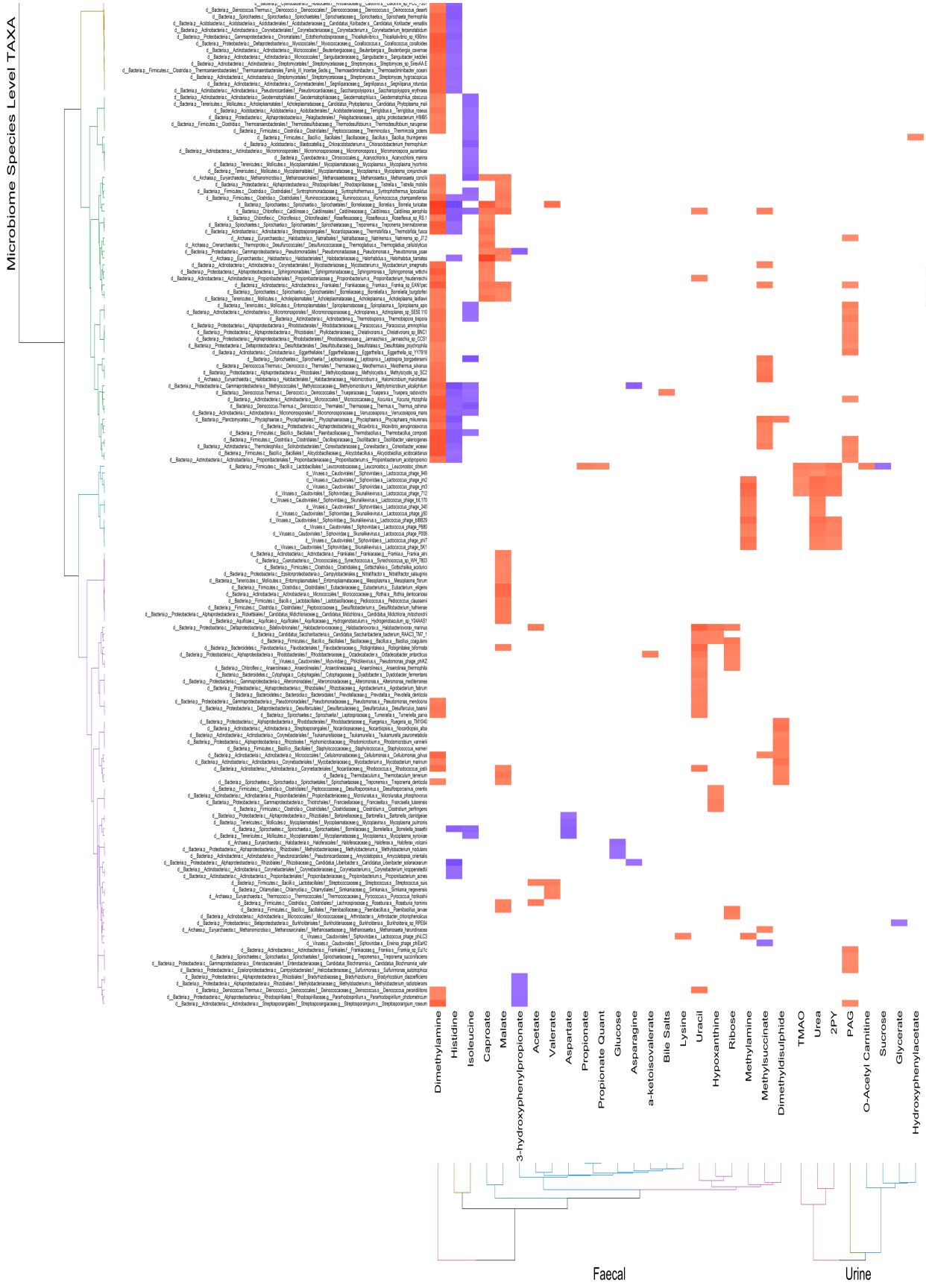
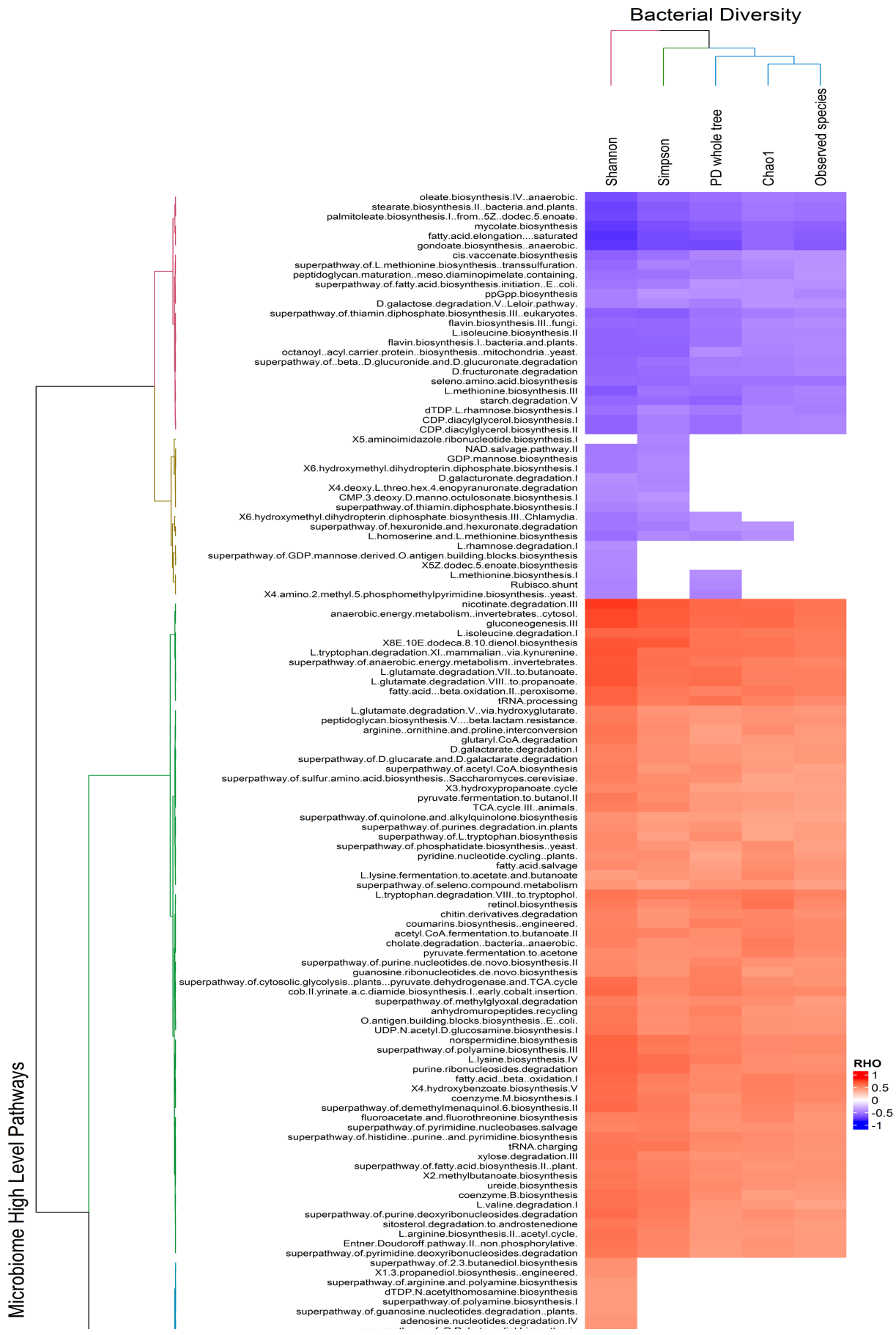


Figure 4.11-2 Gut Species - Metabolite correlations. Significant Spearman's correlations (pFDR <0.01) between microbial species Vs faecal and urinary metabolic datasets are shown, shaded according to strength of correlation coefficient (Rho). Correlations are clustered according to Euclidean distances.


Bacterial Diversity
Shannon
Simpson
PD whole tree
Chao1
Observed species
Microbiome High Level Pathways
oleate.biosynthesis.IV..anaerobic.
stearate.biosynthesis.II..bacteria.and.plants.
palmitoleate.biosynthesis.I..from..5Z..dodec.5.enoate.
mycolate.biosynthesis
fatty.acid.elongation....saturated
gondoate.biosynthesis..anaerobic.
cis.vaccenate.biosynthesis
superpathway.of.L.methionine.biosynthesis..transsulfuration.
peptidoglycan.maturation..meso.diaminopimelate.containing.
superpathway.of.fatty.acid.biosynthesis.initiation..E..coli.
ppGpp.biosynthesis
D.galactose.degradation.V..Leloir.pathway.
superpathway.of.thiamin.diphosphate.biosynthesis.III..eukaryotes.
flavin.biosynthesis.III..fungi.
L.isoleucine.biosynthesis.II
flavin.biosynthesis.I..bacteria.and.plants.
octanoyl..acyl.carrier.protein..biosynthesis..mitochondria..yeast.
superpathway.of..beta..D.glucuronide.and.D.glucuronate.degradation
D.fructuronate.degradation
seleno.amino.acid.biosynthesis
L.methionine.biosynthesis.III
starch.degradation.V
dTDP.L.rhamnose.biosynthesis.I
CDP.diacylglycerol.biosynthesis.I
CDP.diacylglycerol.biosynthesis.II
X5.aminoimidazole.ribonucleotide.biosynthesis.I
NAD.salvage.pathway.II
GDP.mannose.biosynthesis
X6.hydroxymethyl.dihydropterin.diphosphate.biosynthesis.I
D.galacturonate.degradation.I
X4.deoxy.L.threo.hex.4.enopyranuronate.degradation
CMP.3.deoxy.D.manno.octulosonate.biosynthesis.I
superpathway.of.thiamin.diphosphate.biosynthesis.I
X6.hydroxymethyl.dihydropterin.diphosphate.biosynthesis.III..Chlamydia.
superpathway.of.hexuronide.and.hexuronate.degradation
L.homoserine.and.L.methionine.biosynthesis
L.rhamnose.degradation.I
superpathway.of.GDP.mannose.derived.O.antigen.building.blocks.biosynthesis
X5Z.dodec.5.enoate.biosynthesis
L.methionine.biosynthesis.I
Rubisco.shunt
X4.amino.2.methyl.5.phosphomethylpyrimidine.biosynthesis..yeast.
nicotinate.degradation.III
anaerobic.energy.metabolism..invertebrates..cytosol.
gluconeogenesis.III
L.isoleucine.degradation.I
X8E.10E.dodeca.8.10.dienol.biosynthesis
L.tryptophan.degradation.XI..mammalian..via.kynurenine.
superpathway.of.anaerobic.energy.metabolism..invertebrates.
L.glutamate.degradation.VII..to.butanoate.
L.glutamate.degradation.VIII..to.propanoate.
fatty.acid...beta.oxidation.II..peroxisome.
tRNA.processing
L.glutamate.degradation.V..via.hydroxyglutarate.
peptidoglycan.biosynthesis.V....beta.lactam.resistance.
arginine..ornithine.and.proline.interconversion
glutaryl.CoA.degradation
D.galactarate.degradation.I
superpathway.of.D.glucarate.and.D.galactarate.degradation
superpathway.of.acetyl.CoA.biosynthesis
superpathway.of.sulfur.amino.acid.biosynthesis..Saccharomyces.cerevisiae.
X3.hydroxypropanoate.cycle
pyruvate.fermentation.to.butanol.II
TCA.cycle.III..animals.
superpathway.of.quinolone.and.alkylquinolone.biosynthesis
superpathway.of.purines.degradation.in.plants
superpathway.of.L.tryptophan.biosynthesis
superpathway.of.phosphatidate.biosynthesis..yeast.
pyridine.nucleotide.cycling..plants.
fatty.acid.salvage
L.lysine.fermentation.to.acetate.and.butanoate
superpathway.of.seleno.compound.metabolism
L.tryptophan.degradation.VIII..to.tryptophol.
retinol.biosynthesis
chitin.derivatives.degradation
coumarins.biosynthesis..engineered.
acetyl.CoA.fermentation.to.butanoate.II
cholate.degradation..bacteria..anaerobic.
pyruvate.fermentation.to.acetone
superpathway.of.purine.nucleotides.de.novo.biosynthesis.II
guanosine.ribonucleotides.de.novo.biosynthesis
superpathway.of.cytosolic.glycolysis..plants...pyruvate.dehydrogenase.and.TCA.cycle
cob.II.yrinate.a.c.diamide.biosynthesis.I..early.cobalt.insertion.
superpathway.of.methylglyoxal.degradation
anhydromuropeptides.recycling
O.antigen.building.blocks.biosynthesis..E..coli.
UDP.N.acetyl.D.glucosamine.biosynthesis.I
norspermidine.biosynthesis
superpathway.of.polyamine.biosynthesis.III
L.lysine.biosynthesis.IV
purine.ribonucleosides.degradation
fatty.acid..beta..oxidation.I
X4.hydroxybenzoate.biosynthesis.V
coenzyme.M.biosynthesis.I
superpathway.of.demethylmenaquinol.6.biosynthesis.II
fluoroacetate.and.fluorothreonine.biosynthesis
superpathway.of.pyrimidine.nucleobases.salvage
superpathway.of.histidine..purine..and.pyrimidine.biosynthesis
tRNA.charging
xylose.degradation.III
superpathway.of.fatty.acid.biosynthesis.II..plant.
X2.methylbutanoate.biosynthesis
ureide.biosynthesis
coenzyme.B.biosynthesis
L.valine.degradation.I
superpathway.of.purine.deoxyribonucleosides.degradation
sitosterol.degradation.to.androstenedione
L.arginine.biosynthesis.II..acetyl.cycle.
Entner.Doudoroff.pathway.II..non.phosphorylative.
superpathway.of.pyrimidine.deoxyribonucleosides.degradation
superpathway.of.2.3.butanediol.biosynthesis
X1.3.propanediol.biosynthesis..engineered.
superpathway.of.arginine.and.polyamine.biosynthesis
dTDP.N.acetylthomosamine.biosynthesis
superpathway.of.polyamine.biosynthesis.I
superpathway.of.guanosine.nucleotides.degradation..plants.
adenosine.nucleotides.degradation.IV
RHO
1
0.5
0
-0.5
-1

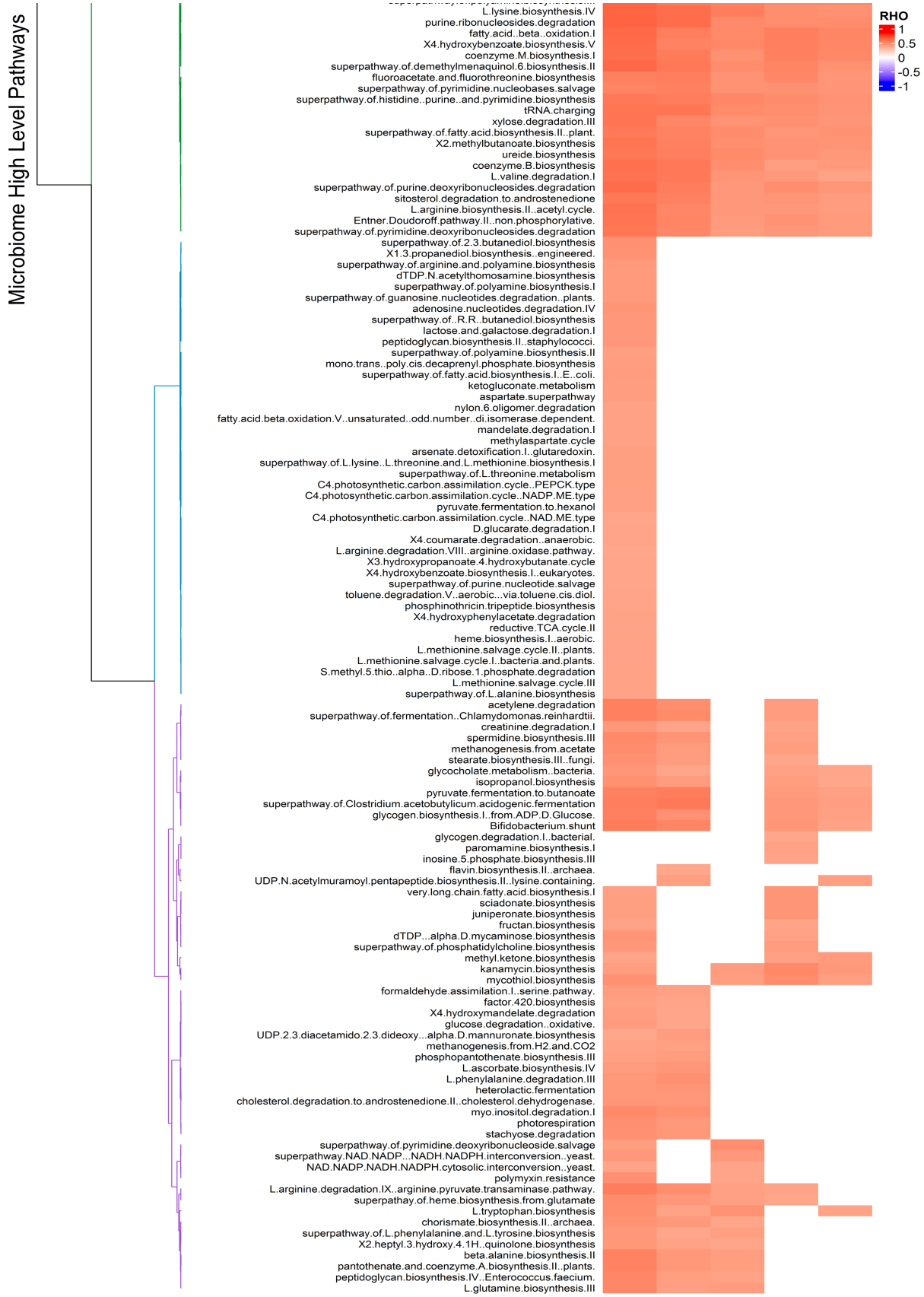


Figure 4.11-3 Metagenome Superpathway – Diversity Indices correlations. Significant Spearman's correlations (pFDR <0.01) between microbial metabolic superpathways and diversity indices (Shannon, Simpson, Whole Tree, Chao1) are shown, shaded according to strength of correlation coefficient (Rho). Correlations are clustered according to Euclidean distances.

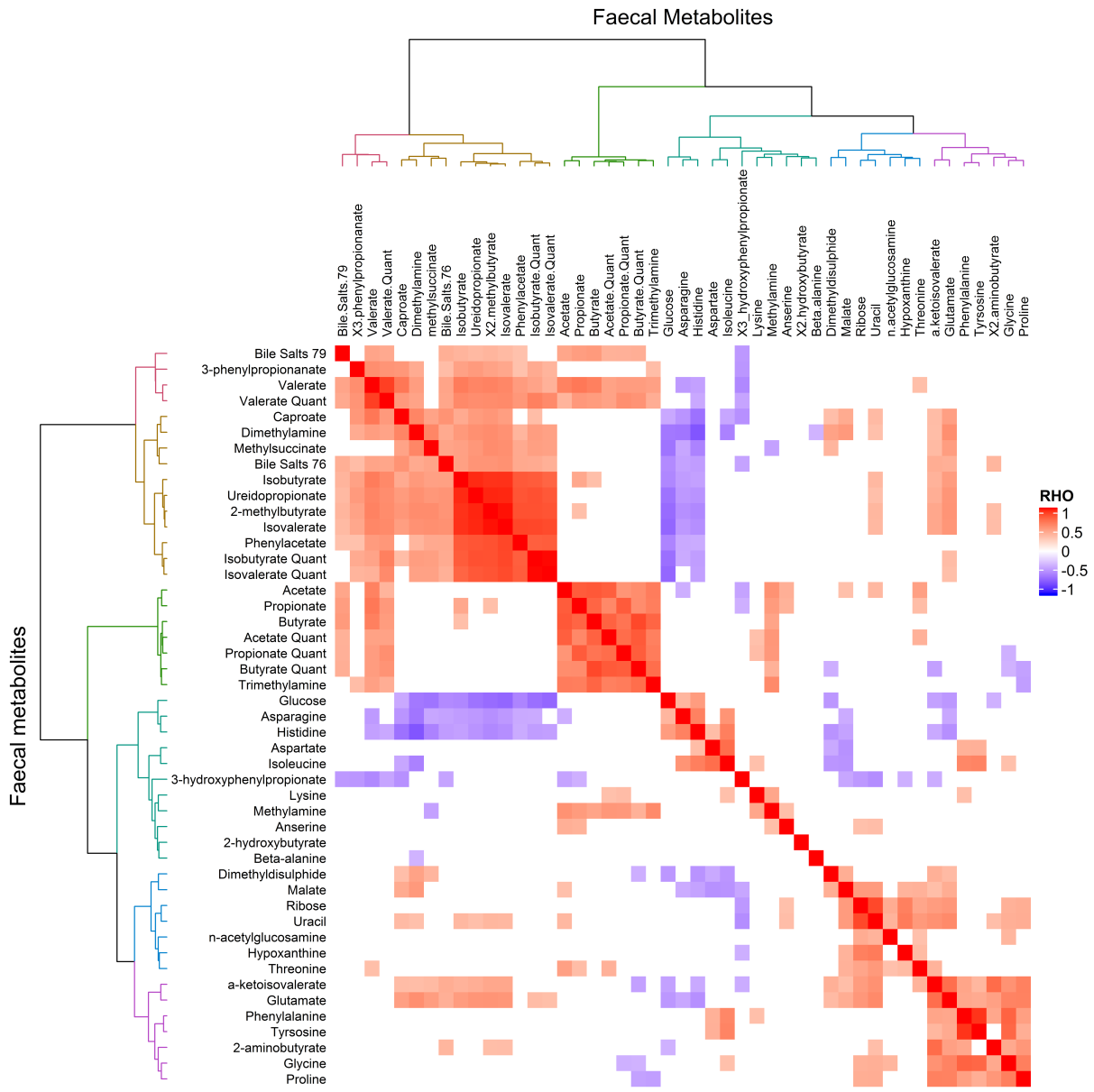


Figure 4.11-4 Faecal – Faecal Metabolite correlations. Significant Spearman's correlations (pFDR <0.05) within the faecal metabolite dataset are shown, shaded according to strength of correlation coefficient (Rho). Correlations are clustered according to Euclidean distances.

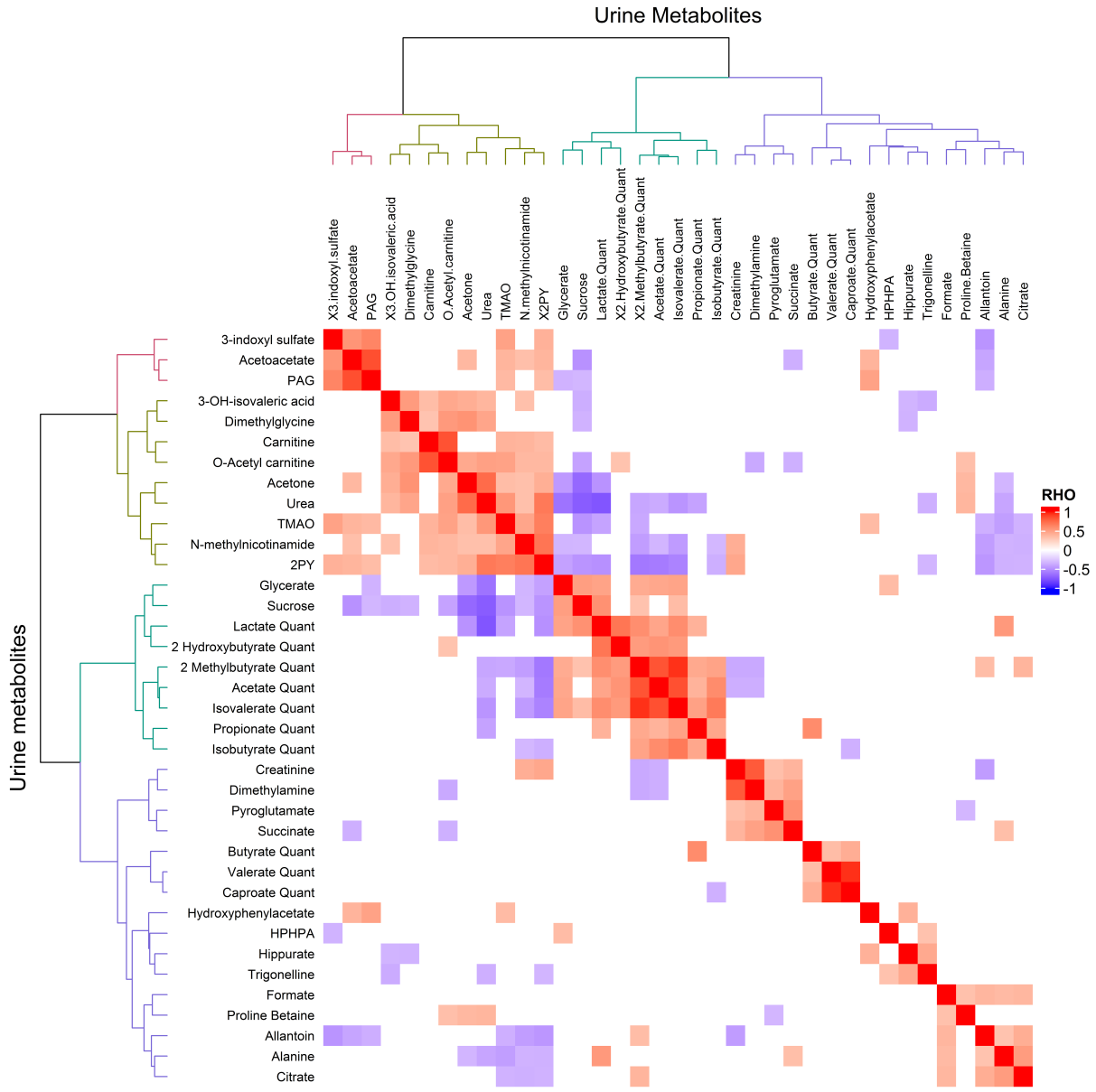


Figure 4.11-5 Urine – Urine Metabolite correlations. Significant Spearman's correlations (pFDR <0.05) within the urine metabolite dataset are shown, shaded according to strength of correlation coefficient (Rho). Correlations are clustered according to Euclidean distances.

4.12 References

5. Holmes E, Loo RL, Stamler J, Bictash M, Yap IK, Chan Q, et al. Human metabolic phenotype diversity and its association with diet and blood pressure. Nature. 2008;453(7193):396-400.

16. Holmes E, Li JV, Athanasiou T, Ashrafian H, Nicholson JK. Understanding the role of gut microbiome-host metabolic signal disruption in health and disease. Trends in microbiology. 2011;19(7):349-59.

20. Turnbaugh PJ, Ley RE, Mahowald MA, Magrini V, Mardis ER, Gordon JI. An obesity-associated gut microbiome with increased capacity for energy harvest. Nature. 2006;444(7122):1027-31.

21. Turnbaugh PJ, Hamady M, Yatsunenko T, Cantarel BL, Duncan A, Ley RE, et al. A core gut microbiome in obese and lean twins. Nature. 2009;457(7228):480-4.

23. Qin J, Li Y, Cai Z, Li S, Zhu J, Zhang F, et al. A metagenome-wide association study of gut microbiota in type 2 diabetes. Nature. 2012;490(7418):55-60.

26. Wang Z, Klipfell E, Bennett BJ, Koeth R, Levison BS, Dugar B, et al. Gut flora metabolism of phosphatidylcholine promotes cardiovascular disease. Nature. 2011;472(7341):57-63.

34. Le Chatelier E, Nielsen T, Qin J, Prifti E, Hildebrand F, Falony G, et al. Richness of human gut microbiome correlates with metabolic markers. Nature. 2013;500(7464):541-6.

41. Lin HV, Frassetto A, Kowalik EJ, Jr., Nawrocki AR, Lu MM, Kosinski JR, et al. Butyrate and propionate protect against diet-induced obesity and regulate gut hormones via free fatty acid receptor 3-independent mechanisms. PloS one. 2012;7(4):e35240.

42. Donohoe DR, Garge N, Zhang X, Sun W, O'Connell TM, Bunger MK, et al. The microbiome and butyrate regulate energy metabolism and autophagy in the mammalian colon. Cell metabolism. 2011;13(5):517-26.

48. Chambers ES, Viardot A, Psichas A, Morrison DJ, Murphy KG, Zac-Varghese SE, et al. Effects of targeted delivery of propionate to the human colon on appetite regulation, body weight maintenance and adiposity in overweight adults. Gut. 2015;64(11):1744-54.

54. Ufnal M, Zadlo A, Ostaszewski R. TMAO: A small molecule of great expectations. Nutrition. 2015;31(11-12):1317-23.

56. Koeth RA, Wang Z, Levison BS, Buffa JA, Org E, Sheehy BT, et al. Intestinal microbiota metabolism of L-carnitine, a nutrient in red meat, promotes atherosclerosis. Nature medicine. 2013;19(5):576-85.

60. Tang WH, Wang Z, Levison BS, Koeth RA, Britt EB, Fu X, et al. Intestinal microbial metabolism of phosphatidylcholine and cardiovascular risk. The New England journal of medicine. 2013;368(17):1575-84.

64. Mueller DM, Allenspach M, Othman A, Saely CH, Muendlein A, Vonbank A, et al. Plasma levels of trimethylamine-N-oxide are confounded by impaired kidney function and poor metabolic control. Atherosclerosis. 2015;243(2):638-44.

65. Dumas ME, Rothwell AR, Hoyles L, Aranias T, Chilloux J, Calderari S, et al. Microbial-Host Co-metabolites Are Prodromal Markers Predicting Phenotypic Heterogeneity in Behavior, Obesity, and Impaired Glucose Tolerance. Cell Rep. 2017;20(1):136-48.

105. Li JV, Ashrafian H, Bueter M, Kinross J, Sands C, le Roux CW, et al. Metabolic surgery profoundly influences gut microbial-host metabolic cross-talk. Gut. 2011;60(9):1214-23.

279. Pechlivanis A, Kostidis S, Saraslanidis P, Petridou A, Tsalis G, Mougios V, et al. (1)H NMR-based metabonomic investigation of the effect of two different exercise sessions on the metabolic fingerprint of human urine. Journal of proteome research. 2010;9(12):6405-16.

281. Estaki M, Pither J, Baumeister P, Little JP, Gill SK, Ghosh S, et al. Cardiorespiratory fitness as a predictor of intestinal microbial diversity and distinct metagenomic functions. Microbiome. 2016;4(1):42.

286. Clarke SF, Murphy EF, O'Sullivan O, Lucey AJ, Humphreys M, Hogan A, et al. Exercise and associated dietary extremes impact on gut microbial diversity. Gut. 2014;63(12):1913-20.

287. Petersen LM, Bautista EJ, Nguyen H, Hanson BM, Chen L, Lek SH, et al. Community characteristics of the gut microbiomes of competitive cyclists. Microbiome. 2017;5(1):98.

311. Garcia-Perez I, Posma JM, Gibson R, Chambers ES, Hansen TH, Vestergaard H, et al. Objective assessment of dietary patterns by use of metabolic phenotyping: a randomised, controlled, crossover trial. The lancet Diabetes & endocrinology. 2017;5(3):184-95.

313. Cloarec O, Dumas ME, Craig A, Barton RH, Trygg J, Hudson J, et al. Statistical total correlation spectroscopy: an exploratory approach for latent biomarker identification from metabolic 1H NMR data sets. Analytical chemistry. 2005;77(5):1282-9.

314. Posma JM, Garcia-Perez I, De Iorio M, Lindon JC, Elliott P, Holmes E, et al. Subset optimization by reference matching (STORM): an optimized statistical approach for recovery of metabolic biomarker structural information from 1H NMR spectra of biofluids. Analytical chemistry. 2012;84(24):10694-701.

339. Barton W, Penney NC, Cronin O, Garcia-Perez I, Molloy MG, Holmes E, et al. The microbiome of professional athletes differs from that of more sedentary subjects in composition and particularly at the functional metabolic level. Gut. 2018;67(4):625-33.

341. Tang WH, Hazen SL. Microbiome, trimethylamine N-oxide, and cardiometabolic disease. Translational research : the journal of laboratory and clinical medicine. 2016.

347. Falony G, Joossens M, Vieira-Silva S, Wang J, Darzi Y, Faust K, et al. Population-level analysis of gut microbiome variation. Science. 2016;352(6285):560-4.

348. Zhernakova A, Kurilshikov A, Bonder MJ, Tigchelaar EF, Schirmer M, Vatanen T, et al. Population-based metagenomics analysis reveals markers for gut microbiome composition and diversity. Science. 2016;352(6285):565-9.

349. Ekelund U, Ward HA, Norat T, Luan J, May AM, Weiderpass E, et al. Physical activity and all-cause mortality across levels of overall and abdominal adiposity in European men and women: the European Prospective Investigation into Cancer and Nutrition Study (EPIC). The American journal of clinical nutrition. 2015;101(3):613-21.

350. Willett WC, Sampson L, Stampfer MJ, Rosner B, Bain C, Witschi J, et al. Reproducibility and validity of a semiquantitative food frequency questionnaire. American journal of epidemiology. 1985;122(1):51-65.

351. Dona AC, Jimenez B, Schafer H, Humpfer E, Spraul M, Lewis MR, et al. Precision high-throughput proton NMR spectroscopy of human urine, serum, and plasma for large-scale metabolic phenotyping. Analytical chemistry. 2014;86(19):9887-94.

352. Garcia-Villalba R, Gimenez-Bastida JA, Garcia-Conesa MT, Tomas-Barberan FA, Carlos Espin J, Larrosa M. Alternative method for gas chromatography-mass spectrometry analysis of short-chain fatty acids in faecal samples. J Sep Sci. 2012;35(15):1906-13.

355. Veselkov KA, Vingara LK, Masson P, Robinette SL, Want E, Li JV, et al. Optimized preprocessing of ultra-performance liquid chromatography/mass spectrometry urinary metabolic profiles for improved information recovery. Analytical chemistry. 2011;83(15):5864-72.

362. Meadows JA, Wargo MJ. Carnitine in bacterial physiology and metabolism. Microbiology. 2015;161(6):1161-74.

363. Fennema D, Philips IR, Shephard EA. Trimethylamine and trimethylamine N-oxide, a flavin-containing monooxygenase 3 (FMO3)-mediated host-microbiome metabolic axis implicated in health and disease. Drug Metab Dispos. 2016.

366. Bennett BJ, de Aguiar Vallim TQ, Wang Z, Shih DM, Meng Y, Gregory J, et al. Trimethylamine-N-oxide, a metabolite associated with atherosclerosis, exhibits complex genetic and dietary regulation. Cell metabolism. 2013;17(1):49-60.

378. Schwabe RF, Jobin C. The microbiome and cancer. Nat Rev Cancer. 2013;13(11):800-12.

379. Kinross J, Mirnezami R, Alexander J, Brown R, Scott A, Galea D, et al. A prospective analysis of mucosal microbiome-metabonome interactions in colorectal cancer using a combined MAS 1HNMR and metataxonomic strategy. Sci Rep. 2017;7(1):8979.

380. Sonnenburg JL, Backhed F. Diet-microbiota interactions as moderators of human metabolism. Nature. 2016;535(7610):56-64.

381. Menni C, Jackson MA, Pallister T, Steves CJ, Spector TD, Valdes AM. Gut microbiome diversity and high-fibre intake are related to lower long-term weight gain. International journal of obesity. 2017;41(7):1099-105.

382. David LA, Maurice CF, Carmody RN, Gootenberg DB, Button JE, Wolfe BE, et al. Diet rapidly and reproducibly alters the human gut microbiome. Nature. 2014;505(7484):559-63.

383. Mika A, Van Treuren W, Gonzalez A, Herrera JJ, Knight R, Fleshner M. Exercise is More Effective at Altering Gut Microbial Composition and Producing Stable Changes in Lean Mass in Juvenile versus Adult Male F344 Rats. PloS one. 2015;10(5):e0125889.

384. Choi JJ, Eum SY, Rampersaud E, Daunert S, Abreu MT, Toborek M. Exercise attenuates PCB-induced changes in the mouse gut microbiome. Environ Health Perspect. 2013;121(6):725-30.

385. Queipo-Ortuno MI, Seoane LM, Murri M, Pardo M, Gomez-Zumaquero JM, Cardona F, et al. Gut microbiota composition in male rat models under different nutritional status and physical activity and its association with serum leptin and ghrelin levels. PloS one. 2013;8(5):e65465.

386. Lamoureux EV, Grandy SA, Langille MGI. Moderate Exercise Has Limited but Distinguishable Effects on the Mouse Microbiome. mSystems. 2017;2(4).

387. Bressa C, Bailen-Andrino M, Perez-Santiago J, Gonzalez-Soltero R, Perez M, Montalvo-Lominchar MG, et al. Differences in gut microbiota profile between women with active lifestyle and sedentary women. PloS one. 2017;12(2):e0171352.

388. Cronin O, Barton W, Skuse P, Penney NC, Garcia-Perez I, Murphy EF, et al. A Prospective Metagenomic and Metabolomic Analysis of the Impact of Exercise and/or Whey Protein Supplementation on the Gut Microbiome of Sedentary Adults. mSystems. 2018;3(3).

389. Craig CL, Marshall AL, Sjostrom M, Bauman AE, Booth ML, Ainsworth BE, et al. International physical activity questionnaire: 12-country reliability and validity. Med Sci Sports Exerc. 2003;35(8):1381-95.

390. Borg G. Borg's perceived exertion and pain scales: Human kinetics; 1998.

391. Kline GM, Porcari JP, Hintermeister R, Freedson PS, Ward A, McCarron RF, et al. Estimation of VO2max from a one-mile track walk, gender, age, and body weight. Med Sci Sports Exerc. 1987;19(3):253-9.

392. Kim Y, Park I, Kang M. Convergent validity of the international physical activity questionnaire (IPAQ): meta-analysis. Public health nutrition. 2013;16(3):440-52.

393. Taesuwan S, Cho CE, Malysheva OV, Bender E, King JH, Yan J, et al. The metabolic fate of isotopically labeled trimethylamine-N-oxide (TMAO) in humans. J Nutr Biochem. 2017;45:77-82.

394. Heianza Y, Sun D, Li X, DiDonato JA, Bray GA, Sacks FM, et al. Gut microbiota metabolites, amino acid metabolites and improvements in insulin sensitivity and glucose metabolism: the POUNDS Lost trial. Gut. 2019;68(2):263-70.

395. Zhuang R, Ge X, Han L, Yu P, Gong X, Meng Q, et al. Gut microbe-generated metabolite trimethylamine N-oxide and the risk of diabetes: A systematic review and dose-response meta-analysis. Obesity reviews : an official journal of the International Association for the Study of Obesity. 2019.

396. Li XS, Obeid S, Klingenberg R, Gencer B, Mach F, Raber L, et al. Gut microbiota-dependent trimethylamine N-oxide in acute coronary syndromes: a prognostic marker for incident cardiovascular events beyond traditional risk factors. Eur Heart J. 2017;38(11):814-24.

397. Senthong V, Li XS, Hudec T, Coughlin J, Wu Y, Levison B, et al. Plasma Trimethylamine N-Oxide, a Gut Microbe-Generated Phosphatidylcholine Metabolite, Is Associated With Atherosclerotic Burden. J Am Coll Cardiol. 2016;67(22):2620-8.

398. Yin J, Liao SX, He Y, Wang S, Xia GH, Liu FT, et al. Dysbiosis of Gut Microbiota With Reduced Trimethylamine-N-Oxide Level in Patients With Large-Artery Atherosclerotic Stroke or Transient Ischemic Attack. J Am Heart Assoc. 2015;4(11).

399. Zhu W, Wang Z, Tang WHW, Hazen SL. Gut Microbe-Generated Trimethylamine N-Oxide From Dietary Choline Is Prothrombotic in Subjects. Circulation. 2017;135(17):1671-3.

400. Wu WK, Sheen LY, Wu MS. Response to the letter: Identification of trimethylamine N-oxide (TMAO)-producer phenotype is interesting, but is it helpful? Gut. 2019.

401. Collins HL, Drazul-Schrader D, Sulpizio AC, Koster PD, Williamson Y, Adelman SJ, et al. L-Carnitine intake and high trimethylamine N-oxide plasma levels correlate with low aortic lesions in ApoE(-/-) transgenic mice expressing CETP. Atherosclerosis. 2016;244:29-37.

402. Poesen R, Claes K, Evenepoel P, de Loor H, Augustijns P, Kuypers D, et al. Microbiota-Derived Phenylacetylglutamine Associates with Overall Mortality and Cardiovascular Disease in Patients with CKD. J Am Soc Nephrol. 2016;27(11):3479-87.

403. Zimmerman L, Egestad B, Jornvall H, Bergstrom J. Identification and determination of phenylacetylglutamine, a major nitrogenous metabolite in plasma of uremic patients. Clin Nephrol. 1989;32(3):124-8.

404. Barrios C, Beaumont M, Pallister T, Villar J, Goodrich JK, Clark A, et al. Gut-Microbiota-Metabolite Axis in Early Renal Function Decline. PloS one. 2015;10(8):e0134311.

405. Collino S, Montoliu I, Martin FP, Scherer M, Mari D, Salvioli S, et al. Metabolic signatures of extreme longevity in northern Italian centenarians reveal a complex remodeling of lipids, amino acids, and gut microbiota metabolism. PloS one. 2013;8(3):e56564.

406. Menni C, Lin C, Cecelja M, Mangino M, Matey-Hernandez ML, Keehn L, et al. Gut microbial diversity is associated with lower arterial stiffness in women. Eur Heart J. 2018;39(25):2390-7.

407. Hazekawa M, Ono K, Nishinakagawa T, Kawakubo-Yasukochi T, Nakashima M. In Vitro Anti-inflammatory Effects of the Phenylbutyric Acid Metabolite Phenylacetyl Glutamine. Biological & pharmaceutical bulletin. 2018;41(6):961-6.

408. Briefel RR, Flegal KM, Winn DM, Loria CM, Johnson CL, Sempos CT. Assessing the nation's diet: limitations of the food frequency questionnaire. Journal of the American Dietetic Association. 1992;92(8):959-62.

409. Wareham NJ, Jakes RW, Rennie KL, Mitchell J, Hennings S, Day NE. Validity and repeatability of the EPIC-Norfolk Physical Activity Questionnaire. Int J Epidemiol. 2002;31(1):168-74.

410. Gu Z, Eils R, Schlesner M. Complex heatmaps reveal patterns and correlations in multidimensional genomic data. Bioinformatics. 2016;32(18):2847-9.

411. Cobb-Clark DA, Kassenboehmer SC, Schurer S. Healthy habits: The connection between diet, exercise, and locus of control. J Econ Behav Organ. 2014;98:1-28.

412. Nieman DC, Gillitt ND, Sha W, Meaney MP, John C, Pappan KL, et al. Metabolomics-Based Analysis of Banana and Pear Ingestion on Exercise Performance and Recovery. Journal of proteome research. 2015;14(12):5367-77.

413. Mayneris-Perxachs J, Lima AA, Guerrant RL, Leite AM, Moura AF, Lima NL, et al. Urinary N-methylnicotinamide and beta-aminoisobutyric acid predict catch-up growth in undernourished Brazilian children. Sci Rep. 2016;6:19780.

414. Kraus D, Yang Q, Kong D, Banks AS, Zhang L, Rodgers JT, et al. Nicotinamide N-methyltransferase knockdown protects against diet-induced obesity. Nature. 2014;508(7495):258-62.

415. Elliott P, Posma JM, Chan Q, Garcia-Perez I, Wijeyesekera A, Bictash M, et al. Urinary metabolic signatures of human adiposity. Science translational medicine. 2015;7(285):285ra62.

416. Xiong X, Liu D, Wang Y, Zeng T, Peng Y. Urinary 3-(3-Hydroxyphenyl)-3-hydroxypropionic Acid, 3-Hydroxyphenylacetic Acid, and 3-Hydroxyhippuric Acid Are Elevated in Children with Autism Spectrum Disorders. Biomed Res Int. 2016;2016:9485412.

417. Emond P, Mavel S, Aidoud N, Nadal-Desbarats L, Montigny F, Bonnet-Brilhault F, et al. GC-MS-based urine metabolic profiling of autism spectrum disorders. Analytical and bioanalytical chemistry. 2013;405(15):5291-300.

418. Lees HJ, Swann JR, Wilson ID, Nicholson JK, Holmes E. Hippurate: the natural history of a mammalian-microbial cometabolite. Journal of proteome research. 2013;12(4):1527-46.

419. Heinzmann SS, Merrifield CA, Rezzi S, Kochhar S, Lindon JC, Holmes E, et al. Stability and robustness of human metabolic phenotypes in response to sequential food challenges. Journal of proteome research. 2012;11(2):643-55.

420. Heimann E, Nyman M, Palbrink AK, Lindkvist-Petersson K, Degerman E. Branched short-chain fatty acids modulate glucose and lipid metabolism in primary adipocytes. Adipocyte. 2016;5(4):359-68.

421. Holecek M. Relation between glutamine, branched-chain amino acids, and protein metabolism. Nutrition. 2002;18(2):130-3.

422. Holecek M. Branched-chain amino acids in health and disease: metabolism, alterations in blood plasma, and as supplements. Nutr Metab (Lond). 2018;15:33.

423. Brosnan JT, Brosnan ME. Branched-chain amino acids: enzyme and substrate regulation. The Journal of nutrition. 2006;136(1 Suppl):207S-11S.

424. Neis EP, Dejong CH, Rensen SS. The role of microbial amino acid metabolism in host metabolism. Nutrients. 2015;7(4):2930-46.

425. Macfarlane GT, Cummings JH, Allison C. Protein degradation by human intestinal bacteria. J Gen Microbiol. 1986;132(6):1647-56.

426. Hughes R, Magee EA, Bingham S. Protein degradation in the large intestine: relevance to colorectal cancer. Curr Issues Intest Microbiol. 2000;1(2):51-8.

5 Longitudinal phenotyping of bariatric surgery patients

5.1 Introduction

Within the UK approximately 1 in 4 adults are now obese. This obesity epidemic is having a dramatic impact on the rise of associated chronic disease states such as type 2 diabetes (T2D), cardiovascular disease and cancer, which in turn carry a significant health and economic burden. The Department of Health estimates the financial cost to the NHS at £5 billion annually. Thus, there is an urgent need for effective preventative and therapeutic strategies for the treatment of obesity. Disappointingly, the encouragement of lifestyle changes such as improved diet and increased exercise together with pharmacological therapies has proved largely ineffectual thus far. Hence surgical procedures have been developed to achieve more sustainable weight-loss and are currently the gold standard treatment for severe obesity. However, in addition to weight-loss they have also been highly successful in the resolution of obesity related co-morbidities including diabetes[77]. The metabolic outcomes are achieved through both weight-dependent and interestingly, weight-independent mechanisms[77, 117]. Indeed, many of the metabolic effects are seen before weight-loss has occurred. This is because bariatric surgery induces a complex systems wide metabolic effect, including a functional modification of the gut microbiome-host metabolic axis. As a result, bariatric surgery provides a unique opportunity to further understand these novel mechanisms and their role in weight-loss and T2D remission.

The microorganisms that reside within the gut and their collective genomes are known as the gut microbiome. Next-generation sequencing technology has significantly reduced the cost of sequencing while simultaneously increasing its throughput, speed and depth. This has been transformative in allowing genome sequencing of entire microbial communities, including unculturable organisms. As a result the gut microbiome has now been linked extensively with numerous disease states and represents an innovative therapeutic target in the treatment of obesity and T2D[22, 23, 34, 36, 40]. A low bacterial richness in the gut is associated with increased insulin resistance, adiposity and dyslipidaemia[34]. Indeed, metagenome wide association studies have demonstrated the ability to identify T2D patients based on their gut microbiome alone[23]. Convincingly, in an effort to establish causality, the colonisation of germ free mice

with the faecal microbiota of twin pairs discordant for obesity results in significantly greater increases in body mass, adiposity and glucose intolerance in mice receiving the faecal microbiota from the obese twin[36]. Furthermore, faecal transplants in humans from lean donors to patients with metabolic syndrome results in increased insulin sensitivity[38]. However, the overwhelming disruption to the gut microbiome caused by bariatric surgery is only just being defined, as is its functional importance. Faecal transplant experiments using the gut microbiota from Roux-en-Y gastric bypass (RYGB) treated mice to transfect non-operated germ free mice, lead to significant weight-loss and decreased fat mass compared to the transfer of gut microbiota from mice who have undergone sham surgery[39]. Multiple mechanisms have been implicated, including: reduced energy harvest of non-digestible food types such complex carbohydrates, modified gut permeability leading to decreased systemic inflammation, altered bile acid metabolism and carbohydrate fermentation products such as short-chain fatty acids (SCFAs) acting as signalling molecules to increase satiety[21, 62].

In particular, BAs have emerged as key signalling molecules, acting through the Farnesoid X Factor nuclear receptor (FXR) and G protein-coupled bile acid receptor (TGR5) to induce a number of physiological changes. I have systematically reviewed the mechanisms through which bile acids mediate **S**atiety, **L**ipid and cholesterol metabolism, **I**ncretins and glucose homeostasis, energy **M**etabolism, the gut **M**icrobiota and **E**ndoplasmic **R**eticulum stress – and named these the 'SLIMMER effects'[71]. In support of this, many of the beneficial effects seen after RYGB are reproduced in rats by simply diverting bile from the common bile duct to the mid to distal jejunum via a catheter[85]. Additionally, following Vertical Sleeve Gastrectomy (VSG) in mice, body fat is reduced and glucose tolerance improved compared to sham-operated controls. However, body fat and glucose tolerance do not significantly differ in FXR knockout mice after VSG. Furthermore, *Bacteroides* were reduced following VSG in the wild type mice but the gut microbiota was not altered in the FXR knockout mice suggesting that FXR signalling is important in mediating the beneficial effects of VSG, in part through its modulation of the gut microbiota[70]. Therapeutically bile acids have been targeted using bile acid binding resins to control and re-establish insulin sensitivity on models of diet-induced obesity[427].

SCFAs, produced through the saccharolytic fermentation of oligosaccharides, are further important signalling molecules influenced by changes to the gut microbiome. For example,

T2D patients are known to have lower levels of butyrate producing bacteria[23]. Butyrate has been demonstrated to reduce appetite[428] and furthermore, improve insulin resistance[41].

5.1.1 Aims and objectives:

Bariatric surgery provides a unique opportunity to study the complex inter relationship between the gut microbiome and the host phenotype through the longitudinal phenotyping of patients' gut microbiome and metabolic profiles before and after surgical intervention. I hypothesise that a functional modification of the gut microbiome occurs following RYGB and VSG surgeries, resulting in altered microbiome – host co-metabolism. In particular I hypothesise that changes to the gut microbiome result in a fundamental shift in bile acid and short-chain fatty acid metabolism. I aim to elucidate these mechanisms with the long-term translational objective of identifying novel, non-surgical, therapeutic targets such as next-generation targeted probiotics.

5.1.2 Preliminary work:

Professor Holmes's research group has pioneered methods to elucidate the mechanisms through which the gut microbiome affects the host phenotype and has developed techniques to apply this to the patient treatment pathway[8]. The group has demonstrated the profound change to the gut microbiota that occurs following bariatric surgery in rats[105]. Specifically, the *Gammaproteobacteria* - *E. hormaechei* correlated with markers of metabolic improvement, while high levels of *Enterobacteriaceae* and *Pasteurellaceae* correlated with weight-loss following bariatric surgery in rats. In addition, the group has identified bile salt hydrolases (BSH) as a key group of bacteria that alter the patient's metabolic phenotype[66]. This is due to the important role of bile acids as essential signalling molecules that act via the FXR and TGR5 bile acid receptors to exert their influence through the so-called 'SLIMMER effects', as reviewed above[71].

5.2 Methods

I conducted a prospective observational study of obese (BMI>30kg/m^2) patients undergoing Roux-en-Y Gastric Bypass (RYGB) or Vertical Sleeve Gastrectomy (VSG) surgery. Patients underwent longitudinal phenotyping pre- and post-surgery, with patients acting as their own

controls. Patients were not randomised and underwent surgical treatment as decided by the Imperial Weight Centre multi-disciplinary team of NHS clinicians.

5.2.1 Recruitment

Patients referred to the Imperial Weight Centre (NHS) Tier 4 service team for consideration of bariatric surgery who were obese (BMI>30kg/m2), aged ≥18, had failed efforts at lifestyle modification and dieting and were willing to comply with the trial protocol were recruited. Diabetics (HbA1c >48mmol/mol or treated) and non-diabetics due to undergo VSG or RYGB were all eligible for recruitment.

Patients who had previously undergone bariatric or major abdominal surgery, were or intended to become pregnant during trial period, or took long-term antibiotics were excluded. Major abdominal surgery included patients who had undergone small or large bowel resection, liver, pancreatic, splenic or stomach surgery, as these could influence the bacteria in the gut and / or the patient's metabolic state. Patients that had previously had an appendicectomy, cholecystectomy or hernia repair were not excluded.

To improve patient compliance sample collection occurred at the time of patients' usual NHS appointments preoperatively and at 3 months and 1 year post operatively.

5.2.2 Confounding factors

Recruitment of different ages, sexes and ethnicities introduced known confounding factors into the analysis. However, it was not feasible to reach the target sample size within a reasonable recruitment period if recruiting from, for example, female Caucasians only. It is proposed that the effect size from these large surgical interventions will outweigh any metabolic differences due to age, sex or ethnicity. Moreover, the longitudinal nature of this study minimises these confounding effects, with each participant acting as their own control. The non-randomised nature of surgical procedure selection also introduced bias. Differences in the baseline demographics of patients undergoing each procedure, such as prevalence of T2D, are explored in the results.

5.2.3 Regulatory approvals

The study received NHS Research Ethics Committee (15/ES/0026) and Imperial College Healthcare NHS Trust approval (15SM2479). In addition, the study was registered with the

Imperial Tissue Bank and ClinicalTrials.gov (NCT02421055). As there was no additional intervention and so no added risk of adverse events as a result of the research, a Trial Steering Committee was not required.

5.2.4 Clinical, Demographic and Dietary data collection

Subjects were assessed at the above time points for: 1) anthropometric & physiological measurements, 2) demographic details, 3) biochemical parameters, 4) oral-hypoglycaemic, insulin and other medication use, length of diabetes diagnosis and other co-morbidities.

In addition, an online self-reported 24-hour dietary recall questionnaire (www.myfood24.org) was utilised to capture detailed dietary intake information from patients at each of the study time points so that changes in diet following surgery could be accounted for in the analysis. Three 24hr recall questionnaires were completed at each time point. Subjects were able to pick from a selection of pictures of corresponding foods to accurately ascertain portion quantities. Collected dietary information was used to calculate Alternative Healthy Eating Index 2010 (AHEI-2010) scores as described previously[429]. In brief, scores of 0-10 were given for 11 components (maximum score 110). High scores were given for a high intake of vegetables, fruit, nuts and legumes, whole grains, long chain omega-3 fats and polyunsaturated fats, moderate intake of alcohol and low intake of sugar, sweetened drinks and fruit juice, red and processed meat, trans-fat and sodium.

5.2.5 Sample collection

Serum, stool and 24-hour urine samples were collected preoperatively and at 3-months and 1-year postoperatively, with informed patient consent. 24-hour urine samples were collected in sterile containers from 9am until 9am on the day of the study visit. Stool samples were collected using a Faecotainer® collection kit and stored on an ice pack provided, as close as possible but not more than 6 hours before the study visit. Serum was collected using red top BD Vacutainer® serum tubes (no additive) and processed according to manufacturer guidelines. After collection, samples were aliquoted and stored at -80°C until analysis. Prior to freezing, a separate aliquot of homogenised stool was used to generate faecal water as follows: approximately 10g of stool was added to 4 parts HPLC grade H_2O (g:ml), vortexed at 2850 rpm for 15min then centrifuged at 10,000g for 15min at 4°C. The resulting supernatant (faecal water) was frozen at -80°C until analysis[430].

A number of faecal water preparation methods have been proposed. Including those that involve the mechanical destruction and lysis of cells to release bacterial metabolites[430, 431]. The method chosen here minimises cell lysis so that the metabolites represent those bioavailable to the host within the sample[430]. In addition, metabolic differences have been demonstrated within topographical differences of the same stool sample, hence care was taken to homogenise samples prior to analyses[430].

Despite these efforts there are still a number of limitations in stool analysis. The most biologically important area of the stool is the mucinous faecal layer that interacts with the bowel mucosa. Furthermore, stool represents the microbiome of the distal colon, while significant levels of bioactivity are thought to occur more proximally in the small bowel and caecum and are not represented in stool samples[432]. However, to overcome both these limitations would have required invasive endoscopic procedures and hence was not practicable in any significant numbers.

5.2.6 Metabolomic analysis

5.2.6.1 ^{1}H-NNMR

Urine and faecal water samples were prepared for analysis by ^{1}H-NMR spectroscopy as follows: frozen samples (-80°C) were thawed, vortexed and then centrifuged at 1600 × g for 10 min to remove particulates and precipitated proteins. Faecal water supernatant was further filtered through Micro centrifuge filters (0.45µm Nylon, Costar) at 16000g for 15 minutes at 4°C. 540 µL of each sample was mixed with 60 µL of 1.5M KH_2PO_4 buffer (pH 7.4, 80% D2O) containing 1 mM of the internal reference standard, 3-(trimethylsilyl)-[2,2,3,3,-$^{2}H_4$]-propionic acid (TSP) and 2mM sodium azide (NaN_3), as described previously[351].

After thawing, serum samples were centrifuged at 12000g for 5 minutes at 4°C. Subsequently, 300µL of serum was mixed with 300µL of 0.075M NaH_2PO_4 buffer (pH 7.4) containing 0.8mM of the internal reference standard, 3-(trimethylsilyl)-[2,2,3,3,-$^{2}H_4$]-propionic acid (TSP) and 3.1mM sodium azide (NaN_3), as described previously[351].

^{1}H-NMR spectroscopy was performed at 300 K on Bruker 600 MHz (urine and serum) and 800 MHz (faecal water) spectrometers (Bruker Biospin, Germany) using the following standard one-dimensional pulse sequence: RD – g_{z1} – 90° – t_1 – 90° – t_m – g_{z2} – 90° – ACQ[351]. The

relaxation delay (RD) was set at 4 s, 90° represents the applied 90° radio frequency pulse, interpulse delay (t_1) was set to an interval of 4 µs, mixing time (tm) was 10 ms, magnetic field gradients (g_{z1} and g_{z2}) were applied for 1 ms and the acquisition period (AQA) was 2.7 s. Water suppression was achieved through irradiation of the water signal during RD and t_m. For the urine samples, each spectrum was acquired using 4 dummy scans followed by 32 scans while faecal spectra were acquired using 256 scans and 4 dummy scans and collected into 64K data points. A spectral width of 12 000Hz was used for all the samples. Prior to Fourier transformation, the free induction decays (FIDs) were multiplied by an exponential function corresponding to a line broadening of 0.3 Hz. Serum samples were analysed by ^{1}H-NMR using the standard one-dimensional pulse sequence described above and Carr-Purcell-Meiboom-Gill (CPMG) one dimensional pulse sequences. CPMG was used to attenuate broad, interfering peaks from lipids and proteins present in serum. The CPMG pulse sequence had the form – RD-90°-(t-180°-t)n-ACQ. The acquisition parameters were set using the same settings as the standard 1D pulse sequence, with the spin-echo delay (t) set at 0.3 ms and 128 loops (n) performed. Continuous wave irradiation was applied at the water resonance frequency during the relaxation delay (RD).

^{1}H-NMR spectra were automatically corrected for phase and baseline distortions and referenced to the TSP singlet at δ 0.0 using TopSpin 3.1 software. Spectra were then digitized into 20k data points at a resolution of 0.0005ppm using an in-house MATLAB R2014a (Mathworks) script. Subsequently, spectral regions corresponding to the internal standard (δ -0.5 to 0.5) and water (δ 4.6 to 5) peaks were removed. In addition, urea (δ 5.4 to 6.3) was removed from the urinary and serum spectra. All spectra were normalised using median fold change normalisation using the median spectrum as the reference[355].

5.2.6.2 Quantitative Bile Acid analysis

Quantitative analysis of 57 bile acids was performed using an established technique[353]. The method was adapted for analysis of bile acids in faecal samples.

5.2.6.2.1 Sample preparation

Bile acids were extracted from serum using the following method: 100 µL of serum was vortexed with 280 µL of MeOH. Samples were centrifuged at 14000g for 15 minutes at 4°C,

followed by incubation at -20°C for 20 minutes. Internal standard (16 deuterated bile acids) was added to the supernatant at a final concentration of 50nM.

Bile acids were extracted from faecal samples using the following method. Faecal samples were first freeze-dried. 100mg of freeze-dried material was then placed in micotubes with 1ml of 2:1:1 H_2O:ACN:IPA and approximately 50mg of 1mm Zirconia beads. This underwent 3x30 seconds bead beating and a Biospec bead beater followed by centrifugation at 16000g for 20 minutes at 4°C. The supernatant was further filtered through Micro centrifuge filters (0.45µm Nylon, Costar) at 16000g for 15 minutes at 4°C. To ensure bile acid concentrations within the dynamic range of the machine extracts were diluted 1:25 and 1:200 prior to analysis using the H_2O:ACN:IPA mix. Internal standard (16 deuterated bile acids) was added to the filtered supernatant at a final concentration of 50nM.

5.2.6.2.2 LC-MS machine conditions

BA analysis was performed using an ACQUITY ultra-performance liquid chromatography (UPLC) coupled to a Xevo triple quadrupole (TQ-S) mass spectrometer.

For liquid chromatography, an ACQUITY BEH C8 column (1.7 µm, 100 mm × 2.1 mm) was used at an operating temperature of 60°C. The mobile phase solvent A consisted of a 1:10 ACN:H_2O, with 1 mM ammonium acetate and pH 4.15 adjusted with acetic acid. Mobile phase solvent B consisted of 1:1 ACN:IPA. The chromatographic gradient was as previously published[353].

Mass spectrometry was performed in negative ionisation mode (ESI-) using the following parameters: capillary voltage 1.5 kV, cone voltage 60 V, source temperature 150°C, desolvation temperature 600°C, desolvation gas flow 1000 L/hr, and cone gas flow 150 L/hr. 57 bile acid species (36 non-conjugated, 12 taurine conjugated, 9 glycine conjugated) were assayed using multiple reaction monitoring (MRM). The transitions for each bile acid and deuterated internal standard was as previously published[353].

5.2.6.3 Quantitative SCFA analysis

5.2.6.3.1 Sample preparation

After defrosting and mixing, 100µL of urine / serum was aliquoted with 500µL of MTBE with 100ppm of internal standard (methyl stearate) and 2µL of HCL. This was vortexed and then shaken for 20 minutes. Following this samples were centrifuged at 10000rcf for 5 minutes at

4°C. Next, 90µL of the polar phase was placed into silanised vial and vortexed with 150 µL of derivatiser MTBSTF + 1% TBDMSCI (*N*-tert-Butyldimethylsilyl-*N*-methyltrifluoroacetamide with 1 % tert-Butyldimethylchloro-silane). This was then incubated for 45 minutes at 60°C before aliquoting into silanised inserts for analysis.

The method was modified to account for higher levels of SCFA in stool. After defrosting, 100mg of stool was aliquoted with 1000µL of MTBE with 100ppm of internal standard (methyl stearate) and 4µL of HCL. 30µL of the polar phase was mixed with 150µL of derivatiser.

5.2.6.3.2 GC-MS machine conditions

Derivatised samples were analysed by GC-MS with a Bruker triple quadrupole (TQ) GC-MS/MS. Helium was used as a carrier gas at a constant flow rate of 1.5 ml/min through the column. The injector temperature was 250°C with a split ratio 1:10. The temperature of the oven was started at 40°C and increased at the rate of 46°C/min to 127°C, 2°C/min to reach 131°C, 30°C/min to reach 160°C, then 50°C/min to reach a final temperature of 300°C. The transfer line to the mass spectrometer was set at 280°C. Targeted analysis of the nine SCFA compounds and internal standard was performed in multiple reaction monitoring mode (MRN) using the following settings:

Compound	**Precursor Ion**	**Product Ion**	**Collision Energy (eV)**
Acetate	117	75	10
Propionate	131	75	10
Butyrate / Isobutyrate	145	75	10
Valerate / Isovalerate	159	75	12
2 Methylbutyrate	159	75	12
2 Hydroxybutyrate	247	73	20
Caproate / Isocaproate	173	75	15

Table 5.2-1 GC-MS/MS machine settings for targeted SCFA analysis.

5.2.6.4 Quantitative Acylcarnitine and Amino Acid analysis

Quantitative acylcarnitine and amino acid analysis of samples was performed using the commercially available Biocrates AbsoluteIDQ® p180 kit, according to the manufacturer guidelines. Samples were analysed using flow injection analysis (FIA)-MS/MS and LC-MS/MS for acylcarnitines and amino acids metabolite groups respectively.

5.2.6.4.1 Sample preparation

10 µL of serum sample / PBS / calibration / QC and 10 µL of the ISTD mix (except in blanks) was added to each well. This was dried for 30 minutes under nitrogen flow. Following this, 50 µL of the derivatization solution was pipetted into each well. The plate was covered and incubated for 20 minutes, then dried for 60 minutes under nitrogen flow. Next, 300 µL of extraction solvent was added to each well, shaken for 30 minutes at 450rpm, then centrifuged for 2 minutes at 500 x g (rcf). For the LC-MS/MS 150 µL was added to 150 µl H_2O. For the FIA, 15 µL was added to 750 µL of FIA mobile phase. Both plates were shaken for 2 minutes at 600 rpm.

5.2.6.4.2 Machine conditions

Samples were analysed using a Waters I-Class UHPLC system and Waters Xevo TQ-S tandem mass spectrometer.

For FIA-MS/MS (direct infusion): the FIA mobile phase consisted of Biocrates Solvent I + 290 mL MeOH. A 2-minute isocratic method was used; starting at 0.15 mL/min for 0.1 minutes, gradually decreasing to 0.03 mL/min at 1 minute, increasing to 0.2 mL/min at 1.5 min, to 0.8 mL/min at 1.60 minutes, and finally decreasing to 0.15 mL/min at 1.95 minutes. MS settings were: capillary voltage 3.2 KV, cone voltage 10 V, source offset 50V, source temp 150°C, desolvation temp 620°C, cone gas 150 L/H, desolvation gas 1000 L/H, collision gas flow 0.15 mL/min, probe position 5 mm.

For LC-MS/MS: A Waters Acquity UPLC BEHC18 1.7 µm 2.1X 75 mm column was used. Mobile phase A: 1000mL H_2O + 2 mL formic acid (FA), Mobile phase B: 500 mL ACN + 1 mL FA. Gradient elution was used; starting at a flow rate of 0.8 mL/min with 100% A for 0.45 minutes, then changing in a linear gradient to 85% A at 3.3 minutes, to 30% A at 5.9 minutes, to 100% B at 6.05 minutes, flow then increased in a concave gradient to 0.9 mL/min 100% B by

6.20min, remaining at 0.9 mL/min 100% B until 6.42 min, before decreasing back in a concave gradient to 0.8mL/min 100% B at 6.52 min. The mobile phase was then changed in a concave gradient from 100% B to 100% A between 6.52 and 6.7 min and remained at 100% A 0.8 ml/min until 7.3 minutes. MS settings were: capillary voltage 3.9 KV, cone voltage 20 V, source offset 50V, source temp 150°C, desolvation temp 350°C, cone gas 150 L/Hr, desolvation Gas 650 L/Hr, collision gas flow 0.15 mL/min, probe position 7 mm.

Data was processed using targetlynx (Waters) and METIDQ (Biocrates; version Carbon) then exported as a CSV file for statistical analysis.

5.2.7 Faecal metagenome analysis

5.2.7.1 DNA extraction

Faecal samples were stored at -80 °C prior to analysis. DNA was extracted using the MoBio PowerFaecal® DNA Isolaion Kit, according to manufacturer's instructions. In brief, DNA was extracted from two separate 0.25 g aliquots of mixed whole stool samples at each analysis point. Samples were homogenised in 2 ml bead beating tubes containing garnet beads. Cell lysis of host and microbial cells was facilitated through both mechanical collisions between beads and chemical disruption of cell membranes. Reagent to precipitate non-DNA organic and inorganic material was then applied. Lastly, DNA was captured on a silica spin column, washed and eluted for downstream analysis. Quality control of DNA quality and quantity was assessed using an Agilent 4200 TapeStation.

5.2.7.2 Shotgun sequencing

Shotgun sequencing was performed using an Illumina HiSeq 4000 with paired-end 150 bp reads. Library preparation was undertaken using the NEBNext Ultra II DNA Library Prep Kit. 15 dual index barcodes (unique at both ends) were custom-designed and ordered from Integrate DNA Technologies (IDT®). Quality control of prepped libraries was performed using the Promega GloMax® and QuantiFluor® dsDNA systems. Each of the "uniquely dual-indexed" libraries were pooled and run on a single lane of the HiSeq4000. A mean of 6.89 Gb sequence data was acquired for each of 120 samples (median 6.84, range 3.88 – 14 Gb).

5.2.7.3 Processing of sequence data

There are known lane-swapping issues with the HiSeq 4000, leading to duplication of some sequencing reads. For this reason, fastq files for each sample were subject to deduplication using FastUniq[433]. Sequencing data were then processed using the Scalable Metagenomics Pipeline (ScaMP)[434], (http://www.imperial.ac.uk/bioinformatics-data- science-group/resources/software/scamp). In brief, raw sequence data were assessed for the presence of adapter sequences and trimmed using Trim Galore! (Babraham Bioinformatics) to remove low-quality bases (Q < 20) from the 3' end of reads and discard trimmed reads shorter than 100 nt. Quality control of trimmed reads was performed using FastQC (Babraham Bioinformatics). Reads that mapped with BWA-MEM[332] to human genome (hg19) were removed from read pairs, as ethical permission is not available for use of human data derived from metagenomes. Remaining reads were assumed to be microbial (bacteria, archaea, virus, fungi, protozoa) and processed further. Trimmed sequence data with human reads removed have been deposited with GenBank, EMBL and DDBJ databases under the BioProject accession number PRJNA473348.

MetaPhlAn2.6[333, 334] was used to determine the bacterial and archaeal taxonomic composition/abundance for each sample. Metagenome assembly was carried out in two rounds using metaSPAdes[335] 3.11.0, with an initial independent assembly carried out for each sample. Unassembled reads were then pooled and subjected to a second round of assembly to improve the representation of low-abundance sequences. *Ab-initio* gene prediction was carried out using MetaGeneMark[435, 436]. The resulting predictions were translated, and the protein sequences clustered using the cluster-fast method of UCLUST[437], with a 95 % identity cut-off. Centroid sequences from each cluster were used to form a non-redundant gene catalogue used for downstream analyses. Gene abundance in each sample was determined by alignment of the reads using BWA-MEM against the gene catalogue, determining the number of reads mapped to each gene sequence and normalising as described[34]. Functional annotation was carried out by mapping centroid sequences to the eggNOG-Mapper database[438] (version 4.5, downloaded on 1 March 2018) using diamond on our in-house server.

Microbial gene richness (MGR) was determined as described previously[34, 439]. Briefly, data were downsized to adjust for sequencing depth and technical variability by randomly selecting 7 million reads mapped to the gene catalogue (of 11,005,136 genes) for each sample and then computing the mean number of genes drawn over 30 random samplings.

5.2.8 Statistical analysis

To correct for dilution differences between samples various correction procedures were applied. Global metabolite data sets were corrected for dilution effects using median fold change normalisation[355]. Targeted metabolites measured within urine samples were corrected for dilution differences using osmolality and creatinine measurements[374]. Metagenome data was expressed as relative abundances.

5.2.8.1 Paired Multivariate analysis

Principal component analysis (PCA) was used to provide an overview of the data. Longitudinally paired global metabolic data, pre and post-intervention, was analysed using Partial Least Squares – Discriminant Analysis (PLS-DA) with Monte-Carlo cross-validation (MCCV)[311]. Data was centred and scaled to account for the repeated-measures design. 1000 MCCV models were generated and used to calculate the mean cross-validated predictive component score (T_{pred}) and variance for each sample[311]. The fit and predictability of the models obtained was determined by the R^2 and Q^2 values respectively. Gaussian kernel density estimates of the T_{pred} in each group were generated for visual interpretation[311].

25 bootstrap resamplings in each of the 1000 models was used to estimate the variance and mean coefficient for each variable and derive a p value for each variable accordingly[311]. Benjamini-Hochberg false discovery corrections were performed and a variable was considered significant with a false discovery rate value (q) ≤ 0.01. Manhattan plots showing $-\log_{10}(q)$ x sign of the variable regression coefficient for each variable within each MCCV-PLS-DA model were generated, with dotted lines added to illustrate the q value significance cut off level on the $\log_{10}$ scale.

5.2.8.2 Paired Univariate analysis

Differences between longitudinally paired samples in quantitative analysis of targeted metabolites and within the gut microbiome were assessed for significance using the Wilcoxon

Rank test. P values were corrected using Benjamini-Hochberg multiple testing corrections. Phylogenetic Trees were generated to illustrate changes using the GraPhlAn[440] script in Python.

5.2.8.3 Microbiome-Metabolome associations

Microbiome-metabolome associations were assessed using Spearman's correlations between datasets in Matlab. As before, p values were corrected using Benjamini-Hochberg multiple testing corrections. Correlations with a false discovery rate value (q) ≤0.05 were displayed using ComplexHeatmap in R[410]. For some microbiome-metabolome datasets the q value was reduced to ≤0.01 to reduce the number of significant associations and aid interpretation. Hierarchical clustering of correlations was performed using Euclidean distances.

5.3 Results

5.3.1 Clinical findings after bariatric surgery

5.3.1.1 Baseline demographics

210 individuals consented to the study. Preoperative serum samples were collected from 158 subjects. Complete sample sets of serum, 24hr urine and stool was collected from 81 of these. 50 patients underwent bariatric surgery (VSG = 26, RYGB = 24) and gave serum samples 3-months post-operatively. 28 of these (VSG = 14, RYGB = 14) gave complete sample sets of serum, 24hr urine and stool 3-months post-operatively. Patients were a mix of sexes, ages and diabetic status, as detailed in Table 5.3-1 and Table 5.3-2. More diabetic patients underwent RYGB than VSG. Otherwise baseline demographics were not significantly different between procedures.

	All (Pre-Surgery)	**VSG (Pre-Surgery)**	**RYGB (Pre-Surgery)**
n	158	26	24
Age *[mean (SD)]*	46 (11)	43 (10)	47 (10)
Sex (F:M)	109 : 49	19 : 7	22 : 2

Height (m) ***[mean (SD)]***	1.67 (0.09)	1.66 (0.09)	1.63 (0.09)
Weight (kg) ***[mean (SD)]***	128.9 (27.5)	128.1 (25.4)	120.3 (20.0)
BMI (kg/m^2) ***[mean (SD)]***	46.0 (8.1)	46.5 (7.9)	45.6 (6.3)
T2D status (T2D:IGT:No) ***(T2D% : IGT% : No%)***	68 : 26 : 64 *(43 : 16 : 41)*	8 : 4 : 14 *(31 : 15 : 54)*	13 : 2 : 9 *(54 : 8 : 38)*
Systolic BP (mmHg) ***[mean (SD)]***	136 (15)	131 (16)	132 (10)
Diastolic BP (mmHg) ***[mean (SD)]***	82 (9)	81 (9)	80 (8)

Table 5.3-1 Baseline demographics of collected serum samples.

	All (Pre-Surgery)	**VSG (Pre-Surgery)**	**RYGB (Pre-Surgery)**
n	81	14	14
Age	48 (11)	44 (10)	50 (8)
Sex (F:M)	48 : 33	9 : 5	12 : 2
Height (m) ***[mean (SD)]***	1.68 (0.09)	1.67 (0.06)	1.62 (0.10)
Weight (kg) ***[mean (SD)]***	133 (27.8)	133.0 (23.0)	120.0 (19.8)
BMI (kg/m^2) ***[mean (SD)]***	47.3 (8.5)	47.8 (8.6)	45.9 (6.9)
T2D status (T2D:IGT:No) ***(T2D% : IGT% : No%)***	43 : 11 : 27 *(53 : 14 : 33)*	4 : 2 : 8 *(29: 14 : 57)*	8 : 2 : 4 *(57 : 14 : 29)*
Systolic BP (mmHg) ***[mean (SD)]***	138 (14)	136 (13)	135 (10)
Diastolic BP (mmHg) ***[mean (SD)]***	82 (10)	83 (7)	79 (8)

Table 5.3-2 Baseline demographics of complete serum, 24hr urine and stool sample sets.

5.3.1.2 Weight loss

Patients who underwent VSG (n=26) had a mean (SD) weight loss, % weight loss and BMI reduction of 21.7 kg (6.8), 17.3 % (5.6) and 7.9 kg/m^2 (2.2) respectively. Patients who underwent RYGB (n=24) had a mean (SD) weight loss, % weight loss and BMI reduction of 24.4 kg (6.9), 20.2 % (4.0) and 9.2 kg/m^2 (2.4) respectively. % Weight loss was significantly greater in the RYGB group (p=0.042), while there was a trend towards a greater reduction in BMI (p=0.051) (see Figure 5.3-1).

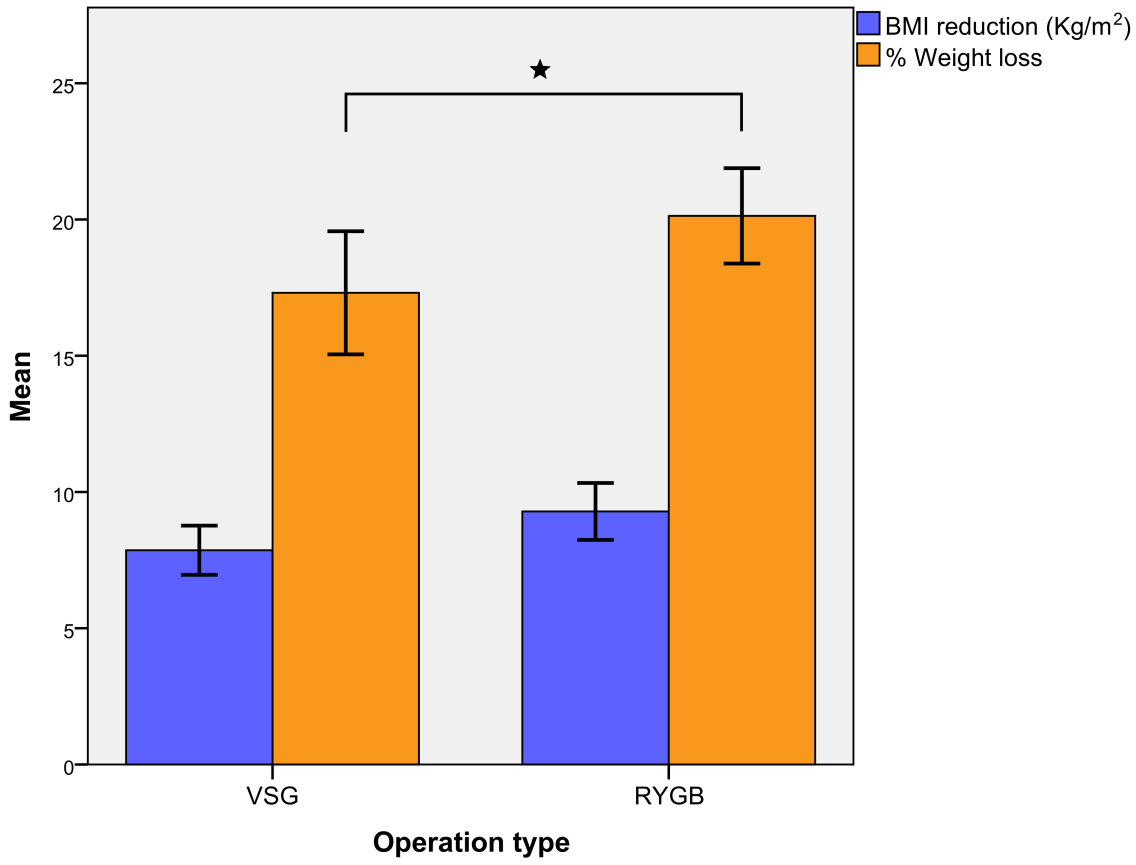


*Figure 5.3-1 Weight loss following VSG and RYGB procedures. Error bars = 95% confidence intervals. * = significant (p=0.042).*

5.3.1.3 Diabetic control

At 3-months post-operatively diabetic patients who underwent VSG (n=8) and RYGB (n=13) had mean (SD) HbA1c reductions of 17.8 (11.2) and 18.6 (12.2) mmol/mol respectively. Relative to baseline HbA1c, VSG and RYGB patients underwent 27.6% (12.1) and similarly

27.6% (14.0) reductions respectively. HbA1c reduction was not significantly different between procedures.

5.3.2 Dietary behaviour following bariatric surgery

3-months following surgery there were large changes in dietary intake. As measured by 3 self-reported 24-hour dietary recall questionnaires collected at each time point, there were significant reductions in calorie, carbohydrate, fat, sugar, protein, fibre, sodium and vegetable intake following surgery (see Figure 5.3-2). In subgroup analysis there was a significant reduction in calorie, carbohydrate, fat, fibre and sodium intake after both RYGB (n=10) and VSG (n=6). In addition, protein intake was significantly reduced after VSG, while saturated fat and sugar intake was significantly reduced after RYGB (see Figure 5.3-3). Dietary healthiness, measured using the Alternative Healthy Eating Index (AHEI-2010)[429], was increased 3 months following surgery (Median 42 Pre Vs 54 Post, p=0.0016) (see Figure 5.3-4).

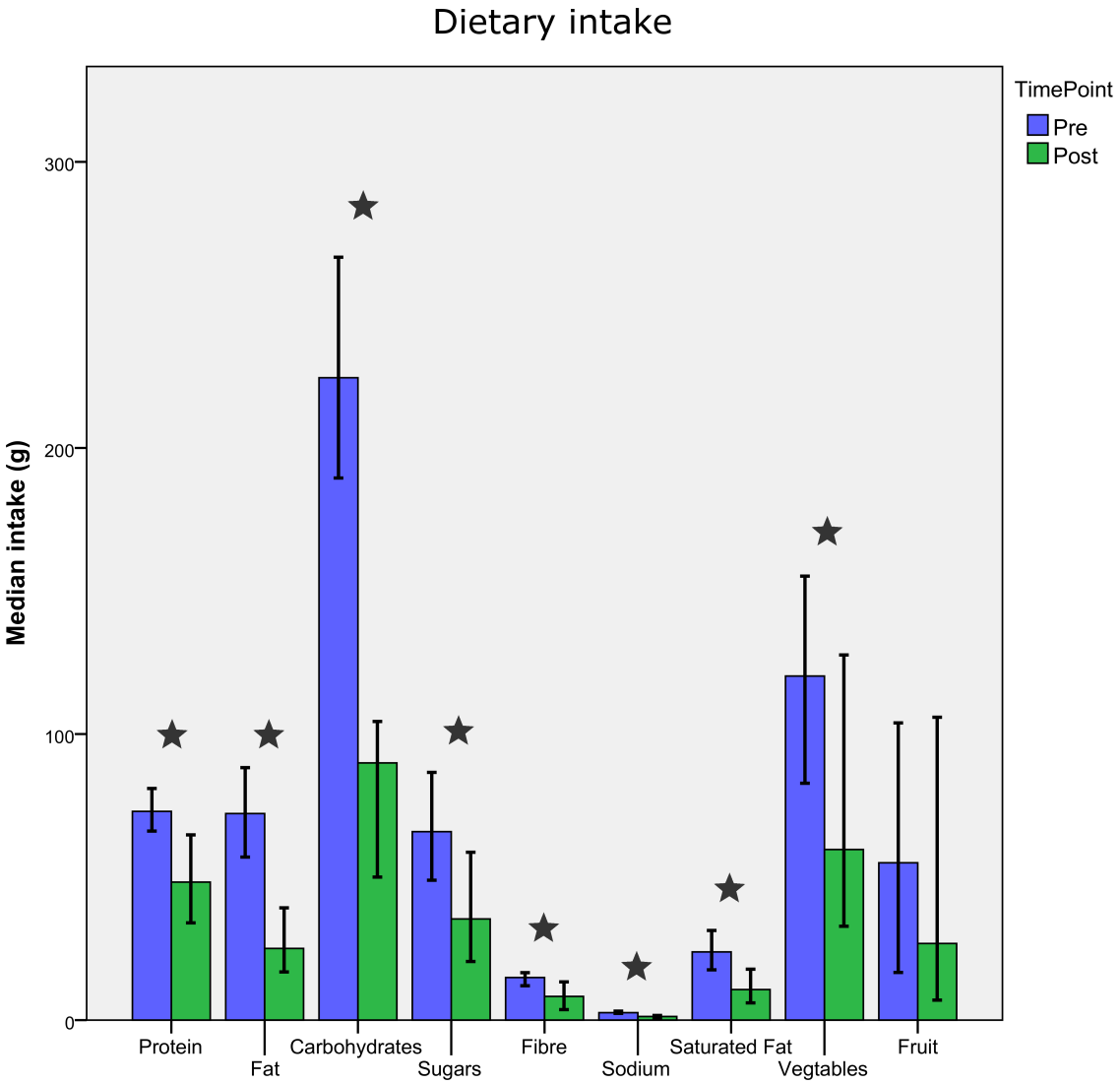


*Figure 5.3-2 Dietary intake Pre (blue) and Post (green) bariatric surgery. Error bars = 95% confidence intervals. * = significant (p<0.05) changes post-surgery.*

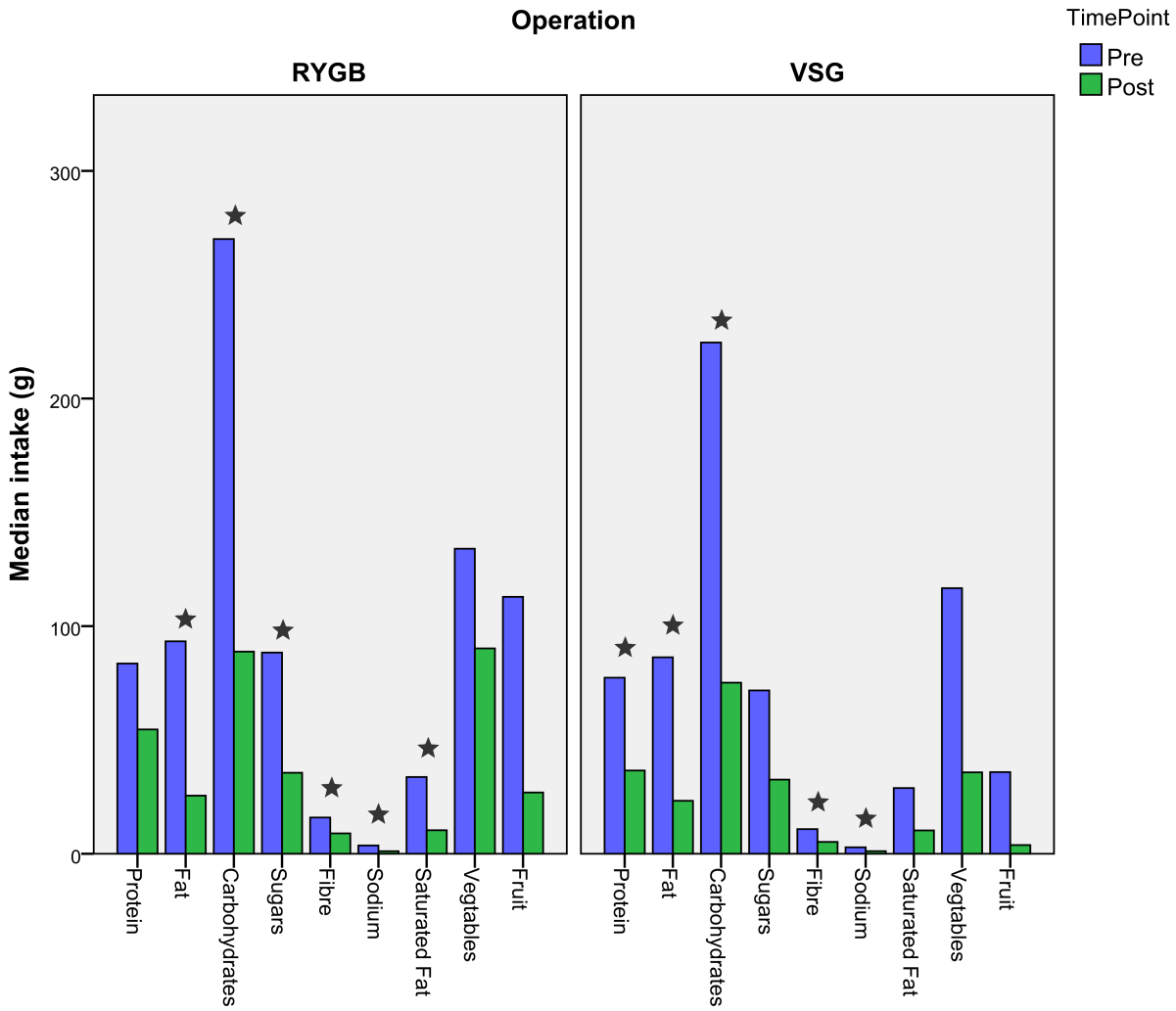


*Figure 5.3-3 Dietary intake Pre (blue) and Post (green) RYGB or VSG surgery. Error bars = 95% confidence intervals. * = significant (p<0.05) changes post-surgery.*

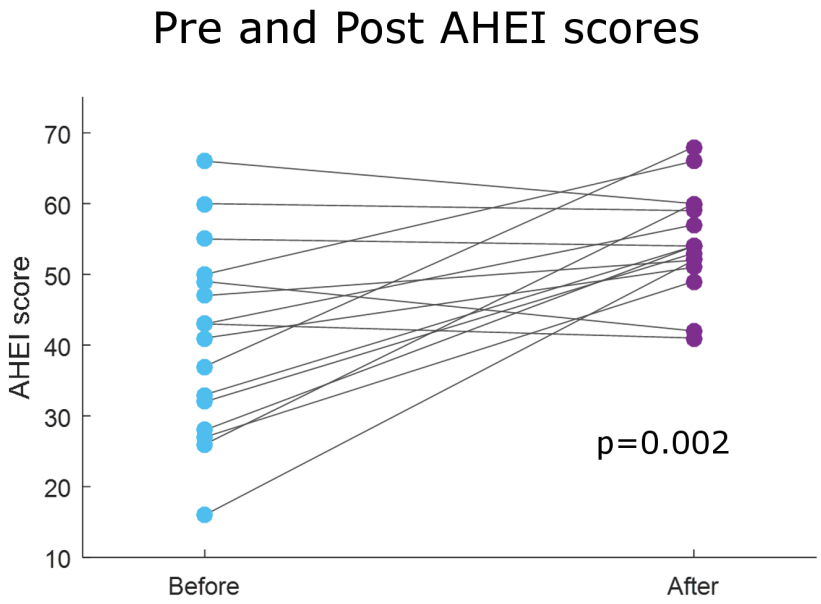


Figure 5.3-4 Alternative Healthy Eating Index 2010 (AHEI) scores Pre and Post bariatric surgery. Scores were significantly increased (p=0.0016, n=16).

5.3.3 Metabolic changes after bariatric surgery

5.3.3.1 Quantitative Bile Acid analysis of serum and faeces

27 bile acids species were fully quantified in the faecal and serum samples. Within the serum samples there were higher levels of secondary (UDCA) and conjugated secondary (GUDCA + TUDCA), and decreased levels of primary (CA + CDCA) and conjugated primary bile aids after bariatric surgery. In addition, the conversion ratio of CDCA to both UDCA and LCA was increased. Furthermore, the ratio of glycine to taurine conjugation in both primary and secondary bile acids was increased. Lastly a number of bile acids found in lower concentrations were increased after bariatric surgery. These included murocholic acid, taurohyocholic acid, 12-dehydrocholic acid, 5-cholenic acid-3β-ol, 3α-hydroxy-7-ketolithocholic acid, isolithocholic acid and glycohyocholic acid. In subgroup analysis, both RYGB and VSG groups had significantly increased UDCA (secondary BA) and GUDCA + TUDCA (conjugated secondary BAs) after surgery. Significant increases in glycine conjugation relative to taurine in both primary and secondary BAs were only seen after RYGB. Whereas significant decreases in primary and conjugated primary bile acids were only seen after VSG. These findings are summarised in Figure 5.3-5.

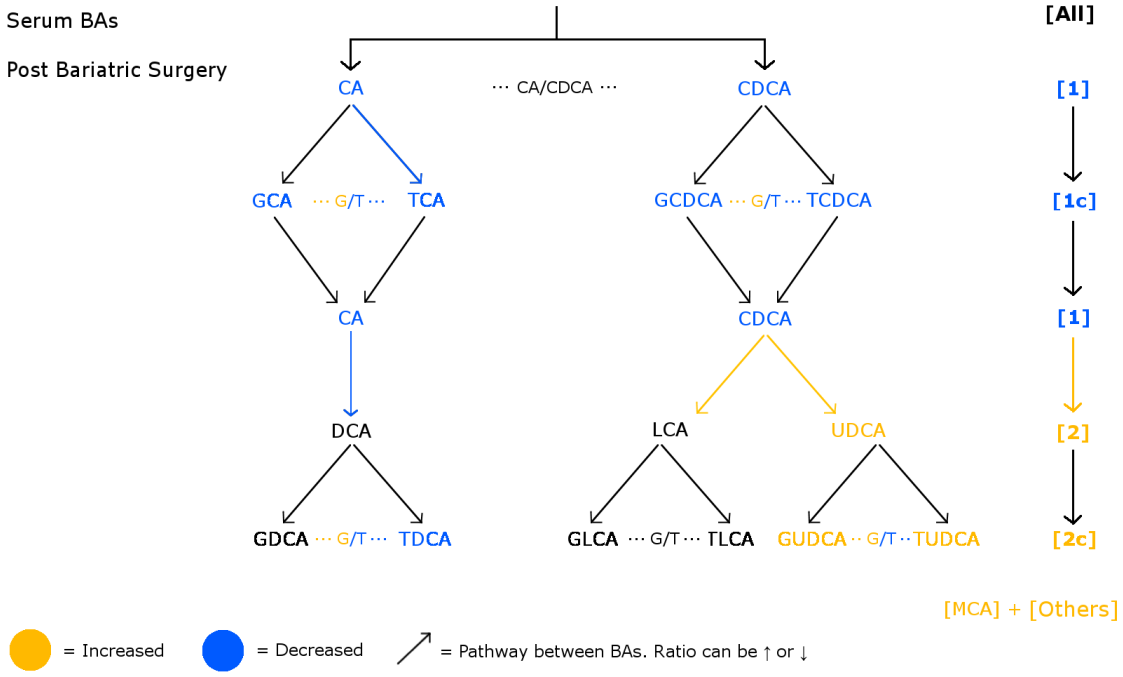


Figure 5.3-5 Serum bile acid profile changes following bariatric surgery. Arrows indicate known pathways between bile acids. Either the ratio between bile acids (pathway arrows), individual bile acids (labels) or bile acids groups (far right labels) can be increased (yellow) or decreased (blue) following bariatric surgery.

1: Primary BAs, 1c: Conjugated Primary BAs, 2: Secondary BAs, 2c: Conjugated secondary BAs, CA: Cholic acid, CDCA: Chenodeoxycholic acid, GCA: Glycocholic acid, TCA: Taurocholic acid, GCDCA: Glycochenodeoxycholic acid, TCDCA: Taurochenodeoxycholic acid, DCA: Deoxycholic acid, LCA: Lithocholic acid, UDCA: Ursodeoxycholic acid, GDCA: Glycodeoxycholic acid, TDCA: Taurodeoxycholic acid, GLCA: Glycolithocholic acid, TLCA: Taurolithocholic acid, GUDCA: Glycoursodeoxycholic acid, TUDCA: Tauroursodeoxycholic acid, MCA: Murocholic acid.

Within faecal samples, although overall levels of primary and secondary BAs decreased, similar to serum there was an increase in the conversion ratio of primary to secondary bile acids after bariatric surgery. This was seen with the conversion ratios of CDCA to UDCA and LCA and also CA to DCA after both RYGB and VSG surgery. Absolute levels of measured primary, secondary, conjugated primary and secondary and overall BAs were decreased after both procedures. These findings are summarised in Figure 5.3-6.

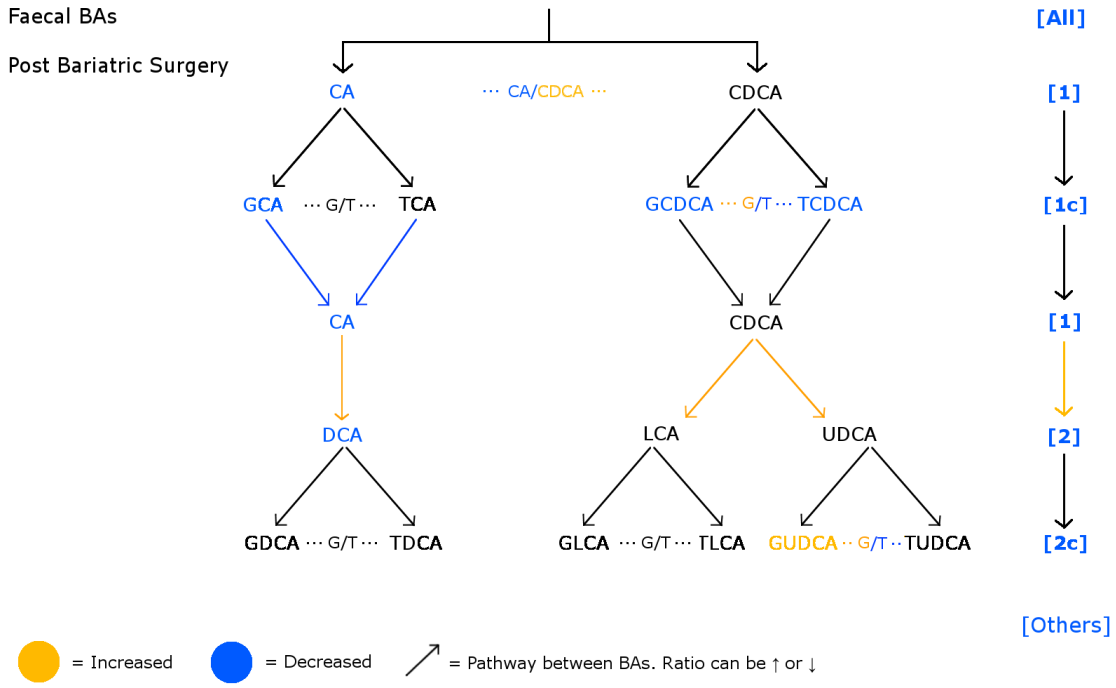


Figure 5.3-6 Faecal bile acid profile changes following bariatric surgery. Arrows indicate known pathways between bile acids. Either the ratio between bile acids (pathway arrows), individual bile acids (labels) or bile acids groups (far right labels) can be increased (yellow) or decreased (blue) following bariatric surgery.

1: Primary BAs, 1c: Conjugated Primary BAs, 2: Secondary BAs, 2c: Conjugated secondary BAs, CA: Cholic acid, CDCA: Chenodeoxycholic acid, GCA: Glycocholic acid, TCA: Taurocholic acid, GCDCA: Glycochenodeoxycholic acid, TCDCA: Taurochenodeoxycholic acid, DCA: Deoxycholic acid, LCA: Lithocholic acid, UDCA: Ursodeoxycholic acid, GDCA: Glycodeoxycholic acid, TDCA: Taurodeoxycholic acid, GLCA: Glycolithocholic acid, TLCA: Taurolithocholic acid, GUDCA: Glycoursodeoxycholic acid, TUDCA: Tauroursodeoxycholic acid, MCA: Murocholic acid.

5.3.3.2 Quantitative Short Chain Fatty Acid analysis in serum, urine and faeces

Analysis of 10 short-medium chain fatty acids was performed in serum, urine and faeces (see Tables 5.3 3-8). This revealed increased levels of 2-methylbutyric acid and isovaleric acid in both urine and faeces after RYGB. This was not seen after VSG. In serum, lactic acid was significantly decreased after RYGB and showed a non-significant trend towards decreasing after VSG. 2-hydroxybutyric acid was significantly reduced in serum after surgery across both groups combined, but this was not significant in subgroup analysis. In faeces, acetic acid was significantly reduced after both VSG and RYGB, whereas butyric acid was significantly reduced after VSG but showed a non-significant trend toward increasing after RYGB. In addition, valeric acid was reduced after VSG.

Serum			
All 3 months (n=51 paired)			
	Median change uM (IQR)	p	pFDR
Acetic acid	3.4 (30.3)	0.471	0.589
Propionic acid	-0.16 (3.63)	0.094	0.235
Isobutyric acid	-0.14 (0.99)	0.245	0.386
Butyric acid	0.01 (0.57)	0.784	0.824
2 Methylbutyric acid	-0.01 (0.06)	0.045	0.150
Isovaleric acid	-0.04 (0.20)	0.169	0.337
Valeric acid	0.00 (0.06)	0.270	0.386
Caproic acid	0.02 (0.25)	0.824	0.824
Lactic acid	-159 (801)	0.005	0.046
2 Hydroxybutyric acid	-10.06 (42.51)	0.009	0.046

Table 5.3-3 Serum SCFA changes after bariatric surgery. Compounds significantly decreased after surgery are highlighted blue.

Serum						
	RYGB 3 months (n=23 paired)			VSG 3 months (n=27 paired)		
	Median change µM (IQR)	p	pFDR	Median change µM (IQR)	p	pFDR
Acetic acid	3.1 (25.5)	0.540	0.665	5.4 (40)	0.413	0.534
Propionic acid	-0.16 (3.01)	0.360	0.562	-0.24 (3.91)	0.248	0.497
Isobutyric acid	-0.14 (0.67)	0.393	0.562	-0.24 (1.04)	0.427	0.534
Butyric acid	-0.12 (0.58)	0.665	0.665	0.01 (0.41)	0.953	0.953
2 Methylbutyric	-0.01 (0.06)	0.234	0.469	-0.02 (0.06)	0.081	0.324
Isovaleric acid	-0.04 (0.17)	0.160	0.469	-0.04 (0.22)	0.336	0.534
Valeric acid	0.00 (0.04)	0.609	0.665	0.00 (0.05)	0.097	0.324
Caproic acid	-0.02 (0.21)	0.211	0.469	0.09 (0.26)	0.220	0.497
Lactic acid	-344 (1166)	0.023	0.233	-146 (626)	0.058	0.324
2 Hydroxybutyric	-12.86 (44.6)	0.119	0.469	-7.25 (40.72)	0.594	0.660

Table 5.3-4 Serum SCFA changes after RYGB or VSG surgery. Compounds significantly decreased after surgery are highlighted blue.

Urine			
All 3 months (n=32 paired)			
	Median change µM (IQR)	p	pFDR
Acetic (Osmo norm)	-23 (557)	0.692	0.877
Acetic (Creat norm)	-2 (493)	0.524	0.873
Propionic (Osmo norm)	12.9 (105)	0.190	0.735
Propionic (Creat norm)	16.1 (96.2)	0.287	0.735
Isobutyric (Osmo norm)	1.16 (8.85)	0.166	0.735
Isobutyric (Creat norm)	0.06 (9.28)	0.638	0.877
Butyric (Osmo norm)	0.15 (8.85)	0.313	0.735
Butyric (Creat norm)	-0.35 (7.93)	0.934	0.963
2 Methylbutyric (Osmo norm)	0.08 (0.4)	0.034	0.454
2 Methylbutyric (Creat norm)	0.05 (0.54)	0.134	0.735
Isovaleric (Osmo norm)	0.05 (0.46)	0.045	0.454
Isovaleric (Creat norm)	0.02 (0.58)	0.331	0.735
Valeric (Osom norm)	-0.03 (0.64)	0.524	0.873
Valeric (Creat norm)	-0.02 (0.56)	0.747	0.877
Caproate (Osmo norm)	0.02 (1.09)	0.625	0.877
Caproate (Creat norm)	-0.08 (0.93)	0.789	0.877
Lactate (Osmo norm)	-32 (294)	0.512	0.873
Lactate (Creat norm)	-30 (328)	0.322	0.735
2 Hydroxybutyric (Osmo norm)	0.35 (10.35)	0.963	0.963
2 Hydroxybutyric (Creat norm)	0.88 (12.02)	0.789	0.877

Table 5.3-5 Urine SCFA changes after bariatric surgery. SCFA concentrations were normalised to urinary osmolality and creatinine. Compounds significantly increased after surgery are highlighted yellow.

Urine						
	RYGB 3 months (n=15 paired)			VSG 3 months (n=17 paired)		
	Median change µM (IQR)	p	pFDR	Median change µM (IQR)	p	pFDR
Acetic (Osmo)	91 (740)	0.847	0.996	-39 (627)	0.329	0.963
Acetic (Creat)	28 (687)	1.000	1.000	-63 (482)	0.243	0.963
Propionic (Osmo)	44.7 (215.7)	0.083	0.301	-19.2 (60.4)	0.927	0.963
Propionic (Creat)	26.8 (192.2)	0.121	0.301	-8.8 (100.9)	0.890	0.963
Isobutyric (Osmo)	1.65 (19.28)	0.073	0.301	0.12 (9.53)	0.963	0.963
Isobutyric (Creat)	0.89 (12.84)	0.229	0.459	-1.21 (6.67)	0.579	0.963
Butyric (Osmo)	2.13 (19.58)	0.135	0.301	-0.22 (8.3)	0.818	0.963
Butyric (Creat)	0.15 (18.1)	0.489	0.752	-2.38 (6.3)	0.517	0.963
2 Methylbutyric (Osmo)	0.18 (0.65)	0.018	0.256	0.02 (0.3)	0.644	0.963
2 Methylbutyric (Creat)	0.35 (0.76)	0.107	0.301	0.03 (0.29)	0.927	0.963
Isovaleric (Osmo)	0.16 (0.69)	0.026	0.256	0.04 (0.28)	0.747	0.963
Isovaleric (Creat)	0.05 (1.01)	0.107	0.301	-0.04 (0.35)	0.747	0.963
Valeric (Osom)	0.21 (0.81)	0.135	0.301	-0.05 (0.42)	0.517	0.963
Valeric (Creat)	0.08 (1.05)	0.277	0.461	-0.09 (0.53)	0.487	0.963
Caproate (Osmo)	0.19 (1.46)	0.277	0.461	-0.03 (1.04)	0.782	0.963
Caproate (Creat)	-0.07 (1.1)	0.679	0.900	-0.1 (0.9)	0.487	0.963
Lactate (Osmo)	-37 (315)	0.679	0.900	-26 (139)	0.782	0.963
Lactate (Creat)	36 (488)	0.720	0.900	-36 (187)	0.329	0.963
2 Hydroxybutyric (Osmo)	0.16 (17.94)	1.000	1.000	0.53 (5.85)	0.963	0.963
2 Hydroxybutyric (Creat)	0.82 (20.88)	0.978	1.000	0.89 (5.57)	0.747	0.963

Table 5.3-6 Urine SCFA changes after RYGB and VSG surgery. SCFA concentrations were normalised to urinary osmolality and creatinine. Compounds significantly increased after surgery are highlighted yellow.

Faeces			
	All 3 months (n=28)		
	Median change µM (IQR)	p	pFDR
Acetic Acid	-17635 (27688)	0.000	0.000
Propionic Acid	-5601 (12203)	0.053	0.178
Isobutyric Acid	12 (1128)	0.678	0.678
Butyric Acid	-5704 (15935)	0.020	0.102
2 Methylbutyric Acid	94 (764)	0.399	0.499
Isovaleric Acid	42 (1211)	0.305	0.436
Valeric Acid	-429 (1615)	0.227	0.436
Caproic Acid	-31 (271)	0.227	0.436
Lactic Acid	-4 (94)	0.582	0.647
2 Hydroxybutyric Acid	-0.36 (3.87)	0.264	0.436

Table 5.3-7 Faecal SCFA changes after bariatric surgery. Compounds significantly decreased after surgery are highlighted blue.

Faeces						
	RYGB 3 months (n=14)			VSG 3 months (n=14)		
	Median change µM (IQR)	p	pFDR	Median change µM (IQR)	p	pFDR
Acetic Acid	-20293 (26802)	0.003	0.034	-16526 (24325)	0.007	0.034
Propionic Acid	-9083 (14255)	0.244	0.488	-5290 (9802)	0.104	0.208
Isobutyric Acid	239 (818)	0.191	0.477	-342 (879)	0.091	0.208
Butyric Acid	1726 (16710)	0.787	0.893	-7188 (12946)	0.005	0.034
2 Methylbutyric	418 (1159)	0.048	0.160	-25 (542)	0.542	0.542
Isovaleric Acid	782 (1843)	0.010	0.052	-124 (610)	0.296	0.329
Valeric Acid	272 (2588)	0.839	0.893	-733 (1303)	0.025	0.082
Caproic Acid	-35 (239)	0.893	0.893	-18 (630)	0.268	0.329
Lactic Acid	12 (87)	0.588	0.840	-24 (108)	0.135	0.225
2 Hydroxybutyric	-0.45 (3.25)	0.340	0.566	-0.65 (3.85)	0.296	0.329

Table 5.3-8 Faecal SCFA changes after RYGB and VSG surgery. Compounds significantly decreased after surgery are highlighted blue, compounds significantly increased are highlighted yellow.

5.3.3.3 Quantitative Amino Acid and Acylcarnitine analysis

Quantitative analysis of amino acids, acylcarnitines and sugar levels was performed in serum (see Tables 5.3 9-12). This found a significant decrease in the majority of amino acids after both RYGB and VSG procedures. This included decreases in the branched chain amino acids leucine, isoleucine and valine and the aromatic amino acids phenylalanine, tryptophan and tyrosine. However, glycine and serine were significantly increased after both procedures, while glutamine was increased after RYGB.

Serum sugar levels were significantly reduced after RYGB, although the baseline level was higher than the VSG group and levels were still higher than the VSG group after intervention.

Short chain acylcarnitines, other than C2 (C0, C3-5), were reduced after bariatric surgery whereas longer chain acylcarnitines (C2, 7, 8, 10, 14, 16, 18) were increased. This was similar after both RYGB and VSG interventions.

Serum				
	Paired All 3 months (n=51)			
Amino Acids	Median Pre [µM]	Median Post [µM]	p (Wilcoxon)	pFDR
Alanine	415.0	364.0	0.0000	0.0000
Arginine	110.0	101.0	0.0437	0.0506
Asparagine	40.9	38.7	0.0476	0.0524
Aspartic acid	23.8	22.2	0.0343	0.0419
Citrulline	25.7	21.2	0.1315	0.1315
Glutamine	612.0	653.0	0.0041	0.0069
Glutamic acid	97.2	64.4	0.0002	0.0005
Glycine	222.0	292.0	0.0000	0.0000
Histidine	77.4	74.3	0.0752	0.0788
Isoleucine	81.6	56.8	0.0001	0.0003
Leucine	146.0	109.0	0.0001	0.0003
Lysine	212.0	198.0	0.0086	0.0118
Methionine	22.3	19.2	0.0028	0.0051
Ornithine	76.5	64.4	0.0083	0.0118
Phenylalanine	79.2	62.5	0.0000	0.0000
Proline	205.0	177.0	0.0014	0.0028
Serine	115.0	135.0	0.0000	0.0000

Threonine	120.0	100.0	0.0099	0.0128
Tryptophan	61.4	49.4	0.0001	0.0003
Tyrosine	75.7	59.6	0.0003	0.0007
Valine	242.0	187.0	0.0000	0.0000
Sugars	5114.0	4630.0	0.0044	0.0069

Table 5.3-9 Serum amino acids and sugar levels pre and post bariatric surgery. Compounds significantly decreased after surgery are highlighted blue, compounds significantly increased are highlighted yellow.

Serum								
Amino Acids	**Paired RYGB 3 months (n=25)**				**Paired VSG 3 months (n=26)**			
	Median Pre [µM]	**Median Post [µM]**	**p**	**pFDR**	**Median Pre [µM]**	**Median Post [µM]**	**p**	**pFDR**
Alanine	415.0	347.0	0.0088	0.0194	412.0	371.5	0.0016	0.0088
Arginine	100.0	97.0	0.7661	0.7661	116.0	104.5	0.0251	0.0460
Asparagine	38.5	37.8	0.2549	0.3299	42.4	39.0	0.0878	0.1073
Aspartic acid	22.5	23.5	0.4145	0.4687	24.5	21.8	0.0318	0.0500
Citrulline	23.8	20.8	0.5827	0.6104	27.1	23.3	0.1340	0.1474
Glutamine	601.0	653.0	0.0061	0.0149	616.5	652.5	0.1583	0.1658
Glutamic acid	97.3	60.5	0.1199	0.1649	92.3	65.6	0.0002	0.0022
Glycine	224.0	297.0	0.0000	0.0000	220.5	270.5	0.0068	0.0299
Histidine	75.4	73.7	0.4261	0.4687	78.6	76.4	0.1090	0.1262
Isoleucine	76.0	56.5	0.0008	0.0035	86.9	58.8	0.0130	0.0359
Leucine	137.0	105.0	0.0012	0.0044	157.0	112.0	0.0143	0.0359
Lysine	211.0	191.0	0.0965	0.1415	222.5	201.0	0.0470	0.0646
Methionine	21.4	18.4	0.0483	0.0817	22.8	20.1	0.0375	0.0550
Ornithine	71.2	66.5	0.3131	0.3827	80.9	63.4	0.0151	0.0359
Phenylalanine	77.3	62.2	0.0000	0.0000	81.9	63.4	0.0001	0.0022
Proline	227.0	177.0	0.0191	0.0350	193.5	182.0	0.0297	0.0500
Serine	113.0	136.0	0.0001	0.0007	118.0	134.0	0.0215	0.0430

Threonine	106.0	94.5	0.0957	0.1415	129.5	106.5	0.0636	0.0823
Tryptophan	54.1	45.5	0.0007	0.0035	67.9	53.9	0.0163	0.0359
Tyrosine	71.5	55.9	0.0115	0.0230	78.3	63.7	0.0140	0.0359
Valine	234.0	182.0	0.0015	0.0047	254.5	189.5	0.0011	0.0081
Sugars	6190.0	5206.0	0.0034	0.0094	4645.5	4517.5	0.2370	0.2370

Table 5.3-10 Serum amino acids and sugar levels pre and post RYGB or VSG surgery. Compounds significantly decreased after surgery are highlighted blue, compounds significantly increased are highlighted yellow.

Serum				
	Paired All 3 months (n=51)			
Acylcarnitines	Median Pre [µM]	Median Post [µM]	p (Wilcoxon)	pFDR
C0	41.300	37.300	0.0492	0.0841
C2	6.090	8.530	0.0001	0.0009
C3	0.329	0.243	0.0000	0.0001
C3-DC (C4-OH)	0.061	0.085	0.0061	0.0184
C3-OH	0.013	0.011	0.0030	0.0099
C3:1	0.011	0.008	0.0011	0.0044
C4	0.184	0.152	0.0099	0.0263
C4:1	0.012	0.013	0.2320	0.2900
C5	0.144	0.097	0.0000	0.0001
C5-DC (C6-OH)	0.023	0.024	0.0960	0.1370
C5-M-DC	0.022	0.022	0.5874	0.6183
C5-OH (C3-DC-M)	0.033	0.028	0.0000	0.0000
C5:1	0.021	0.019	0.0064	0.0184
C5:1-DC	0.016	0.015	0.0577	0.0890
C6 (C4:1-DC)	0.073	0.071	0.6749	0.6922
C6:1	0.014	0.013	0.2101	0.2712
C7-DC	0.024	0.032	0.0007	0.0031
C8	0.139	0.173	0.0440	0.0839
C9	0.024	0.021	0.0993	0.1370
C10	0.175	0.217	0.0260	0.0571
C10:1	0.313	0.355	0.2998	0.3527
C10:2	0.053	0.048	0.0271	0.0571

C12	0.081	0.089	0.2965	0.3527
C12-DC	0.044	0.044	0.7928	0.7928
C12:1	0.223	0.253	0.0655	0.0971
C14	0.061	0.063	0.3192	0.3648
C14:1	0.062	0.068	0.0470	0.0841
C14:1-OH	0.013	0.014	0.0245	0.0571
C14:2	0.022	0.027	0.0318	0.0636
C14:2-OH	0.007	0.006	0.4219	0.4687
C16	0.102	0.117	0.0002	0.0009
C16-OH	0.006	0.007	0.0505	0.0841
C16:1	0.026	0.030	0.0172	0.0429
C16:1-OH	0.010	0.012	0.0001	0.0005
C16:2	0.008	0.009	0.1059	0.1413
C16:2-OH	0.013	0.013	0.0578	0.0890
C18	0.033	0.035	0.4825	0.5216
C18:1	0.112	0.155	0.0000	0.0000
C18:1-OH	0.008	0.010	0.0004	0.0021
C18:2	0.038	0.044	0.0015	0.0055

Table 5.3-11 Serum acylcarnitine levels pre and post bariatric surgery. Compounds significantly decreased after surgery are highlighted blue, compounds significantly increased are highlighted yellow.

Serum								
	Paired RYGB 3 months (n=25)				Paired VSG 3 months (n=26)			
Acylcarnitines	Median Pre [µM]	Median Post [µM]	p	pFDR	Median Pre [µM]	Median Post [µM]	p	pFDR
C0	37.500	39.300	0.4620	0.5280	43.150	35.500	0.0357	0.0953
C2	6.700	9.380	0.0096	0.0482	5.760	8.100	0.0071	0.0286
C3	0.325	0.247	0.0081	0.0461	0.335	0.242	0.0006	0.0057
C3-DC (C4-OH)	0.065	0.099	0.0559	0.1399	0.056	0.077	0.0659	0.1464
C3-OH	0.013	0.011	0.2364	0.3783	0.013	0.011	0.0013	0.0106
C3:1	0.011	0.008	0.0735	0.1730	0.012	0.008	0.0049	0.0216
C4	0.184	0.173	0.4459	0.5246	0.185	0.138	0.0017	0.0115
C4:1	0.013	0.015	0.1198	0.2083	0.012	0.013	0.9201	0.9201
C5	0.128	0.098	0.0122	0.0542	0.155	0.096	0.0002	0.0056
C5-DC (C6-OH)	0.024	0.025	0.1113	0.2023	0.022	0.023	0.4765	0.5956

C5-M-DC	0.023	0.023	0.2166	0.3610	0.021	0.021	0.5242	0.6247
C5-OH (C3-DC-M)	0.031	0.027	0.0027	0.0268	0.036	0.028	0.0004	0.0056
C5:1	0.021	0.020	0.2750	0.4075	0.021	0.019	0.0022	0.0127
C5:1-DC	0.015	0.015	0.8166	0.8828	0.018	0.015	0.0120	0.0437
C6 (C4:1-DC)	0.075	0.073	0.9941	0.9941	0.071	0.069	0.5826	0.6473
C6:1	0.014	0.015	0.8910	0.9378	0.014	0.013	0.1010	0.2126
C7-DC	0.024	0.031	0.0400	0.1316	0.024	0.032	0.0048	0.0216
C8	0.139	0.173	0.0232	0.0928	0.142	0.159	0.5408	0.6247
C9	0.022	0.021	0.3483	0.4804	0.026	0.024	0.1975	0.3591
C10	0.175	0.237	0.0475	0.1356	0.173	0.206	0.3027	0.4658
C10:1	0.325	0.367	0.2605	0.4008	0.304	0.309	0.7078	0.7536
C10:2	0.055	0.052	0.4221	0.5246	0.050	0.045	0.0153	0.0474
C12	0.081	0.093	0.4458	0.5246	0.085	0.087	0.5466	0.6247
C12-DC	0.044	0.043	0.4296	0.5246	0.044	0.044	0.2996	0.4658
C12:1	0.223	0.277	0.0839	0.1864	0.218	0.221	0.4487	0.5956
C14	0.061	0.065	0.3023	0.4318	0.061	0.061	0.7160	0.7536
C14:1	0.058	0.073	0.0559	0.1399	0.065	0.065	0.4189	0.5778
C14:1-OH	0.013	0.015	0.0428	0.1316	0.014	0.014	0.2987	0.4658
C14:2	0.022	0.028	0.0942	0.1884	0.024	0.027	0.1707	0.3251
C14:2-OH	0.006	0.006	0.9424	0.9666	0.007	0.006	0.3629	0.5377
C16	0.102	0.117	0.0054	0.0371	0.102	0.118	0.0154	0.0474
C16-OH	0.006	0.007	0.4296	0.5246	0.006	0.007	0.0567	0.1333
C16:1	0.025	0.035	0.0335	0.1218	0.027	0.029	0.2220	0.3862
C16:1-OH	0.010	0.013	0.0016	0.0216	0.010	0.012	0.0182	0.0521
C16:2	0.007	0.009	0.1104	0.2023	0.009	0.009	0.4655	0.5956
C16:2-OH	0.013	0.013	0.0901	0.1884	0.013	0.014	0.4037	0.5767
C18	0.033	0.034	0.5407	0.6007	0.035	0.036	0.8367	0.8581
C18:1	0.108	0.160	0.0000	0.0020	0.115	0.151	0.0004	0.0056
C18:1-OH	0.008	0.010	0.0056	0.0371	0.009	0.010	0.0509	0.1273
C18:2	0.036	0.043	0.0002	0.0050	0.038	0.046	0.1623	0.3247

Table 5.3-12 Serum acylcarnitine levels pre and post RYGB or VSG surgery. Compounds significantly decreased after surgery are highlighted blue, compounds significantly increased are highlighted yellow.

5.3.3.4 Global ^{1}H-NMR profiling

5.3.3.4.1 PCA models comparing ^{1}H-NMR spectra of subjects before and after bariatric surgery in serum, urine and faecal biofluids

Principal component analysis (PCA) of serum samples analysed by ^{1}H-NMR, computed with two principal components, had a model score of R^2 0.23, Q^2 0.20. The unsupervised analysis showed initial clustering of patients according to their time point pre or post bariatric surgery. There was also clustering seen according to diabetes status and gender.

PCA of urine samples analysed by ^{1}H-NMR, computed with two principal components, had a model score of R^2 0.14, Q^2 0.09. The unsupervised analysis showed initial clustering of patients according to their time point pre or post bariatric surgery. There was also clustering seen according to diabetes status, but not gender.

PCA of faecal water samples analysed by ^{1}H-NMR, computed with two principal components, had a model score of R^2 0.34, Q^2 0.29. The unsupervised analysis did not show any clustering according to sample time point, diabetes status or gender.

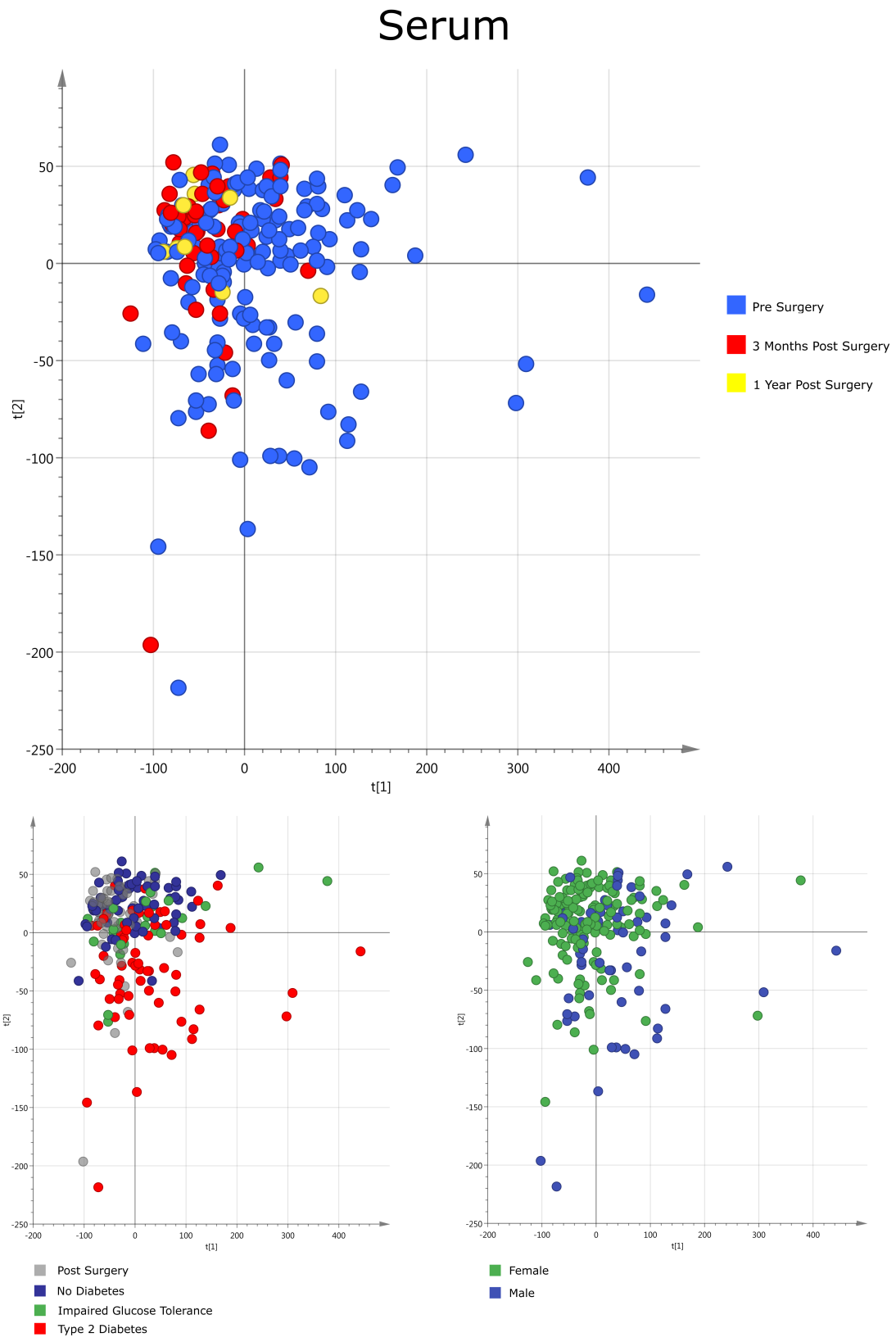


Figure 5.3-7 PCA scores plots of ^{1}H-NMR analysis comparing participants serum samples pre, 3-months post and 1-year post bariatric surgery. Models are comprised of 2 principal components. Model score: R^2 0.23, Q^2 0.20. Samples are colour coded according to i) Time point, ii) Diabetes status, iii) Sex.

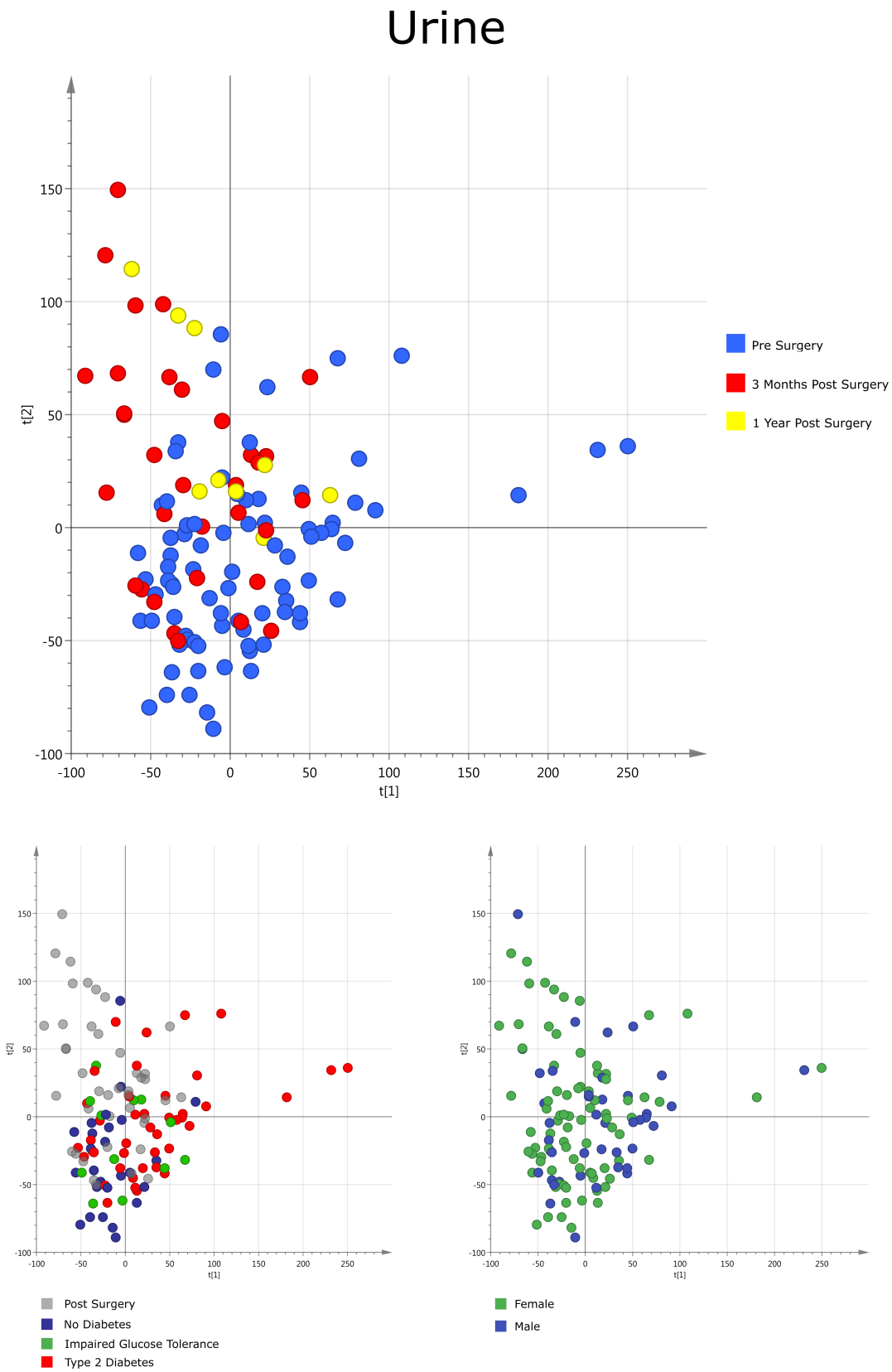


Figure 5.3-8 PCA scores plots of ^{1}H-NMR analysis comparing participants urine samples pre, 3-months post and 1-year post bariatric surgery. Models are comprised of 2 principal components. Model score: R^2 0.14, Q^2 0.09. Samples are colour coded according to i) Time point, ii) Diabetes status, iii) Sex.

Faeces

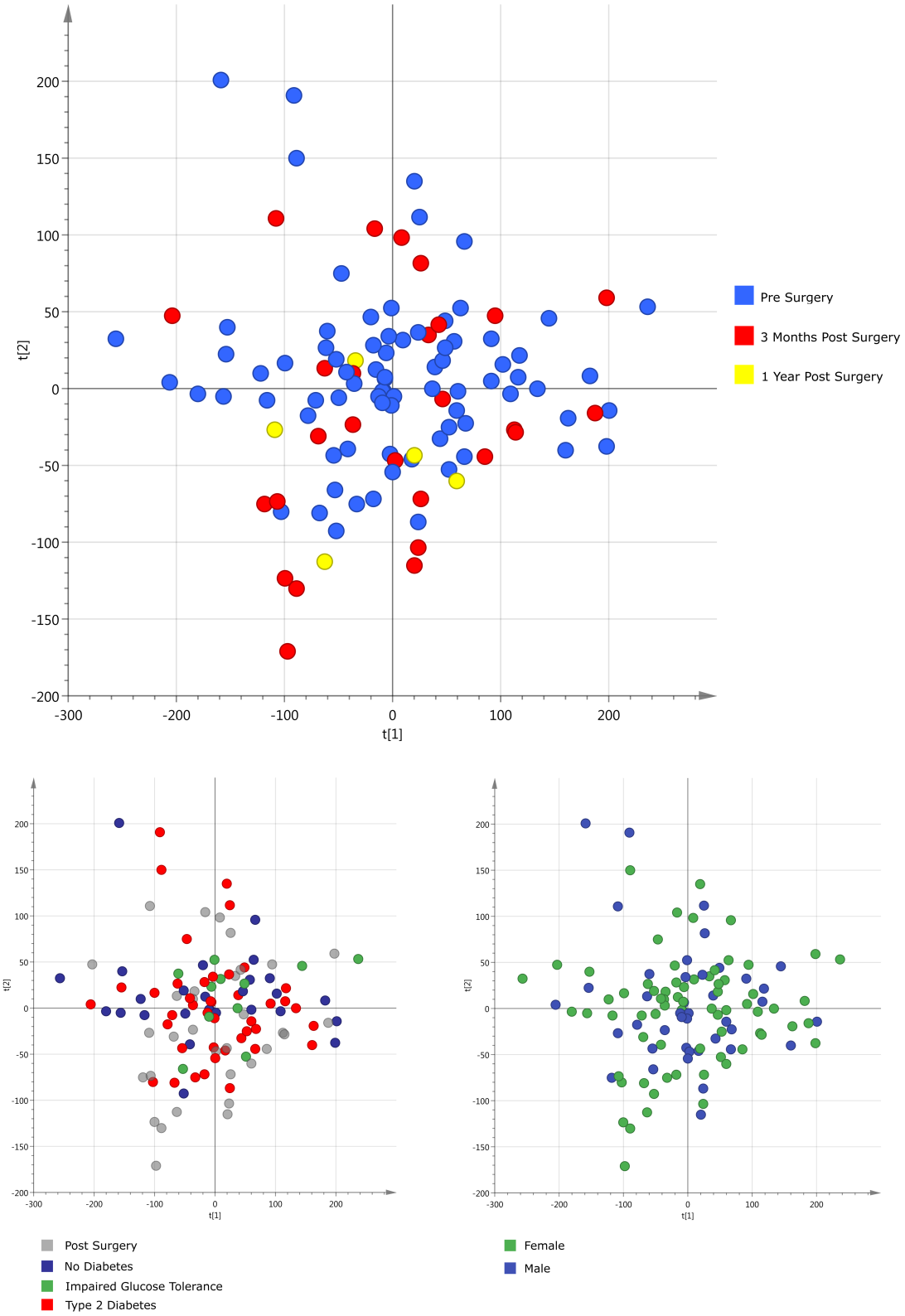


Figure 5.3-9 PCA scores plots of ^{1}H-NMR analysis comparing participants serum samples pre, 3-months post and 1-year post bariatric surgery. Models are comprised of 2 principal components. Model score: R^2 0.34, Q^2 0.29. Samples are colour coded according to i) Time point, ii) Diabetes status, iii) Sex.

5.3.3.4.2 Longitudinal MCCV-PLS-DA models comparing ^{1}H-NMR spectra of subjects before and after bariatric surgery in serum, urine and faecal biofluids

5.3.3.4.2.1 Serum ^{1}H-NMR analysis

MCCV-PLS-DA models of longitudinally paired serum samples analysed by ^{1}H-NMR found good separation between pre and post-surgery time points in overall and subgroup analyses. The resulting models were as follows: i) All 3months (n=50), R^2 0.92, Q^2 0.65 (see Figure 5.3-10); ii) RYGB (n=24), R^2 0.99, Q^2 0.42, iii) VSG 3 months (n=26), R^2 0.96, Q^2 0.51; iv) 1 Year (n=9), R^2 1.00, Q^2 0.35 (see Figure 5.3-11).

The significant serum metabolite changes derived from the loadings plot included: amino acids changes, consistent with changes seen in the targeted amino acid analysis, with increases in glycine and glutamine and decreases in tyrosine, proline, lysine and the BCAAs leucine, isoleucine and valine after surgery. Lipid changes with VLDL/LDL, HDL, lipid glycerol and choline decreasing at 3 months after surgery, while HDL and choline appear to increase by 1 year. Ketone bodies acetone, acetoacetate and 3-hydroxybutyrate were increased after bariatric surgery. Furthermore, evidence of changes to the Krebs cycle was seen, with citrate increasing and pyruvate decreasing. In addition, in the RYGB and 1-year post surgery group, lactate decreased, consistent with the quantitative SCFA analysis. Lastly, in the 1-year subgroup analysis serum α glucose was decreased.

Serum

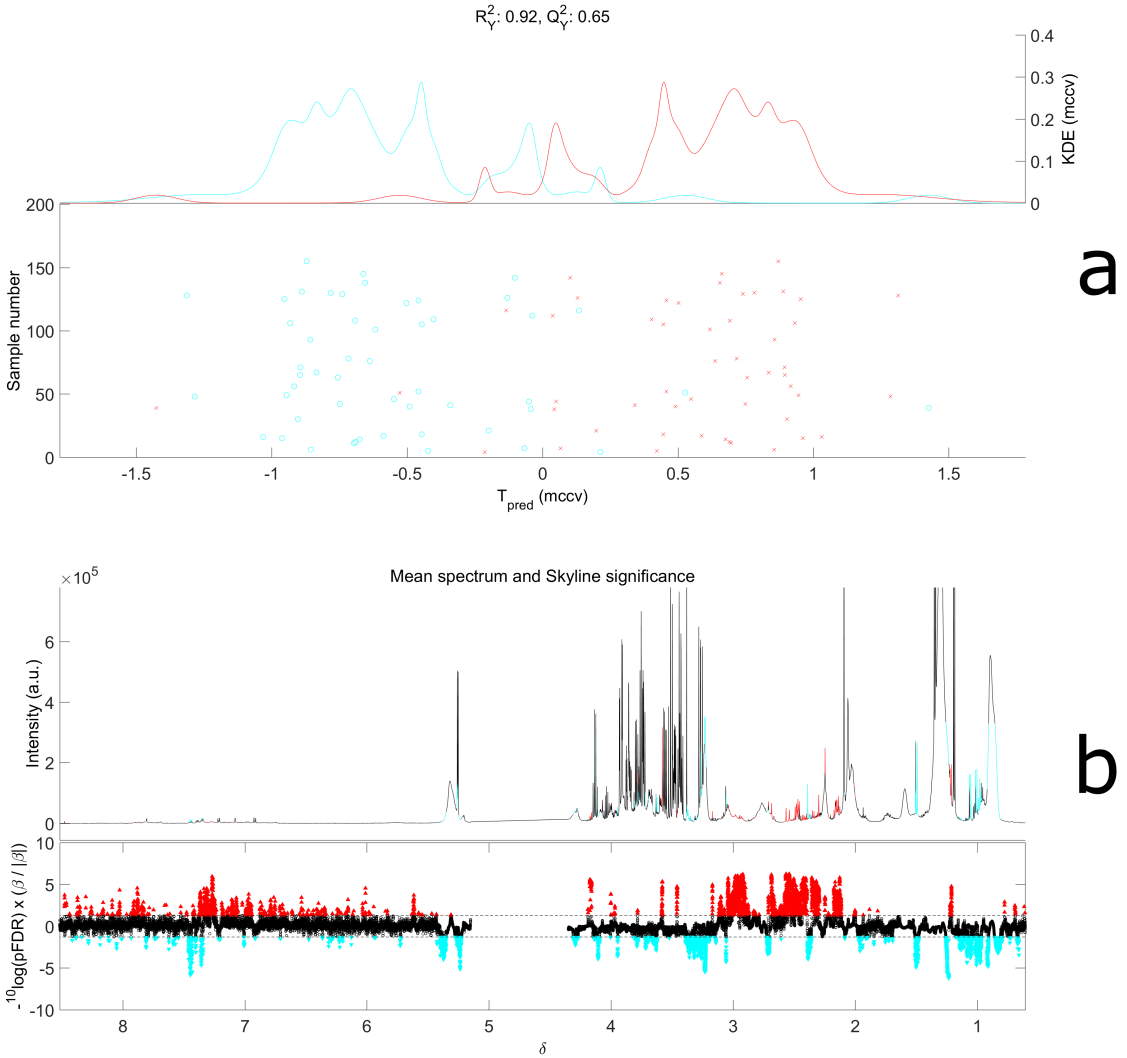


Figure 5.3-10 Serum ^{1}H-NMR paired MCCV-PLS-DA analysis. a) Paired MCCV-PLS-DA scores plots of ^{1}H-NMR analysis comparing participant serum samples pre and 3-months post bariatric surgery. Models are comprised of 1 predictive and 1 orthogonal component. Model score: R^2 0.92, Q^2 0.65. b) Mean spectrum and Manhattan plot. Manhattan plot showing -log_{10}(pFDR) x sign of the variable regression coefficient for each variable within the MCCV-PLS-DA model. Dotted lines illustrate the pFDR significance cut off level (0.01) on the log_{10} scale. Spectra considered significant are highlighted in the Manhattan plot and mean spectrum. Red spectra are significantly increased after surgery, blue spectra are significantly decreased.

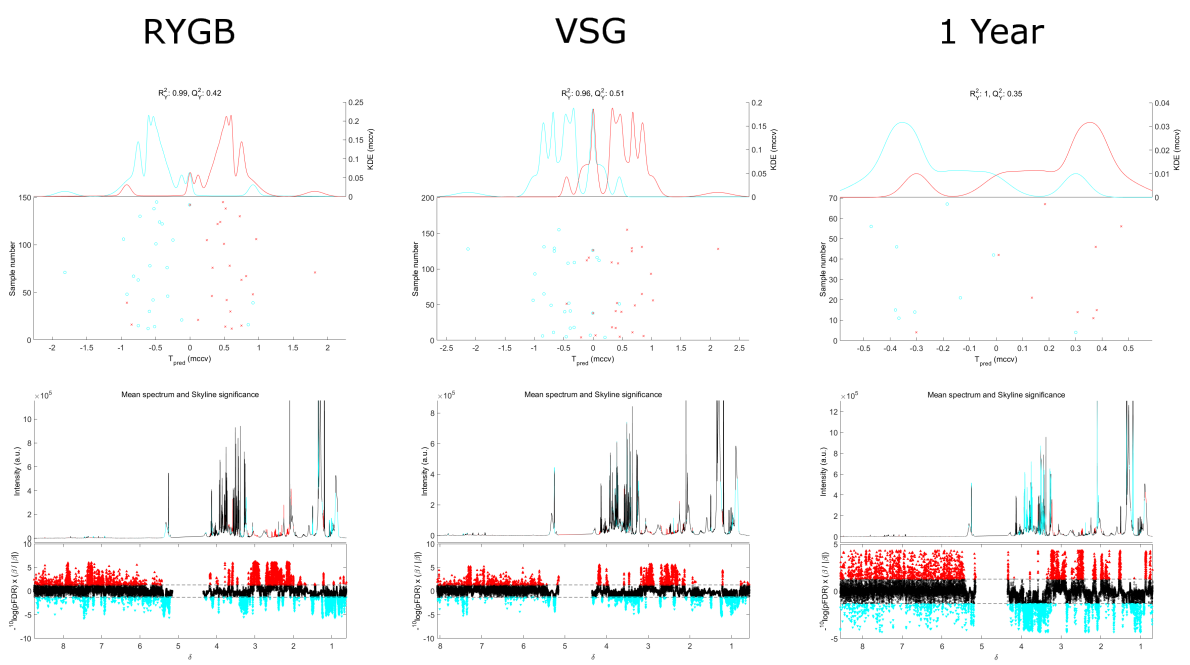


Figure 5.3-11 Serum ^{1}H-NMR paired MCCV-PLS-DA subgroup analysis. a) Paired MCCV-PLS-DA scores plots of ^{1}H-NMR analysis comparing participant serum samples pre and 3-month post RYGB or VSG surgery and 1-year post bariatric surgery. Models are comprised of 1 predictive and 1 orthogonal component. Model scores: i) RYGB 3 months R^2 0.99, Q^2 0.42, ii) VSG 3 months R^2 0.96, Q^2 0.51, iii) 1 Year R^2 1.00, Q^2 0.35. b) Mean spectrum and Manhattan plots. Manhattan plots show -log_{10}(pFDR) x sign of the variable regression coefficient for each variable within the MCCV-PLS-DA model. Dotted lines illustrate the pFDR significance cut off level (0.01) on the log_{10} scale. Spectra considered significant are highlighted in the Manhattan plot and mean spectrum. Red spectra are significantly increased after surgery, blue spectra are significantly decreased.

Serum			
Metabolite	**^{1}H chemical shift δ (multiplicity[a])**	**Association**	**Model**
3-Hydroxybutyrate	4.17 (m), 2.32 (m), 2.42 (m), 1.22 (d)	↑	All
Glycine	3.58 (s)	↑	All
Citrate	2.56 (ABx), 2.70 (ABx)	↑	All
Dimethylglycine	2.93 (s)	↑	All
Glutamine	2.15 (m), 2.47 (m), 3.77 (t)*	↑	All
Formate	8.47 (s)	↑	All
Unknown A	7.88 (d)	↑	All
Acetoacetate	3.46 (s), 2.30 (s)	↑	All
Acetone	2.25 (s)	↑	All
Unknown B	3.17 (s) no stocsy/storm	↑	All
Histidine	7.08 (s), 7.80 (s)	↑	1Yr only
HDL	0.86 (m)	↑	1Yr only
Glycerophosphocholine / phosphocholine / choline	3.23 (s broad)	↑	1Yr only
Phenylalanine	7.35 (m), 7.39 (m), 7.45 (m), 4.00 (m)	↓	All
Glycerol from lipid	5.22	↓	All
Alanine	1.5 (d), 3.79 (q)*	↓	All
Lysine	[1.48 (m), 1.73 (m), 1.91 (m), 3.03 (t), 3.76 (t)]	↓	All
VLDL/LDL	0.89 (t), 1.29 (m), 1.59 (m)	↓	All

HDL	0.86 (m)	↓	3m / RYGB / VSG
Valine	1.01 (d), 1.06 (d), 2.28 (m), 3.63 (d)	↓	All
Isoleucine	0.96 (t), 1.03 (d), 1.48 (m), 1.26 (m)*, 1.98 (m)*, 3.68 (d)*	↓	All
Leucine	0.98 (t), 1.71 (m), 3.73 (t)*	↓	All
Proline	2.01 (m)*, 2.07 (m)*, 2.37 (m), 3.36 (m), 3.43 (m)*, 4.13 (dd)	↓	All
Pyruvate	2.39 (s) Storm – lactate	↓	All
Creatine	3.06 (s), 3.95 (s)	↓	All
Glycerophosphocholine / phosphocholine / choline	3.23 (s broad)	↓	3m / RYGB / VSG
Lactate	4.13 (q)	↓	RYGB + 1Yr only
Tyrosine	3.06 (Abx), 3.16 (Abx)*, 3.94 (Abx)*, 6.92 (d), 7.21 (d)	↓	RYGB only
α Glucose	5.25 (d) + 3.23 (dd), 3.40 (m), 3.46 (m), 3.52 (dd), 3.73 (m), 3.82 (m), 3.88 (dd)	↓	1Yr only
Glycoproteins	2.09 (s)	↓	1Yr only

Table 5.3-13 Serum metabolites discriminating between classes. Table shows serum metabolites increasing or decreasing after bariatric surgery in individual or all MCCV-PLS-DA models as indicated. [o]Multiplicity key is as follows: s=singlet, d=doublet, t=triplet, q=quartet, dd=doublet of doublets, m=multiplet. [1]H shifts marked by an asterisk (*) were not confirmed experimentally due to the absence of unambiguous resonance values and are taken from the Human Metabolome Database (HMDB).

5.3.3.4.2.2 Urine ^{1}H-NMR analysis

MCCV-PLS-DA models of longitudinally paired urine samples analysed by ^{1}H-NMR found good separation between pre and post-surgery time points in overall and subgroup analyses. The resulting models were as follows: i) All 3months (n=32), R^2 0.97, Q^2 0.77 (see Figure 5.3-12); ii) RYGB (n=15), R^2 0.99, Q^2 0.79, iii) VSG 3 months (n=16), R^2 0.99, Q^2 0.58; iv) 1 Year (n=9), R^2 0.99, Q^2 0.75 (see Figure 5.3-13).

The significant urinary metabolite changes after bariatric surgery derived from the loadings plot included: increases in a number of microbially derived metabolites such as PAG, 4PY, 4-cresol sulfate, hippurate and TMAO. Ethanol, from consumption or potentially microbially derived, was also increased. Decreased urinary excretion of the amino acids lysine, alanine, leucine and valine occurred. As well as decreased 3-hydroxyisovaleric acid excretion, a leucine degradation by product that has been reported to increase in biotin deficiency and smokers[441] and decreased excretion of the common analgaesics paracetamol and ibuprofen after surgery. Urinary lactate was reduced after bariatric surgery in all sub group analyses and urinary α and β Glucose reduced by 1-year following surgery.

Urine

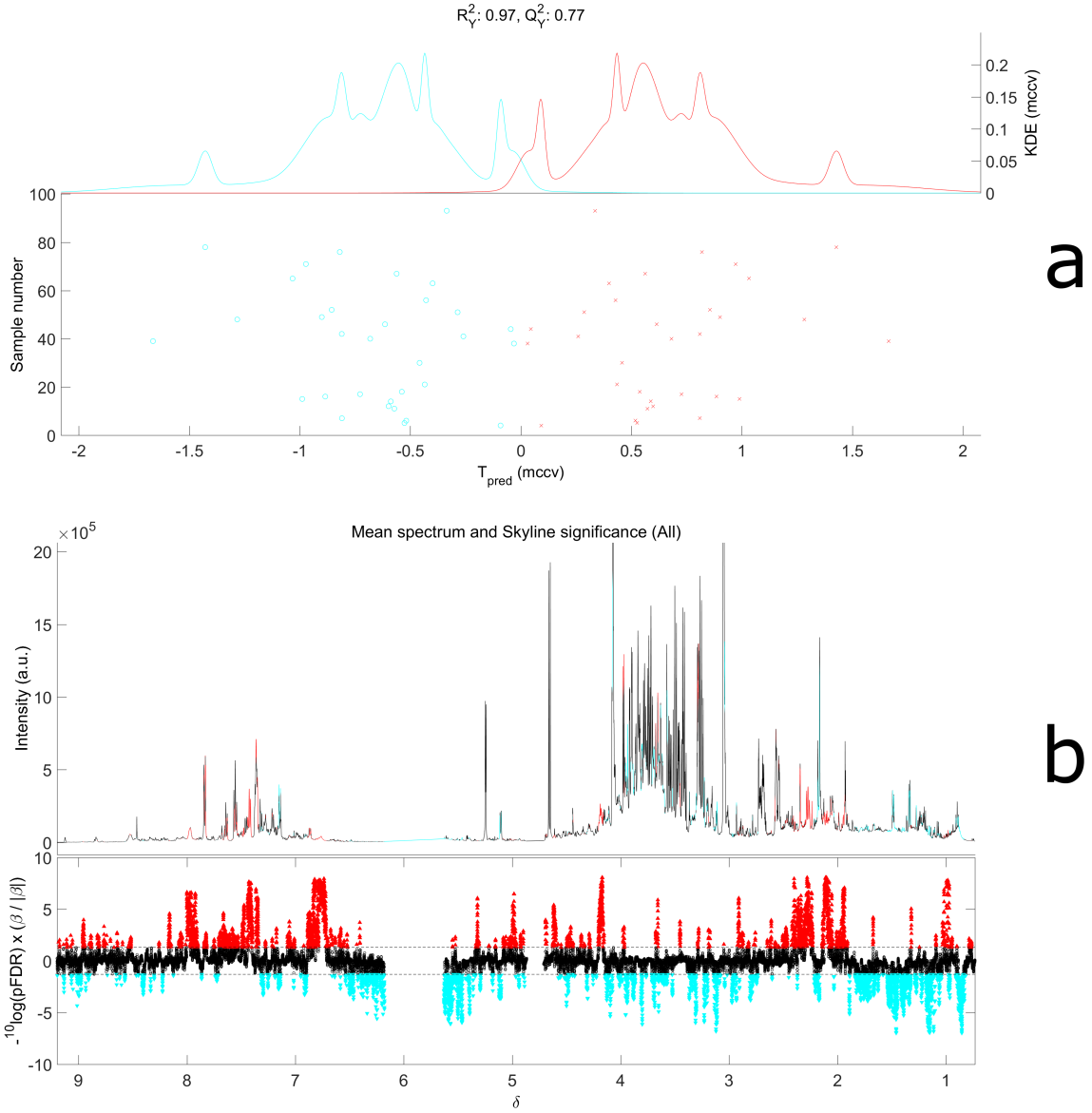


Figure 5.3-12 Urine ^{1}H-NMR paired MCCV-PLS-DA analysis. a) Paired MCCV-PLS-DA scores plots of ^{1}H-NMR analysis comparing participant 24-hour urine samples pre and 3-months post bariatric surgery. Models are comprised of 1 predictive and 1 orthogonal component. Model score: R^2 0.97, Q^2 0.77. b) Mean spectrum and Manhattan plot. Manhattan plot showing $-\log_{10}$(pFDR) x sign of the variable regression coefficient for each variable within the MCCV-PLS-DA model. Dotted lines illustrate the pFDR significance cut off level (0.01) on the $\log_{10}$ scale. Spectra considered significant are highlighted in the Manhattan plot and mean spectrum. Red spectra are significantly increased after surgery, blue spectra are significantly decreased.

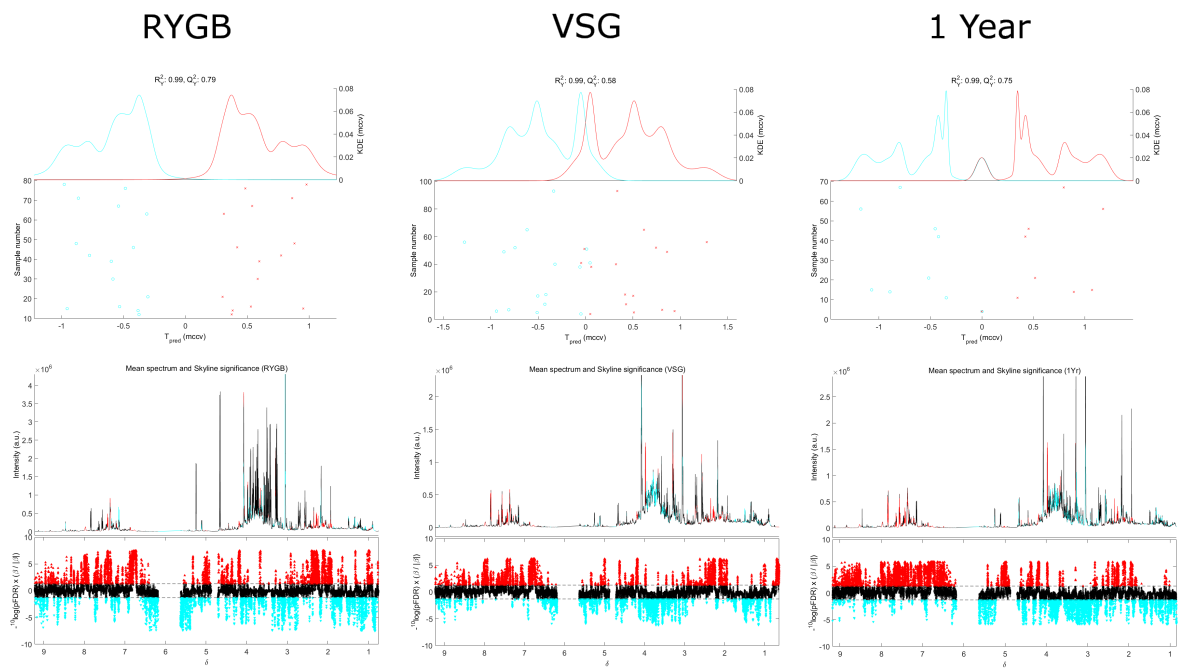


Figure 5.3-13 Urine ^{1}H-NMR paired MCCV-PLS-DA subgroup analysis. a) Paired MCCV-PLS-DA scores plots of ^{1}H-NMR analysis comparing participant 24-hour urine samples pre and 3-month post RYGB or VSG surgery and 1-year post bariatric surgery. Models are comprised of 1 predictive and 1 orthogonal component. Model scores: i) RYGB 3 months R^2 0.99, Q^2 0.79, ii) VSG 3 months R^2 0.99, Q^2 0.58, iii) 1 Year R^2 0.99, Q^2 0.75. b) Mean spectrum and Manhattan plots. Manhattan plots show -log_{10}(pFDR) x sign of the variable regression coefficient for each variable within the MCCV-PLS-DA model. Dotted lines illustrate the pFDR significance cut off level (0.01) on the log_{10} scale. Spectra considered significant are highlighted in the Manhattan plot and mean spectrum. Red spectra are significantly increased after surgery, blue spectra are significantly decreased.

Urine			
Metabolite	**^{1}H chemical shift δ (multiplicity[a])**	**Association**	**Model**
Phenylacetylglutamine (PAG)	2.11 (m), 2.27 (m), 3.67 (m), 4.19 (m), 7.36 (t), 7.43 (t)	↑	All
Unknown C	6.76 (m) 7.97 (d) (STORM – PAG, Glutamine related)	↑	All
Hippurate	3.97 (d), 7.55 (t), 7.64 (t), 7.84 (d), 8.52 (m)	↑	All
4 Hydroxyphenylacetate	6.86 (m), 7.17 (m), 3.45 (s)	↑	All
Ethanol	1.19 (t), 3.66 (q)	↑	All
TMAO	3.28 (s)	↑	All
Citrate	2.55~ (d), 2.69~ (d)	↑	All
4-cresol sulfate	2.34 (s), 7.21 (d), 7.28 (d)	↑	All
Unknown D	1.32 (s)	↑	All
2-aminobutyrate[ϕ]	0.98 (t), 1.90 (m)*, 3.72 (t)*	↑	All
Butanone[ϕ]	1.02(t)	↑	All
N1-methyl-4-pyridone 5 carboxamide (4PY)	8.55 (d)	↑	RYGB only
Levoglucosan	5.46 (s/t)	↓	All
Acetaminophen (paracetamol) glucuronide	2.16 (s), 3.63 (m), 5.11(d), 7.14 (d), 7.36 (d)	↓	All

Acetaminophen (paracetamol) sulfate	2.17 (s), 7.31 (d), 7.45 (d)	↓	All
Creatine	3.04 (s), 3.94 (s)	↓	All
Lysine	1.48 (m), 1.73 (m), 1.91 (m), 3.03 (t), 3.76 (t)	↓	All
Alanine	1.49 (d), 3.79 (q)*	↓	All
Unknown E	1.52 (m)	↓	All
Ibuprofen$^{\phi}$	1.39 (d)	↓	All
Ibuprofen Glucuronide$^{\phi}$	1.15 (d) (STORM 1.66 (s), 5.50 (m))	↓	All
Isobutyrate	1.11 (d), 3.02 (m)*	↓	All
Lactate	1.34 (d), 4.22 (q)	↓	All
3 hydroxyisovaleric acid	1.27 (s), 2.37 (s)	↓	All
Leucine	0.97 (t), 1.71 (m)*, 3.73 (t)*	↓	All
Valine	1.01 (d), 1.06 (d), 2.28 (m)*, 3.63 (d)	↓	All
Creatinine	3.05 (s), 4.06 (s)	↓	RYGB + 1Yr only
Formate	8.46 (s)	↓	RYGB only
α Glucose	5.25 (d) + 3.23 (dd), 3.40 (m), 3.46 (m), 3.52 (dd), 3.73 (m), 3.82 (m), 3.88 (dd)	↓	1Yr only
β Glucose	4.66 (d) + 3.23 (dd), 3.40 (m), 3.46 (m), 3.52 (dd), 3.73 (m), 3.82 (m), 3.88 (dd)	↓	1Yr only

Table 5.3-14 Urinary metabolites discriminating between classes. Table shows urinary metabolites increasing or decreasing after bariatric surgery in individual or all MCCV-PLS-DA models as indicated. [a]Multiplicity key is as follows: s=singlet, d=doublet, t=triplet, q=quartet, dd=doublet of doublets, m=multiplet. [1]H shifts marked by an asterisk (*) were not confirmed experimentally due to the absence of unambiguous resonance values and are taken from the Human Metabolome Database (HMDB). $^{\phi}$= tentative assignment

5.3.3.4.2.3 Faecal Water ^{1}H-NMR analysis

MCCV-PLS-DA models of longitudinally paired faecal water samples analysed by ^{1}H-NMR did not show as strong separation between pre and post-surgery time points as the serum and urine models. However, there was some separation seen in subgroup analyses. The resulting models were as follows: i) All 3months (n=25), R^2 0.83, Q^2 0.03 (see Figure 5.3-14); ii) RYGB (n=11), R^2 0.95, Q^2 0.30, iii) VSG 3 months (n=14), R^2 0.96, Q^2 0.15; iv) 1 Year (n=5), R^2 1.00, Q^2 0.62 (see Figure 5.3-15).

The significant faecal water metabolite changes after bariatric surgery derived from the loadings plot included: increased levels of the essential amino acids phenylalanine and lysine as well as increases in the amino acid metabolites: 1) tyramine, produced from the decarboxylation of tyrosine, 2) acetyllysine, produced by the acetylation of lysine and 3) putrescine, produced from the microbial breakdown of arginine. In keeping with the quantitative SCFA analysis, acetate was significantly reduced in all groups, whereas butyrate

was decreased after VSG but showed a trend towards increasing after RYGB. Similarly, isovalerate and valerate decreased after VSG, but following RYGB isovalerate and 2-methylbutyrate increased. Similar to serum and urine, lactate was decreased in faecal water after bariatric surgery (all subgroups). Methanol, formate and 3-hydroxyphenylpropionate levels, products of microbial metabolism, reduce. While trimethylamine, resulting from microbial metabolism of choline, is increased after RYGB surgery. Lastly, α Glucose reduces after surgery in all sub-group analyses.

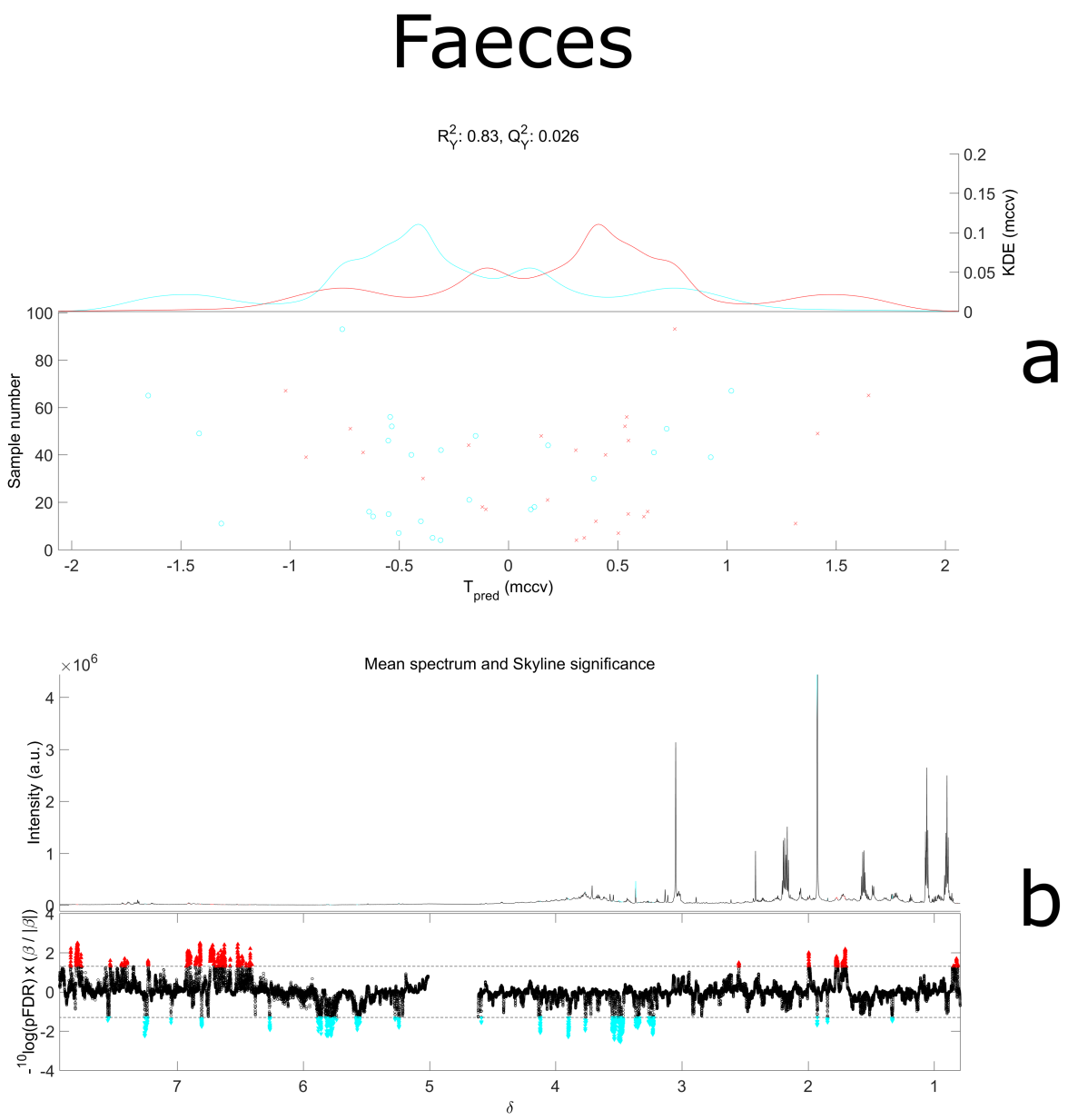


Figure 5.3-14 Faecal ^{1}H-NMR paired MCCV-PLS-DA analysis. a) Paired MCCV-PLS-DA scores plots of ^{1}H-NMR analysis comparing participant faecal samples pre and 3-months post bariatric surgery. Models are comprised of 1 predictive and 1 orthogonal component. Model score: R^2 0.83, Q^2 0.03. b) Mean spectrum and Manhattan plot. Manhattan plot showing -

log_{10}(pFDR) x sign of the variable regression coefficient for each variable within the MCCV-PLS-DA model. Dotted lines illustrate the pFDR significance cut off level (0.01) on the log_{10} scale. Spectra considered significant are highlighted in the Manhattan plot and mean spectrum. Red spectra are significantly increased after surgery, blue spectra are significantly decreased.

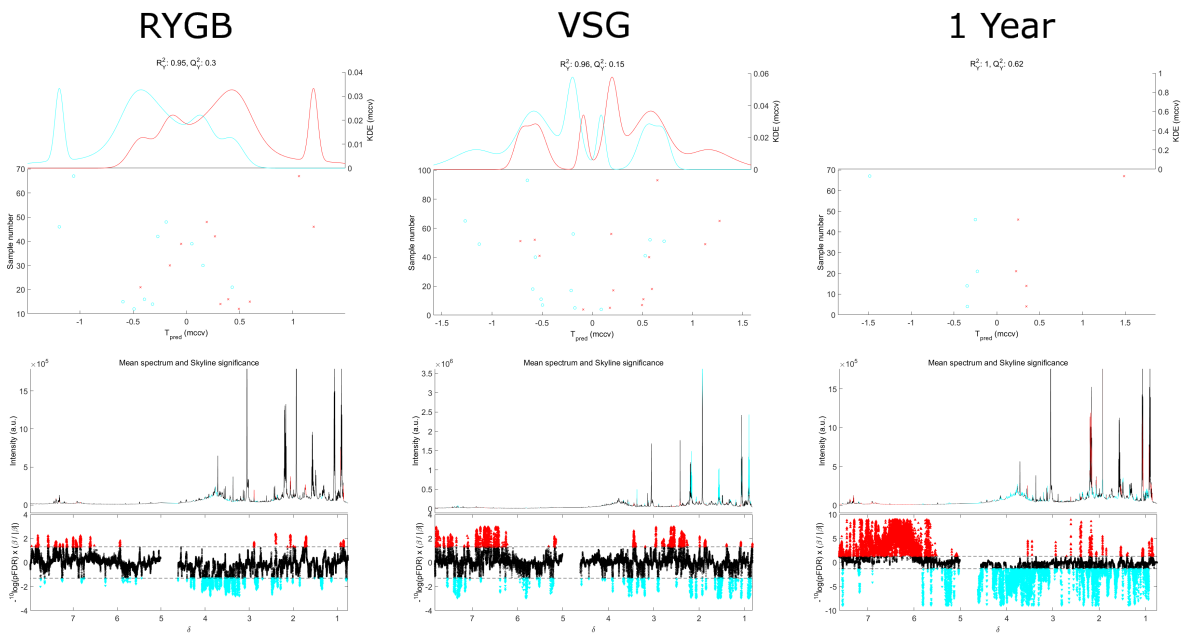


Figure 5.3-15 Faecal ^{1}H-NMR paired MCCV-PLS-DA subgroup analysis. a) Paired MCCV-PLS-DA scores plots of ^{1}H-NMR analysis comparing participant faecal samples pre and 3-month post RYGB or VSG surgery and 1-year post bariatric surgery. Models are comprised of 1 predictive and 1 orthogonal component. Model scores: i) RYGB 3 months R^2 0.95, Q^2 0.30, ii) VSG 3 months R^2 0.96, Q^2 0.15, iii) 1 Year R^2 1.0, Q^2 0.62. b) Mean spectrum and Manhattan plots. Manhattan plots show -log_{10}(pFDR) x sign of the variable regression coefficient for each variable within the MCCV-PLS-DA model. Dotted lines illustrate the pFDR significance cut off level (0.01) on the log_{10} scale. Spectra considered significant are highlighted in the Manhattan plot and mean spectrum. Red spectra are significantly increased after surgery, blue spectra are significantly decreased.

Faeces			
Metabolite	**^{1}H chemical shift δ (multiplicity)**	**Association**	**Model**
Phenylalanine	3.20 (dd), 3.29 (dd), 3.99 (dd), 7.34 (d), 7.38 (m), 7.43 (m)	↑	All
Tyramine	6.92 (d), 7.22 (d), 2.93 (t), 3.24 (t)	↑	All
3,4 Dihydroxyphenylacetate	6.73 (d), 6.82 (s), 6.87 (d), 3.4 (s)	↑	All
Lysine	1.46 (m), 1.72 (m), 3.03 (t), 3.76 (t)*	↑	All
Putrescine	1.77 (m), 3.06 (m)	↑	All
n-acetyllysine	2.00 (s), 1.41 (m), 1.56 (m), 1.87 (m), 3.19 (q), 3.74 (t)*	↑	All
Isovalerate	0.91 (d), 1.96 (m), 2.06 (d)	↑	RYGB only
2-methylbutyrate	0.86 (t), 1.05 (d), 1.39 (m), 1.5 (m), 2.21 (m)	↑	RYGB only
Trimethylamine	2.89 (s)	↑	RYGB only
Lactate	1.33 (d), 4.12 (q)	↓	All
Nicotinate	8.95 (d), 8.62 (dd), 8.26 (dt), 7.53 (dd)	↓	All
Formate	8.46 (s)	↓	All
Hypoxanthine	8.21 (d)	↓	All

Uracil	5.81 (d), 7.54 (d)	↓	All
Unknown A	8.09 (t)	↓	All
3-hydroxyphenylpropionate	2.47 (t), 2.84 (t), 6.76 (m), 6.81 (t), 6.87 (m), 7.25 (t)	↓	All
α Glucose	5.24 (d) + 3.50 (t)	↓	All
Acetate	1.93 (s)	↓	All
Methanol	3.37 (s) – STORM ethanol + acetate	↓	All
Butyrate	0.90 (t), 1.56 (m), 2.16 (t)	↓	VSG only
Valerate	0.89 (t), 1.30 (m), 1.54 (m), 2.18 (t)	↓	VSG only
Isovalerate	0.91 (d), 1.96 (m), 2.06 (d)	↓	VSG only

Table 5.3-15 Faecal metabolites discriminating between classes. Table shows faecal metabolites increasing or decreasing after bariatric surgery in individual or all MCCV-PLS-DA models as indicated. [a]Multiplicity key is as follows: s=singlet, d=doublet, t=triplet, q=quartet, dd=doublet of doublets, m=multiplet. [1]H shifts marked by an asterisk (*) were not confirmed experimentally due to the absence of unambiguous resonance values and are taken from the Human Metabolome Database (HMDB).

5.3.4 Gut microbiome changes after bariatric surgery

Taxonomic analysis of the distal colon gut microbiota reveals a profound change in microbial composition after bariatric surgery (see Figure 5.3-16).

Subgroup analyses reveals a major change after RYGB, but much more subtle changes after VSG. 3 months after RYGB participants had higher faecal levels of the genera; *Veillonella*, *Gemella*, *Granulicatella*, *Enterococcus*, *Stretococcus* and *Clostridium (Firmicutes)*, *Fusobacterium (Fusobacteria)*, *Klebsiella* and *Escherichia (Proteobacteria)*, *Actinomyces* and *Anaerotruncus (Actinobacteria)* and *Prevotella (Bacterodetes)* and decreased levels of; *Holdemania*, *Eubacterium*, *Faecalibacterium*, *Subdoligranulum*, *Ruminococcus*, *Dorea* and *Anaerostipes (Firmicutes)*, *Burkholderiales (Proteobacteria)*, *Bifidobacterium* and *Collinsella (Actinobacteria)* (see Figure 5.3-17).

3 months after VSG participants had increases in a select number of species within the genera; *Streptococcus*, *Eubacterium* and *Anaerotruncus (Firmicutes)* and *Escherichia (Proteobacteria)* and decreased species within; *Faecalibacterium*, *Dorea*, *Anaerostipes, Roseburia* and *Coprococcus (Firmicutes)* (see Figure 5.3-18).

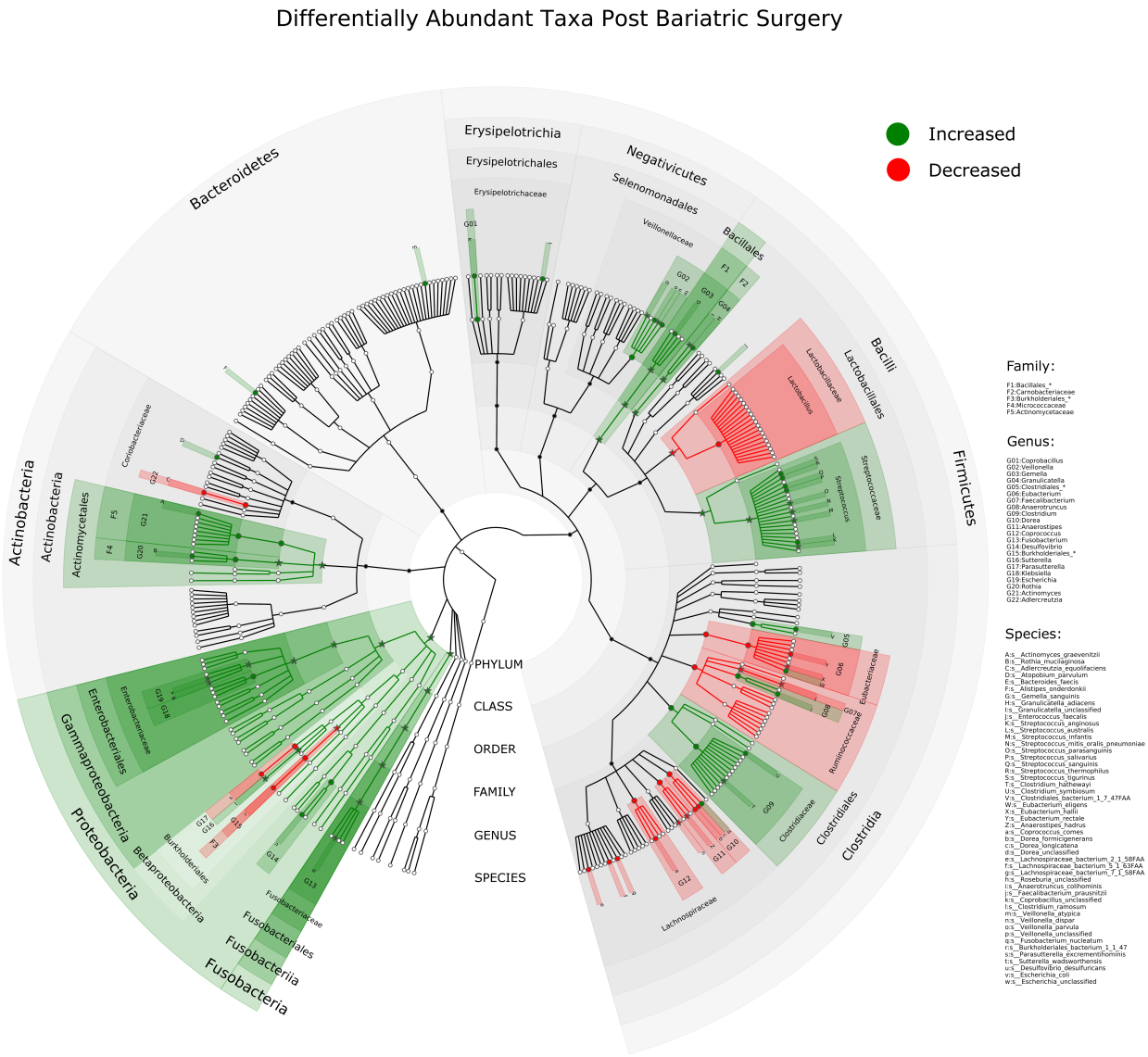


Figure 5.3-16 Phylogenetic tree of differentially abundant taxa post bariatric surgery. Taxa significantly increased are shown in green, taxa significantly decreased are shown in red. Changes that remain significant after Benjamini-Hochberg multiple testing corrections are denoted with a star (*).

Differentially Abundant Taxa Post Roux-en-Y Gastric Bypass

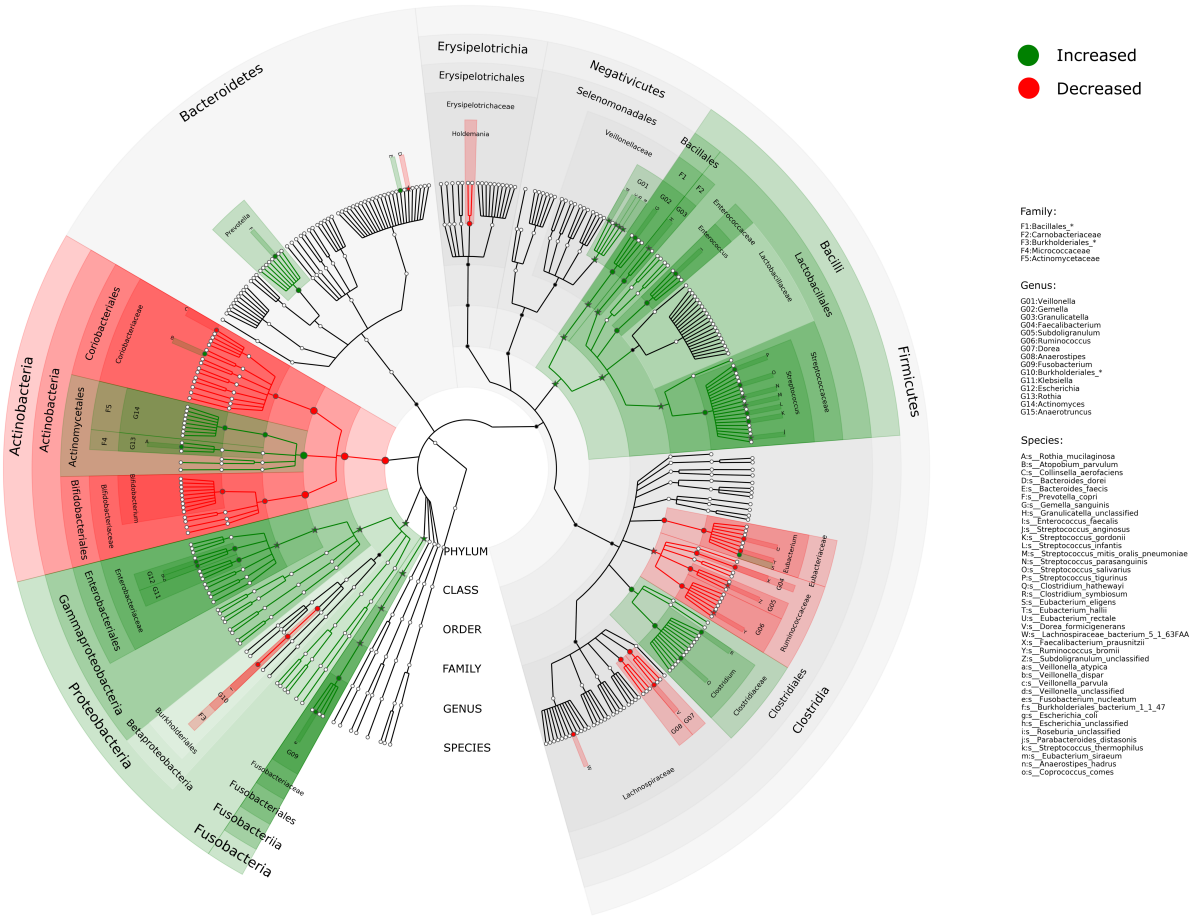


Figure 5.3-17 Phylogenetic tree of differentially abundant taxa post RYGB surgery. Taxa significantly increased are shown in green, taxa significantly decreased are shown in red. Changes that remain significant after Benjamini-Hochberg multiple testing corrections are denoted with a star (*).

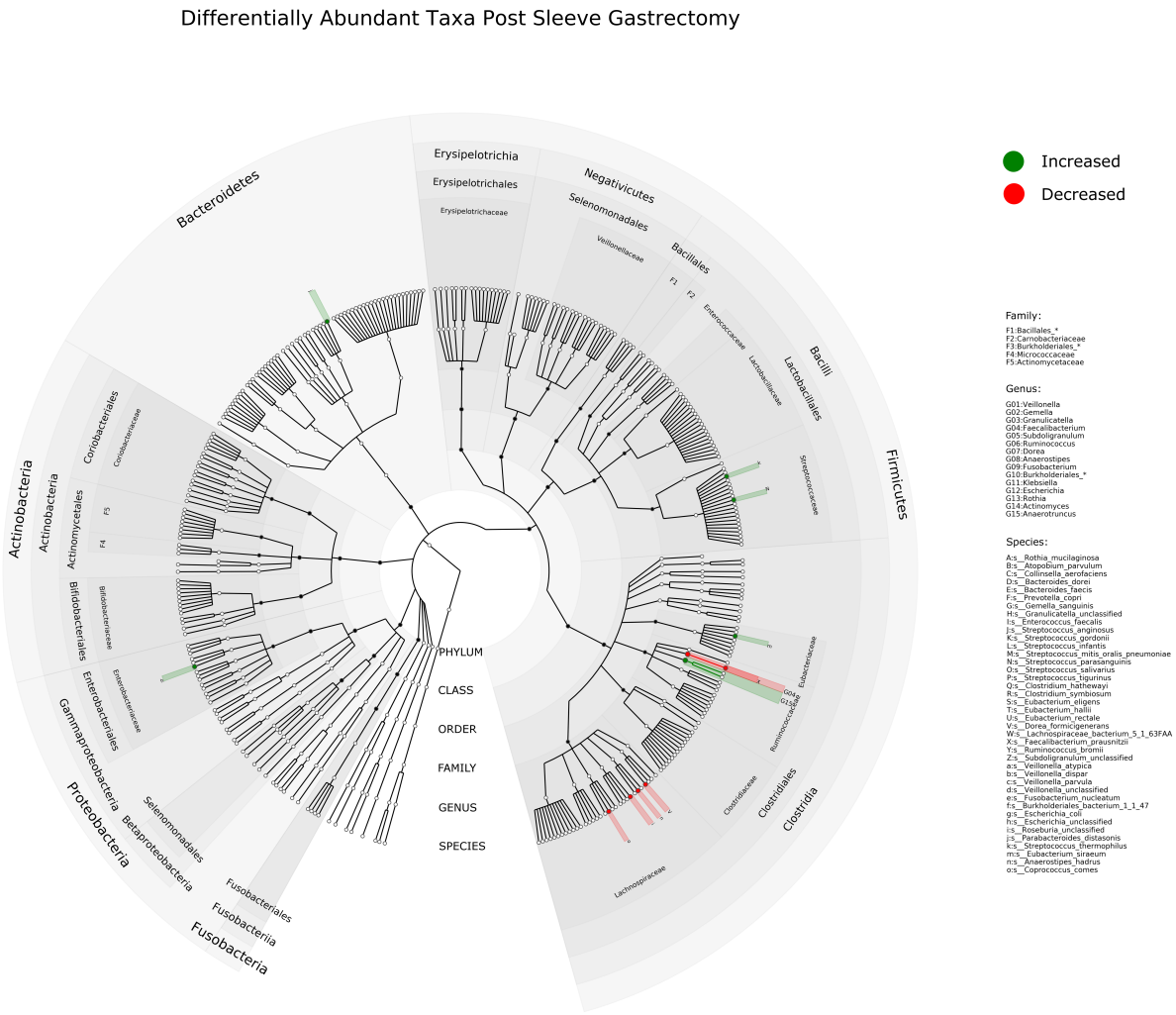


Figure 5.3-18 Phylogenetic tree of differentially abundant taxa post VSG surgery. Taxa significantly increased are shown in green, taxa significantly decreased are shown in red. Changes that remain significant after Benjamini-Hochberg multiple testing corrections are denoted with a star (*).

5.3.5 Gut Microbiome – Host Metabonome Associations

Gut microbiome – host metabonome association analysis revealed a number of significant correlations between bacterial species and bile acid, SCFA, amino acid and acylcarnitine levels. Significant associations (pFDR<0.05) are shown in Figures 9.3-19-22.

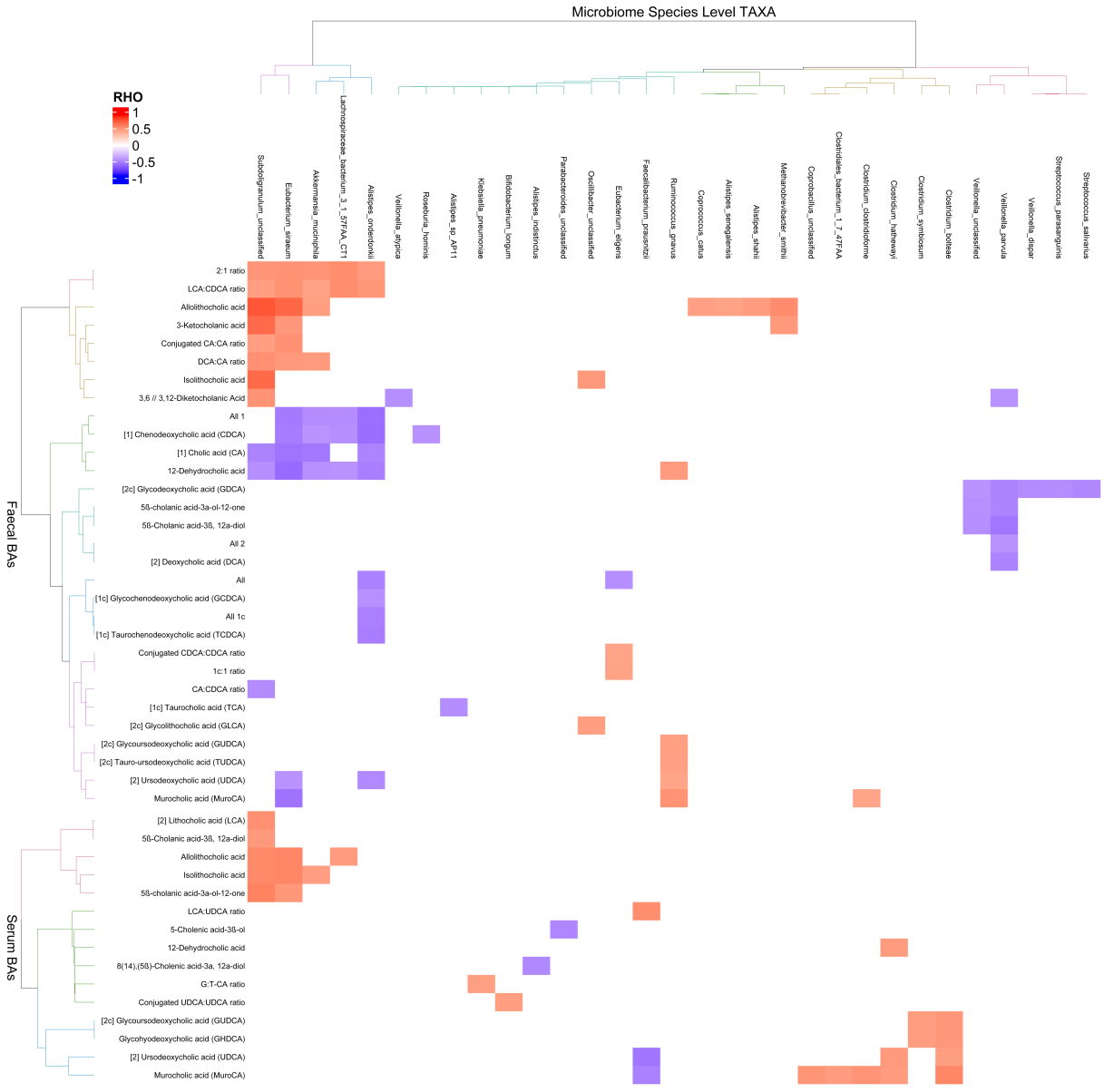


Figure 5.3-19 Gut Species – Bile acid correlations. Significant Spearman's correlations (pFDR <0.01) between microbial species Vs faecal and urinary bile acid datasets are shown, shaded according to strength of correlation coefficient (Rho). Correlations are clustered according to Euclidean distances.

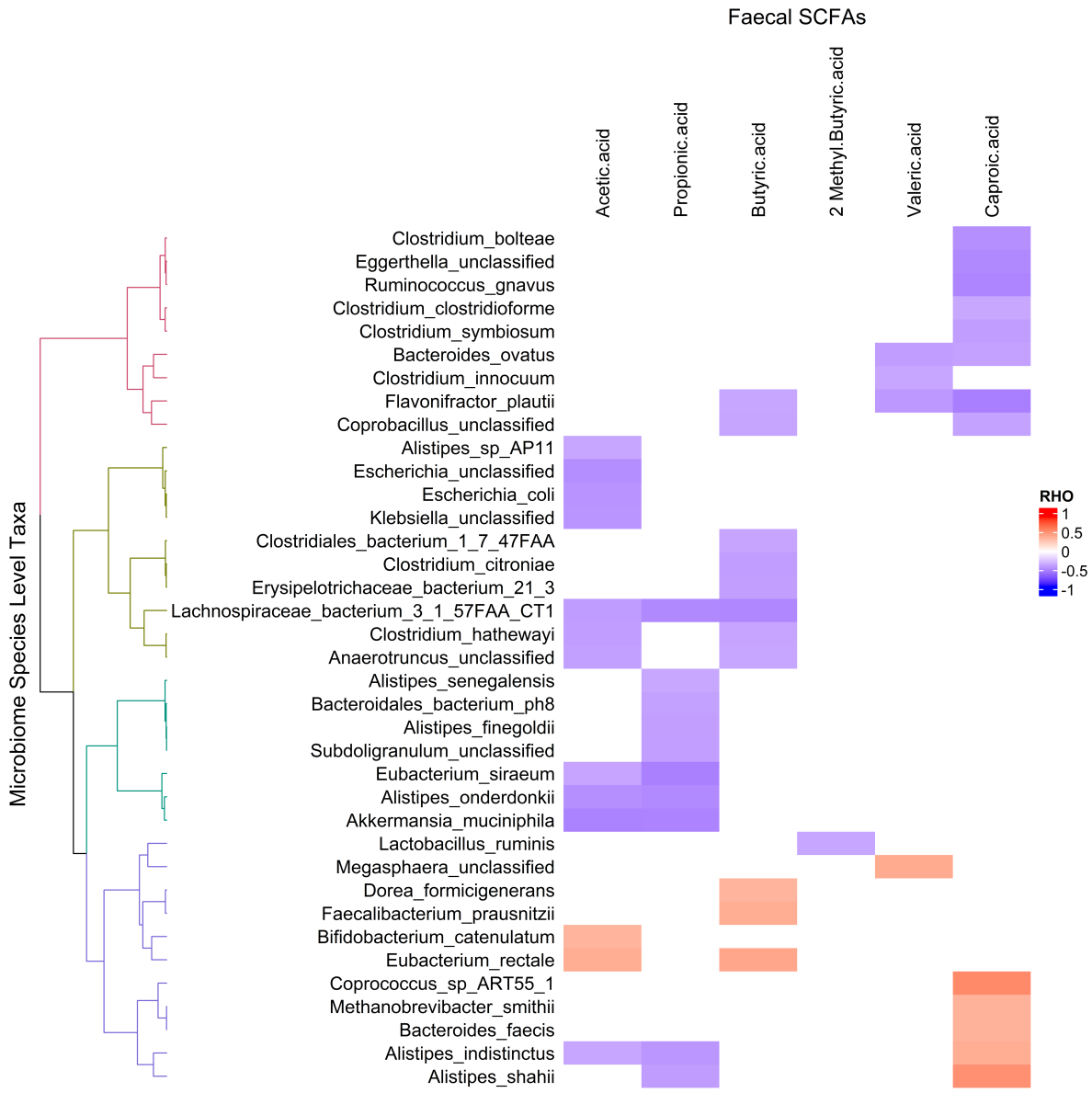


Figure 5.3-20 Gut Species – Faecal SCFA correlations. Significant Spearman's correlations (pFDR <0.01) between microbial species Vs faecal SCFA datasets are shown, shaded according to strength of correlation coefficient (Rho). Correlations are clustered according to Euclidean distances.

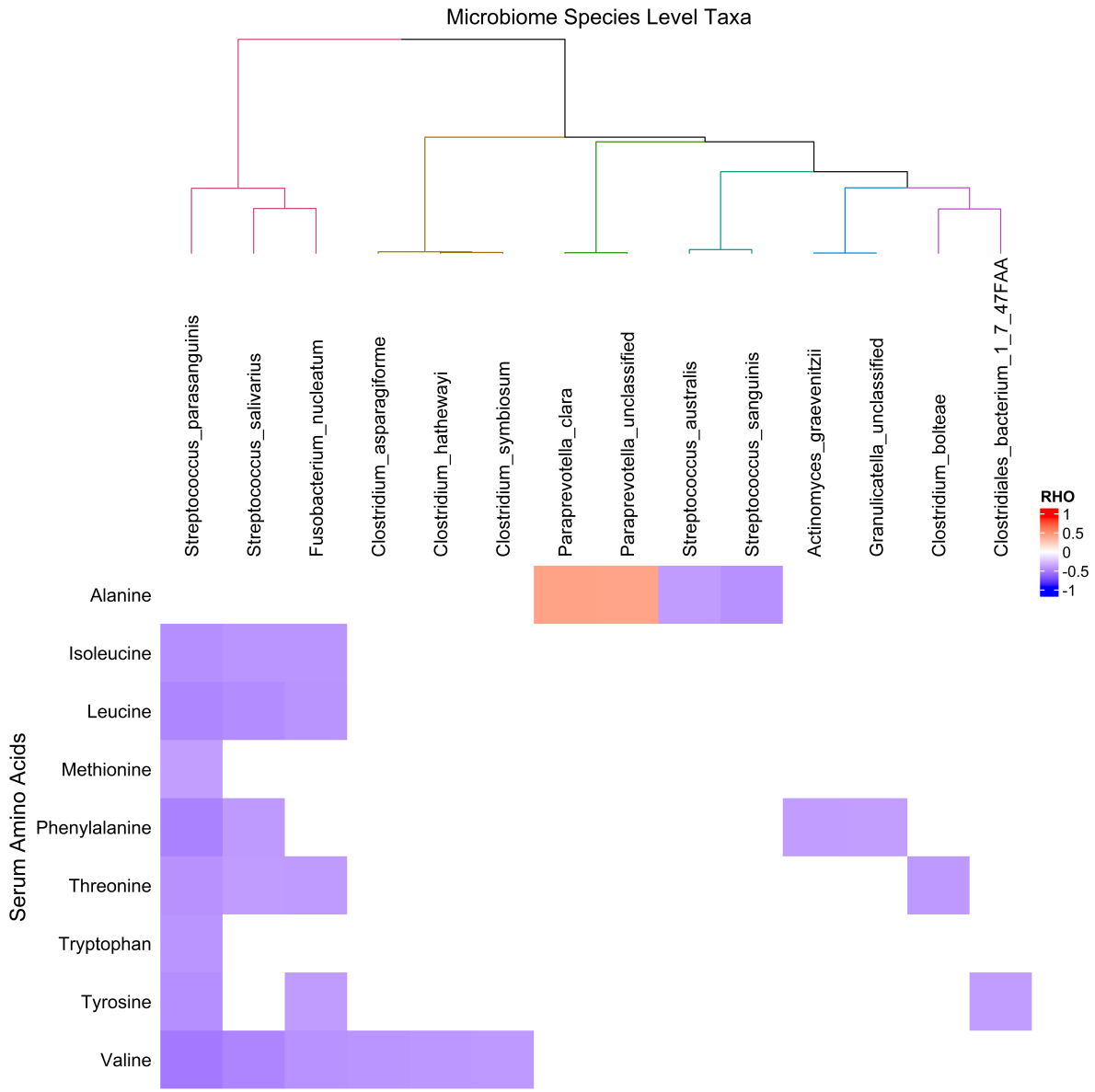


Figure 5.3-21 Gut Species – Serum Amino Acid correlations. Significant Spearman's correlations (pFDR <0.01) between microbial species Vs serum amino acid datasets are shown, shaded according to strength of correlation coefficient (Rho). Correlations are clustered according to Euclidean distances.

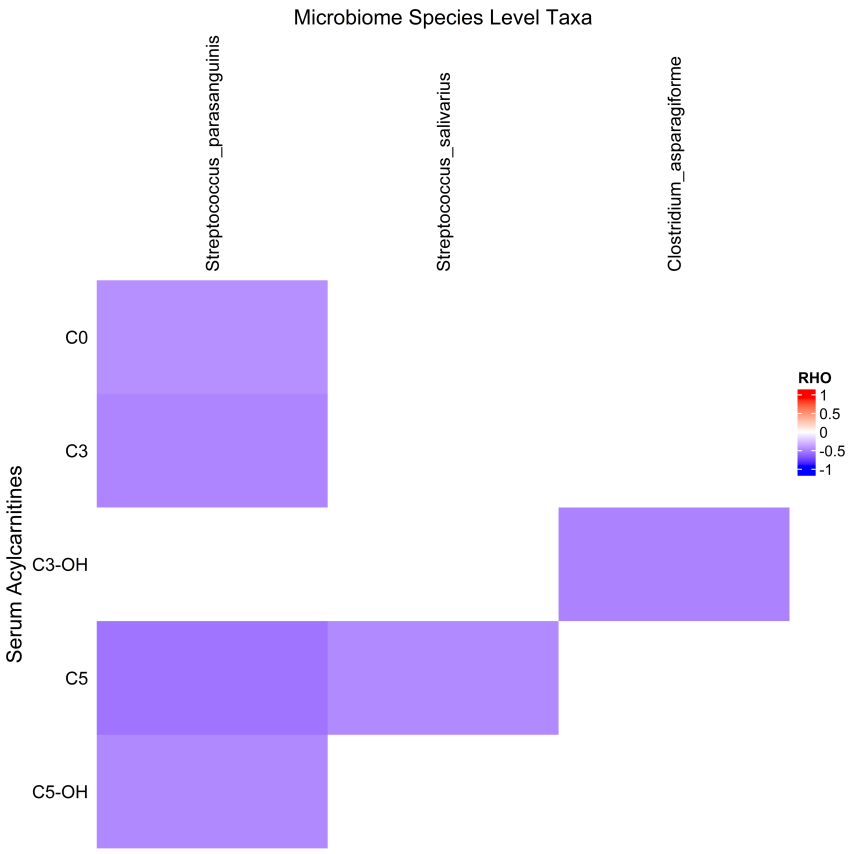


Figure 5.3-22 Gut Species – Serum Acylcarnitine correlations. Significant Spearman's correlations (pFDR <0.01) between microbial species Vs serum acylcarnitine datasets are shown, shaded according to strength of correlation coefficient (Rho). Correlations are clustered according to Euclidean distances.

5.4 Discussion

5.4.1 Clinical findings after bariatric surgery

5.4.1.1 Weight and Diabetic control

The large reductions in weight after RYGB and VSG are consistent with the well characterised weight-loss effects of both procedures[442, 443]. Further, the impressive improvement in glycaemic control, measured by HbA1c, seen 3-months after both RYGB and VSG is consistent with a number of randomised controlled trials and large cohort studies indicating that bariatric surgery is more effective than intensive medical therapy alone in decreasing and, in some cases, resolving hyperglycaemia[75-79].

5.4.1.2 Dietary behaviour following bariatric surgery

Large reductions in the intake of all food groups, in particular carbohydrate, fat, sugar and fibre are noted after both RYGB and VSG. In addition to the restrictive elements of both procedures through a reduction stomach size, bariatric procedures are known to reduce hunger and increase satiety[444]. This is in part due to due to early and exaggerated anorexigenic hormone responses[444]. In addition, patients have a lower brain-hedonic response to food[109]. Moreover, following bariatric surgery, patients are known to change their food preferences and these changes are dependent on the type of procedure[445, 446]. Whilst the restrictive nature of these procedures would be expected to cause a decrease in portion sizes, a change in food preferences suggests a change in the underlying physiological response to food. Changes include an increase in sensitivity to sweet and fatty taste stimuli and a decreased preference to sweet tasting stimuli, as well as increased smell acuity[445, 447]. This appears to be reflected here with an increase in dietary healthiness, measured using the AHEI-2010 score, after surgery. The AHEI-2010 score reflects a high intake of whole grains, polyunsaturated fatty acids, omega-3 fats and nuts and low intake of red or processed meats, sugary drinks and refined grains. Higher scores have been associated with a lower incidence of obesity, diabetes, cardiovascular disease, cancer and COPD as well as a reduced risk of cardiovascular, cancer and all-cause mortality[429, 448-451]. However, it should be noted that all self-reported dietary data is subject to misreporting, with under reporting of unhealthy food and over reporting of healthy foods[452-454]. Moreover, under-reporting is more common in

obese individuals and this is likely to be more pronounced following surgery due to patient perceptions that healthcare professionals will expect them to have improved their diet[454].

5.4.2 Biological interpretation of metabolic and gut microbiome changes after bariatric surgery

5.4.2.1 Gut microbiome

The microbial composition of the gut changes along its length. This is due to a gradient in a number of variable factors such as nutrient availability, oxygen levels, pH and antimicrobial activity including bile acid levels[455]. The changes to the gut bacteria seen after RYGB in this cohort represent a shift in the colonic bacteria towards those usually found in higher concentrations in the small bowel such as; *Clostridium*, *Streptococcus*, *Escherichia* and *Veillonella*[456-458]. In addition, a number of obligate anaerobes increase. This includes *Clostridium* and *Veillonella* as mentioned, as well as obligate anaerobes from the genera *Fusobacterium*, *Prevotella* and *Actinomyces*. Whereas fermentative bacteria usually found in high concentrations in the caecum and distal large bowel such as *Subdoligranulum, Faecalibacterium and Ruminococcus* (*Ruminococcaceae)* and *Lachnospiraceae* decreased after RYGB surgery in this cohort[458-461]. As expected, due to the fact that VSG maintains continuity of the GI tract and results in less changes to pH and bile flow, the microbial changes following VSG are more subtle. Nevertheless, there are increases in species from a number of similar genera, namely *Streptococcus*, *Eubacterium* and *Escherichia* and decreases within *Lachnospiraceae*. Initial studies investigating obesity and the gut microbiome found a higher *Firmicutes* / *Bacteroidetes* ratio in obese individuals[20, 22, 29]. A number of further studies have reported contrasting results, finding the opposite changes or no difference[30, 462]. Here, consistent with early reports, the *Firmicutes* / *Bacteroidetes* proportion decreases after VSG from 0.34 to 0.23, whereas after RYGB it remains constant measuring 0.36 pre and 0.35 post-surgery. Indeed, RYGB results in greater weight loss and would therefore be expected to results in a greater change to the *Firmicutes* / *Bacteroidetes* ratio. This supports the notion that the picture is much more complex than changes at a Phylum level as originally portrayed and changes at lower taxonomic levels may be of more relevance[463].

5.4.2.2 Bile Acids

Bile acid circulation appears to fundamentally change after bariatric surgery in both RYGB and VSG procedures. This is expected after RYGB where the bile flow anatomy is profoundly changed such that the bile enters the bowel much further downstream than the usual anatomical configuration. Here it is exposed to an altered environment including altered pH, gut microbiome and a reduced length of bowel for reabsorption. Changes after VSG are less expected, although consistent with previous literature reports[70, 118]. After VSG the removal of the greater curve of the stomach reduces its ability to produce acid, thus increasing gut pH and altering the gut microbiome with subsequent effects on BAs.

In this study there is an increased overall conversion of primary to secondary bile acids in the faeces and serum, with higher levels of secondary and conjugated secondary bile acids circulating in the serum. However, total levels of primary and secondary faecal bile acids decrease. This is likely to confer health benefits with increased bile acid signally via FXR and TGR5 receptors, due to the increased agonist potency of secondary bile acids versus primary, leading to increased satiety and insulin sensitivity, as described previously[71, 464]. Furthermore, lower levels of faecal bile acids seen here reduce concerns raised regarding the deleterious local effects of bile acid cytotoxicity on the gut mucosa[218-220].

Conversion of primary conjugated bile acids to secondary bile acids is performed by the gut bacteria and the changes seen in the bile acid profiles here are likely explained by the changes to the gut microbiome that result from these procedures. The initial step in bile acid biotransformation performed by bacteria containing the bile salt hydrolase (BSH) enzyme. This is found in a number of *Clostridium* species, increased in this cohort after RYGB. It has also been reported in *Bifidobacterium* (decreased) and *Lactobacillus* (no change)[66, 464]. A number of further biotransformations can then occur. The predominant transformations, 7α dehydroxylation of CA and CDCA to DCA and LCA respectively or 7β-dehydroxylaion of UDCA to LCA, appear to be almost exclusively performed by Clostridium[464, 465]. In addition, hydroxysteroid dehydrogenase (HSDH) enzymes are widely present within the gut microbiota. For example, 7α/β-HSDH has been reported in *Escherichia*, *Clostridium* and *Bacteroides*[466]. Bacteria from the genera *Clostridium* and *Escherichia* are both increased after RYGB in this study and may explain the changes seen in bile acids. Indeed, in this study a number of

Clostridium species show a significant positive correlation with serum levels of ursodeoxycholic acid and glycoursodeoxycholic acid. UDCA is widely accepted to be a non-toxic bile acid with anti-inflammatory and immunomodulatory properties[467]. In patients with primary biliary cirrhosis it has been used to improve liver biochemistry, reduce disease progression and increase transplant free survival[468, 469]. However, in the faeces a number of significant correlations with gut bacteria cannot be readily explained. For example, *Subdoligranulum* is associated with an increased 2:1 conversion ratio and a number of other bile acids such as allolithocholic acid, ketocholanic and diketocholanic acid, but is decreased after RYGB. However, a number of other bacteria from the genera *Eubacterium*, *Akkermansia* and *Alistipes* also show similar correlations and, although they do no significantly change individually after bariatric surgery, may explain the overall increase seen in faeces.

In addition, there is a consistent increase in the ratio of glycine to taurine conjugation in both faecal and serum conjugated bile acids, matching with the increase in measured free glycine within serum. This is in agreement with previous studies that have also shown increased glycine conjugation relative to taurine after bariatric surgery[108, 112, 124]. Changes in the glycine : taurine ratio can result from changes in their bioavailability for conjugation in the liver[470]. Others have also demonstrated changes as a result of different diets, which may relate to alterations in deconjugation in the gut[471]. Differences in glycine / taurine conjugation alter BAs solubility, absorbability and potency against BA receptors. Different conjugation patterns have been shown to alter the size of the BA pool, excretion and synthesis rates[470]. However, the overall metabolic effects of differences in the conjugation pattern are difficult to predict and currently poorly understood.

Use or manipulation of BAs could be utilised as a potential pharmacological therapeutic target for metabolic diseases. So far BAs such as UDCA have predominantly been administered to humans to treat cholestatic liver diseases[472]. Alternate strategies could include targeted use of probiotics to increased secondary BAs within the BA pool or direct targeting of BA receptors. Indeed, FXR and TGR5 agonists are being developed[473, 474]. However, both receptors have widespread systemic effects – some of which are deleterious, so agonists need to be developed that are specific for the desired end-organ effects. For example, TGR5 agonists that are gut specific[474].

5.4.2.3 SCFA

SCFA analysis found a decrease in faecal acetate after bariatric surgery, with a decrease in butyrate after VSG but trend towards increasing after RYGB. Whereas 2-methylbutyrate and isovalerate increased in faeces and urine after RYGB. The decrease in faecal acetate and butyrate after VSG is likely largely due to a reduction in fibre, complex carbohydrate and protein intake following surgery.

Interestingly, a number of significant positive correlations seen here between faecal SCFA and gut bacteria levels match existing knowledge about known butyrate producers such as *Faecalibacterium parausnitzii* and *Eubacterium rectale* and acetate producers such as *Bifidobacterium*[475, 476]. In this study *Faecalibacterium prausnitzii* was lower after both VSG and RYGB, contrary to previous reports where it was found to be lower in T2D patients relative to non-diabetic controls[23, 37]. However, in a further previous study, although *Faecalibacterium prausnitzii* was negatively correlated with markers of insulin resistance, this disappeared after adjusting for dietary fat intake, suggesting that these changes could be influenced by dietary differences[477].

Furthermore, a number of clostridium species, known to be butyrate degraders, such as *Clostridium hathewayi* and *Clostridium citroniae* negatively correlated with Butyrate[476]. While two *Escherichia* species, which have been shown to hold the ability to metabolise acetate, negatively correlate with acetate[478]. There were a number of other negative correlations not previously reported, suggesting that bacteria utilising or degrading SCFAs are as important in the final homeostatic balance as those producing them. Interestingly, a number of bacterial species are also associated with increased faecal caproate levels. Caproate is also known to have an affinity for the GPR43 (FFAR2) and GPR41 (FFAR3) receptors[476]. Subsequently, if these bacteria are confirmed to be caproate producers, they are likely to impact on host health.

5.4.2.4 Amino Acids

There were large changes to amino acid profiles after both bariatric procedures. In serum this included decreases in the concentrations of branched chain amino acids (BCAAs) leucine, isoleucine and valine and the aromatic amino acids (AAAs) phenylalanine, tryptophan and tyrosine as well as increases in glycine and serine after both procedures, with glutamine also increased after RYGB. Similarly, there was decreased urinary excretion of lysine, alanine,

leucine and valine. While faecal levels of the essential amino acids phenylalanine and lysine were increased, as well as breakdown products of tyrosine, lysine and arginine.

BCAAs and AAAs have previously been documented as higher in obese diabetic patients relative to controls, while glycine was decreased[479]. Recently perturbations in BCAA and AAA homeostasis have also been significantly associated with insulin resistance[480] and future risk of diabetes in a nested case control study within the Framingham Offspring Study[6]. In particular, those in the top quartile for levels of leucine, isoleucine, valine, tyrosine and phenylalanine had a fivefold increase in diabetes risk[6]. This is thought to be a causative effect. BCAA supplementation in rats leads to the development of insulin resistance[481]. Similarly amino acid infusion in humans increases insulin resistance[481, 482]. Proposed mechanisms include the activation of the mammalian target of rapamycin complex 1 (mTORC1) and its downstream mediators such as S6 kinase-1[482, 483]. mTORC1 acts to sense a variety of nutrients, in particular amino acids and its activation promotes anabolic processes including protein synthesis as well as feedback inhibition of the insulin signalling cascade[484]. Thus, this suggests that the changes in amino acid profiles seen here after bariatric surgery are likely to be an important factor driving improved insulin resistance.

Recent studies have demonstrated that the gut microbiome has the potential to influence the serum BCAA profile of individuals and consequently their insulin resistance[485, 486]. Similar to the findings in this study, subjects who underwent VSG were shown to reduce BCAA and AAA levels to that of lean controls and this corresponded to gut microbiome taxonomic and functional changes[486]. Furthermore, oral gavage of mice with *Bacteroides thetaiotaomicron* led to a reduction in glutamate, phenylalanine, leucine and valine[486]. Indeed, germ free mice have significantly altered profiles of amino acids absorbed from the gut into the systemic circulation via the portal vein relative to those with a normal gut microbiome[487]. This is due to the large number of bacteria involved in amino acid biosynthesis or fermentation. For example, *Paraprevotella* is highly capable of producing amino acids, particularly BCAAs[485]. In this study two species of *Paraprevotella* correlate with serum alanine levels. *Prevotelllaceae* have previously been reported to be significantly enriched in obesity[202]. Interestingly there are also large number of significant negative associations between bacterial species and amino acid levels identified in this study, indicating that fermentation and utilisation of amino acids by gut bacteria may be an important pathway influencing human amino acids profiles.

In particular, a number of bacteria from genera previously shown to be important amino acid fermenters such as *Streptococcus*, *Fusobacterium* and *Clostridium*[488] are shown here to correlate with a reduction in serum BCAAs (leucine, isoleucine and valine).

5.4.2.5 Acylcarnitines

After bariatric surgery even chain acylcarnitines, which largely represent intermediates of mitochondrial fatty acid oxidation, are predominantly increased. Whereas C3 and C5 acylcarnitines, which are markers of amino acid oxidation decrease. These findings are similar to those of brown bears in hibernation that switch their metabolism towards increased lipolysis and altered amino acid metabolism[489]. Furthermore, pyruvate, lactate and a number of gluconeogenic amino acids decrease, whereas citrate is increased after bariatric surgery, suggesting a change in energy metabolism. The negative correlations between C3 and C5 acylcarnitines and the bacteria *Streptococcous parasanguinis*, *Streptococcus salivarius* and *Clostridium asparagiforme* suggests that may result in part from increased fermentation and degradation of amino acids within the gut, resulting in lower levels of serum amino acids and hence lower substrate availability for gluconeogenesis. On the contrary, higher levels of phenylalanine and lysine detected in the faeces after surgery, suggest an alternative mechanism.

5.4.2.6 Other microbial metabolites

TMAO excretion is increased in urine after both RYGB and VSG, while TMA is also increased in faeces after RYGB. These findings are similar to our previous findings in elite athletes relative to sedentary controls[339]. As discussed, TMAO has been described as pro-atherogenic and a predictor of cardiovascular disease by others[26, 56, 60]. However, the causative effect of cardiovascular disease from high TMAO is disputed and these results may have been due to confounders in these studies such as reduced kidney function and poor metabolic control[64]. Other evidence such as the presence of high concentrations of TMAO in the tissues of cold water-dwelling fish where it acts as an osmolyte antifreeze agent and also in the urine of Japanese populations whose diet contains a high portion of fish and who do not have high risk for cardiovascular disease, suggests that these findings may not be due to causative mechanisms[5]. Moreover, TMAO was recently found to protect against impaired glucose tolerance and reduce endoplasmic reticulum stress[65]. After bariatric surgery, patients have a

lower relative risk of both cardiovascular events or death from cardiovascular disease[78, 490], hence these results provide further weight to the suggestion that the described association between cardiovascular disease and high TMAO is not due to a causative mechanism.

Ethanol excretion is increased in urine after bariatric surgery in this cohort. Metabolism of ethanol after gastric bypass has previously been shown to be impaired with higher peak breath alcohol and longer times required to become sober for a matched alcohol intake[491]. Consequently, patients are counselled on reducing alcohol intake prior to surgery. Nevertheless, increased excretion over a 24hr period suggests higher overall intake post-surgery. Contrary to this, methanol and its degradation product formate are both decreased in faeces after bariatric surgery. Formate is a naturally occurring metabolite derived from exogenous sources such as fruits, vegetables and alcoholic beverages in the diet. However, both ethanol and methanol can also results from fermentation by gut bacteria[492]. Indeed, the increase in urinary ethanol seen here after surgery suggests an increased intake of alcoholic beverages post-surgery which would be expected to increase methanol[492]. Yet, despite this possible increase in exogenous intake, faecal methanol decreases. In addition, a number of methanol producing bacteria, such as *Eubacterium rectale*, are decreased after bariatric surgery[493]. Together this suggests a role for the gut microbiome in these changes, which may have important health consequences for the host. Methanol undergoes first pass metabolism within the liver, here excess levels of methanol result in higher levels of its toxic breakdown products formaldehyde and formate, which result in liver damage. Hence, a reduction in gut methanol production may be a novel mechanism in the known improvement of non-alcoholic steatohepatosis (NASH) after bariatric surgery[494].

In addition, a number of other microbial metabolites are also increased in urine after bariatric surgery. These include PAG and 4-cresol sulfate, metabolites of phenylalanine and tyrosine metabolism and hippurate, the glycine conjugate of benzoate. In keeping, PAG has previously been associated with a lean phenotype[415] and was previously higher after models of RYGB in rats[105]. While higher hippurate levels have been correlated with a lean phenotype and lower blood pressure as well as fruit intake[5, 419]. Recently hippurate has also been correlated with markers of gut bacterial diversity and reduced risk of metabolic syndrome, independent of diet[495].

5.5 Conclusion

As expected, the intense physiological disruption induced after both RYGB and VSG procedures results in gross changes to body morphology, glycaemic control, metabolic and gut microbiome profiles. A number of significant novel associations are found between the gut microbiota and host metabolites such as bile acids, SCFAs and amino acids. The changes to bile acids following bariatric surgery has been precisely characterised and shows an overall shift towards secondary bile acids. Interestingly, a number of bacterial species that increase after bariatric surgery correlate with reductions in BCAA and this may play an important role in the improved diabetic control seen after surgery. Crucially, although the overall changes appear to be towards a healthier phenotype there may also be some negative consequences of surgery. It is not clear if the exposure of the colon to a shift towards a gut microbiome usually found within the small bowel, changes in bile acids and other metabolites results in increased or reduced oncogenic risk. In addition, SCFAs are known to be important signalling metabolites in host satiety, insulin resistance and colonocyte health. The reduction seen here in acetate and butyrate after VSG may represent a deleterious effect of bariatric surgery. Nevertheless, it is likely, in part at least, to be due to the large dietary changes, including reduced fibre and carbohydrate, that occur after bariatric surgery.

Although these associations do not establish causation, they suggest that metabolite signalling after bariatric surgery through changes to gut microbiome – host co-metabolism, has a direct influence on host health. Further understanding of this area could enable adjuncts to enhance the beneficial effects of surgery or indeed non-surgical therapies for weight loss such as next-generation targeted probiotics or organ specific FXR / TGR5 agonists.

5.6 References

5. Holmes E, Loo RL, Stamler J, Bictash M, Yap IK, Chan Q, et al. Human metabolic phenotype diversity and its association with diet and blood pressure. Nature. 2008;453(7193):396-400.

6. Wang TJ, Larson MG, Vasan RS, Cheng S, Rhee EP, McCabe E, et al. Metabolite profiles and the risk of developing diabetes. Nature medicine. 2011;17(4):448-53.

8. Nicholson JK, Holmes E, Kinross JM, Darzi AW, Takats Z, Lindon JC. Metabolic phenotyping in clinical and surgical environments. Nature. 2012;491(7424):384-92.

20. Turnbaugh PJ, Ley RE, Mahowald MA, Magrini V, Mardis ER, Gordon JI. An obesity-associated gut microbiome with increased capacity for energy harvest. Nature. 2006;444(7122):1027-31.

21. Turnbaugh PJ, Hamady M, Yatsunenko T, Cantarel BL, Duncan A, Ley RE, et al. A core gut microbiome in obese and lean twins. Nature. 2009;457(7228):480-4.

22. Ley RE, Turnbaugh PJ, Klein S, Gordon JI. Microbial ecology: human gut microbes associated with obesity. Nature. 2006;444(7122):1022-3.

23. Qin J, Li Y, Cai Z, Li S, Zhu J, Zhang F, et al. A metagenome-wide association study of gut microbiota in type 2 diabetes. Nature. 2012;490(7418):55-60.

26. Wang Z, Klipfell E, Bennett BJ, Koeth R, Levison BS, Dugar B, et al. Gut flora metabolism of phosphatidylcholine promotes cardiovascular disease. Nature. 2011;472(7341):57-63.

29. Ley RE, Backhed F, Turnbaugh P, Lozupone CA, Knight RD, Gordon JI. Obesity alters gut microbial ecology. Proceedings of the National Academy of Sciences of the United States of America. 2005;102(31):11070-5.

30. Schwiertz A, Taras D, Schafer K, Beijer S, Bos NA, Donus C, et al. Microbiota and SCFA in lean and overweight healthy subjects. Obesity. 2010;18(1):190-5.

34. Le Chatelier E, Nielsen T, Qin J, Prifti E, Hildebrand F, Falony G, et al. Richness of human gut microbiome correlates with metabolic markers. Nature. 2013;500(7464):541-6.

36. Ridaura VK, Faith JJ, Rey FE, Cheng J, Duncan AE, Kau AL, et al. Gut microbiota from twins discordant for obesity modulate metabolism in mice. Science. 2013;341(6150):1241214.

37. Karlsson FH, Tremaroli V, Nookaew I, Bergstrom G, Behre CJ, Fagerberg B, et al. Gut metagenome in European women with normal, impaired and diabetic glucose control. Nature. 2013;498(7452):99-103.

38. Vrieze A, Van Nood E, Holleman F, Salojarvi J, Kootte RS, Bartelsman JF, et al. Transfer of intestinal microbiota from lean donors increases insulin sensitivity in individuals with metabolic syndrome. Gastroenterology. 2012;143(4):913-6 e7.

39. Liou AP, Paziuk M, Luevano JM, Jr., Machineni S, Turnbaugh PJ, Kaplan LM. Conserved shifts in the gut microbiota due to gastric bypass reduce host weight and adiposity. Science translational medicine. 2013;5(178):178ra41.

40. Nicholson JK, Holmes E, Kinross J, Burcelin R, Gibson G, Jia W, et al. Host-gut microbiota metabolic interactions. Science. 2012;336(6086):1262-7.

41. Lin HV, Frassetto A, Kowalik EJ, Jr., Nawrocki AR, Lu MM, Kosinski JR, et al. Butyrate and propionate protect against diet-induced obesity and regulate gut hormones via free fatty acid receptor 3-independent mechanisms. PloS one. 2012;7(4):e35240.

56. Koeth RA, Wang Z, Levison BS, Buffa JA, Org E, Sheehy BT, et al. Intestinal microbiota metabolism of L-carnitine, a nutrient in red meat, promotes atherosclerosis. Nature medicine. 2013;19(5):576-85.

60. Tang WH, Wang Z, Levison BS, Koeth RA, Britt EB, Fu X, et al. Intestinal microbial metabolism of phosphatidylcholine and cardiovascular risk. The New England journal of medicine. 2013;368(17):1575-84.

62. Tremaroli V, Backhed F. Functional interactions between the gut microbiota and host metabolism. Nature. 2012;489(7415):242-9.

64. Mueller DM, Allenspach M, Othman A, Saely CH, Muendlein A, Vonbank A, et al. Plasma levels of trimethylamine-N-oxide are confounded by impaired kidney function and poor metabolic control. Atherosclerosis. 2015;243(2):638-44.

65. Dumas ME, Rothwell AR, Hoyles L, Aranias T, Chilloux J, Calderari S, et al. Microbial-Host Co-metabolites Are Prodromal Markers Predicting Phenotypic Heterogeneity in Behavior, Obesity, and Impaired Glucose Tolerance. Cell Rep. 2017;20(1):136-48.

66. Jones BV, Begley M, Hill C, Gahan CG, Marchesi JR. Functional and comparative metagenomic analysis of bile salt hydrolase activity in the human gut microbiome. Proceedings of the National Academy of Sciences of the United States of America. 2008;105(36):13580-5.

70. Ryan KK, Tremaroli V, Clemmensen C, Kovatcheva-Datchary P, Myronovych A, Karns R, et al. FXR is a molecular target for the effects of vertical sleeve gastrectomy. Nature. 2014;509(7499):183-8.

71. Penney NC, Kinross J, Newton RC, Purkayastha S. The role of bile acids in reducing the metabolic complications of obesity after bariatric surgery: a systematic review. International journal of obesity. 2015;39(11):1565-74.

75. Adams TD, Davidson LE, Litwin SE, Kolotkin RL, LaMonte MJ, Pendleton RC, et al. Health benefits of gastric bypass surgery after 6 years. JAMA : the journal of the American Medical Association. 2012;308(11):1122-31.

76. Ikramuddin S, Korner J, Lee WJ, Connett JE, Inabnet WB, Billington CJ, et al. Roux-en-Y gastric bypass vs intensive medical management for the control of type 2 diabetes, hypertension, and hyperlipidemia: the Diabetes Surgery Study randomized clinical trial. JAMA : the journal of the American Medical Association. 2013;309(21):2240-9.

77. Schauer PR, Bhatt DL, Kirwan JP, Wolski K, Brethauer SA, Navaneethan SD, et al. Bariatric surgery versus intensive medical therapy for diabetes--3-year outcomes. The New England journal of medicine. 2014;370(21):2002-13.

78. Eliasson B, Liakopoulos V, Franzen S, Naslund I, Svensson AM, Ottosson J, et al. Cardiovascular disease and mortality in patients with type 2 diabetes after bariatric surgery in Sweden: a nationwide, matched, observational cohort study. The lancet Diabetes & endocrinology. 2015;3(11):847-54.

79. Schauer PR, Bhatt DL, Kirwan JP, Wolski K, Aminian A, Brethauer SA, et al. Bariatric Surgery versus Intensive Medical Therapy for Diabetes - 5-Year Outcomes. The New England journal of medicine. 2017;376(7):641-51.

85. Kohli R, Setchell KD, Kirby M, Myronovych A, Ryan KK, Ibrahim SH, et al. A surgical model in male obese rats uncovers protective effects of bile acids post-bariatric surgery. Endocrinology. 2013;154(7):2341-51.

105. Li JV, Ashrafian H, Bueter M, Kinross J, Sands C, le Roux CW, et al. Metabolic surgery profoundly influences gut microbial-host metabolic cross-talk. Gut. 2011;60(9):1214-23.

108. Werling M, Vincent RP, Cross GF, Marschall HU, Fandriks L, Lonroth H, et al. Enhanced fasting and post-prandial plasma bile acid responses after Roux-en-Y gastric bypass surgery. Scandinavian journal of gastroenterology. 2013;48(11):1257-64.

109. Scholtz S, Miras AD, Chhina N, Prechtl CG, Sleeth ML, Daud NM, et al. Obese patients after gastric bypass surgery have lower brain-hedonic responses to food than after gastric banding. Gut. 2014;63(6):891-902.

112. Simonen M, Dali-Youcef N, Kaminska D, Venesmaa S, Kakela P, Paakkonen M, et al. Conjugated bile acids associate with altered rates of glucose and lipid oxidation after Roux-en-Y gastric bypass. Obesity surgery. 2012;22(9):1473-80.

117. Cummings BP, Bettaieb A, Graham JL, Stanhope KL, Kowala M, Haj FG, et al. Vertical sleeve gastrectomy improves glucose and lipid metabolism and delays diabetes onset in UCD-T2DM rats. Endocrinology. 2012;153(8):3620-32.

118. Myronovych A, Kirby M, Ryan KK, Zhang W, Jha P, Setchell KD, et al. Vertical sleeve gastrectomy reduces hepatic steatosis while increasing serum bile acids in a weight-loss-independent manner. Obesity. 2014;22(2):390-400.

124. Mencarelli A, Renga B, D'Amore C, Santorelli C, Graziosi L, Bruno A, et al. Dissociation of intestinal and hepatic activities of FXR and LXRalpha supports metabolic effects of terminal ileum interposition in rodents. Diabetes. 2013;62(10):3384-93.

202. Zhang H, DiBaise JK, Zuccolo A, Kudrna D, Braidotti M, Yu Y, et al. Human gut microbiota in obesity and after gastric bypass. Proceedings of the National Academy of Sciences of the United States of America. 2009;106(7):2365-70.

218. Katona BW, Anant S, Covey DF, Stenson WF. Characterization of enantiomeric bile acid-induced apoptosis in colon cancer cell lines. The Journal of biological chemistry. 2009;284(5):3354-64.

219. Bernstein H, Bernstein C, Payne CM, Dvorak K. Bile acids as endogenous etiologic agents in gastrointestinal cancer. World journal of gastroenterology : WJG. 2009;15(27):3329-40.

220. Pearson JR, Gill CI, Rowland IR. Diet, fecal water, and colon cancer--development of a biomarker. Nutrition reviews. 2009;67(9):509-26.

311. Garcia-Perez I, Posma JM, Gibson R, Chambers ES, Hansen TH, Vestergaard H, et al. Objective assessment of dietary patterns by use of metabolic phenotyping: a randomised, controlled, crossover trial. The lancet Diabetes & endocrinology. 2017;5(3):184-95.

332. Li H. Aligning sequence reads, clone sequences and assembly contigs with BWA-MEM. arXiv. 2013.

333. Truong DT, Franzosa EA, Tickle TL, Scholz M, Weingart G, Pasolli E, et al. MetaPhlAn2 for enhanced metagenomic taxonomic profiling. Nat Methods. 2015;12(10):902-3.

334. Segata N, Waldron L, Ballarini A, Narasimhan V, Jousson O, Huttenhower C. Metagenomic microbial community profiling using unique clade-specific marker genes. Nat Methods. 2012;9(8):811-4.

335. Nurk S, Meleshko D, Korobeynikov A, Pevzner PA. metaSPAdes: a new versatile metagenomic assembler. Genome Res. 2017;27(5):824-34.

339. Barton W, Penney NC, Cronin O, Garcia-Perez I, Molloy MG, Holmes E, et al. The microbiome of professional athletes differs from that of more sedentary subjects in composition and particularly at the functional metabolic level. Gut. 2018;67(4):625-33.

351. Dona AC, Jimenez B, Schafer H, Humpfer E, Spraul M, Lewis MR, et al. Precision high-throughput proton NMR spectroscopy of human urine, serum, and plasma for large-scale metabolic phenotyping. Analytical chemistry. 2014;86(19):9887-94.

353. Sarafian MH, Lewis MR, Pechlivanis A, Ralphs S, McPhail MJ, Patel VC, et al. Bile acid profiling and quantification in biofluids using ultra-performance liquid chromatography tandem mass spectrometry. Analytical chemistry. 2015;87(19):9662-70.

355. Veselkov KA, Vingara LK, Masson P, Robinette SL, Want E, Li JV, et al. Optimized preprocessing of ultra-performance liquid chromatography/mass spectrometry urinary metabolic profiles for improved information recovery. Analytical chemistry. 2011;83(15):5864-72.

374. Warrack BM, Hnatyshyn S, Ott KH, Reily MD, Sanders M, Zhang H, et al. Normalization strategies for metabonomic analysis of urine samples. Journal of chromatography B, Analytical technologies in the biomedical and life sciences. 2009;877(5-6):547-52.

410. Gu Z, Eils R, Schlesner M. Complex heatmaps reveal patterns and correlations in multidimensional genomic data. Bioinformatics. 2016;32(18):2847-9.

415. Elliott P, Posma JM, Chan Q, Garcia-Perez I, Wijeyesekera A, Bictash M, et al. Urinary metabolic signatures of human adiposity. Science translational medicine. 2015;7(285):285ra62.

419. Heinzmann SS, Merrifield CA, Rezzi S, Kochhar S, Lindon JC, Holmes E, et al. Stability and robustness of human metabolic phenotypes in response to sequential food challenges. Journal of proteome research. 2012;11(2):643-55.

427. Watanabe M, Morimoto K, Houten SM, Kaneko-Iwasaki N, Sugizaki T, Horai Y, et al. Bile acid binding resin improves metabolic control through the induction of energy expenditure. PloS one. 2012;7(8):e38286.

428. Frost G, Sleeth ML, Sahuri-Arisoylu M, Lizarbe B, Cerdan S, Brody L, et al. The short-chain fatty acid acetate reduces appetite via a central homeostatic mechanism. Nature communications. 2014;5:3611.

429. Chiuve SE, Fung TT, Rimm EB, Hu FB, McCullough ML, Wang M, et al. Alternative dietary indices both strongly predict risk of chronic disease. The Journal of nutrition. 2012;142(6):1009-18.

430. Gratton J, Phetcharaburanin J, Mullish BH, Williams HR, Thursz M, Nicholson JK, et al. Optimized Sample Handling Strategy for Metabolic Profiling of Human Feces. Analytical chemistry. 2016;88(9):4661-8.

431. Klinder A, Karlsson PC, Clune Y, Hughes R, Glei M, Rafter JJ, et al. Fecal water as a non-invasive biomarker in nutritional intervention: comparison of preparation methods and refinement of different endpoints. Nutrition and cancer. 2007;57(2):158-67.

432. Hillman ET, Lu H, Yao T, Nakatsu CH. Microbial Ecology along the Gastrointestinal Tract. Microbes Environ. 2017;32(4):300-13.

433. Xu H, Luo X, Qian J, Pang X, Song J, Qian G, et al. FastUniq: a fast de novo duplicates removal tool for paired short reads. PloS one. 2012;7(12):e52249.

434. Hoyles L, Fernandez-Real JM, Federici M, Serino M, Abbott J, Charpentier J, et al. Molecular phenomics and metagenomics of hepatic steatosis in non-diabetic obese women. Nature medicine. 2018;24(7):1070-80.

435. Zhu W, Lomsadze A, Borodovsky M. Ab initio gene identification in metagenomic sequences. Nucleic Acids Res. 2010;38(12):e132.

436. Besemer J, Borodovsky M. Heuristic approach to deriving models for gene finding. Nucleic Acids Res. 1999;27(19):3911-20.

437. Edgar RC. Search and clustering orders of magnitude faster than BLAST. Bioinformatics. 2010;26(19):2460-1.

438. Huerta-Cepas J, Forslund K, Coelho LP, Szklarczyk D, Jensen LJ, von Mering C, et al. Fast Genome-Wide Functional Annotation through Orthology Assignment by eggNOG-Mapper. Mol Biol Evol. 2017;34(8):2115-22.

439. Qin N, Yang F, Li A, Prifti E, Chen Y, Shao L, et al. Alterations of the human gut microbiome in liver cirrhosis. Nature. 2014;513(7516):59-64.

440. Asnicar F, Weingart G, Tickle TL, Huttenhower C, Segata N. Compact graphical representation of phylogenetic data and metadata with GraPhlAn. PeerJ. 2015;3:e1029.

441. Sealey WM, Teague AM, Stratton SL, Mock DM. Smoking accelerates biotin catabolism in women. The American journal of clinical nutrition. 2004;80(4):932-5.

442. Buchwald H, Avidor Y, Braunwald E, Jensen MD, Pories W, Fahrbach K, et al. Bariatric surgery: a systematic review and meta-analysis. JAMA : the journal of the American Medical Association. 2004;292(14):1724-37.

443. Gloy VL, Briel M, Bhatt DL, Kashyap SR, Schauer PR, Mingrone G, et al. Bariatric surgery versus non-surgical treatment for obesity: a systematic review and meta-analysis of randomised controlled trials. Bmj. 2013;347:f5934.

444. le Roux CW, Aylwin SJ, Batterham RL, Borg CM, Coyle F, Prasad V, et al. Gut hormone profiles following bariatric surgery favor an anorectic state, facilitate weight loss, and improve metabolic parameters. Annals of surgery. 2006;243(1):108-14.

445. Ahmed K, Penney N, Darzi A, Purkayastha S. Taste Changes after Bariatric Surgery: a Systematic Review. Obesity surgery. 2018;28(10):3321-32.

446. Ernst B, Thurnheer M, Wilms B, Schultes B. Differential changes in dietary habits after gastric bypass versus gastric banding operations. Obesity surgery. 2009;19(3):274-80.

447. Behary P, Miras AD. Food preferences and underlying mechanisms after bariatric surgery. The Proceedings of the Nutrition Society. 2015;74(4):419-25.

448. Boggs DA, Rosenberg L, Rodriguez-Bernal CL, Palmer JR. Long-term diet quality is associated with lower obesity risk in young African American women with normal BMI at baseline. The Journal of nutrition. 2013;143(10):1636-41.

449. Varraso R, Chiuve SE, Fung TT, Barr RG, Hu FB, Willett WC, et al. Alternate Healthy Eating Index 2010 and risk of chronic obstructive pulmonary disease among US women and men: prospective study. Bmj. 2015;350:h286.

450. Reedy J, Krebs-Smith SM, Miller PE, Liese AD, Kahle LL, Park Y, et al. Higher diet quality is associated with decreased risk of all-cause, cardiovascular disease, and cancer mortality among older adults. The Journal of nutrition. 2014;144(6):881-9.

451. Samieri C, Sun Q, Townsend MK, Chiuve SE, Okereke OI, Willett WC, et al. The association between dietary patterns at midlife and health in aging: an observational study. Annals of internal medicine. 2013;159(9):584-91.

452. Lafay L, Mennen L, Basdevant A, Charles MA, Borys JM, Eschwege E, et al. Does energy intake underreporting involve all kinds of food or only specific food items? Results from the Fleurbaix Laventie Ville Sante (FLVS) study. International journal of obesity and related metabolic disorders : journal of the International Association for the Study of Obesity. 2000;24(11):1500-6.

453. Poslusna K, Ruprich J, de Vries JH, Jakubikova M, van't Veer P. Misreporting of energy and micronutrient intake estimated by food records and 24 hour recalls, control and adjustment methods in practice. The British journal of nutrition. 2009;101 Suppl 2:S73-85.

454. Rennie KL, Coward A, Jebb SA. Estimating under-reporting of energy intake in dietary surveys using an individualised method. The British journal of nutrition. 2007;97(6):1169-76.

455. Donaldson GP, Lee SM, Mazmanian SK. Gut biogeography of the bacterial microbiota. Nature reviews Microbiology. 2016;14(1):20-32.

456. Zoetendal EG, Raes J, van den Bogert B, Arumugam M, Booijink CC, Troost FJ, et al. The human small intestinal microbiota is driven by rapid uptake and conversion of simple carbohydrates. ISME J. 2012;6(7):1415-26.

457. Mu C, Yang Y, Su Y, Zoetendal EG, Zhu W. Differences in Microbiota Membership along the Gastrointestinal Tract of Piglets and Their Differential Alterations Following an Early-Life Antibiotic Intervention. Frontiers in microbiology. 2017;8:797.

458. Suzuki TA, Nachman MW. Spatial Heterogeneity of Gut Microbial Composition along the Gastrointestinal Tract in Natural Populations of House Mice. PloS one. 2016;11(9):e0163720.

459. Gu S, Chen D, Zhang JN, Lv X, Wang K, Duan LP, et al. Bacterial community mapping of the mouse gastrointestinal tract. PloS one. 2013;8(10):e74957.

460. Miquel S, Martin R, Bridonneau C, Robert V, Sokol H, Bermudez-Humaran LG, et al. Ecology and metabolism of the beneficial intestinal commensal bacterium Faecalibacterium prausnitzii. Gut microbes. 2014;5(2):146-51.

461. Abell GC, Cooke CM, Bennett CN, Conlon MA, McOrist AL. Phylotypes related to Ruminococcus bromii are abundant in the large bowel of humans and increase in response to a diet high in resistant starch. FEMS Microbiol Ecol. 2008;66(3):505-15.

462. Duncan SH, Lobley GE, Holtrop G, Ince J, Johnstone AM, Louis P, et al. Human colonic microbiota associated with diet, obesity and weight loss. International journal of obesity. 2008;32(11):1720-4.

463. Flint HJ, Scott KP, Louis P, Duncan SH. The role of the gut microbiota in nutrition and health. Nature reviews Gastroenterology & hepatology. 2012;9(10):577-89.

464. Ridlon JM, Harris SC, Bhowmik S, Kang DJ, Hylemon PB. Consequences of bile salt biotransformations by intestinal bacteria. Gut microbes. 2016;7(1):22-39.

465. Wells JE, Berr F, Thomas LA, Dowling RH, Hylemon PB. Isolation and characterization of cholic acid 7alpha-dehydroxylating fecal bacteria from cholesterol gallstone patients. Journal of hepatology. 2000;32(1):4-10.

466. Ridlon JM, Kang DJ, Hylemon PB. Bile salt biotransformations by human intestinal bacteria. Journal of lipid research. 2006;47(2):241-59.

467. Poupon R. Ursodeoxycholic acid and bile-acid mimetics as therapeutic agents for cholestatic liver diseases: an overview of their mechanisms of action. Clin Res Hepatol Gastroenterol. 2012;36 Suppl 1:S3-12.

468. Poupon RE, Lindor KD, Cauch-Dudek K, Dickson ER, Poupon R, Heathcote EJ. Combined analysis of randomized controlled trials of ursodeoxycholic acid in primary biliary cirrhosis. Gastroenterology. 1997;113(3):884-90.

469. Gong Y, Huang Z, Christensen E, Gluud C. Ursodeoxycholic acid for patients with primary biliary cirrhosis: an updated systematic review and meta-analysis of randomized clinical trials using Bayesian approach as sensitivity analyses. The American journal of gastroenterology. 2007;102(8):1799-807.

470. Hardison WG, Grundy SM. Effect of bile acid conjugation pattern on bile acid metabolism in normal humans. Gastroenterology. 1983;84(3):617-20.

471. Ide T, Kano S, Murata M, Yanagita T, Sugano M. Dietary modifications of the biliary bile acid glycine:taurine ratio and activity of hepatic bile acid-CoA:amino acid N-acyltransferase (EC 2.3.1) in the rat. The British journal of nutrition. 1994;72(1):93-100.

472. Hofmann AF. Biliary secretion and excretion in health and disease: current concepts. Ann Hepatol. 2007;6(1):15-27.

473. Han CY. Update on FXR Biology: Promising Therapeutic Target? International journal of molecular sciences. 2018;19(7).

474. Cao H, Chen ZX, Wang K, Ning MM, Zou QA, Feng Y, et al. Intestinally-targeted TGR5 agonists equipped with quaternary ammonium have an improved hypoglycemic effect and reduced gallbladder filling effect. Sci Rep. 2016;6:28676.

475. Louis P, Young P, Holtrop G, Flint HJ. Diversity of human colonic butyrate-producing bacteria revealed by analysis of the butyryl-CoA:acetate CoA-transferase gene. Environ Microbiol. 2010;12(2):304-14.

476. Basson A, Trotter A, Rodriguez-Palacios A, Cominelli F. Mucosal Interactions between Genetics, Diet, and Microbiome in Inflammatory Bowel Disease. Front Immunol. 2016;7:290.

477. Brahe LK, Le Chatelier E, Prifti E, Pons N, Kennedy S, Hansen T, et al. Specific gut microbiota features and metabolic markers in postmenopausal women with obesity. Nutr Diabetes. 2015;5:e159.

478. Clark DP, Cronan JE. Two-Carbon Compounds and Fatty Acids as Carbon Sources. EcoSal Plus. 2005;1(2).

479. Felig P, Marliss E, Cahill GF, Jr. Plasma amino acid levels and insulin secretion in obesity. The New England journal of medicine. 1969;281(15):811-6.

480. Tai ES, Tan ML, Stevens RD, Low YL, Muehlbauer MJ, Goh DL, et al. Insulin resistance is associated with a metabolic profile of altered protein metabolism in Chinese and Asian-Indian men. Diabetologia. 2010;53(4):757-67.

481. Tremblay F, Krebs M, Dombrowski L, Brehm A, Bernroider E, Roth E, et al. Overactivation of S6 kinase 1 as a cause of human insulin resistance during increased amino acid availability. Diabetes. 2005;54(9):2674-84.

482. Tremblay F, Brule S, Hee Um S, Li Y, Masuda K, Roden M, et al. Identification of IRS-1 Ser-1101 as a target of S6K1 in nutrient- and obesity-induced insulin resistance. Proceedings of the National Academy of Sciences of the United States of America. 2007;104(35):14056-61.

483. Howell JJ, Manning BD. mTOR couples cellular nutrient sensing to organismal metabolic homeostasis. Trends Endocrinol Metab. 2011;22(3):94-102.

484. Langenberg C, Savage DB. An amino acid profile to predict diabetes? Nature medicine. 2011;17(4):418-20.

485. Pedersen HK, Gudmundsdottir V, Nielsen HB, Hyotylainen T, Nielsen T, Jensen BA, et al. Human gut microbes impact host serum metabolome and insulin sensitivity. Nature. 2016;535(7612):376-81.

486. Liu R, Hong J, Xu X, Feng Q, Zhang D, Gu Y, et al. Gut microbiome and serum metabolome alterations in obesity and after weight-loss intervention. Nature medicine. 2017;23(7):859-68.

487. Mardinoglu A, Shoaie S, Bergentall M, Ghaffari P, Zhang C, Larsson E, et al. The gut microbiota modulates host amino acid and glutathione metabolism in mice. Molecular systems biology. 2015;11(10):834.

488. Dai ZL, Wu G, Zhu WY. Amino acid metabolism in intestinal bacteria: links between gut ecology and host health. Front Biosci (Landmark Ed). 2011;16:1768-86.

489. Sommer F, Stahlman M, Ilkayeva O, Arnemo JM, Kindberg J, Josefsson J, et al. The Gut Microbiota Modulates Energy Metabolism in the Hibernating Brown Bear Ursus arctos. Cell Rep. 2016;14(7):1655-61.

490. Sjostrom L, Peltonen M, Jacobson P, Sjostrom CD, Karason K, Wedel H, et al. Bariatric surgery and long-term cardiovascular events. JAMA : the journal of the American Medical Association. 2012;307(1):56-65.

491. Woodard GA, Downey J, Hernandez-Boussard T, Morton JM. Impaired alcohol metabolism after gastric bypass surgery: a case-crossover trial. Journal of the American College of Surgeons. 2011;212(2):209-14.

492. Dorokhov YL, Komarova TV, Petrunia IV, Kosorukov VS, Zinovkin RA, Shindyapina AV, et al. Methanol may function as a cross-kingdom signal. PloS one. 2012;7(4):e36122.

493. Dorokhov YL, Shindyapina AV, Sheshukova EV, Komarova TV. Metabolic methanol: molecular pathways and physiological roles. Physiological reviews. 2015;95(2):603-44.

494. Lassailly G, Caiazzo R, Buob D, Pigeyre M, Verkindt H, Labreuche J, et al. Bariatric Surgery Reduces Features of Nonalcoholic Steatohepatitis in Morbidly Obese Patients. Gastroenterology. 2015;149(2):379-88; quiz e15-6.

495. Pallister T, Jackson MA, Martin TC, Zierer J, Jennings A, Mohney RP, et al. Hippurate as a metabolomic marker of gut microbiome diversity: Modulation by diet and relationship to metabolic syndrome. Sci Rep. 2017;7(1):13670.

6 Conclusion and Planned future work

6.1 Summary of findings

In this thesis I have applied metabolic and gut microbiome profiling techniques to three separate and contrasting cohorts to elucidate the physiological relationship between the gut microbes and extreme lifestyle factors. I have investigated i) the extreme healthy state of elite athletes compared to healthy controls, ii) participants randomised to an exercise regime, a high protein diet or both and iii) the extreme unhealthy state of obese patients undergoing bariatric surgery. The physiological extremes found within these cohorts have helped to reveal a host of novel findings that increase the body of knowledge characterising the effects of gut microbiome - host co-metabolism and diet on host health (see Figure 6.1-1).

The study of elite athletes demonstrated distinct metabolic and gut microbiome phenotypes between athletes and sedentary controls, with changes resulting from both dietary differences and levels of aerobic and anaerobic exercise and fitness. Further, the analysis confirmed higher gut bacterial diversity in athletes relative to healthy controls. Metabolic differences were dominated by metabolites associated with muscle turnover, those derived from vitamins, recovery supplements and a high protein diet in addition to those derived from gut microbes. However, the study does not allow the separation of these components and indeed conflates changes due to exercise with those due to diet.

To further explore the separate components of this paradigm two further studies were undertaken. Firstly, a prospective study of short-to-medium term exercise and/or whey protein supplementation in healthy, physically inactive adults was performed. This did not induce significant detectable metabolic alterations, although some changes including alteration of urinary TMAO and PAG excretion were evident. This suggests that the alterations in microbial diversity, composition, and metabolic profiles observed in professional athletes may be a late response to exercise or fitness.

In contrast, a second study which grouped participants based on an objective measure of their dietary healthiness and exercise levels elicited novel insights into this complex, multi-factorial relationship. The model synthesis enabled control of a number of closely related confounders, which consequently enabled more accurate ascertainment of the individual biological

sequelae of diet healthiness and exercise respectively, with each exercise / diet group exhibiting a distinct metabolic and functional microbial phenotype. Further analysis of the influence of gut bacterial diversity, which has previously been associated with a healthy state[21, 34], was associated with a number of microbially derived metabolites such as SCFA but also metabolites produced through proteolytic fermentation by gut bacteria. Protein metabolism within the gut has been associated with the production of toxic compounds such as ammonia, amines and sulphides. Thus, indicating that in this cohort the effects of increased diversity may include deleterious as well as beneficial effects on the host.

As expected, the intense physiological disruption induced after both RYGB and VSG procedures results in gross changes to metabolic and gut microbiome profiles. A number of significant associations were found between the gut microbiota and host metabolites such as bile acids, SCFAs and amino acids.

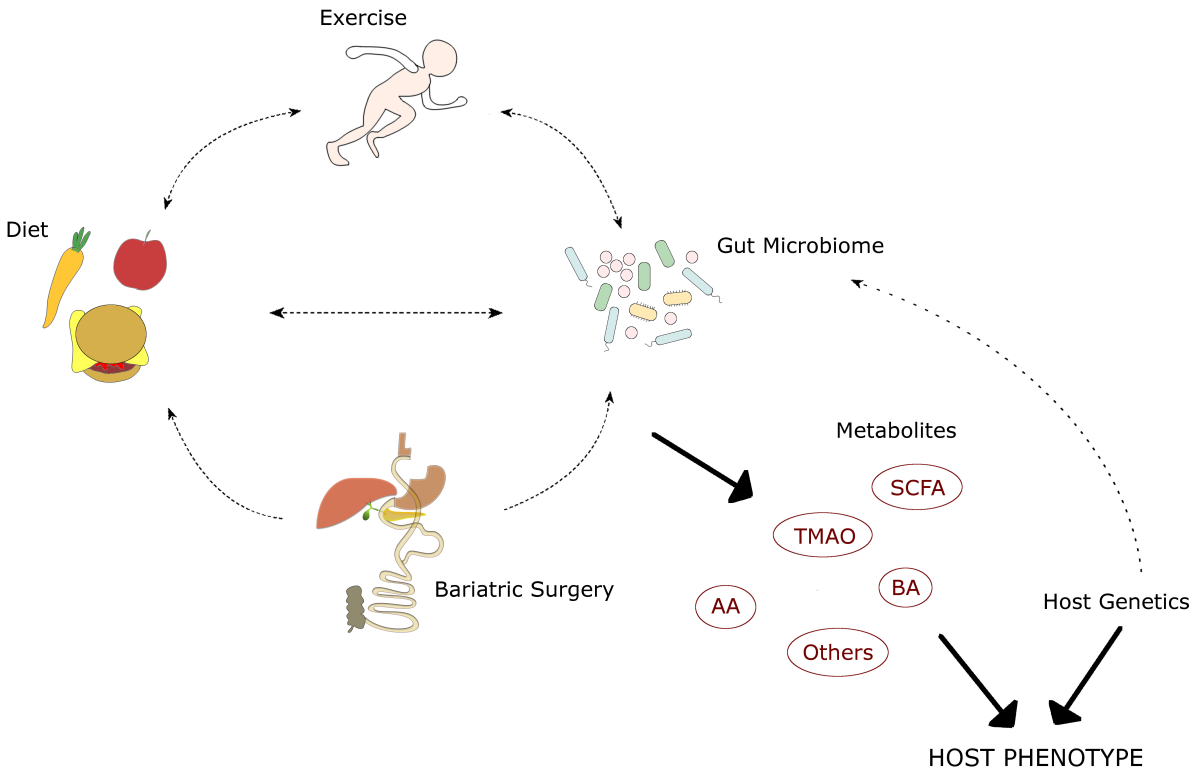


Figure 6.1-1 Summary of findings. Extremes of exercise, diet and changes to the gut microbiome following bariatric surgery utilised to expose their individual influence on host metabolism and phenotype.

6.2 Impact on host physiology

Changes to several metabolite groups, known to be microbial in origin, recurred between different cohorts within this thesis. Earlier studies have associated SCFAs with a lean phenotype and numerous health benefits[36, 356, 357]. In corroboration with this, here, athletes have an enriched faecal SCFA profile. Interestingly, within the faecal SCFAs, two distinct correlation clusters were observed; acetic acid, propionic acid and butyric acid correlated predominantly with dietary contributors (fibre with butyric acid and protein with propionic acid), while isobutyric acid, isovaleric acid and valeric acid correlated with microbial diversity. The same SCFA clusters were observed when correlating with individual bacterial taxa. Contrary to this, after bariatric surgery, although subjects become leaner, SCFA levels were reduced. This is likely due to the large dietary changes, including reduced fibre and protein intake, that occur after surgery.

As discussed within this thesis, TMAO has previously been associated with atherosclerosis and cardiovascular disease[26, 56, 60]. However, the causative role of TMAO in cardiovascular disease is disputed[5, 65]. Indeed, in each separate cohort studied here TMAO is found in higher concentrations in the 'healthier' group, associated with lower cardiovascular disease. This included athletes versus controls, subjects with a healthier diet (controlling for exercise levels), subjects with higher exercise levels (controlling for diet healthiness) and longitudinally matched subjects after bariatric surgery. Thus, providing further evidence to dispute the link between TMAO levels and cardiovascular disease and indicating that bacterial degradation of dietary choline is dependent on multiple interacting factors.

Bile acids are important signalling molecules that have key metabolic effects on host metabolism and the gut microbiome in a bi-directional manner, as reviewed herein[71]. Semi targeted bile acid analysis of faecal samples in athletes versus controls did not reveal significant differences. Although some subtle differences in bile acid profiles were detected in subjects with exercise or diet healthiness differences using ^{1}H-NMR, these were difficult to characterise. The use of a quantitative targeted bile acid analysis of subject samples pre and post bariatric surgery enabled more accurate and comprehensive measurement of bile acid changes and revealed a shift towards higher secondary and conjugated secondary bile acids after bariatric surgery that correlated in part with changes to the gut microbiota.

Interestingly a number of significant negative associations between bacterial species and amino acid levels were identified pre and post bariatric surgery, indicating that fermentation and utilisation of amino acids by gut bacteria may be an important pathway influencing human amino acids profiles. This includes the association of reduced serum BCAA (leucine, isoleucine and valine), important modifiers of insulin resistance, with amino acid fermenters in the gut.

6.3 Future work

A number of different associations between gut bacteria and metabolites are witnessed throughout this thesis. Although these associations do not establish causation, they suggest that altered metabolite signalling, through changes to gut microbiome – host co-metabolism, has a direct influence on host health. However, future mechanistic studies of the gut microbiome are required to clarify which changes are caused by the gut, rather than solely non-causal associations. These future studies may include *in vitro* studies of cultured organisms of interest[496]. For example, a recent study utilised *in vitro* models of the human faecal microbiota to elucidate specific bacteria – bile acid associations[497]. In addition, *in vivo* studies using faecal transplants into germ free rodent models have previously provided key insights into the role of the gut microbiome[20, 36] and could be used to assess the impact of isolated bacteria of interest[20, 36]. Nonetheless, with all these approaches it is important to caution that the gut-microbiome and its interaction with the host is complex and multidirectional and analysing small parts of the paradigm in isolation may not reveal their true overall impact. Thus, a dual approach combining a 'top-down' or systems methodology with the 'bottom-up' or model driven approach should be used to further advance understanding of this complex relationship.

Increased knowledge of gut microbiome – host co-metabolism could lead to future medical therapies to treat a number of different disease states including obesity, diabetes and cardiovascular disease. Gut microbiome composition can be modified using various strategies including prebiotics, probiotics, faecal microbiota transplant or phage therapy. Studies are ongoing to ascertain the best method of altering the gut microbiome to benefit these and other disease states and to establish the optimal dosing, longevity of effect and any

potentially harmful side-effects[498]. In addition, improved knowledge of co-metabolites such as BAs and SCFAs could lead to novel pharmacological targets. For example, FXR and TGR5 agonists are currently being developed[473, 474]. However, both receptors have widespread systemic effects – some of which are deleterious, so agonists need to be developed that are specific for the desired end-organ effects. Such as TGR5 agonists that are gut specific[474].

From a clinical perspective, national and international guidelines for bariatric surgery have historically been based predominantly on weight. However, bariatric surgery is also highly successful in achieving remission of co-morbidities such as T2D. This does not appear to be weight-dependent[499]. Consequently, the latest guidelines by the National Institute for Health and Care Excellence (NICE 2014) have been updated to reflect the convincing body of evidence that surgery is also a highly successful and cost-effective treatment for T2D patients who are less obese (BMI>30kg/m^2). However, unfortunately up to 30% of T2D patients who undergo bariatric surgery do not achieve diabetes remission[499]. There is currently no reliable method of identifying these patients preoperatively. Therefore, novel preoperative biomarkers to individually stratify patients according to their likely metabolic outcomes following bariatric surgery and help guide clinicians select the ideal surgical candidates are urgently required. Through further extension and analysis of the dataset collected I hope to identify biomarkers to enable the preoperative stratification of bariatric surgery candidates according to their chance of T2D remission. This will allow both patients and clinicians to accurately assess the likely benefits and risks from bariatric surgery and thus enable truly personalised healthcare.

6.4 References

5. Holmes E, Loo RL, Stamler J, Bictash M, Yap IK, Chan Q, et al. Human metabolic phenotype diversity and its association with diet and blood pressure. Nature. 2008;453(7193):396-400.

20. Turnbaugh PJ, Ley RE, Mahowald MA, Magrini V, Mardis ER, Gordon JI. An obesity-associated gut microbiome with increased capacity for energy harvest. Nature. 2006;444(7122):1027-31.

21. Turnbaugh PJ, Hamady M, Yatsunenko T, Cantarel BL, Duncan A, Ley RE, et al. A core gut microbiome in obese and lean twins. Nature. 2009;457(7228):480-4.

26. Wang Z, Klipfell E, Bennett BJ, Koeth R, Levison BS, Dugar B, et al. Gut flora metabolism of phosphatidylcholine promotes cardiovascular disease. Nature. 2011;472(7341):57-63.

34. Le Chatelier E, Nielsen T, Qin J, Prifti E, Hildebrand F, Falony G, et al. Richness of human gut microbiome correlates with metabolic markers. Nature. 2013;500(7464):541-6.

36. Ridaura VK, Faith JJ, Rey FE, Cheng J, Duncan AE, Kau AL, et al. Gut microbiota from twins discordant for obesity modulate metabolism in mice. Science. 2013;341(6150):1241214.

56. Koeth RA, Wang Z, Levison BS, Buffa JA, Org E, Sheehy BT, et al. Intestinal microbiota metabolism of L-carnitine, a nutrient in red meat, promotes atherosclerosis. Nature medicine. 2013;19(5):576-85.

60. Tang WH, Wang Z, Levison BS, Koeth RA, Britt EB, Fu X, et al. Intestinal microbial metabolism of phosphatidylcholine and cardiovascular risk. The New England journal of medicine. 2013;368(17):1575-84.

65. Dumas ME, Rothwell AR, Hoyles L, Aranias T, Chilloux J, Calderari S, et al. Microbial-Host Co-metabolites Are Prodromal Markers Predicting Phenotypic Heterogeneity in Behavior, Obesity, and Impaired Glucose Tolerance. Cell Rep. 2017;20(1):136-48.

71. Penney NC, Kinross J, Newton RC, Purkayastha S. The role of bile acids in reducing the metabolic complications of obesity after bariatric surgery: a systematic review. International journal of obesity. 2015;39(11):1565-74.

356. Koh A, De Vadder F, Kovatcheva-Datchary P, Backhed F. From Dietary Fiber to Host Physiology: Short-Chain Fatty Acids as Key Bacterial Metabolites. Cell. 2016;165(6):1332-45.

357. Hamer HM, Jonkers DM, Bast A, Vanhoutvin SA, Fischer MA, Kodde A, et al. Butyrate modulates oxidative stress in the colonic mucosa of healthy humans. Clinical nutrition (Edinburgh, Scotland). 2009;28(1):88-93.

473. Han CY. Update on FXR Biology: Promising Therapeutic Target? International journal of molecular sciences. 2018;19(7).

474. Cao H, Chen ZX, Wang K, Ning MM, Zou QA, Feng Y, et al. Intestinally-targeted TGR5 agonists equipped with quaternary ammonium have an improved hypoglycemic effect and reduced gallbladder filling effect. Sci Rep. 2016;6:28676.

496. Marx V. Microbiology: the return of culture. Nat Methods. 2016;14(1):37-40.

497. Martin G, Kolida S, Marchesi JR, Want E, Sidaway JE, Swann JR. In Vitro Modeling of Bile Acid Processing by the Human Fecal Microbiota. Frontiers in microbiology. 2018;9:1153.

498. McCarville JL, Caminero A, Verdu EF. Novel perspectives on therapeutic modulation of the gut microbiota. Therap Adv Gastroenterol. 2016;9(4):580-93.

499. Panunzi S, De Gaetano A, Carnicelli A, Mingrone G. Predictors of Remission of Diabetes Mellitus in Severely Obese Individuals Undergoing Bariatric Surgery: Do BMI or Procedure Choice Matter? A Meta-analysis. Annals of surgery. 2015;261(3):459-67.